SYNTHESIS, POLYMERIZATION KINETICS, AND APPLICATIONS OF NOVEL MACROMONOMER-BASED DEGRADABLE MATERIALS

by

Thomas Richard Rooney

A thesis submitted to the Department of Chemical Engineering

In conformity with the requirements for the

Degree of Doctor of Philosophy

Queen's University

Kingston, Ontario, Canada

April, 2017

Abstract

The ability to design materials with controlled degradation rates has stimulated the development of polyesters for a range of applications, from biomedical to environmental. Although attractive because they become increasingly hydrophilic upon hydrolysis, many polyester materials need high molecular weight (MW) for the good colloidal stability and mechanical properties required for end-use applications. As degradation rates are directly linked to polyester chain length, this precludes potential applications that require both high MW and fast hydrolysis. "Grafting through" radical polymerization (RP) of short-chain polyester macromonomers (1-5 units) decouples hydrolysis time and MW by efficiently imparting polyester material properties onto a much higher MW comb-polymer frame. These macromonomers are synthesized by a ring opening polymerization (ROP) in which the type and stoichiometric ratio of cyclic monomer to initiator controls the final comb-polymer degradability.

In this work, several ROP initiators are implemented to produce four new methacrylate macromonomer families with different end-group functionalities (alkyl, tertiary amine, quaternary ammonium, and carboxyl). The utility of these new end-group functionalities in comb-polymer materials is demonstrated by proof of concept application developments conducted in cooperation with three research groups. Alkyl macromonomers provide a means to delay the onset of comb-polymer hydrolysis, cationic macromonomers are polymerized to produce novel flocculants with hydrolysis-triggered enhanced sediment dewaterability, while a biorenewable material is modified with tertiary amine macromonomers to have both pH responsive and tunable hydrophobicity characteristics. In each application, the ability to easily tune the material's performance by specifying the functional group density in the ROP step is emphasized.

To facilitate the efficient production of comb-polymer materials, macromonomer radical (co)polymerization kinetics are studied in bulk, solution, and micellar media. The alkyl terminated macromonomer bulk homopropagation rate constants determined by pulsed laser polymerization are invariant to the number of polyester units in the methacrylic ester side chain. In addition, macromonomer relative consumption behavior in solution copolymerization with styrene is determined by the chemical

identity up to several units away from the methacrylic ester, independent of the polyester type, length, and end-group functionality. As further product development opportunities emerge, this kinetic knowledge will enable improved control of comb-polymer composition and MW.

Co-Authorship

The bulk of the research in this thesis was conducted independently under the supervision of Dr. Robin Hutchinson at Queen's University.

The materials presented in Chapters 3, 4, 6 (first half), and 8 have been published in a variety of peer-reviewed journals as detailed later on in the thesis. In addition, the material presented in Chapter 5 has been submitted for publication in a peer-reviewed journal.

The pulsed laser experiments in Chapter 7 were performed by myself in Dr. Igor Lacík's lab at the Polymer Institute of the Slovak Academy of Sciences. In Chapter 6, the flocculant settling and sediment dewaterability tests were performed by Sarang Gumfekar in the lab of Dr. João Soares at the University of Alberta, while the cellulose nanocrystals modifications and characterizations were performed by Dr. Omar Garcia-Valdez in the lab of Dr. Michael Cunningham at Queen's University.

Acknowledgements

Thanks to the people who helped shape the last 4.5 years of my life:

First and foremost I would like to thank Professor Robin Hutchinson who encouraged me to pursue graduate studies in the first place. He has since continually challenged me to be a better scientist and has always supported me in achieving my goals. I am greatly appreciative of the many opportunities he has provided me with, both near and afar, to grow as a researcher.

I am grateful to Professor Davide Moscatelli who invited me to spend one year in his lab at Politecnico di Milano, and stimulated my excitement for new fields of research. In addition, it was from Davide that I learned the most about transforming research ideas into reality. Thanks to all of his students who helped make my stay such a memorable experience; in particular, Evangelos Mavroudakis, and Claudio Colombo who was always willing to follow curiosity with me.

Thanks to Dr. Igor Lacík for giving me the opportunity to spend four months in his lab at the Polymer Institute in Bratislava, and introducing me to the exciting albeit overwhelming complexities of aqueous propagation kinetics. His love for learning is truly contagious. A special thanks to Anna Chovancová, whose endless resourcefulness in the lab aided me on numerous occasions.

At Queen's I am grateful to Kevin Payne and Elijah Bultz who helped me in the lab when I was just starting – especially to Eli for his sage wisdom. Thanks to Sean George and Omar Garcia-Valdez for our fantastic scientific discussions and constant pursuit of the money shot. Also to Jan Schier and Joaquin Arredondo who were always available to help or to bounce ideas off of.

Finally I want to acknowledge the support of my friends, Catherine Normandeau and Stuart Young, who have also been my role models. Last but not least, I would like to thank my parents and siblings for their unconditional support that has undoubtedly helped me make it this far.

Table of Contents

List of Figures

List of Schemes

List of Tables

List of Abbreviations

A	Arrhenius pre-exponential factor
ACA	alkyl cyanoacrylate
AIBN	2,2'-Azobis(2-methylpropionitrile)
BCA	n-butyl cyanoacrylate
BMA	n-butyl methacrylate
BuOH	n-butanol
$CDCl_3$	deuterated chloroform
CL	ε-caprolactone
CMC	critical micelle concentration
CNC	cellulose nanocrystals
CST	capillary suction time
DLS	dynamic light scattering
DMA	dodecyl methacrylate
DMF	N, N dimethylformamide
DMPA	2,2-dimethoxy-2-phenylacetophenone
DMSO	dimethyl sulfoxide
dn/dc	differential refractive index
E_A	activation energy
EMA	ethyl methacrylate
ETL	ethyl lactate
EtOAc	ethyl acetate
f_i	mole fraction monomer i
F_i	instantaneous mole fraction repeat unit i

F_i^{cum}	cumulative mole fraction repeat unit i
FFT	fluid fine tailings
HB	hydrogen bonding
HEA	2-hydroxyethyl acrylate
HEMA	2-hydroxyethyl methacrylate
IR	infrared spectroscopy
k_p	homopropagation rate coefficient
k_p^{app}	apparent k_p
$k_{p,\infty}$	k_p at infinite dilution
$k_{p,cop}$	copolymerization propagation rate coefficient
k_t	termination rate coefficient
LA	lactide
L_i	chain length of i^{tth} inflection point
LiTPO	lithium phenyl-2,4,6-trimethylbenzoylphosphinate
LS	light scattering
LTL	low termination limit
$[M]$	monomer concentration
MAA	methacrylic acid
MALLS	multi angle laser light scattering
MeOH	methanol
MFT	mature fine tailings
MH	Mark-Houwink
MMA	methyl methacrylate
MMD	molar mass distribution
MRP	micellar radical polymerization

MW	molecular weight
NaCl	sodium chloride
NP	nanoparticle
PAM	polyacrylamide
PCL	polycaprolactone
PDI	polydispersity index
PLA	polylactic acid
PLP	pulsed laser polymerization
$[R\cdot]$	radical concentration
RI	refractive index
r_i	TM reactivity ratio of monomer i
ROP	ring opening polymerization
RP	radical polymerization
SDS	sodium dodecyl sulfate
SEC	size exclusion chromatography
$Sn(oct)_2$	tin(II) 2-ethylhexanoate
ST	styrene
t_0	time between pulses
TEA	triethylamine
TEM	transmission electron microscopy
T_g	glass transition temperature
THF	Tetrahydrofuran
TM	terminal model of copolymerization
TS	transition state
V_i	molar volume of component i

x   molar conversion

xMA   generic methacrylate

List of Publications

(7)   Rooney, T. R.; Lacík, I.; Hutchinson, R. A. "Pulsed Laser Studies of Cationic Reactive Surfactant Radical Propagation",. **2017**, *in preparation*.

(6)   Rooney, T. R.; Moscatelli, D.; Hutchinson, R. A. "Polylactic Acid Macromonomer Radical Propagation Kinetics and Degradation Behavior", **2017**, *Accepted for publicationin Reaction Chemistry & Engineering*.

(5)   Rooney, T. R.; Monyatsi, O.; Hutchinson, R. A. "Polyester Macromonomer Syntheses and Radical Copolymerization Kinetics with Styrene", *Macromolecules* **2017**, *50*, 784.

(4)   Rooney, T. R.; Gumfekar, S. P.; Soares, J. B. P.; Hutchinson, R. A. "Cationic Hydrolytically Degradable Flocculants with Enhanced Water Recovery for Oil Sands Tailings Remediation", *Macromol. Mater. Eng.* **2016**, *301*, 1248.

(3)   Rooney, T. R.; Mavroudakis, E.; Lacik, I.; Hutchinson, R. A.; Moscatelli, D. "Pulsed-laser and Quantum Mechanics Study of *n*-Butyl Cyanoacrylate and Methyl Methacrylate Free-Radical Copolymerization", *Polym. Chem.* **2015,** *6*, 1594.

(2)   Liang, K.; Rooney, T. R.; Hutchinson, R. A. "Solvent Effects on Kinetics of 2-Hydroxyethyl Methacrylate Semibatch Radical Copolymerization", *Ind. Eng. Chem. Res.* **2013**, 53, 7296.

(1)   Ferrari, R.; Rooney, T. R.; Lupi, M.; Ubezio, P.; Hutchinson, R. A.; Moscatelli, D. "A Methyl Methacrylate–HEMA-CL$_n$ Copolymerization Investigation: From Kinetics to Bioapplications ", *Macromol. Biosci.* **2013**, *13*, 1347.

Chapter 1

Introduction

One of the desirable properties of polyesters is their hydrolytic degradability, a feature which can transition a material from hydrophobic to increasingly hydrophilic over time. This feature may benefit many applications, especially those in which the prolonged exposure to and/or accumulation of a polymeric material is undesirable (e.g., intravenous drug delivery vehicles for biomedical applications and environmental remediation applications such as oil sands tailings dewatering). Since the rate of polyester hydrolysis is correlated with the number and type of repeat unit, the design of any polyester device must balance the intended timescale for degradation with other material properties. However, in many cases, high molecular weight (MW) polymer is requisite to ensure good colloidal stability or adequate mechanical properties; therefore, the corresponding hydrolysis times are also elevated, precluding many potential applications.

To decouple polyester degradation time and MW, "grafting through" macromonomer polymerization is an attractive approach which combines the productivity of radical polymerization (RP) with the material properties of polyesters. As illustrated by Scheme 1.1, macromonomer synthesis, via ring opening polymerization (ROP) of cyclic esters, allows the user to specify well-defined graft properties such as polyester type, average number of degradable units (typically n=1-5), and end-group functionality, which are then efficiently imparted onto a much higher MW comb-polymer frame via RP (e.g., via the methacrylate group). Since the methacrylic backbone is not hydrolytically degradable, the term "degradation" is applied throughout this thesis to refer to the hydrolysis of the pendant polyesters that elicits a change in the material's relative hydrophobicity. Thus, the comb-polymer's degradability and functional group density are specified in the macromonomer synthesis step, independent of the material's overall MW. Furthermore, through
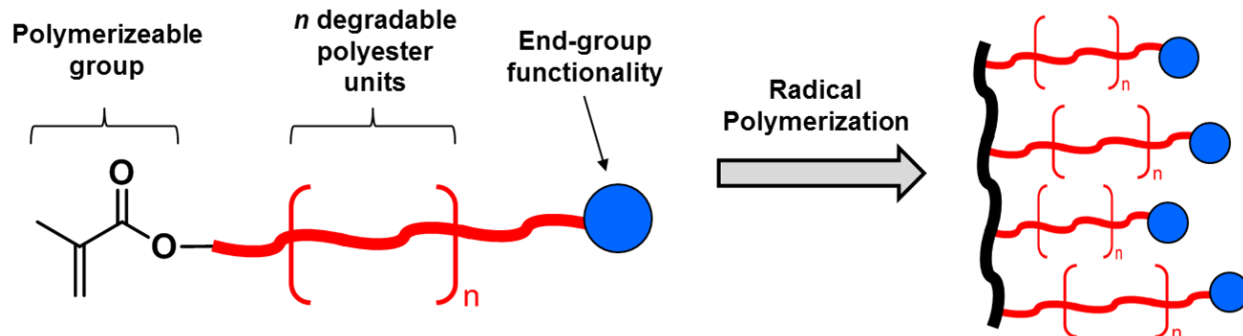
Scheme 1.1: Features of comb-polymers produced by macromonomer radical polymerization.

macromonomer radical copolymerization, an even greater diversity of materials with tunable properties and architectures is accessible.

The advantages of "grafting through" RP have been demonstrated extensively by the Moscatelli group (Politecnico di Milano) who developed a host of materials for biomedical applications based on short-chain polyester macromonomers produced via the ROP of cyclic esters using 2-hydroxyethyl methacrylate (HEMA) as initiator. Emulsion RP of the resulting hydroxyl terminated polyester macromonomers yields hydrolytically degradable nanoparticles (NP) whose degradation time can be tuned from days to weeks based on macromonomer design. In particular, the NP degradation time is controlled by ROP specifications such as the ratio of cyclic ester to HEMA as well as polyester type; in order of decreasing hydrophobicity, the choice of cyclic ester includes: ε-caprolactone, lactide, or a mixture of lactide and glycolide.

1.1 Research Objectives

The work in this thesis encompasses aspects of both product and process development for hydrolytically degradable macromonomer-based materials. Four new families of polyester macromonomers, amenable to RP, are synthesized according to different end-group functionalities: alkyl, tertiary amine, quaternary ammonium, and carboxyl. For these new macromonomer systems, the utility of degradable comb-polymers with such functional groups needs to be justified by proof

of concept application development. In addition, the ability to tune comb-polymer performance, by specifying its functional group density via the macromonomer synthesis step, must be demonstrated.

Given the vast portfolio of currently available as well as new monomers emerging for specialized applications, one of the goals of the polymerization kinetics community is to establish generalized family type behaviors such that simulations can support the accurate prediction of structure/property relationships for a diversity of polymer products. Since macromonomer polyester length, type, and end-group functionality distinguish the performance properties of the final comb-polymer materials, the impact of these features on macromonomer propagation kinetics must be examined with the aim of generalizing macromonomer propagation behavior so as to guide the design of new macromonomer-based materials. The specific research objectives are summarized below:

1. Expand the library of polyester macromonomers to include alkyl, tertiary amine, quaternary ammonium, and carboxyl end-group functionalities.

2. Develop specific applications for each macromonomer system to demonstrate the utility of new end-group functionalities in comb-polymer materials.

3. Demonstrate that final material performance can be easily tuned by specifying the density of functional groups in the macromonomer ROP synthesis step.

4. Determine the effect of polyester macromonomer chain length on radical homopropagation behavior.

5. Evaluate the effect of macromonomer polyester type, size, and end-group functionality on its radical copolymerization behavior in terms of well-documented solvent and hydrogen bonding effects.

1.2 Thesis Outline

This thesis is presented in manuscript format, with some modifications to improve readability and continuity. Chapter 2 covers the relevant background for polyester macromonomer synthesis and measurement of propagation kinetic parameters with emphasis on structural considerations relevant to macromonomer propagation behavior. Chapter 3 summarizes the library of new macromonomer families synthesized in this thesis. The application development for the alkyl macromonomer is summarized by the second part of Chapter 5, while the quaternary ammonium tertiary amine macromonomer applications are presented in Chapter 6.

The rest of the thesis is devoted to macromonomer propagation kinetics. The initial macromonomer copolymerization kinetics investigations presented in Chapter 4 highlight the experimental difficulties associated with applying pulsed laser polymerization (PLP) techniques to functionalized macromonomer systems. Then, the first part of Chapter 5 details how these challenges were overcome in order to establish a clear relationship between macromonomer bulk homopropagation rate coefficients as a function of macromonomer average chain length. In Chapter 7, PLP is applied for the first time to a self-assembled cationic monomer system to study the kinetics of micellar RP.

Chapter 8 aims to generalize macromonomer copolymer composition behavior in terms of polyester type, length, and end-group functionality as well as the solvent and hydrogen bonding effects that are known to have a significant impact on traditional monomer copolymerization systems. Building on these findings, Chapter 9 details a new framework which captures the peculiar copolymer composition behaviors that have been documented for hydroxyl-bearing monomer systems, and is supported by kinetic Monte Carlo simulations. Finally, Chapter 10 summarizes the thesis and offers an outlook for future work.

Chapter 2

Literature Review

This chapter covers background material relevant to the synthesis of short-chain polyester macromonomers as well as the measurement of their propagation rate coefficients in radical polymerization (RP). Additional literature relevant to the specific macromonomer systems and kinetic investigations studied in this thesis is reviewed in the subsequent chapters.

2.1 Polyesters

Polycaprolactone (PCL), polylactic acid (PLA), and polylactic-*co*-glycolic acid (PLGA; not covered in this work) are polyesters whose good material properties[1-3] combined with hydrolytic degradability to yield non-toxic degradation products[3-5] has resulted in their use in diverse applications especially in the biomedical field.[6-8] Moreover, PLA is particularly attractive because it is produced from 100% biorenewable resources.[9]

2.1.1 Synthesis

Although polyesters can be produced via polycondensation, removal of the liberated water is a serious challenge posing difficulties in controlling the molecular weight (MW) characteristics that influence material performance.[10-12] As an alternative, PCL and PLA can be synthesized from the ring-opening polymerization (ROP) of their cyclic monomers, ε-caprolactone and lactide, respectively, in the melt phase using a variety of catalysts, with tin(II) ethyl 2-ethylhexanoate $(Sn(Oct)_2)$ most commonly employed because of its relatively low toxicity.[13,14] ROP allows for good control over MW characteristics,[15] and the user may select functional ROP initiators to impart customized features onto the final polyester material.[16,17] Some of the drawbacks of ROP include its sensitivity to acidic impurities as well as susceptibility to side reactions, such as inter- and intramolecular transesterifications, that can lead to a significant broadening of the molar mass

distribution (MMD).[18] Operating at lower temperatures and preventing the ROP from reaching complete conversion are both strategies to mitigate significant MMD broadening.[19]

2.1.2 Polyester Hydrolysis

Polyester hydrolysis may be catalyzed by acid, base, or enzyme action,[20,21] with the rate dependent on material properties such as crystallinity, morphology, and hydrophobicity,[22-24] as well as external factors like temperature and pH.[25] Mainly due to its increased hydrophobicity, PCL materials degrade more slowly than PLA and PLGA.[26-28] The rate of polyester hydrolysis is also directly related to the number of polyester repeat units in the chain.[25,29] In addition, there is a difference in hydrolysis reactivities for backbone and terminal esters[30] due to a preferential chain-end scission mechanism in both basic and acidic media,[31-33] a result ascribed to better solvation of the terminal carboxylic acid or alcohol units.[30]

Since polyester hydrolysis is autocatalyzed by the carboxylic acid end groups of degraded oligomers, mass transfer considerations are important.[34] Bulk hydrolysis describes the situation where the rate of water diffusion in a material is faster than the rate of hydrolysis, whereas surface erosion describes the case where hydrolysis occurs faster than water diffusion. Thus, hydrolysis of polyester materials must also take into consideration material dimensions and topology (e.g., surface, bulk, solution).[35]

2.1.3 Polyester Macromonomer

Typically, nanoparticles (NP) for intravenous drug delivery applications are produced via the nanoprecipitation of high molecular weight (MW) PCL, PLA, or PLGA,[36] necessitating the use of solvent and/or surfactant. Moreover, the degradation of such high MW materials can take up to several months,[37] while even the most advanced nanoprecipitation techniques are limited by low yields and production rates.[38]

Recently, the Moscatelli group has developed a solvent and surfactant-free emulsion polymerization strategy to produce polymeric NPs from short-chain polyester macromonomers.[26]

Bulk ROP of ε-caprolactone, lactide, or glycolide using 2-hydroxyethyl methacrylate (HEMA) as initiator yields short-chain (average $n=1$–5 polyester units per chain) PCL,[39] PLA,[40] or PLGA[41] macromonomers amenable to RP, herein termed HEMA-PCL$_n$ and HEMA-PLA$_{2n}$. Macromonomer emulsion RP produces NPs consisting of comb-polymers that hydrolytically degrade via a swelling mechanism to yield a final hydrophilic poly(HEMA) backbone. The degradation time is controlled by the type of cyclic monomer selected in the ROP synthesis step as well as by the specified stoichiometric ratio of cyclic monomer to initiator. For example, by changing n from 2 to 5 for HEMA-PCL$_n$ and n from 2 to 4 for HEMA-PLA$_{2n}$, NP degradation time in cell medium at 37 °C is tuned from 56 hours to more than 4 weeks,[42] and from 46 hours to 58 hours,[26] respectively.

Other research groups have also employed similar HEMA-PLA$_{2n}$ macromonomers in radical miniemulsion polymerization[43,44] and in solution RP.[45-47] Thus, there is a need to develop a better understanding of macromonomer RP to produce comb-polymer materials more efficiently.

2.2 Radical Polymerization Kinetics

Although there are many emerging technologies based on controlled radical polymerization techniques,[48,49] the more robust radical polymerization (RP) still accounts for the majority of industrial processes used to manufacture polymeric materials. In RP, one of the central considerations to reactor design (e.g., heat removal requirements, reactor size and type) is the rate of (co)polymerization, given by Eqns. 2.1 and 2.2, where $[M]$ is the monomer concentration, $[M]_{tot}$ is the total monomer concentration in a copolymerization system, and $[R\cdot]$ is the total concentration of radicals.

$$-\frac{d[M]}{dt} = k_p \cdot [M] \cdot [R\cdot] \tag{2.1}$$

$$-\frac{d[M]_{tot}}{dt} = k_{p,cop} \cdot [M]_{tot} \cdot [R\cdot] \tag{2.2}$$

Thus, the homopropagation rate coefficient (k_p) and overall composition-averaged copolymer propagation rate coefficient ($k_{p,cop}$) significantly affect the overall rate of reaction. In addition, k_p

and $k_{p,cop}$ have a large impact on the polymer molar mass distribution (MMD) and the molecular weight (MW) averages that greatly influence the polymeric material properties. The favorable properties of homopolymers can be combined through radical copolymerization (Eqns. 2.3-2.6); the copolymer properties depend not only on the relative amounts of incorporated monomer but also on the copolymer sequence distribution (e.g., block, random, gradient, or alternating) which are described by the reactivity ratios, r_A and r_B, in Eqns. 2.7 and 2.8.

$$A \cdot + A \xrightarrow{k_{p,AA}} AA \cdot \tag{2.3}$$

$$A \cdot + B \xrightarrow{k_{p,AB}} AB \cdot \tag{2.4}$$

$$B \cdot + A \xrightarrow{k_{p,BA}} BA \cdot \tag{2.5}$$

$$B \cdot + B \xrightarrow{k_{p,BB}} BB \cdot \tag{2.6}$$
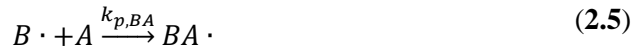
$$r_A = \frac{k_{p,AA}}{k_{p,AB}} \tag{2.7}$$

$$r_B = \frac{k_{p,BB}}{k_{p,BA}} \tag{2.8}$$

This section reviews the experimental techniques employed to measure the kinetic parameters k_p, $k_{p,cop}$, r_A, and r_B with particular emphasis on the challenges associated with methacrylate-type macromonomer systems.

2.2.1 Measurement of Homopropagation Rate Coefficients

In 1987 Olaj et al. introduced the pulsed-laser polymerization (PLP) technique[50] which has enabled the measurement of k_p values for a variety of monomer systems, as is described in comprehensive detail by Beuermann and Buback.[51] Briefly, a monomer solution containing photoinitiator is exposed to periodic laser pulses to generate a pseudostationary state characterized by a periodic radical concentration profile. At each laser pulse, there is a burst of primary radicals generated, chains begin to grow during the dark time between pulses, t_0, and then immediately following the

8

subsequent laser pulse many chains are terminated with length, L_1. Chains which escaped termination and continue to grow throughout the second dark time are terminated following the next pulse with length, L_2. Once the characteristic chain lengths, L_i, are identified from the inflection points of a low-conversion PLP-generated polymer's MMD measured by size exclusion chromatography (SEC), the k_p may be assessed according to Eqn. 2.9. PLP-SEC has also been applied to the measurement of $k_{p,cop}$ (Eqn. 10) for binary[52-54] and ternary[55] copolymerizations systems. In order to report a k_p or $k_{p,cop}$ measurement, the following PLP-SEC consistency criteria must be met: the length of L_2 must equal $2 \cdot L_1$, and the k_p estimations must be invariant to laser energy, photoinitiator concentration, and pulse repetition rate.[56]

$$L_i = i \cdot k_p \cdot [M] \cdot t_0 \tag{2.9}$$

$$L_i = i \cdot k_{p,cop} \cdot [M]_{tot} \cdot t_0 \tag{2.10}$$

PLP-SEC is recommended by the IUPAC *subcommittee on "Modeling of Polymerization Kinetics and Processes"* as the most accurate and reliable method for determining k_p, such that benchmark data sets have been established for common bulk monomer systems such as styrene,[57] methyl methacrylate (MMA),[58] and methyl acrylate.[59] In order to systematically investigate k_p for a particular monomer system several challenges must be overcome. In addition to selecting the non-trivial appropriate conditions for the SEC setup,[60] the significant uncertainty introduced to k_p estimations by SEC broadening and calibration must be taken into consideration.[51] Furthermore, each class of monomer has unique features which influence the interpretation of PLP-SEC experiments in different ways: acrylates can undergo an intramolecular chain-transfer event, known as backbiting, to yield more stable mid-chain radicals,[61] vinyl esters undergo head-to-head additions to yield less reactive CH_2 adducts,[62,63] while methacrylates exhibit significant depropagation behavior at high temperatures (>100 °C) and low monomer concentrations.[64] Also important to the application of PLP-SEC is the system's termination behavior,[65] the influence of monomer functional groups,[66] as well as solvent type and concentration in some cases.[67]

Due to the increasing diversity of available monomers, there is strong impetus in the polymerization kinetics community to establish family type behaviors such that k_p can be modeled and predicted for new and existing systems;[56,68,69] the following sections specifically examine the operating conditions and solvent effects relevant to the study of k_p for new methacrylate type macromonomer systems.

2.2.2 Low Termination Limit of PLP

Well-structured PLP MMDs are produced from experimental conditions selected to carefully balance the rate of radical generation with the rate of radical termination such that the increase in radical concentration, $[\Delta R\cdot]$, at each pulse is sufficient to terminate most of the growing chains produced by the previous pulse, but still allow a fraction of those growing chains to survive a second dark time and terminate with length $2\cdot L_1$. The situation is described by Eqn. 2.11, where β is the fraction of radicals generated by a pulse which are terminated between two pulses, $[R\cdot]_{max}$ is the maximum concentration of radicals during the experiment, and k_t is the termination rate coefficient.[70]

$$\beta = \frac{[\Delta R\cdot]}{[R\cdot]_{max}} = \frac{k_t \cdot [R\cdot]_{max} \cdot t_0}{1 + k_t \cdot [R\cdot]_{max} \cdot t_0} \qquad (2.11)$$

A low propensity for termination in highly viscous (e.g., macromonomers) or in aqueous ionized monomer systems (anionic or cationic[71]) can be described by the so-called low-termination limit (LTL) of the PLP technique where only about 20% of the radicals produced by a laser pulse are terminated by the subsequent pulse.[65] PLP experiments performed near the LTL result in the production of a MMD whose primary inflection point may lead to an overestimation of k_p by 10-20%, and therefore estimation of k_p from the secondary inflection point is more reliable.[72] In order to improve the quality of PLP MMDs for LTL systems, experimental conditions must be selected to augment β, such as increasing t_0 by operating at lower pulse repetition rates, increasing $[R\cdot]_{max}$

by multipulse initiation or higher initiator concentrations,[73] or increasing temperature to reduce system viscosity.[70]
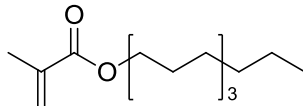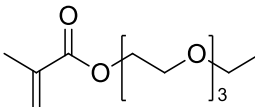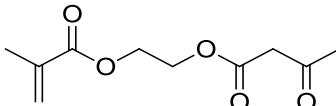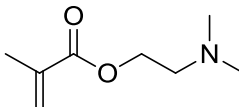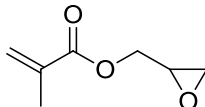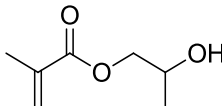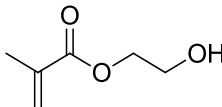
2.2.3 Trends in Methacrylate Homopropagation Rate Coefficients

The IUPAC subcommittee on "Modeling of Polymerization Kinetics and Processes" has benchmarked Arrhenius parameters for the bulk k_p of several alkyl ester methacrylates: MMA,[58] ethyl methacrylate (EMA), n-butyl methacrylate (BMA), and dodecyl methacrylate (DMA) with similar activation energies (E_A) in the range of 23.4–21.0 kJ·mol^{-1}.[74] Furthermore, an increase in the length of the alkyl ester side chain correlates to an increase in bulk k_p measured by PLP-SEC; this trend was more recently reported to extend to behenyl methacrylate (average of 19.9 C atoms in ester side chain).[68] Buback has explained this behavior based on entropic reasons in terms of transition state (TS) for propagation theory,[75] where longer alkyl side chains can better shield the dipolar interactions (between methacrylate groups) to afford greater mobility to the TS and consequently increase k_p.[76] Consistent with this interpretation, a similar increase in bulk k_p with increasing ester side chain length was reported for polyethylene glycol ethyl ether methacrylate (PEGEEMA, 3 PEG units) compared to 2-ethoxyethyl methacrylate (EEMA, 1 PEG unit);[77] however, no additional increase in bulk k_p was found for polyethylene glycol methyl ether methacrylate (PEGMA, 7-8 PEG units).[72]

The propagation behavior for methacrylates containing heteroatoms or sterically hindered groups in the ester side chain is less well-understood. Although the bulk k_p for cyclic ester methacrylates glycidyl methacrylate (GMA), cyclohexyl methacrylate, benzyl methacrylate, and isobornyl methacrylate (iBoMA) can be described by a single Arrhenius relation of $E_A = 21.9$ kJ·mol^{-1} with pre-exponential (A) of 4.24×10^6 L·mol^{-1}·s^{-1},[56] the bulk k_p for several other methacrylates with steric hindrances further away from the methacrylic group could not be described by the same fit,[68] indicating the importance of functional group location (with respect to the polymerizable group) in the ester side chain.

The Arrhenius parameters for the bulk k_p of methacrylates containing various functional groups in the ester side chain are summarized by Table 2.1. Despite having lower MW than the linear alkyl methacrylate DMA, acetoacetoxyethyl methacrylate (AAEMA), 2-(*N*, *N* dimethylamino)ethyl methacrylate (DMAEMA), and GMA all have k_p values that are higher than that of DMA, confirming that the presence of functional groups in the ester side is significant. Further discussions of the structure reactivity trends relevant to macromonomer polymerization are continued in the macromonomer homopropagation PLP and copolymerization studies in Chapters 5 and 8, respectively. Furthermore, it should be noted that the hydroxyl-bearing monomers 2-hydroxyethyl methacrylate (HEMA) and 2-hydroxypropyl methacrylate (HPMA) exhibit markedly elevated k_p because of hydrogen bonding effects.[66,78]

Table 2.1: Summary of Arrhenius parameters for propagation of diverse methacrylates in bulk.

Methacrylate		k_p at 50 °C ($L \cdot mol^{-1} \cdot s^{-1}$)	E_A ($kJ \cdot mol^{-1}$)	A ($10^6 \ L \cdot mol^{-1} \cdot s^{-1}$)
DMA[74]		1009	21.0	2.51
PEGEEMA[77]		1053	24.4	9.3
AAEMA[79]		1399	19.7	2.13
DMAEMA[80]		1185	20.7	2.64
GMA[56]		1219	21.9	4.24
HPMA[78]		1510	21.7	4.85
HEMA[66]		2554	21.9	8.89

2.2.4 Solvent Effects on Homopropagation Rate Coefficients

Solvent effects on radical homopropagation kinetics can arise from both non-specific as well as specific interactions between monomer and solvent.[67] In the case of non-specific solvent interactions, the k_p measured by PLP-SEC can manifest as an apparent value (k_p^{app}) which may be different than the bulk k_p depending on the differences in molar volumes of monomer and solvent. For example, in toluene solution, the $k_p^{app}/k_{p,bulk}$ for MMA (lower molar volume than toluene) is greater than unity, while the $k_p^{app}/k_{p,bulk}$ for iBoMA (higher molar volume than toluene) is less than unity.[81] This phenomenon can be explained as a competition between solvent and monomer molecules for positioning at the radical site; if the monomer size is less than that of a solvent molecule, then the concentration of monomer at the reaction site will be greater than its analytical concentration such that the k_p^{app} measured by PLP-SEC will be higher than $k_{p,bulk}$, and vice versa. The same phenomenon of decreasing k_p measured for linear alkyl acrylates in toluene solution has been explained by Buback as an entropic effect in which an increasing molar volume of monomer relative to that of the solvent results in a more hindered TS for propagation and consequently lower value of k_p.[76,82]

Specific hydrogen bonding interactions between a hydroxyl group and the methacryloyl carbonyl can reduce the electron density at the monomeric double bond making the monomer more reactive towards radical addition.[67] As illustrated by Scheme 2.1, hydrogen bonding between monomers in bulk HEMA solution[66] can be disrupted by solvents such as tetrahydrofuran (THF) or dimethylformamide (DMF) to reduce the monomer's reactivity towards that of a typical linear alkyl ester methacrylate such as BMA.[78,83] Hydrogen bonding can also be promoted in methacrylate systems by alcohol solvents.[84] PLP-SEC experiments of BMA in n-butanol solutions showed a significant reduction in E_A compared to bulk BMA, indicating that the effect of hydrogen bonding on k_p is enthalpic in origin.[85]

H-Bond Disruptor   H-Bond Promoter
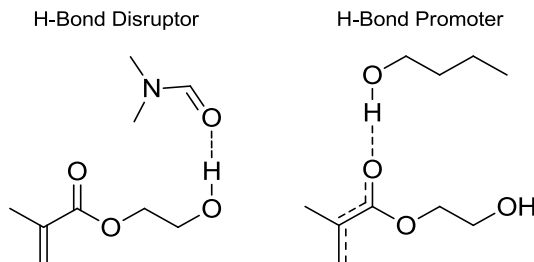
Scheme 2.1: Simplified illustration of hydrogen bond disruption and promotion in methacrylate solution polymerization.

The effect of solvent on aqueous monomer propagation kinetics is much more complex and beyond the scope of this thesis. However, it can be briefly summarized that non-ionized aqueous monomer systems tend to exhibit a sharp increase in k_p towards more dilute conditions, an effect which is interpreted as entropic in origin.[72,86-88] On the other hand, PLP-SEC studies of partially and fully ionized methacrylic acid (MAA) showed the opposite trend, where a slight reduction in E_A with increasing ionic strength (IS) results in a small increase in k_p towards more concentrated conditions.[89]

2.2.5 Measurement of Copolymerization Reactivity Ratios

Depending on the monomer reactivity ratios r_A and r_B, defined by Eqns. 2.7 and 2.8, the composition (and therefore material properties) of copolymer produced at the beginning of a batch radical copolymerization may differ significantly from the copolymer produced towards the end. Thus, knowledge of system-specific r_A and r_B is required in order to guide the design of a monomer feeding strategy aimed at minimizing such compositional drift.

In general, methacrylate/acrylate yields methacrylate-rich copolymers,[54] methacrylate/methacrylate copolymerize with equal addition probabilities,[90,91] and methacrylate/styrene tends towards an alternating sequence.[83] Exceptions to these trends occur when hydroxyl-bearing monomers are copolymerized.[83,92] For example, the copolymer produced from bulk HEMA/BMA is enriched by HEMA at all compositions, but when the same

copolymerization is performed in the hydrogen bond disrupting solvent, DMF, the reactivity ratios return to unity (i.e., the copolymer composition is that of the comonomer mixture) as expected for typical methacrylate/methacrylate systems.[93] Lastly, trends in macromonomer reactivity are not clear; while the chemical nature of the polymerizable group has been identified as the most important factor influencing macromonomer reactivity,[94] the importance of macromonomer MW and polymerization solvent cannot be disregarded.

The monomer reactivity ratios, r_A and r_B, are frequently estimated from the Mayo-Lewis relationship (Eqn. 2.12)[95] by measuring the instantaneous molar composition of low-conversion copolymer (F_A) produced from monomer mixtures with different molar composition (f_A).

$$F_A = \frac{r_A f_A^2 + f_A f_B}{r_A f_A^2 + 2 f_A f_B + r_B f_B^2} \tag{2.12}$$

Recently, the possibility to directly estimate monomer reactivity ratios from the integrated Mayo-Lewis relationship (Eqn. 2.13) has been demonstrated using monomer composition drift profiles measured by in situ ^{1}H NMR experiments for a variety of aqueous copolymerization systems.[96-98] The main benefit of this approach is convenience and simplicity – isolation, purification, and subsequent analysis of copolymers is not necessary. The only requirement is that each comonomer exhibits a distinct ^{1}H NMR signal, and that a peak whose integration is invariant with time can be identified to establish a measurement of conversion throughout the batch.

$$\frac{df_A}{dx} = \frac{f_A - F_A}{1 - x} \tag{2.13}$$

The PLP-SEC technique as well as in situ ^{1}H NMR experiments and low-conversion copolymer composition analyses are used in this work to study the RP propagation kinetics, in bulk and solution (co)polymerizations, of methacrylate type polyester macromonomer systems for which there is little available data in the literature.

2.3 References

(1)   Schué, F. Polymer International **2000**, 49, 472.

(2)   Karjalainen, T.; Hiljanen-Vainio, M.; Malin, M.; Seppälä, J. Journal of Applied Polymer Science **1996**, 59, 1299.

(3)   Jamshidian, M.; Tehrany, E. A.; Imran, M.; Jacquot, M.; Desobry, S. Comprehensive Reviews in Food Science and Food Safety **2010**, 9, 552.

(4)   Chiellini, E.; Solaro, R. Advanced Materials **1996**, 8, 305.

(5)   Davachi, S. M.; Kaffashi, B. Polymer-Plastics Technology and Engineering **2015**, 54, 944.

(6)   Kumari, A.; Yadav, S. K.; Yadav, S. C. Colloids and Surfaces B: Biointerfaces **2010**, 75, 1.

(7)   Ulery, B. D.; Nair, L. S.; Laurencin, C. T. Journal of Polymer Science Part B: Polymer Physics **2011**, 49, 832.

(8)   Mondal, D.; Griffith, M.; Venkatraman, S. S. International Journal of Polymeric Materials and Polymeric Biomaterials **2016**, 65, 255.

(9)   Drumright, R. E.; Gruber, P. R.; Henton, D. E. Advanced Materials **2000**, 12, 1841.

(10)   Moon, S. I.; Lee, C. W.; Taniguchi, I.; Miyamoto, M.; Kimura, Y. Polymer **2001**, 42, 5059.

(11)   Achmad, F.; Yamane, K.; Quan, S.; Kokugan, T. Chemical Engineering Journal **2009**, 151, 342.

(12)   Filachione, E. M.; Fisher, C. H. Industrial & Engineering Chemistry **1944**, 36, 223.

(13)   Dechy-Cabaret, O.; Martin-Vaca, B.; Bourissou, D. Chemical Reviews **2004**, 104, 6147.

(14)   Carlmark, A.; Larsson, E.; Malmström, E. European Polymer Journal **2012**, 48, 1646.

(15)   Nuyken, O.; Pask, S. Polymers **2013**, 5, 361.

(16)   van den Berg, S. A.; Zuilhof, H.; Wennekes, T. Macromolecules **2016**, 49, 2054.

(17)   Okuda, T.; Ishimoto, K.; Ohara, H.; Kobayashi, S. Macromolecules **2012**, 45, 4166.

(18)   Yu, Y.; Storti, G.; Morbidelli, M. Macromolecules **2009**, 42, 8187.

(19)   Ferrari, R.; Pecoraro, C. M.; Storti, G.; Moscatelli, D. RSC Advances **2014**, 4, 12795.

(20)   Herzog, K.; Müller, R. J.; Deckwer, W. D. Polymer Degradation and Stability **2006**, 91, 2486.

(21) Jung, J. H.; Ree, M.; Kim, H. Catalysis Today **2006**, 115, 283.

(22) Lee, W.-K.; Gardella, J. A. Langmuir **2000**, 16, 3401.

(23) Ahmed, F.; Discher, D. E. Journal of Controlled Release **2004**, 96, 37.

(24) Vert, M.; Li, S.; Garreau, H.; Mauduit, J.; Boustta, M.; Schwach, G.; Engel, R.; Coudane, J. Die Angewandte Makromolekulare Chemie **1997**, 247, 239.

(25) Lazzari, S.; Codari, F.; Storti, G.; Morbidelli, M.; Moscatelli, D. Polymer Degradation and Stability **2014**, 110, 80.

(26) Colombo, C.; Dragoni, L.; Gatti, S.; Pesce, R. M.; Rooney, T. R.; Mavroudakis, E.; Ferrari, R.; Moscatelli, D. Industrial & Engineering Chemistry Research **2014**, 53, 9128.

(27) Ye, W. P.; Du, F. S.; Jin, W. H.; Yang, J. Y.; Xu, Y. Reactive and Functional Polymers **1997**, 32, 161.

(28) Malin, M.; Hiljanen-Vainio, M.; Karjalainen, T.; Seppälä, J. Journal of Applied Polymer Science **1996**, 59, 1289.

(29) Antheunis, H.; van der Meer, J.-C.; de Geus, M.; Heise, A.; Koning, C. E. Biomacromolecules **2010**, 11, 1118.

(30) Codari, F.; Lazzari, S.; Soos, M.; Storti, G.; Morbidelli, M.; Moscatelli, D. Polymer Degradation and Stability **2012**, 97, 2460.

(31) van Nostrum, C. F.; Veldhuis, T. F. J.; Bos, G. W.; Hennink, W. E. Polymer **2004**, 45, 6779.

(32) de Jong, S. J.; Arias, E. R.; Rijkers, D. T. S.; van Nostrum, C. F.; Kettenes-van den Bosch, J. J.; Hennink, W. E. Polymer **2001**, 42, 2795.

(33) Shih, C. Journal of Controlled Release **1995**, 34, 9.

(34) Grizzi, I.; Garreau, H.; Li, S.; Vert, M. Biomaterials **1995**, 16, 305.

(35) Xu, L.; Crawford, K.; Gorman, C. B. Macromolecules **2011**, 44, 4777.

(36) Mora-Huertas, C. E.; Fessi, H.; Elaissari, A. International Journal of Pharmaceutics **2010**, 385, 113.

(37) Burkersroda, F. v.; Schedl, L.; Göpferich, A. Biomaterials **2002**, 23, 4221.

(38) Karnik, R.; Gu, F.; Basto, P.; Cannizzaro, C.; Dean, L.; Kyei-Manu, W.; Langer, R.; Farokhzad, O. C. Nano Letters **2008**, 8, 2906.

(39)   Ferrari, R.; Yu, Y.; Morbidelli, M.; Hutchinson, R. A.; Moscatelli, D. Macromolecules **2011**, 44, 9205.

(40)   Yu, Y.; Ferrari, R.; Lattuada, M.; Storti, G.; Morbidelli, M.; Moscatelli, D. Journal of Polymer Science Part A: Polymer Chemistry **2012**, 50, 5191.

(41)   Ferrari, R.; Colombo, C.; Dossi, M.; Moscatelli, D. Macromolecular Materials and Engineering **2013**, 298, 730.

(42)   Ferrari, R.; Colombo, C.; Casali, C.; Lupi, M.; Ubezio, P.; Falcetta, F.; D'Incalci, M.; Morbidelli, M.; Moscatelli, D. International Journal of Pharmaceutics **2013**, 453, 551.

(43)   Ishimoto, K.; Arimoto, M.; Ohara, H.; Kobayashi, S.; Ishii, M.; Morita, K.; Yamashita, H.; Yabuuchi, N. Biomacromolecules **2009**, 10, 2719.

(44)   Ishimoto, K.; Arimoto, M.; Okuda, T.; Yamaguchi, S.; Aso, Y.; Ohara, H.; Kobayashi, S.; Ishii, M.; Morita, K.; Yamashita, H.; Yabuuchi, N. Biomacromolecules **2012**, 13, 3757.

(45)   Lim, D. W.; Choi, S. H.; Park, T. G. Macromolecular Rapid Communications **2000**, 21, 464.

(46)   Eguiburu, J.; Fernandez-Berridi, M. J.; Román, J. S. Polymer **1996**, 37, 3615.

(47)   Shinoda, H.; Matyjaszewski, K. Macromolecules **2001**, 34, 6243.

(48)   Braunecker, W. A.; Matyjaszewski, K. Progress in Polymer Science **2007**, 32, 93.

(49)   Matyjaszewski, K.; Spanswick, J. Materials Today **2005**, 8, 26.

(50)   Olaj, O. F.; Bitai, I.; Hinkelmann, F. Die Makromolekulare Chemie **1987**, 188, 1689.

(51)   Beuermann, S.; Buback, M. Progress in Polymer Science **2002**, 27, 191.

(52)   Coote, M. L.; Zammit, M. D.; Davis, T. P.; Willett, G. D. Macromolecules **1997**, 30, 8182.

(53)   Hutchinson, R. A.; McMinn, J. H.; Paquet, D. A.; Beuermann, S.; Jackson, C. Industrial & Engineering Chemistry Research **1997**, 36, 1103.

(54)   Buback, M.; Feldermann, A.; Barner-Kowollik, C.; Lacík, I. Macromolecules **2001**, 34, 5439.

(55)   Li, D.; Hutchinson, R. A. Macromolecular Rapid Communications **2007**, 28, 1213.

(56)   Beuermann, S.; Buback, M.; Davis, T. P.; García, N.; Gilbert, R. G.; Hutchinson, R. A.; Kajiwara, A.; Kamachi, M.; Lacík, I.; Russell, G. T. Macromolecular Chemistry and Physics **2003**, 204, 1338.

(57) Buback, M.; Gilbert, R. G.; Hutchinson, R. A.; Klumperman, B.; Kuchta, F.-D.; Manders, B. G.; O'Driscoll, K. F.; Russell, G. T.; Schweer, J. Macromolecular Chemistry and Physics **1995**, 196, 3267.

(58) Beuermann, S.; Buback, M.; Davis, T. P.; Gilbert, R. G.; Hutchinson, R. A.; Olaj, O. F.; Russell, G. T.; Schweer, J.; van Herk, A. M. Macromolecular Chemistry and Physics **1997**, 198, 1545.

(59) Barner-Kowollik, C.; Beuermann, S.; Buback, M.; Castignolles, P.; Charleux, B.; Coote, M. L.; Hutchinson, R. A.; Junkers, T.; Lacik, I.; Russell, G. T.; Stach, M.; van Herk, A. M. Polym. Chem. **2014**, 5, 204.

(60) Lacík, I.; Stach, M.; Kasák, P.; Semak, V.; Uhelská, L.; Chovancová, A.; Reinhold, G.; Kilz, P.; Delaittre, G.; Charleux, B.; Chaduc, I.; D'Agosto, F.; Lansalot, M.; Gaborieau, M.; Castignolles, P.; Gilbert, R. G.; Szablan, Z.; Barner-Kowollik, C.; Hesse, P.; Buback, M. Macromolecular Chemistry and Physics **2015**, 216, 23.

(61) Junkers, T.; Barner-Kowollik, C. Journal of Polymer Science Part A: Polymer Chemistry **2008**, 46, 7585.

(62) Barner-Kowollik, C.; Beuermann, S.; Buback, M.; Hutchinson, R. A.; Junkers, T.; Kattner, H.; Manders, B.; Nikitin, A. N.; Russell, G. T.; van Herk, A. M. Macromolecular Chemistry and Physics **2017**, 218, 1600357.

(63) Monyatsi, O.; Hutchinson, R. A. Macromolecular Chemistry and Physics **2016**, 217, 51.

(64) Hutchinson, R. A.; Paquet, D. A.; Beuermann, S.; McMinn, J. H. Industrial & Engineering Chemistry Research **1998**, 37, 3567.

(65) Drawe, P.; Buback, M. Macromolecular Theory and Simulations **2016**, 25, 74.

(66) Buback, M.; Kurz, C. H. Macromolecular Chemistry and Physics **1998**, 199, 2301.

(67) Beuermann, S. Macromolecular Rapid Communications **2009**, 30, 1066.

(68) Haehnel, A. P.; Schneider-Baumann, M.; Hiltebrandt, K. U.; Misske, A. M.; Barner-Kowollik, C. Macromolecules **2013**, 46, 15.

(69) Haehnel, A. P.; Schneider-Baumann, M.; Arens, L.; Misske, A. M.; Fleischhaker, F.; Barner-Kowollik, C. Macromolecules **2014**, 47, 3483.

(70) Beuermann, S.; Paquet, D. A.; McMinn, J. H.; Hutchinson, R. A. Macromolecules **1996**, 29, 4206.

(71) Kattner, H.; Drawe, P.; Buback, M. Macromolecular Chemistry and Physics **2015**, 216, 1737.

(72) Smolne, S.; Weber, S.; Buback, M. Macromolecular Chemistry and Physics **2016**, 217, 2391.

(73)   Vana, P.; Yee, L. H.; Davis, T. P. Macromolecules **2002**, 35, 3008.

(74)   Beuermann, S.; Buback, M.; Davis, T. P.; Gilbert, R. G.; Hutchinson, R. A.; Kajiwara, A.; Klumperman, B.; Russell, G. T. Macromolecular Chemistry and Physics **2000**, 201, 1355.

(75)   Heuts, J. P. A.; Gilbert, R. G.; Radom, L. Macromolecules **1995**, 28, 8771.

(76)   Buback, M. Macromolecular Symposia **2009**, 275–276, 90.

(77)   Siegmann, R.; Jeličić, A.; Beuermann, S. Macromolecular Chemistry and Physics **2010**, 211, 546.

(78)   Beuermann, S.; Nelke, D. Macromolecular Chemistry and Physics **2003**, 204, 460.

(79)   Zoller, A.; Kockler, K. B.; Rollet, M.; Lefay, C.; Gigmes, D.; Barner-Kowollik, C.; Guillaneuf, Y. Polym. Chem. **2016**, 7, 5518.

(80)   Kockler, K. B.; Fleischhaker, F.; Barner-Kowollik, C. Macromolecules **2016**, 49, 8572.

(81)   Beuermann, S.; García, N. Macromolecules **2004**, 37, 3018.

(82)   Buback, M. Macromolecular Rapid Communications **2015**, 36, 1979.

(83)   Liang, K.; Hutchinson, R. A. Macromolecules **2010**, 43, 6311.

(84)   O'Driscoll, K. F.; Monteiro, M. J.; Klumperman, B. Journal of Polymer Science Part A: Polymer Chemistry **1997**, 35, 515.

(85)   Beuermann, S. Macromolecules **2004**, 37, 1037.

(86)   Beuermann, S.; Buback, M.; Hesse, P.; Lacík, I. Macromolecules **2006**, 39, 184.

(87)   Stach, M.; Lacík, I.; Kasák, P.; Chorvát, D.; Saunders, A. J.; Santanakrishnan, S.; Hutchinson, R. A. Macromolecular Chemistry and Physics **2010**, 211, 580.

(88)   Stach, M.; Lacík, I.; Chorvát, D.; Buback, M.; Hesse, P.; Hutchinson, R. A.; Tang, L. Macromolecules **2008**, 41, 5174.

(89)   Lacík, I.; Učňová, L.; Kukučková, S.; Buback, M.; Hesse, P.; Beuermann, S. Macromolecules **2009**, 42, 7753.

(90)   Stahl, G. A. Journal of Polymer Science: Polymer Chemistry Edition **1979**, 17, 1883.

(91)   Grassie, N.; Torrance, B. J. D.; Fortune, J. D.; Gemmell, J. D. Polymer **1965**, 6, 653.

(92)   Schier, J. E. S.; Hutchinson, R. A. Polym. Chem. **2016**, 7, 4567.

(93)   Liang, K.; Rooney, T. R.; Hutchinson, R. A. Industrial & Engineering Chemistry Research **2013**, 53, 7296.

(94)   Meijs, G. F.; Rizzardo, E. Journal of Macromolecular Science, Part C **1990**, 30, 305.

(95)   Mayo, F. R.; Lewis, F. M. Journal of the American Chemical Society **1944**, 66, 1594.

(96)   Preusser, C.; Ezenwajiaku, I. H.; Hutchinson, R. A. Macromolecules **2016**, 49, 4746.

(97)   Preusser, C.; Hutchinson, R. A. Macromolecular Symposia **2013**, 333, 122.

(98)   Cuccato, D.; Storti, G.; Morbidelli, M. Macromolecules **2015**, 48, 5076.

Chapter 3

Macromonomer Syntheses

Preface

Comb-polymers produced from short-chain hydroxyl terminated macromonomers have been employed extensively by the Moscatelli group, particularly in the biomedical field. In order to expand the diversity of applications and to improve the understanding of macromonomer radical polymerization (RP) kinetics, four new macromonomer families with alkyl, tertiary amine, quaternary ammonium, and carboxyl end-group functionalities were synthesized. The purpose of this Chapter is to provide a summary of the synthesis details, ^{1}H NMR characterizations, and oligomeric distributions measured by size exclusion chromatography (SEC) of the materials studied in the subsequent Chapters. These details are extracted from the published works, such that the later Chapters focus primarily on macromonomer polymerization kinetics and applications.

Abstract

The syntheses of five new methacrylate type macromonomers, comprising ethyl and propionate esters, tertiary amine, quaternary ammonium, and carboxyl end-group functionalities, are described with corresponding ^{1}H NMR and SEC characterizations provided. The new materials include: polylactic acid ethyl ester methacrylate (PLA$_N$EMA; for N=1, 5, 7, and 9), polycaprolactone 2-(N,N-dimethylamino)ethyl ester methacrylate (PCL$_n$DeMA; for n=2 and 3), and polycaprolactone choline iodide ester methacrylate (PCL$_n$ChMA; for n=3), as well as the derivatives of hydroxyl terminated HEMA-PCL$_3$: propionate ester end-capped (HEMA-PCL$_3$-PR) and mono-succinic acid ester (HEMA-PCL$_3$-COOH). All syntheses were performed in > 65% yields with cyclic monomer conversions of 94-97% and macromonomer average chain lengths within 10% of the target value. The dn/dc for several comb-polymers in THF are also provided.

3.1 Introduction

The average number of polyester units (n) per macromonomer, specified by the stoichiometric ratio of cyclic monomer to initiator in the ROP step, controls the hydrolytic degradability and functional group density of the final comb-polymer material. The synthesis of macromonomers with hydroxyl functional group is conveniently straightforward because the vinyl group, which makes the macromonomer amenable to RP, is already included in the ROP initiator (e.g., 2-hydroxyethyl methacrylate). To produce macromonomers with different end-group functionalities, the strategy outlined in Scheme 3.1 is adopted, where functional ROP initiators are selected, and post-ROP acylation is performed using an acid chloride (e.g., methacryloyl chloride) to impart vinyl functionality on to the short-chain polyesters. Acylation with acryloyl chloride or the ring opening of maleic anhydride via terminal hydroxyl of the macromonomer, could also be implemented to produce macromonomers with different RP kinetic behaviors. Finally, since acid chlorides are generally expensive and their reaction must be performed in solution with appropriate acid scavenger, the acid chloride acylation step could eventually be replaced by esterification of the analogous carboxylic acid in bulk at high temperature.
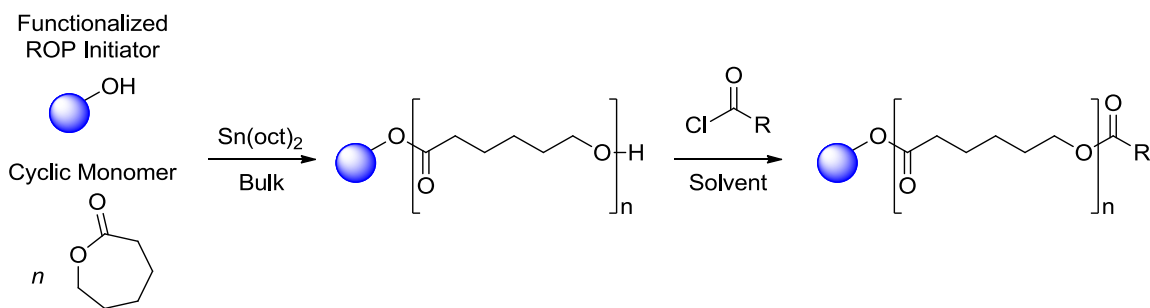
Scheme 3.1: Generalized synthetic strategy for producing bifunctional short-chain polyesters.

In this work, several short-chain methacryloyl-terminated polyester macromonomers with similar average molecular weight (MW) yet different end-group functionalities – alkyl, tertiary amine, quaternary ammonium, hydroxyl, and carboxyl – were synthesized by ROP and subsequent modification, with the structures shown in Scheme 3.2. In the biomedical field, the hydroxyl

terminated macromonomers (e.g., HEMA-PCL$_3$ and HEMA-PLA$_5$ in Scheme 3.2, where the subscript denotes the average number of polycaprolactone (PCL) or polylactic acid (PLA) units in the macromonomer, respectively) have been extensively employed to make materials with tunable hydrolytic degradability,[1,2] with the carboxyl terminated macromonomers (e.g., HEMA-PCL$_3$-COOH) as a variant to afford post-polymerization esterification to cross-link or attach specific molecules to the final material. The alkyl terminated (macro)monomers (PLA$_1$EMA and PLA$_5$EMA) are investigated in Chapter 5 as hydrolytic degradation rate modifiers, and for their ability to improve the selectivity of post-polymerization esterification reactions through use as a comonomer spacer with hydroxyl or carboxyl terminated macromonomers. In addition, tunable charge density and hydrophobicity are important features of both quaternary ammonium (e.g., PCL$_3$ChMA) and tertiary amine end-functionalized (e.g., PCL$_3$DeMA) macromonomer systems, which are investigated in Chapter 6 to produce degradable flocculants and to modify biorenewables with p*H*-responsive polymers such that the final material can reversibly transition from a hydrophobic to a hydrophilic state using carbon dioxide as a stimulus. Finally, the propionate ester end-capped version of HEMA-PCL$_3$, termed HEMA-PCL$_3$-PR, is used in a kinetics study in Chapter 8 to gain a better understanding of the role of hydrogen bonding in organic solution copolymerization kinetics.

PLA$_5$EMA

PLA$_1$EMA

PCL$_3$DeMA

PCL$_3$ChMA

HEMA-PLA$_5$

HEMA-PCL$_3$-COOH

HEMA-PCL$_3$

HEMA-PCL$_3$-PR
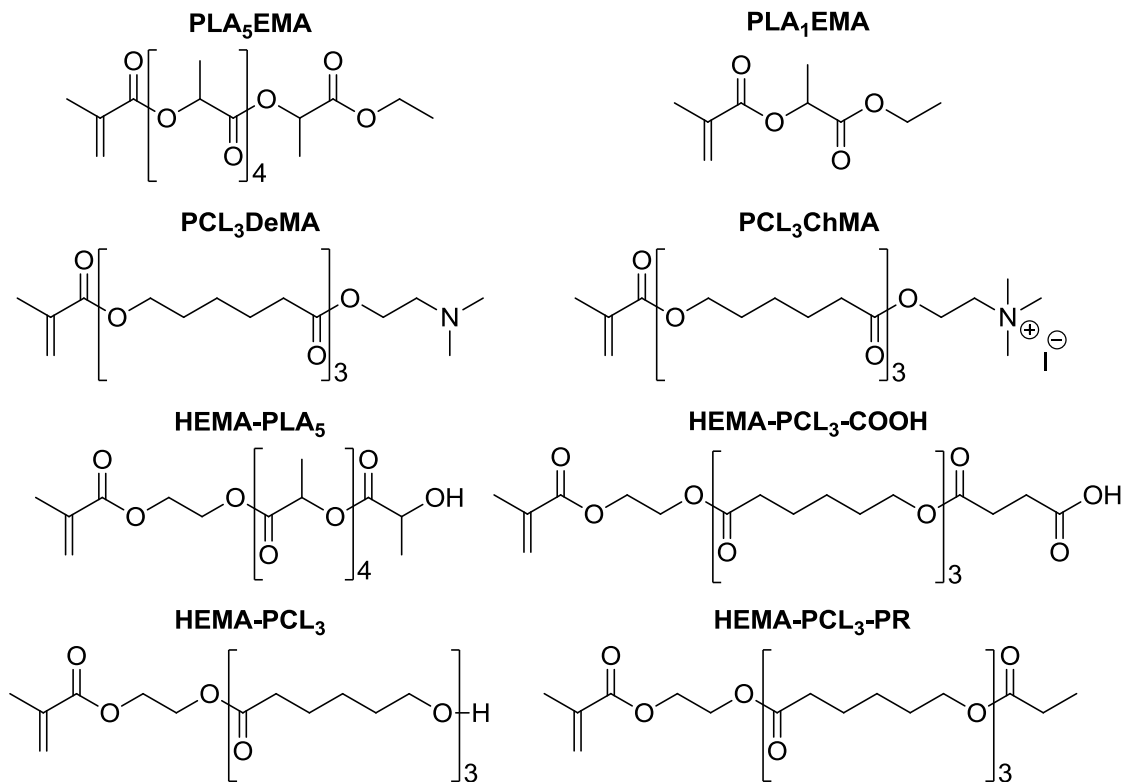
Scheme 3.2: Structures of short-chain polyester methacrylate (macro)monomers synthesized in this work.

3.2 Materials

ε-Caprolactone (CL, 97%), 2-(dimethylamino)ethanol (De, >98%), (3S)-*cis*-3,6-dimethyl-1,4-dioxane-2,5-dione (LA, 98%), ethyl 2-hydroxypropionate (ETL, ≥98%), succinic anhydride (≥99%), propionyl chloride (98%), tin(II) 2-ethylhexanoate (Sn(oct)$_2$, 92.5-100.0%), triethylamine (TEA, ≥99.5%), basic alumina (Brockmann 1), methyl iodide (ICH$_3$, 99%), 2-hydroxyethyl methacrylate (HEMA, 97%), and 2,2'-azobis(2-methylpropionitrile) (AIBN, 98%) were purchased from Sigma Aldrich and used as received. Tetrahydrofuran (THF, >99%, ACP Chemicals), ethyl acetate (EtOAc, reagent grade, ACP Chemicals), hexanes (reagent grade, ACP Chemicals), methanol (reagent grade, ACP Chemicals), hydroquinone (reagent grade, Fisher Scientific), anhydrous diethyl ether (≥99.0%, ACP Chemicals), and chloroform-d (CDCl$_3$, 99.8% D, Sigma

Aldrich) were used as received. Methacryloyl chloride (MACl, 97%, Sigma Aldrich) was distilled immediately before use.

3.3 Methods

All ^{1}H NMR characterizations of (macro)monomers synthesized in this work were performed on a Bruker Avance instrument operating at 400 MHz. The oligomeric distributions of all macromonomers were assessed by size exclusion chromatography (SEC) using a Waters 2960 separation module instrument with a Waters 410 differential refractometer (DRI) and a Wyatt Instruments Dawn EOS 690 nm laser photometer multiangle light scattering (LS) detector. Four Styragel columns (HR 0.5, 1, 3, 4) were maintained at 35 °C with distilled THF as eluent at 0.3 mL/minute. The DRI detector was calibrated using 14 narrow polymethyl methacrylate (PMMA) standards (302–853,000 Da). The differential refractive indices (dn/dc) of homopolymers were measured using a Wyatt Optilab DSP refractometer at 690 nm calibrated with sodium chloride. Six homopolymer samples of 1-20 mg·mL^{-1} were prepared in THF and injected sequentially to construct a curve with slope dn/dc, with values summarized by Table 3.1. The homopolymers were prepared by reacting 5 g of macromonomer with 200 mg AIBN in 20 mL THF at 60 °C overnight. After the THF was evaporated *in vacuo*, the homopolymers were purified by repeated precipitations at -20 °C in an appropriate solvent (Table 3.1), and then dried under vacuum overnight at 40 °C.

Table 3.1: Solvents which can selectively precipitate the respective comb-polymer from its macromonomer at -20 °C, and polymer differential refractive indices.

Homopolymer	Precipitation Solvent	dn/dc (mL·g^{-1})
PLA$_1$EMA	Hexanes	0.069
PLA$_5$EMA	Methanol	0.055
HEMA-PCL$_3$	Diethyl Ether	0.063[4]
PCL$_3$DeMA	Hexanes	0.074

3.4 Macromonomer Syntheses

In general, the ring opening polymerization (ROP) of CL or LA was performed in bulk using a suitable hydroxyl-bearing initiator. Except for HEMA-initiated ROP, methacrylation of the terminal hydroxyl group is performed to yield macromonomers amenable to radical polymerization (RP).

3.4.1 Alkyl Terminated Monomer: PLA_1EMA

In a sealed 3 neck 100 mL round bottom flask, ETL (4.25 g, 36.0 mmol) was dissolved in 60 mL EtOAc to which 15 mL TEA (108.4 mmol) was added. The solution was cooled to 0 °C using an external ice bath, bubbled with nitrogen for 10 min, and then 4.6 mL freshly distilled MACl (47.1 mmol) was fed over 20 min using a glass syringe. The reaction mixture was maintained at 0 °C for 3 hours, filtered to remove the TEA salt, and then passed through a column of basic alumina. Approximately 1 mg of hydroquinone was added to the product solution before the solvent was evaporated *in vacuo* to afford 4.51 g 2-ethoxy-1-methyl-2-oxoethyl methacrylate or polylactic acid ethyl ester (PLA_1EMA) with number average $N=1$ in 67 % yield. The ^1H NMR spectrum is provided as **Error! Reference source not found.**Figure A.1 of Appendix A.

3.4.2 Alkyl Terminated Macromonomers: PLA_NEMA for $N=5, 7,$ and 9

The PLA_NEMA synthesis is described for the $N=5$ macromonomer, where characterizations for the $N=7$ and $N=9$ syntheses are detailed by Table A.1 with oligomeric MMDs shown in Figure A.11 of Appendix A. LA (5.27 g, 36.6 mmol) was loaded into a 50 mL sealed round bottom flask, purged with nitrogen, and then heated to 130 °C. A $Sn(oct)_2$/ETL mixture with molar ratio 1:400 was prepared separately (1:200 for the $N=9$ synthesis), then 2.17 g of this mixture (corresponding to 18.3 mmol ETL) was added to the LA by syringe and allowed to react for 4 hours at 130 °C to afford polylactic acid ethyl ester (PLA_nE) with number average $n = 5.5$ and LA conversion ≈ 94 % (as determined by ^1H NMR in Figure A.2 of Appendix A).

Next, in a sealed 3 neck 100 mL round bottom flask, PLA$_n$E (7.44 g, 18.3 mmol -OH) was dissolved in 38 mL EtOAc to which 7 mL TEA (50.6 mmol) was then added. The solution was cooled to 0 °C using an external ice bath, bubbled with nitrogen for 10 min, and then 2.3 mL freshly distilled MACl (23.6 mmol) was fed over 20 minutes using a glass syringe. The reaction mixture was maintained at 0 °C for 3 hours, filtered to remove the TEA salt, and then passed through a column of basic alumina. Approximately 1 mg of hydroquinone was added to the product solution before the solvent was evaporated *in vacuo* to afford 6.21 g polylactic acid ethyl ester methacrylate (PLA$_5$EMA) with number average N=5.3 in 77 % yield (according to ^{1}H NMR in Figure A.3 of Appendix A).

3.4.3 Tertiary Amine Macromonomer: PCL$_n$DeMA for *n*=2 and 3

The PCL$_n$DeMA synthesis is described for the *n*=3 macromonomer, where characterizations for the *n*=2 synthesis are detailed by Table A.2 with oligomeric MMDs shown in Figure A.12 of Appendix A. A catalyst/monomer mixture with molar ratio of 1:500 consisting of Sn(oct)$_2$ (39.0 mg, 96.3 µmol) and CL (5.49 g, 48.2 mmol), was loaded into a 50 mL sealed round bottom flask, purged with nitrogen, and then heated to 130 °C. De (1.43 g, 16.1 mmol) was added to the catalyst/monomer mixture by syringe and allowed to react for 110 minutes at 130 °C to yield polycaprolactone 2-(*N,N*-dimethylamino)ethyl ester (PCL$_3$De) with number average $n = 3.0$ and CL conversion $\approx$ 94 % (as determined by the ^{1}H NMR spectrum in Figure A.4 of Appendix A).

Next, in a sealed 3 neck 100 mL round bottom flask, PCL$_3$De (6.96 g, 16.2 mmol -OH) was dissolved in 26 mL THF to which 20 mL TEA (144.6 mmol) was then added. The solution was cooled to 0 °C using an external ice bath, bubbled with nitrogen for 10 minutes, and then 2.0 mL freshly distilled methacryloyl chloride (MACl, 20.5 mmol), diluted by 5.5 mL THF, was fed over 1 hour using a glass syringe. The reaction mixture was maintained at 0 °C for 3 hours, filtered to remove the TEA salt, and then passed through a column of basic alumina. The solvent was evaporated *in vacuo* to afford 6.11 g polycaprolactone 2-(*N,N* -dimethylamino)ethyl ester

methacrylate (PCL$_3$DeMA) with number average n = 3.0 (according to ^{1}H NMR in Figure A.5 of Appendix A) in 76 % yield.

3.4.4 Quaternary Ammonium Macromonomer: PCL$_3$ChMA

PCL$_3$DeMA (5.89 g, 11.2 mmol) was dissolved in 160 mL diethyl ether, cooled to 0 °C using an external ice bath, and kept under constant flow of nitrogen. Approximately 2.5 mL ICH$_3$ (40 mmol) was injected by syringe then the reaction was allowed to warm to room temperature and proceed for 48 hours. The white waxy precipitate was collected by filtration, washed with cold diethyl ether, and dried in vacuum oven at 40 °C overnight to afford 5.20 g polycaprolactone choline iodide ester methacrylate (PCL$_3$ChMA) (72 % methylation yield) whose ^{1}H NMR is provided as Figure A.6 of Appendix A.

3.4.5 Hydroxyl Terminated Macromonomers and Derivative: HEMA-PLA$_5$, HEMA-PCL$_3$, and HEMA-PCL$_3$-PR

The syntheses of hydroxyl terminated macromonomers HEMA-PLA$_5$ and HEMA-PCL$_3$ and were achieved by bulk ROP of LA and CL, respectively, using a previously reported procedure[3,4] with minor modification. In each reaction, 1-2 mg hydroquinone was added to LA (5.68 g, 39.4 mmol) or CL (5.03 g, 44.1 mmol), loaded into a 50 mL sealed round bottom flask, purged with nitrogen, and then heated to 130 °C. Separately, a Sn(oct)$_2$/HEMA mixture with molar ratio 1:400 was prepared, then 2.05 g or 1.91 g of this mixture (corresponding to 15.8 and 14.7 mmol HEMA) was added to the LA or CL by syringe, and then allowed to react at 130 °C for 2 and 2.5 hours, respectively. The LA conversion was ≈ 96% for HEMA-LA$_5$ with n = 5.3 and the CL conversion was ≈ 94% for HEMA-PCL$_3$ with n = 3.3 (as determined by ^{1}H-NMR spectra in Figure A.7 and Figure A.8 of Appendix A, respectively).

The hydroxyl end group of HEMA-PCL$_3$ was converted to its propionate ester by reaction with propionyl chloride to afford HEMA-PCL$_3$-PR. In a sealed 3 neck 100 mL round bottom flask, HEMA-PCL$_3$ (6.50 g, 13.8 mmol -OH) was dissolved in 28 mL THF to which 5.7 mL TEA (41.2

mmol) was then added. The solution was cooled to 0 °C using an external ice bath, bubbled with nitrogen for 10 minutes, and then 1.6 mL propionyl chloride (18.3 mmol), diluted by 3.3 mL THF, was fed over 1 hour using a glass syringe. The reaction mixture was maintained at 0 °C for 3 hours, filtered to remove the TEA salt, and then passed through a column of basic alumina. The solvent was evaporated *in vacuo* to afford 6.15 g HEMA-PCL$_3$-PR with number average *n* = 3.3 (determined by ^{1}H NMR in Figure A.9 of Appendix A) in 84 % yield.

3.4.6 Carboxyl Terminated Macromonomer: HEMA-PCL$_3$-COOH

The hydroxyl end group of HEMA-PCL$_3$ was converted to its mono-succinic acid ester (HEMA-PCL$_3$-COOH) by bulk ring opening of succinic anhydride. HEMA-PCL$_3$ (6.90 g, 14.6 mmol) and succinic anhydride (1.52 g, 15.2 mmol) were purged with nitrogen, and heated to 90 °C for 24 hours to afford HEMA-PCL$_3$-COOH with *n* = 3.3 (according to ^{1}H NMR in Figure A.10 of Appendix A) in quantitative yield. No attempt was made to purify the minor excess of succinic anhydride from the final product.

3.5 Results and Discussion

The ^{1}H NMR peak assignments for PLA$_1$EMA monomer as well as all macromonomers and corresponding precursors are detailed in Figures A.1-A.10 of Appendix A. For each macromonomer synthesis, the ROP proceeded to high cyclic monomer conversion (>94%) and was stopped before exceeding 97% conversion to minimize the occurrence of side reactions which broaden the oligomeric MW distribution.[5] The average polyester chain lengths, *n*, measured for each macromonomer by ^{1}H NMR are in close agreement with the target values specified by initiator and cyclic monomer stoichiometry, as summarized by Table 3.2. Furthermore, SEC for macromonomer oligomeric molar mass distributions (MMD), in terms of weight fraction (Figure A.13) and number fraction (Figure A.14), show that the majority of the macromonomer weight comprises the target chain length, while the most numerous fractions correspond to the lowest chain lengths.

Table 3.2: Number average macromonomer chain lengths measured by ^{1}H NMR compared to target values as well as dn/dc for select macromonomer homopolymers in THF.

Macromonomer	n	
	Target	^{1}H NMR
PLA$_1$EMA	1	1
PLA$_5$EMA	5	5.3
HEMA-PLA$_5$	5	5.3
HEMA-PCL$_3$	3	3.3
HEMA-PCL$_3$-COOH	3	3.3
HEMA-PCL$_3$-PR	3	3.3
PCL$_3$DeMA	3	3.0
PCL$_3$ChMA	3	3.0

Compared to HEMA-PCL$_3$, the oligomeric distributions of its derivatives, HEMA-PCL$_3$-PR and HEMA-PCL$_3$-COOH, are uniformly shifted to higher MW and have similar broadness. In addition, the successful functionalization of all chains in the oligomeric distributions of the derived materials is confirmed by ^{1}H NMR (Figure A.9 and Figure A.10) where disappearance of the methylene signal adjacent to the terminal hydroxyl group (δ = 3.64 ppm for HEMA-PCL$_3$ in Figure A.8) is accompanied by a commensurate increase in integration for methylene signals adjacent to the repeating ester units (δ = 4.06 ppm). The average n of the PLA$_5$E (precursor to PLA$_5$EMA) decreased slightly from 5.5 to 5.3 after methacrylation because the significant amount of unreacted ETL initiator ($\approx$10%), shown in Figure A.2 of Appendix A, becomes PLA$_1$EMA upon functionalization, thus lowering the average n of the final PLA$_5$EMA distribution. Finally, it should be noted that although HEMA-PLA$_5$ and PLA$_5$EMA have similar average MW, the HEMA-PLA$_5$ oligomers are predominantly even-numbered (i.e., n = 2, 4, 6) whereas PLA$_5$EMA oligomers are predominantly odd-numbered (i.e., n = 3, 5, 7) because the ETL initiator fragment contributes a single PLA unit to each polyester chain.

3.6 References

(1)   Lupi, M.; Colombo, C.; Frapolli, R.; Ferrari, R.; Sitia, L.; Dragoni, L.; Bello, E.; Licandro, S. A.; Falcetta, F.; Ubezio, P.; Bigini, P.; Salmona, M.; D'Incalci, M.; Morbidelli, M.; Moscatelli, D. *Nanotechnology* **2014,** *25* (33), 335706

(2)   Colombo, C.; Dragoni, L.; Gatti, S.; Pesce, R. M.; Rooney, T. R.; Mavroudakis, E.; Ferrari, R.; Moscatelli, D. *Ind. Eng. Chem. Res.* **2014,** *53* (22), 9128-9135.

(3)   Yu, Y.; Ferrari, R.; Lattuada, M.; Storti, G.; Morbidelli, M.; Moscatelli, D. *J. Polym. Sci. Part A: Polym. Chem.* **2012,** *50* (24), 5191-5200.

(4)   Ferrari, R.; Yu, Y.; Morbidelli, M.; Hutchinson, R. A.; Moscatelli, D. *Macromolecules* **2011,** *44* (23), 9205-9212.

(5)   Ferrari, R.; Pecoraro, C. M.; Storti, G.; Moscatelli, D. *RSC Adv.* **2014,** *4* (25), 12795-12804.

Chapter 4

Copolymer Propagation Kinetics for (Macro)monomers
Relevant to Biomedical Applications

Preface

In the beginning (pre-2015), the work in this PhD was primarily focused on a collaboration with the group of Dr. Davide Moscatelli (Politecnico di Milano) who was developing nanocarriers for intravenous drug delivery applications. Due to the high variability of *in vitro* and *in vivo* conditions, it is important that the production of any biomedical device is robust, reproducible, and that its material properties may be easily controlled. Thus, the Moscatelli group has been investigating the biomedical applications of cyanoacrylate and polyester macromonomer based materials produced by radical polymerization (RP). During the year 2013-2014, I was fortunate to spend one year at Politecnico di Milano, working closely on the applications side of research; however, my main contribution is to the RP propagation kinetics of these systems. This Chapter combines and summarizes the understandings developed for the copolymerization propagation kinetics of methyl methacrylate (MMA) with *n*-butyl cyanoacrylate (BCA) and HEMA-PCL$_n$, which have been published as full papers in Polymer Chemistry (2015, vol. 6, 1594-1603) and Macromolecular Bioscience (2013, vol. 13, 1347-1357), respectively. The contributions by co-authors Evangelos Mavroudakis (Quantum Mechanics), Raffaele Ferrari (nanocarrier production) as well as Dr. Monica Lupi and Dr. Paolo Ubezio (*in vitro* studies) are omitted. I also performed some of the BCA/MMA kinetic studies in Dr. Igor Lacík's lab during my 2014 visit to the Polymer Institute of the Slovak Academy of Sciences. The Supporting Information for each work can be found online.

4.1 BCA/MMA

Abstract

The radical polymerization (RP) kinetics for *n*-butyl cyanoacrylate (BCA) and methyl methacrylate (MMA) copolymerization are studied in bulk at 30-70 °C using a pulsed laser polymerization (PLP) technique Through the addition of 1 v% dichloroacetic acid, the notoriously rapid anionic polymerization of α-cyanoacrylates (ACA) is successfully suppressed without affecting the RP process. A strongly alternating copolymer sequence distribution is confirmed by reactivity ratio estimates determined using ^{1}H NMR composition analysis (r_{BCA}=0.236±0.042 and r_{MMA}=0.057±0.008. For MMA-rich monomer mixtures ($0.50 \leq f_{MMA} \leq 0.97$), overall propagation rate coefficients ($k_{p,cop}$) greater than twice the value for MMA homopolymerization ($k_{p,MMA}$) are facilitated by the strongly alternating copolymerization kinetics, whereas the BCA propagation rate coefficient ($k_{p,BCA}$) is estimated to be only 336±20 L·mol^{-1}·s^{-1} at 50 °C, approximately half the value of $k_{p,MMA}$.

4.1.1 Introduction

Alkyl cyanoacrylates (ACAs) are renowned for their extremely rapid anionic polymerization that can be initiated by trace amounts of weak base at room temperature without catalyst.[1,2] Even moisture from ambient air is sufficient to initiate the fast polymerization and thus ACAs have found widespread applications as 'fast-acting' adhesives.[3] In addition to remarkable mechanical properties and biocompatibility, poly(alkyl cyanoacrylates) (PACA) demonstrate biodegradability, drug compatibility and permeability that establish them as excellent raw materials for drug delivery systems.[4-6] Although myriad experimental investigations show PACA nanoparticles (NP) to be promising polymeric colloidal carriers, highly variable *in vitro* and *in vivo* results arising from an incomplete control over factors influencing polymerization kinetics, such as competitive initiation by formulation components (i.e., bioactives, excipients, etc.), have been identified as prominent barriers preventing PACA NP drug delivery systems from entering the market.[6]

Indeed, the predominant mechanism for PACA production remains anionic polymerization[7-9] because of the ease of initiation and the fact that high molecular weights (MW) on the order of 10^5-10^6 g·mol^{-1} can be achieved within seconds.[10,11] However, such rapid polymerization is both sensitive and aggressive, necessitating a careful control of operating conditions through the addition of acid stabilizers (e.g., SO_2, sulfonic acid, etc).[7] As a further complication, base catalyzed proton abstraction at the polymer's chain end facilitates a rapid depolymerization mechanism followed by a repolymerization to form new lower MW daughter chains.[10,11] This depolymerization-repolymerization behavior makes the anionic polymerization of ACA systems difficult to study, while their remarkably high anionic reactivity limits the choice of suitable monomers for copolymerization.

Recently, the possibility to copolymerize ACAs with more stable and common monomers (e.g., methacrylates) by radical polymerization (RP) disclosed new opportunities to control PACA degradation rates.[12] Although the RP of alkyl cyanoacrylates is reported to proceed much slower than its anionic polymerization,[4] the ability to copolymerize ACAs through RP enables a greater control over polymer MW characteristics and degradative behavior while providing a means to tailor polymer properties otherwise inaccessible by anionic polymerization. Furthermore, Robello et al. confirmed that the copolymerization of ethyl cyanoacrylate (ECA) with only 5 wt% methyl methacrylate (MMA) is sufficient to halt the depolymerization of the poly(ECA) backbone in basic medium.[10]

The current understanding of ACA reactivity is incomplete; for methacrylate/cyanoacrylate copolymerization systems, Kinsinger et al. report equal addition probabilities in bulk and a strongly alternating copolymer sequence distribution in benzene solution,[13] while the work of Yamada et al. claims reactivity ratios well-below unity in bulk.[14] Furthermore, the high-conversion experiments of Han and Kim indicate near equal addition probabilities for the bulk copolymerization of ECA/MMA.[12] Also scarce in the literature are

investigations aimed at the estimation of individual ACA radical propagation rate coefficients (k_p); using the rotating sector method, Yamada et al. estimated a bulk k_p of 1622 L·mol^{-1}·s^{-1} for ECA at 30 °C, approximately 3.6 times their estimate for the bulk k_p of MMA.[14] The same group found that the cyano group (–CN) at the α- position has a similar influence on propagation kinetics as the α-chloro substituent,[15] and leads to a 45% increase in k_p compared to the α-fluoro substituent,[16] with a recent computational study performed by Değirmenci et al. supporting these experimental findings.[17] A common feature of all these experimental works is that the authors emphasize the difficulty in suppressing anionic polymerization during RP and isolation of the low-conversion copolymer.

The current experimental study was undertaken to resolve these inconsistencies seen in previous literature, and to provide a detailed understanding of BCA RP kinetics from which PACAs may be synthesized with highly reproducible final properties. In this work, PLP-SEC is implemented to study the propagation kinetics of the *n*-butyl cyanoacrylate (BCA) and MMA copolymerization system. MMA is selected as comonomer because of its frequent use in biomedical applications,[18] confirmed ability to halt depolymerization of PACA backbone,[10] and well-documented RP kinetics.[19] A computational approach based on density functional theory (DFT) was also performed to support and enrich the BCA/MMA copolymerization experiments.

4.1.2 Experimental

Materials

Methyl methacrylate (MMA, 99%, Sigma Aldrich), *n*-butyl cyanoacrylate (BCA, Henkel Biomedical, Dublin, Ireland), 2,2-dimethoxy-2-phenylacetophenone (DMPA, 99%, Sigma Aldrich), dichloroacetic acid (DCAA, ≥99%, Sigma Aldrich), methacrylic acid (MAA, 99 %, Sigma Aldrich), chloroform-d (CDCl$_3$, 99.8 % D, Cambridge Isotope Laboratories), methanol (MeOH, reagent grade, ACP Chemicals Inc.), and acetone (reagent grade, ACP Chemicals Inc.) were all used as received.

Pulsed Laser Polymerization

Low-conversion copolymerizations of BCA/MMA were conducted at Queen's University using a pulsed laser setup consisting of a Coherent Xantos XS-500 laser operating at the XeF line of 351 nm and capable of producing laser energy of 1-6 mJ per pulse at repetition rates up to 500 Hz, while a similar setup was also used at the Polymer Institute of the Slovak Academy of Sciences (Polymer Institute SAS).[25]

Monomer mixtures of various BCA/MMA composition were prepared in bulk with 1 v% DCAA and 5 mmol·L^{-1} DMPA photoinitiator. Approximately 1 mL of the monomer mixture was added to a Quartz cuvette of 10 mm pathlength (CV10Q3500S, Thorlabs), heated to 50 °C using a circulating oil bath, and exposed to laser energy while the temperature was monitored and controlled to within 50±1 °C. In addition, several experiments were also carried out at 30±1 °C and 70±1 °C. Experiments were conducted using laser repetition rates between 10 and 100 Hz (see Table S4 of the Supporting Information for the exact operating conditions employed for each sample).

Following PLP experiments, the residual MMA monomer was removed under constant air stream. The resulting copolymer/BCA monomer mixture was treated with methanol (MeOH) containing 5 v% MAA at room temperature, centrifuged at 6000 rpm for 10 minutes, with the supernatant then decanted to collect the copolymer precipitate. This procedure was repeated by dissolving the copolymer in a minimum amount of acetone followed by precipitation in non-acidified MeOH, centrifugation, and isolation of the copolymer product. Monomer conversion for each experiment was less than 3 % as measured by gravimetry. Copolymer composition was determined by ^{1}H NMR using a Bruker Avance instrument operating at 400 MHz.

Size Exclusion Chromatography

The molecular weights of all copolymer samples produced at Queen's University were determined using the SEC setup described in Section 3.3. The SEC analysis of the samples produced at the

Polymer Institute SAS was also performed with THF as eluent using a setup described elsewhere.[21] In both setups, the RI detector was calibrated using polystyrene standards, while both RI and LS output were interpreted using the literature and measured calibration parameters listed in Table 4.1. The copolymer MW was calculated as a composition-weighted average of the homopolymer values using literature MH parameters, while a composition-weighted dn/dc value was used to interpret the LS output. The dn/dc value for PBCA was measured as described by Section 3. Finally, the monomer densities were measured at temperatures between 20 and 70 °C using a Paar DMA 48 Density Meter, with best-fit parameters reported in Table 4.1.

Table 4.1: Parameters for interpretation of SEC results and calculation of $k_{p,cop}$.

Monomer	ρ (g·mL^{-1})	dn/dc (mL·g^{-1})	Mark–Houwink parameters		
			K (10^{-4}·dL·g^{-1})	a	Ref.
Styrene	-	0.185	1.14	0.716	22
MMA	0.9671–0.001117T/°C^a	0.089[23]	0.944	0.719	24
BCA	1.0140–0.009326T/°C^a	0.074^a	2.00	0.571	25

^{a} parameters measured in this work

4.1.3 Results and Discussion – BCA/MMA

Copolymer Composition Analysis

Low-conversion free-radical generated copolymer compositions estimates are difficult to obtain for ACA systems because of the extremely rapid anionic polymerization of the monomer. Previous authors have attempted to mitigate this issue by precipitating their desired polymer from solution using methanol (MeOH) containing 5 wt% hydrochloric acid (HCl).[12,25] Although MeOH itself is a nucleophile the presence of HCl is designed to quickly cap any anionic species formed. In this work, MeOH acidified with 5 wt% HCl was unsuitable to isolate low-conversion PLP-generated RP copolymers, as subtle changes in HCl solubility in MeOH with temperature and during centrifugation inevitably led to the formation of anionic PBCA during isolation. Instead, MeOH containing 5 v% methacrylic acid (MAA) was used to effectively precipitate low conversion RP-

generated copolymer from residual monomer at room temperature. When MAA, whose density is similar to that of BCA, is used as the acidic end-capping agent the residual monomer is not segregated during centrifugation and therefore the formation of anionic PBCA is prevented altogether. As outlined in the Supporting Information, the ^{1}H-NMR spectra of the isolated RP copolymer provided three independent estimates of copolymer composition for which the presence of any anionically-generated PBCA homopolymer leads to a distinct disagreement.

Copolymer composition results were only deemed as reliable (i.e., not contaminated by PBCA homopolymer formed during sample workup) if the three independent calculations of copolymer composition were within 3 % of each other. As a further validation of the effectiveness of this copolymer isolation technique, several samples were produced at different repetition rates for each initial monomer composition and the corresponding copolymer compositions were estimated with excellent reproducibility. The final results are presented in Figure 4.1, where the 50 °C data is fitted according to the Terminal Model with reactivity ratios estimated by non-linear parameter estimation. There is excellent agreement at the 95 % confidence level between the values (r_{BCA}=0.236±0.042 and r_{MMA}=0.057±0.008) fitted to experimental data with the values (r_{BCA}=0.272 and r_{MMA}=0.057) predicted by Quantum Mechanics. Included in Figure 4.1 are copolymer compositions for samples produced at 30 and 70 °C; as the data are in excellent agreement with both sets of reactivity ratio estimates at 50 °C, it can be concluded that there is no significant variation in bulk BCA/MMA reactivity ratios over the 30-70 °C temperature range.
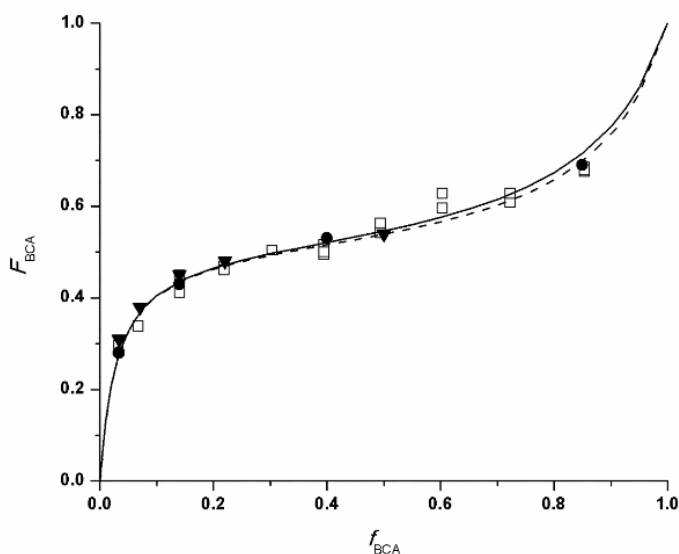
Figure 4.1: BCA/MMA copolymer composition vs initial molar fraction of BCA polymerized in bulk at 30 °C (▼), 50 °C (□), and 70 °C (●) with 1 v% DCAA to suppress anionic polymerization. Experimental data at 50 °C fitted by the terminal model with r_{BCA}=0.236±0.042 and r_{MMA}=0.057±0.008 (dashed line), while the solid line indicates Terminal Model predictions with r_{BCA}=0.0272 and r_{MMA}=0.057 estimated computationally.

Copolymer composition estimates beyond f_{BCA}=0.85 were not reliable, as the copolymer could not be successfully isolated from the residual monomer without inducing anionic polymerization. This difficulty introduces higher uncertainty in the estimate of r_{BCA} from experimental data. Nevertheless, the amount and reproducibility of the data presented in Figure 4.1 is sufficient to show that the BCA/MMA copolymerization system is well-represented by the Terminal Model, and demonstrates its strongly alternating character, in agreement with the findings of Yamada et al. in bulk[14] and Kinsinger et al. in benzene.[13] The direct low-conversion estimates in this work confirm a strongly alternating system which facilitates BCA incorporation while minimizing the mutual repulsion between dipolar –CN groups. This is supported by QM calculations which indicate that the BCA dimer radical structure which possesses the minimum

energy is pro-syndiotactic as well as the work of Markova et al. in which it is reported that the anionic polymerization of BCA also adopts a syndiotactic configuration to minimize the repulsion between adjacent dipolar –CN groups.[30] Furthermore, the reproducibility of the low-conversion data in Figure 4.1 confirms that the incorporation of MMA through RP successfully halts the well-known depolymerization-repolymerization behavior of PACAs over a wide range of initial monomer compositions. Although Robello et al. reported that an initial composition containing only 5 wt% MMA (f_{BCA}=0.93) is enough to halt depolymerization of the PACA backbone in basic medium,[10] the number of incorporated MMA units corresponding to f_{BCA}=0.93 could not be confirmed by experimentation. However, the reactivity ratio estimates used to fit the data in Figure 4.1 indicate that depolymerization is halted when at least 2 of every 10 units in a copolymer sequence are MMA (i.e., f_{BCA}=0.93 yields copolymer of composition F_{BCA}=0.8).

Composition -Averaged Copolymer Propagation Rate Coefficient Estimation

Pulsed-laser polymerization experiments were performed for various mixtures of BCA/MMA in bulk at 50 °C and repetition rates ranging from 10-100 Hz. In this work, BCA/MMA samples are pulsed in the presence of 1 v% DCAA to suppress the anionic polymerization of BCA. Robello et al. showed that DCAA can effectively inhibit ACA anionic polymerization in solution,[10] and the validation of the copolymer composition results in Figure 4.1 confirms that 1 v% DCAA is sufficient to suppress BCA anionic polymerization under bulk RP conditions at 30, 50, and 70 °C. As described in the Supporting Information, the estimation of k_p from PLP-SEC analysis of bulk MMA homopolymerization is not affected when 1 v% DCAA is added to the reaction mixture, and there is also no significant change in $k_{p,cop}$ estimation when the content of DCAA is systematically varied from 0.1 to 3.0 v%. Supporting the conclusion that the addition of acid does not affect the estimation of k_p, Yamada et al. found no effect of acid type in the study of ECA bulk radical homopolymerization at 30 °C using the rotating sector method, with two different acids employed

to suppress anionic polymerization.[14] Given the above observations it can be safely concluded that the addition of 1 v% DCAA does not influence the radical copolymerization propagation kinetics over the range of reaction conditions studied in this work.

As previously outlined, a major challenge associated with applying the PLP-SEC technique to the BCA/MMA system is to isolate the low-conversion RP-generated copolymer without inducing anionic polymerization of residual BCA monomer. If reduced temperature or MeOH containing 5 wt% HCl are employed to precipitate the PLP samples from residual monomer the resulting MMD and 1st derivative plots will resemble those shown in Figure 4.2, where *Blank* corresponds to the polymer formed (presumably by anionic polymerization of BCA) during work-up of a comonomer mixture which was not exposed to laser energy but was still treated with MeOH containing 5 wt% HCl. Note the presence of the inflection point near $\log(MW) = 4.7$ on the high-MW side of the distribution in each sample, regardless of PLP reaction temperature. This peak must be a result of the anionic polymerization of BCA during the isolation procedure, for if it had been produced during the PLP experiment a shift in MW corresponding to reaction temperature would be expected. The PLP distributions are found at lower MW than the contaminant peak and the primary inflection points increase with reaction temperature, as expected. However, the secondary inflection points expected from the PLP experiment are obscured by the contaminant PBCA peak, preventing the accurate determination of $k_{p,cop}$ by negatively affecting the PLP consistency checks.[27,28] When MeOH containing 5 v% MAA is employed at room temperature the issue of contaminant PBCA is averted to yield typical MMDs and 1st derivative plots like those presented in Figure 4.3.
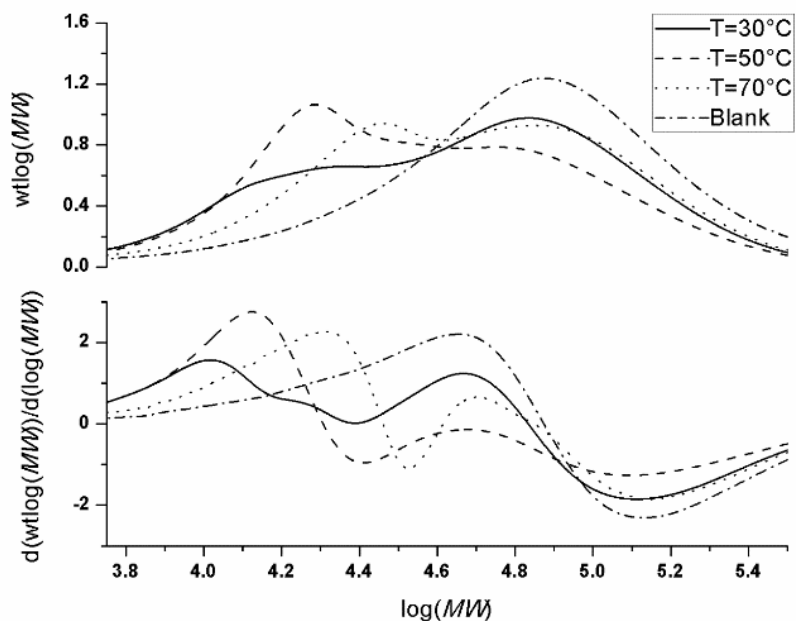
Figure 4.2: MMDs and 1st derivative plots from RI output when reduced temperature or MeOH containing 5 wt% HCl is employed to precipitate PLP samples generated from f_{BCA}=0.22 and 100 Hz at various temperatures. Blank corresponds to a PLP sample which underwent identical treatment except it was not exposed to laser energy.

The MMDs and 1st derivative plots in Figure 4.3 indicate that the polymer was produced and isolated without significant amounts of contaminant PBCA and show good PLP structure from both RI and LS detectors. Furthermore, when all acidic species are removed, by re-dissolving the isolated PLP samples in a minimum amount of acetone and re-precipitating in MeOH, a good agreement is achieved between the RI and LS estimates for $k_{p,cop}$ over the entire composition range. The differences between detectors do not exceed 15 % which justifies the composition-weighted approaches to interpreting RI and LS data as well as the measurement of the *dn/dc* and the usage of literature Mark-Houwink parameters for PBCA.[25] PLP samples produced from BCA compositions greater than f_{BCA}=0.85 could not be isolated from residual monomer without exposing them to a lower temperature (-10 °C) or treating them with MeOH containing less than 5 v% MAA.
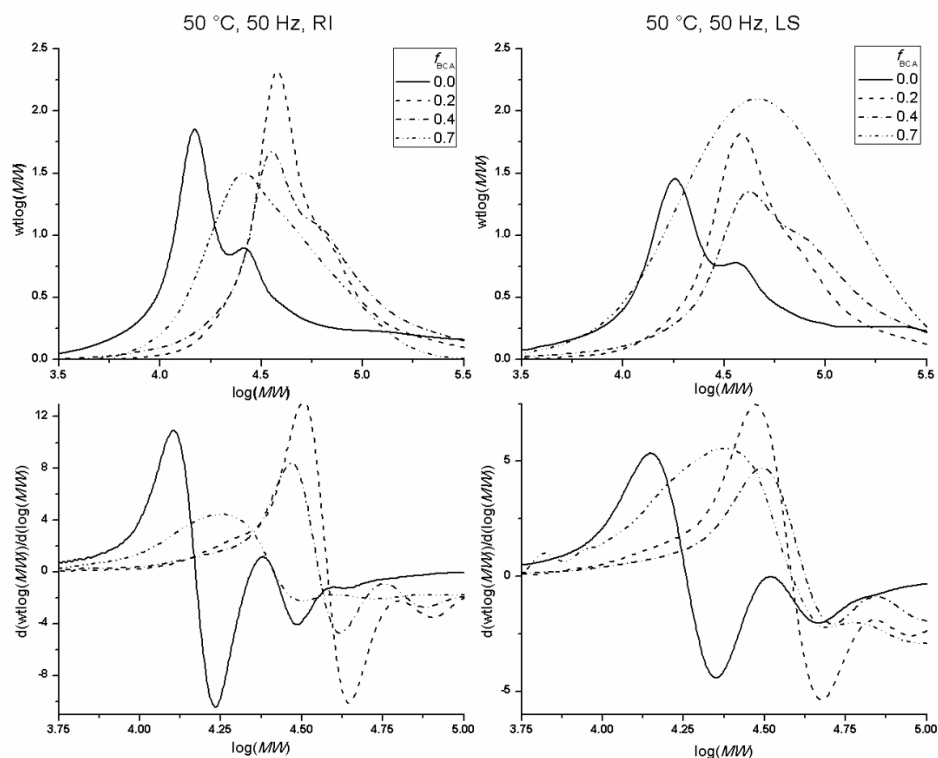
Figure 4.3: MMDs and 1st derivative plots from RI and LS detectors for BCA/MMA bulk PLP experiments at 50 °C and 50 Hz with 1 v% DCAA and 5 mmol·L⁻¹ DMPA photoinitiator. PLP polymer isolation was performed with MeOH containing 5 v% MAA at room temperature.

This compromise inevitably led to the appearance of contaminant PBCA in the SEC traces, and therefore reliable $k_{p,cop}$ estimation could not be made for samples produced from BCA compositions greater than $f_{BCA}=0.85$.

Individual $k_{p,cop}$ estimates were deemed reliable only if the ratio of secondary to primary inflection point (L_2/L_1) was contained within the interval of 1.8–2.2 and if there was consistency between estimates made from the same composition yet different repetition rates (see Supporting Information). In general, repetition rates of 33 and 50 Hz led to MMDs with the best PLP structures, but for higher BCA content systems lower repetition rates were favorable. This observation is likely

related to the fact that lower repetition rates generate higher MW copolymer which facilitates an easier precipitation of the copolymer from residual monomer. Estimations for the $k_{p,cop}$ at f_{BCA}=0.93 could be inferred from the primary inflection point location amongst samples pulsed at different repetition rates, but lack of suitable L_2/L_1 for any of the samples makes them unreliable. As shown in the Supporting Information, no discernible PLP structure could be obtained from the bulk homopolymerization of BCA at 50 or 75 °C due to the rapid depolymerization of the PBCA backbone while awaiting injection into the THF-based SEC instrument.

Reliable $k_{p,cop}$ estimates from the SEC RI analysis of PLP-generated polymer produced by BCA/MMA bulk polymerizations at 50 °C are presented in Figure 4.4 as a function of comonomer composition. The excellent agreement between experiments performed in the laboratories of Queen's University and the Polymer Institute SAS further strengthens the reliability of the $k_{p,cop}$ data set for this experimentally challenging polymerization system. However, since a value of $k_{p,BCA}$ could not be obtained experimentally, it was estimated by fitting the $k_{p,cop}$ data to the Terminal Model with $k_{p,BCA}$ the only unknown parameter. The non-linear parameter estimation was done twice, using the two sets of reactivity ratios determined in Figure 4.1 as well as an average of the $k_{p,MMA}$ values measured in this work.

The shape of the $k_{p,cop}$ data is well-represented by both fits at the 95 % confidence level, with the corresponding estimates for bulk $k_{p,BCA}$ at 50 °C of 379±32 and 336±20 L·mol^{-1}·s^{-1}, when using Quantum Mechanics and experimentally-fit reactivity ratios, respectively. It is worth mentioning that as described in the literature,[29,30] QM calculations are more accurate for the prediction of relative rate coefficients than the prediction of absolute values. Therefore, to reduce uncertainty in the computational $k_{p,cop}$ plot, the computationally obtained propagation rate coefficients for the homopolymerization of MMA and BCA were not used; the experimental values for $k_{p,MMA}$ and $k_{p,BCA}$ (fitted using the procedure described above) were used instead.
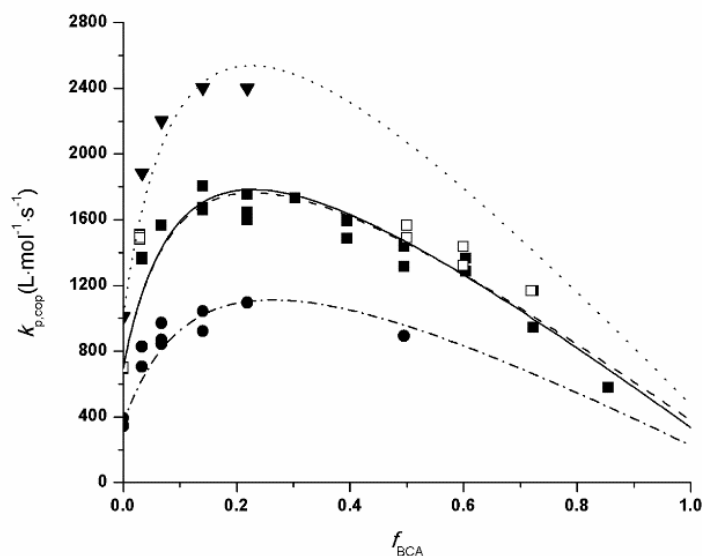
Figure 4.4: $k_{p,cop}$ **experimental estimates using RI detector output for bulk BCA/MMA copolymerizations with 1 v% DCAA and 5 mmol·L^{-1} DMPA. Experiments performed at 50 °C at Queen's University (■) and the Polymer Institute SAS (□) are fitted to the Terminal Model using reactivity ratios from Quantum Mechanics (solid line) of** r_{BCA}**=0.272 and** r_{MMA}**=0.057 as well as from experimental (dashed line) of** r_{BCA}**=0.236 and** r_{MMA}**=0.057. Experimental reactivity ratios are also used for Terminal Model fits to** $k_{p,cop}$ **using estimates made at 70°C (▼, dotted line) and 30 °C (●, dash-dotted line).**

It is well-known that the Terminal Model is not always able to simultaneously represent both the composition and propagation rate for binary copolymerization systems.[31,32] In the case of styrene/MMA copolymerization, the penultimate unit effect must be taken into account to accurately describe the moderately alternating system.[31] The more strongly alternating character of the BCA/MMA system indicates that a terminal BCA unit is generally only associated with a penultimate MMA unit and vice versa. While the Terminal Model reasonably describes both composition and $k_{p,cop}$ data over the experimentally accessible range ($f_{BCA}\leq 0.85$), it may be that some penultimate effects are hidden in our estimate for $k_{p,BCA}$, which was not available from independent experimentation.

The satisfactory fit of the Terminal Model at 50 °C prompted some additional $k_{p,cop}$ measurements at 30 and 70 °C which are also presented in Figure 4.4 along with their corresponding

Terminal Model fits. The confirmed invariance of BCA/MMA reactivity between 30 and 70 °C allowed the same extrapolation procedure used for the 50 °C data to be applied to the limited 30 and 70 °C data sets in order to estimate a value for $k_{p,BCA}$ of 226±32 L·mol^{-1}·s^{-1} and 475±95 L·mol^{-1}·s^{-1}, respectively. Unfortunately, due to the current inaccessibility of a direct measure for $k_{p,BCA}$, and the inherent uncertainty associated with the extrapolated estimates for $k_{p,BCA}$, the estimation of Arrhenius parameters for BCA was not attempted.

In Table 4.2, the extrapolated estimates of $k_{p,BCA}$ at 30, 50, and 70 °C are compared to the only other available ACA k_p estimate in the literature as well as the k_p estimates for other acrylic monomers differing in α-substituent. Although some of the k_p values are for monomers whose alkyl chain lengths are shorter than that of BCA, the results are still comparable, as an increase in alkyl chain length leads to only a slight increase in k_p for methacrylates.[28] To compensate for differences in experimental conditions and techniques, the k_p values of the α-substituted monomers are expressed relative to the k_p of their methacrylate analogs. Included in the table is the study of Yamada et al. that measured both $k_{p,ECA}$ and $k_{p,MMA}$ in bulk at 30 °C using the rotating sector method. Their results indicate that the RP of ECA is 3.6 times faster than MMA.[14] Although their finding is supported by the computational work of Değirmenci et al.,[17] in this work BCA is estimated to have a k_p approximately 50% lower than that of MMA between 30 and 70 °C. Despite the fact that these estimates for $k_{p,BCA}$ are extrapolated values, it is clear from the $k_{p,cop}$ data in Figure 4.4 that $k_{p,BCA}$ should be lower or similar to $k_{p,MMA}$, contrary to the previously published value of Yamada et al. for ECA.[14]

The two electron withdrawing groups, –CN and –COOR, which are responsible for the renowned reactivity of the anionic polymerization of ACAs, do not result in the same effect on the RP of BCA. The presence of these two electron withdrawing groups increases the lability of the hydrogen atom on the adjacent vinyl carbon leading to the generation of a stable and poorly reactive BCA radical, which can be inferred from the decreasing $k_{p,cop}$ measurements in Figure 4.4 towards

Table 4.2: Comparison of k_p for bulk BCA radical homopolymerization estimated in this work to other published values for ACAs and different α-substituted acrylic monomers.

Monomer	α-substituent	Medium	Temperature (°C)	$k_p/k_{p,\text{methacrylate}}$	k_p (L·mol^{-1}·s^{-1})	Ref.
n-butyl α-cyanoacrylate	–CN	Bulk	50	0.55 · MMA	379 ± 32	[a]
		Bulk	30	0.63 · MMA	226 ± 32	[b]
		Bulk	50	0.46 · MMA	336 ± 20	[b]
		Bulk	70	0.47 · MMA	475 ± 95	[b]
ethyl α-cyanoacrylate	–CN	Bulk	30	3.6 · MMA	1610-1622	14
n-butyl methacrylate	–CH$_3$	Bulk	50	-	753	33
n-butyl acrylate	–H	Bulk	52	39.5 · BMA	29774	34
ethyl α-hydroxy methacrylate	–CH$_2$OH	Solution	15	2.5-8.3·EMA	580-1860	35,36

[a,b] Fitted in this work using Quantum Mechanics and experimental reactivity ratios, respectively.

BCA-rich monomer mixture ($f_{\text{MMA}}<0.5$). Furthermore, it is likely that mutual repulsion between dipolar –CN groups further contributes to the increased difficulty of BCA homopropagation. On the other hand, compared to MMA radical homopropagation, the –CN electron-withdrawing substituent at the α-position clearly facilitates an elevated level of BCA monomer cross-propagation. This rapid cross-propagation is evidenced by the high $k_{p,\text{cop}}$ values for copolymerizations with initial compositions rich in MMA (i.e., for copolymerizations with $0.50 \leq f_{\text{MMA}} \leq 0.97$, the $k_{p,\text{cop}}$ is at least double the experimental $k_{p,\text{MMA}}$ value at 50 °C). Thus, it is clear that the identity of the α-substituent manifests special kinetic considerations beyond the typical acrylate RP kinetic scheme. An investigation aimed at solvent effects on the BCA/MMA copolymerization kinetics system could be useful to gain insight into the –CN group's dual impact on RP propagation kinetics, and to see if solvent choice can be used to further manipulate polymer final properties.

4.1.4 Conclusions

In this work, the PLP-SEC technique was applied to study the RP propagation kinetics of the n-butyl cyanoacrylate (BCA) and methyl methacrylate (MMA) copolymerization system in bulk at 30, 50, and 70 °C with 1 v% DCAA to suppress the anionic polymerization of BCA. Low-conversion RP-generated copolymers were successfully isolated without inducing the rapid anionic polymerization of residual BCA monomer using methanol containing 5 v% methacrylic acid at room temperature. This procedure enabled an accurate and highly reproducible ^{1}H NMR copolymer composition analysis for copolymers produced from initial monomer compositions up to f_{BCA}=0.85. A Mayo-Lewis plot was constructed and fitted to the 50 °C data with reactivity ratio estimates of r_{BCA}=0.236±0.042 and r_{MMA}=0.057±0.008, in excellent agreement with the experimental copolymer composition data at 30 and 70 °C as well as the values (r_{BCA}=0.272 and r_{MMA}=0.057) predicted by Quantum Mechanics at 50 °C. This confirms and clarifies that BCA/MMA copolymerization is well-represented by the Terminal Model as a strongly alternating system over the 30-70 °C temperature range.

Reliable estimates for bulk $k_{p,cop}$ at 50 °C were determined from low-conversion PLP experiments as a function of comonomer composition (up to f_{BCA}=0.85) with excellent agreement between estimates made from RI and LS detectors as well as samples produced from the same composition at different repetition rates. Since a direct estimate for $k_{p,BCA}$ could not be obtained experimentally, the $k_{p,cop}$ data were fitted to the terminal model using reactivity ratios predicted by Quantum Mechanics and determined by experimental composition analysis to extrapolate estimates for bulk $k_{p.BCA}$ at 50 °C of 379±32 L·mol^{-1}·s^{-1} and 336±20 L·mol^{-1}·s^{-1}, respectively. These results, supported by smaller sets of $k_{p,cop}$ experiments performed at 30 and 70 °C, indicate that $k_{p,BCA}$ is about 50 % the value of $k_{p,MMA}$, contrary to the previously published value of 3.6·$k_{p,MMA}$ for $k_{p,ECA}$ at 30 °C.[14] This detailed investigation of the RP kinetics for BCA/MMA copolymerization has not

only updated our understanding of ACA systems in general, but has also demonstrated that a high level of control over MW and degradation can now be achieved.

4.2 HEMA-PCL$_n$/MMA

Abstract

The radical copolymerization propagation kinetics of MMA/HEMA-PCL$_n$ in bulk are studied by PLP at 50 °C. Bulk MMA/HEMA-PCL$_n$ reactivity ratios are determined to be near unity, while poor solubility of the HEMA-PCL$_n$ homopolymer precludes a direct estimate of its bulk k_p. However, the apparent linear increase in $k_{p,cop}$ (for w_{macro}=0-0.8) indicates that the k_p for HEMA-PCL$_3$ is at least $2.69 \cdot k_{p,MMA}$ because of its longer alkyl ester side chain and hydrogen bonding provided by its terminal hydroxyl. For w_{macro}=0.5, the small difference in $k_{p,cop}/k_{p,MMA}$ of 1.81 ± 0.09 and 1.86 ± 0.05 for n=2 and n=3 indicates that no further increase in methacrylate k_p is afforded by the additional grafted PCL unit.

4.2.1 Introduction

In the context of synthetic polymeric drug delivery systems, the use of copolymers allows for the improvement of final material properties.[37,38] For example, copolymers based on MMA and methacrylic acid, combined with others comonomers, are commonly used for drug encapsulation to produce pills for oral administration because the copolymer exhibits swelling behavior at different biological pH.[38-40]

In this work, a copolymer system based on MMA and a recently reported macromonomer of 2-hydroxyethyl methacrylate (HEMA) functionalized with n ε-caprolactone (CL) units, termed HEMA-PCL$_n$, is studied. After macromonomer RP, these grafted PCL units have tunable hydrolytic degradation time when exposed to biological environment.[41] Copolymerization of HEMA-PCL$_n$ with MMA accesses a wider range of final polymer properties including degradation time, pH resistance, hydrophobicity, and mechanical resistance, as demonstrated by other copolymer systems based on MMA and PCL.[42-45] Therefore, the investigation of the copolymerization kinetics

50

of these macromonomers is essential to efficiently produce copolymers with the desired properties, such as MW and copolymer composition, which dictate polymer performance.

4.2.2 Experimental

Additional materials not listed by Section 4.1.2 include: HEMA-PCL$_2$ and HEMA-PCL$_3$ (n=2.4 and n=3.2 by ^{1}H NMR) synthesized according to Section 3.4. Acetone-d6 and diethyl ether were used as received from Sigma Aldrich.

Low-conversion bulk copolymerizations of MMA/HEMA-PCL$_n$ were conducted in the pulsed laser setup described in Section 4.1.2 at 50 °C with HEMA-PCL$_n$ weight fractions in the monomer mixture varied from 0 and 90 wt% using laser repetition rates of 10, 20, 25, and 33 Hz. Polymer samples produced from 0 to 10 wt% macromonomer were precipitated using MeOH, while higher macromonomer content polymers were precipitated using diethyl ether.

The SEC setup described in Section 3.3 was employed with polystyrene calibration. Both RI and LS output were interpreted using the literature calibration parameters listed in Table 4.3. (Macro)monomer densities were measured using a Paar DMA 48 Density Meter. In this study, LS output was less reliable than the RI output because of low signal response due to the low solubility of the copolymers in THF. However, when available, LS molecular weight results were used to verify the MW measurements from the RI detector. The dn/dc and Mark-Houwink parameters for poly(HEMA-PCL$_3$) were taken from a previous work,[41] and were also implemented for poly(HEMA-PCL$_2$) analyses.

Table 4.3: Parameters for calculation of $k_{p,cop}$ from SEC analysis in THF at 35 °C of PLP generated copolymer samples of MMA and HEMA-PCL$_n$.

Monomer	ρ at 50 °C (g·mL^{-1})	dn/dc (mL·g^{-1})	Mark–Houwink parameters	
			K (10^{-4}·dL·g^{-1})	a
Styrene[22]	-	0.1800	1.14	0.716
MMA[24]	0.908	0.089	0.944	0.719
HEMA-PCL$_2$[41]	1.0606	0.0627	2.00	0.571
HEMA-PCL$_3$[41]	1.066	0.0627	2.00	0.571

4.2.3 Results and Discussion

Copolymer Composition

^{1}H NMR was used to estimate the composition of MMA/HEMA-PCL$_3$ and MMA/HEMA-PCL$_2$ copolymers produced by PLP at 50 °C over a range of initial comonomer compositions. Full details of peak assignments and copolymer composition analysis are presented as Supporting Information. There was increased uncertainty in determining the composition of copolymers produced with higher macromonomer content (f_{macro}>0.25; w_{macro}>0.6) due to reduced polymer solubility and poor peak separation. Figure 4.5 plots the copolymer composition for both n=2 and n=3 MMA/HEMA-PCL$_n$ systems, where each comonomer composition produced from 0 to 60 wt% macromonomer was successfully verified by at least two independent experiments. Because of the large difference in MMA (100 g·mol^{-1}) and macromonomer average molar masses (HEMA-PCL$_2$=358 g·mol^{-1}, HEMA-PCL$_3$=473 g·mol^{-1}), the data are presented both on a weight fraction composition basis as well as a molar composition basis (i.e., a Mayo-Lewis plot).
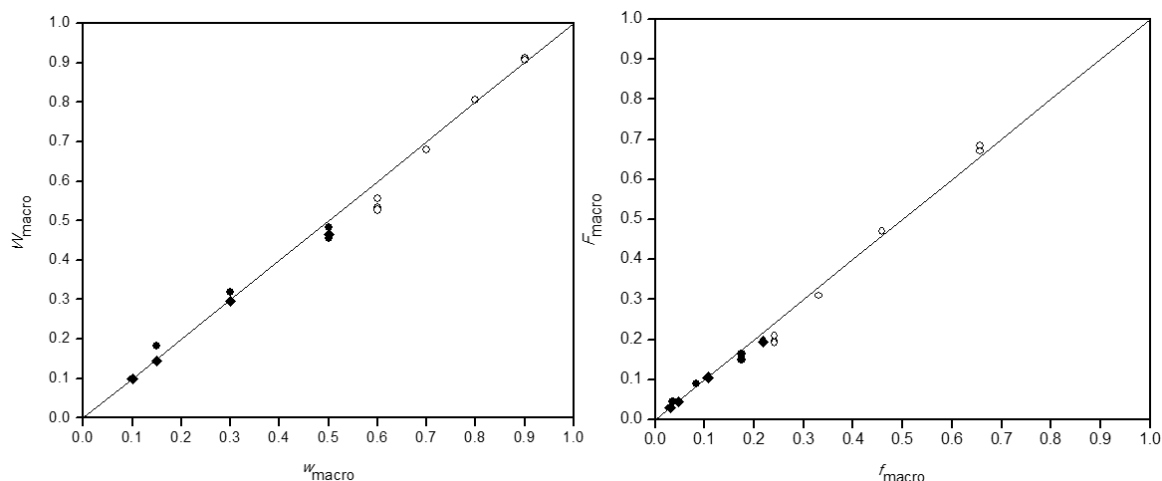
Figure 4.5: Weight fraction HEMA-PCL$_n$ in copolymer (W_{macro}) vs weight fraction in comonomer (left panel) and mole fraction HEMA-PCL$_n$ in copolymer (F_{macro}) vs mole fraction in comonomer (right panel) for bulk radical copolymerization of MMA/HEMA-PCL$_n$ at 50 °C for macromonomer with n=2 (♦) and n=3 (●). Estimates from high initial HEMA-PCL$_3$ compositions (○) are included albeit with reduced reliability.

For both chain lengths $n=2$ and $n=3$ the copolymer composition does not vary greatly from the comonomer composition for macromonomer contents of up to 50 wt% (22 and 17 mol%, respectively). At greater HEMA-PCL$_n$ fractions, the data remain close to the diagonal indicating that the reactivity ratios for both MMA and HEMA-PCL$_n$ are near unity. However, given the difficulty in estimating copolymer composition for samples with high macromonomer content, there is significant uncertainty in these estimates. What can be safely concluded is that copolymer composition is very close to comonomer composition in the composition range of interest for this work ($w_{macro} \leq 0.5$). Thus, there will be negligible composition drift over the course of a batch copolymerization. This behavior is expected as seen in previous works in which the composition of MMA and dodecyl methacrylate (DMA) copolymerized at 60 °C was described by $r_{MMA}=1.216\pm0.140$ and $r_{DMA}=0.837\pm0.100$,[46] and copolymerization of MMA and ethyl methacrylate (EMA) at 60 °C was represented by $r_{MMA}=1.09\pm0.1$ and $r_{EMA}=0.98\pm0.1$.[47] These examples all support the observation that methacrylates copolymerize with equal addition probabilities.

Copolymer-Averaged Propagation Rate Coefficient Estimation

A series of MMA/HEMA-PCL$_2$ and MMA/HEMA-PCL$_3$ low conversion bulk copolymerizations were performed at 50 °C with various initial (macro)monomer compositions. The experiments were conducted at laser repetition rates between 10-33 Hz, but only samples pulsed at 10, 20, and 25 Hz generated adequate PLP structures from which reliable $k_{p,cop}$ estimations can be made.[27] The $k_{p,cop}$ was estimated for each system using the primary inflection point of the MMD. Figure 4.6 shows a set of typical MMDs and corresponding first derivative plots, while the specific operating conditions of each experiment are summarized in the Supporting Information.

The $k_{p,cop}$ estimates from the RI detector were only included if the MW of the secondary inflection point was twice that of the primary inflection point. The $k_{p,cop}$ values estimated from LS
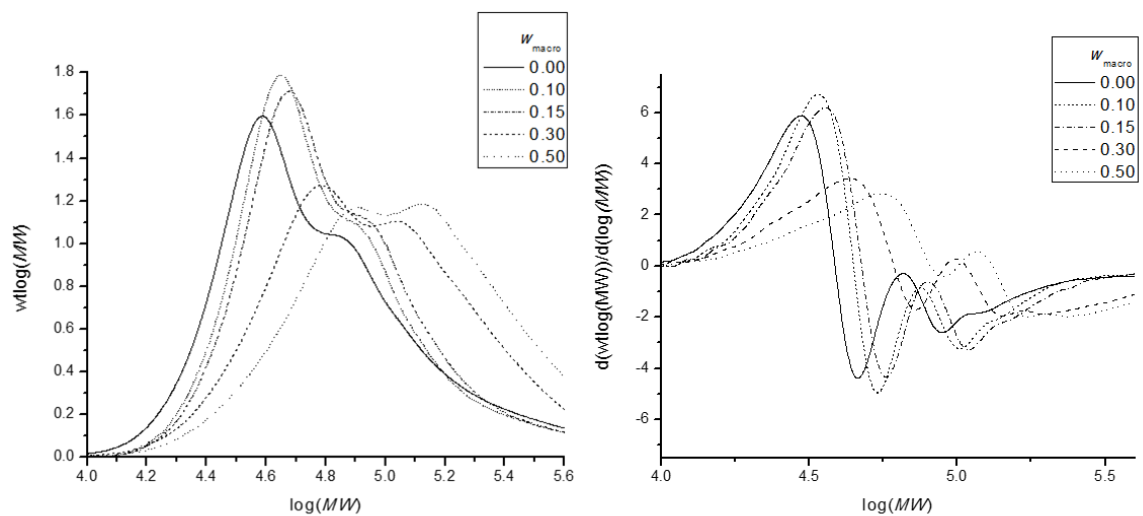
Figure 4.6: MMDs (left) and corresponding first derivative (right) plots from RI output for copolymers generated from various initial compositions of bulk MMA/HEMA-PCL$_3$ mixtures at 50 °C and a pulse repetition rate of 20 Hz.
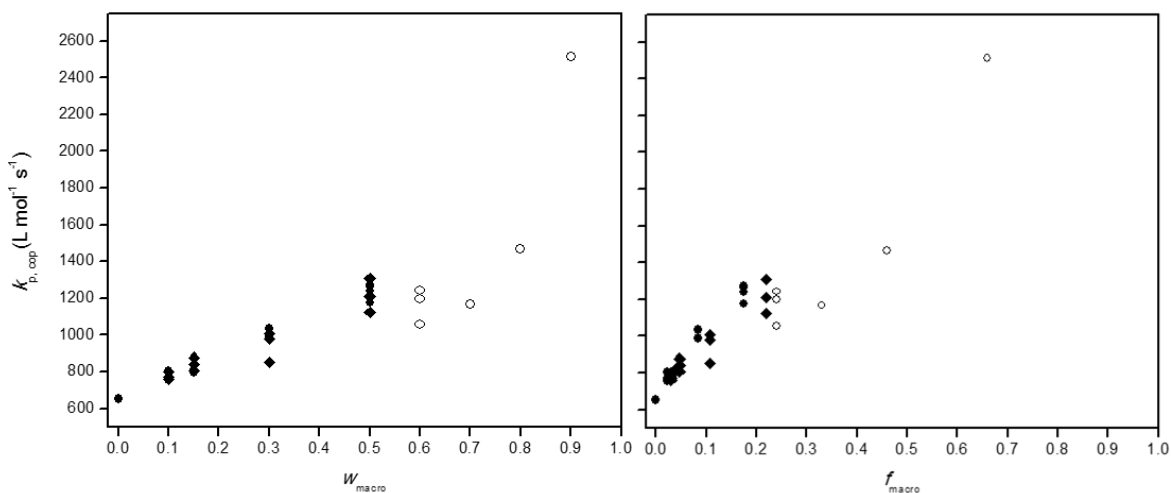
Figure 4.7: Plot of $k_{p,cop}$ calculated from RI detector output vs the initial weight fraction (left) and initial mole fraction (right) of HEMA-PCL$_n$ macromonomer with n=2 (♦) and n=3 (●) copolymerized with MMA at 50 °C in bulk. Estimates from high initial HEMA-PCL$_3$ compositions (○) are included albeit with reduced reliability.

output were usually within 25 % of the value estimated from the RI output, but showed significant scatter in some cases due to low copolymer solubility in THF. Further details of the $k_{p,cop}$ analyses are summarized in the Supporting Information. The $k_{p,cop}$ results for bulk MMA/HEMA-PCL$_3$ and MMA/HEMA-PCL$_2$ systems pulsed at 50 °C are presented in Figure 4.7. The data are plotted as a function of both weight (left) and mole (right) fraction of macromonomer in the monomer mixture.

On a molar basis, there is no significant difference in $k_{p,cop}$ between the HEMA-PCL$_2$ and HEMA-PCL$_3$ copolymerizations; however, on a weight fraction basis, $k_{p,cop}$ values for HEMA-PCL$_2$ are slightly higher than the corresponding for HEMA-PCL$_3$. There is a clear increase in the copolymer-averaged propagation rate coefficient from the MMA homopolymer values; the latter varied between 600 L·mol^{-1}·s^{-1} and 700 L·mol^{-1}·s^{-1}, in good agreement with the best-fit value of 648 L·mol^{-1}·s^{-1} at 50 °C reported from an IUPAC benchmark study.[19] Further experiments were performed to measure the $k_{p,cop}$ for bulk MMA/HEMA-PCL$_3$ system with 70-100 wt% initial macromonomer composition in the feed, but limited polymer solubility in THF made the samples difficult to analyze by SEC (see the Supporting Information for PLP structure of these high macromonomer content copolymers). These data points are included in the plot, but are of reduced reliability. The data presented in Figure 4.7 were determined from three different sets of experiments conducted over a span of several months. To reduce the variation introduced by SEC calibrations, the $k_{p,cop}$ values have been ratioed to the corresponding $k_{p,MMA}$ value measured at the same conditions and in the same experimental set; these ratios are summarized in Table 4.4 and plotted in Figure 4.8. At macromonomer content of 50 wt%, $k_{p,cop}$ values are 80-90 % higher than $k_{p,MMA}$. This increase is substantial, considering that 50 wt% HEMA-PCL$_n$ corresponds to a much lower macromonomer content on a molar basis; $f_{HEMA-PCL3}$=0.17 and $f_{HEMA-PCL2}$=0.22.

Table 4.4: Average increase of $k_{p,cop}$ over $k_{p,MMA}$ estimated from RI output for $n=2$ and $n=3$ MMA/HEMA-PCL$_n$ bulk copolymerizations at 50 °C, with N the number of results included.

w_{macro}	$n=3$		$n=2$	
	$k_{p,cop}/k_{p,MMA}$ $(L \cdot mol^{-1} \cdot s^{-1})$	N	$k_{p,cop}/k_{p,MMA}$ $(L \cdot mol^{-1} \cdot s^{-1})$	N
0	1.00	11	1.00	11
0.10	1.17 ± 0.02	5	1.15 ± 0.03	3
0.15	1.21 ± 0.01	3	1.22 ± 0.08	3
0.30	1.52 ± 0.07	4	1.50 ± 0.03	3
0.50	1.86 ± 0.05	4	1.81±0.09	3
0.60	1.99 ± 0.11	3	-	-

As shown in Figure 4.8, for w_{macro}=0-0.8 the increase in $k_{p,cop}$ is relatively linear with composition, with a R^2=0.97 when a linear fit is applied. Thus, the ratio of HEMA-PCL$_n$ homopropagation to MMA homopropagation can be roughly estimated by extrapolating the data to a value of 2.69 for $k_{p,macro}/k_{p,MMA}$. Note, however, that this extrapolation is significantly below the data point obtained for copolymerization with 90 wt% HEMA-PCL$_3$. Although this point has high uncertainty, it indicates that the extrapolated value of 1740 $L \cdot mol^{-1} \cdot s^{-1}$ for HEMA-PCL$_3$ homopropagation may underestimate the true value. The increase in macromonomer k_p relative to MMA can be ascribed to two effects that are well-documented in the literature. The first is the systematic increase in k_p of methacrylates with increasing alkyl length. At 50 °C there is a 47% increase in k_p of bulk DMA over MMA due to the extended length of the alkyl ester side chain.[28] Siegmann et. al. documented an increase of only 15% for ethyl ether methacrylate (EEMA; MW=158 $g \cdot mol^{-1}$) compared to MMA for bulk polymerizations at 25 °C, but a corresponding increase in k_p of 70% for the PEGylated methacrylate monomer polyethylene glycol ethyl ether methacrylate (PEGEEMA; MW=246 $g \cdot mol^{-1}$).[48] Therefore, upon consideration of these two examples, the length of the ester side chain of HEMA-PCL$_n$ must contribute to the observed increase in $k_{p,cop}$.

Secondly, hydrogen bonding has been shown to significantly increase the reactivity of 2-hydroxyethyl methacrylate (HEMA) in bulk copolymerization conditions compared to alkyl methacrylates of similar MW.[49] The k_p of HEMA at 50 °C is 3.96 times larger than that of MMA,[50] a result attributed to a specific hydrogen bonding interaction between HEMA's hydroxyl and methacryloyl carbonyl groups which reduce the electron density at the double bond, making it more reactive towards radical addition.[49] In this work, the effect of hydrogen bonding is most likely diluted compared to HEMA, as the HEMA-PCL$_n$ contains only one terminal hydroxyl group capable of providing hydrogen bonding whereas there are $n+1$ carbonyls capable of accepting hydrogen bonding. Thus, it seems reasonable that the increase in bulk $k_{p,macro}$ relative to $k_{p,MMA}$ should be less than that of bulk HEMA yet larger than that of the bulk PEGylated methacrylate system, which is not capable of hydrogen bonding.
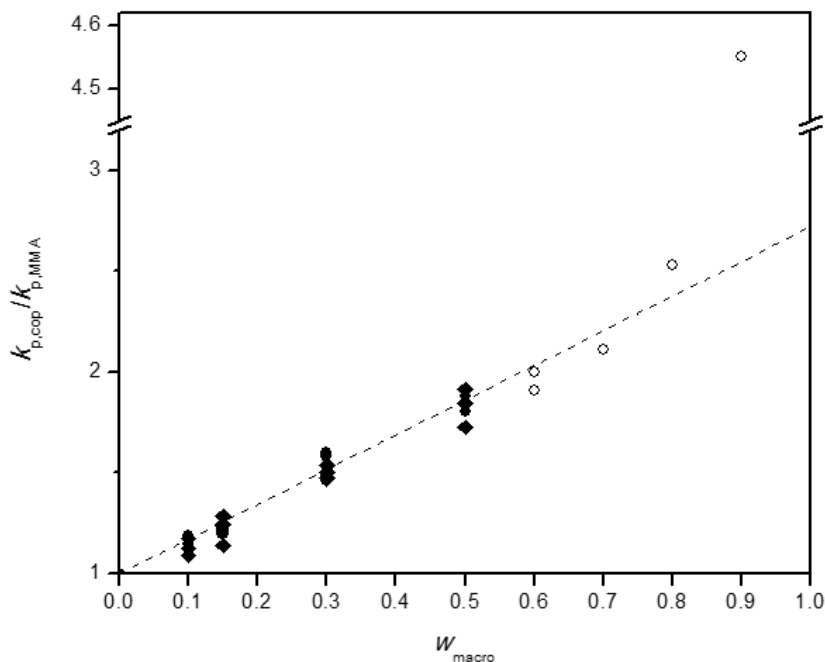
Figure 4.8: Plot of $k_{p,cop}$ calculated from RI detector output vs the initial weight fraction of HEMA-PCL$_n$ macromonomer with $n=2$ (♦) and $n=3$ (●) copolymerized with MMA at 50 °C in bulk. Estimates from high initial HEMA-PCL$_3$ compositions (○) are included albeit with reduced reliability. A line of best fit (- - -) is applied to the $n=3$ system, using data from $0 \leq w_{macro} \leq 0.8$, with $R^2=0.97$ to extrapolate a value for the macromonomer homopropagation rate coefficient of $2.69 \cdot k_{p,MMA}$.

4.2.4 Conclusions

A series of PLP-SEC experiments were successfully conducted at 50 °C for bulk MMA/HEMA-PCL$_2$ and MMA/HEMA-PCL$_3$ systems with initial monomer compositions varied from 0 to 90 wt% macromonomer. Copolymer composition analysis by ^{1}H NMR was reliable for copolymers generated from 0-50 wt% macromonomer, while analysis of higher macromonomer content copolymers was of reduced reliability due to lower copolymer solubility. Nevertheless, as is typical for methacrylate/methacrylate copolymerization systems, for $w_{macro}\leq0.5$, the bulk reactivity ratios can be safely assumed to be near unity.

The significant increases in $k_{p,cop}$ over $k_{p,MMA}$ documented for all macromonomer copolymerizations is due to both the larger size of ester side chain and the effect of hydrogen bonding (provided by the terminal hydroxyl of HEMA-PCL$_n$) to promote methacrylate reactivity. At 50 wt% macromonomer in the feed, a 1.81±0.09 and 1.86±0.05 increase in $k_{p,cop}/k_{p,MMA}$ was determined for the n=2 and n=3 cases, respectively, which indicates that further increasing the average number of grafted PCL units in the methacrylate ester side chain from 2 to 3 has minimal influence on HEMA-PCL$_n$ propagation behavior. Although bulk $k_{p,cop}$ estimates made for monomer mixtures with initial macromonomer content greater than 50 wt% were of reduced reliability, the data are well-represented by a linear relationship over the 0-80 wt% macromonomer composition range for both n=2 and n=3 copolymerization systems. Moreover, the insolubility of HEMA-PCL$_n$ homopolymer in THF precluded a direct estimate for its k_p. Instead, a value of $2.69 \cdot k_{p,MMA}$ for k_p of HEMA-PCL$_3$ at 50 °C was extrapolated from the $k_{p,cop}/k_{p,MMA}$ data; however, this is likely an underestimation of the true value. Thus, Chapter 5 is devoted to overcoming experimental challenges which limited the study of macromonomer propagation kinetics encountered in this work.

4.3 References

(1)   C. Limouzin, A. Caviggia, F. Ganachaud and P. Hémery, *Macromolecules* **2003**, *36*, 667.

(2)   M. Dossi, G. Storti and D. Moscatelli, *Macromol. Symp.* **2010**, *289*, 124.

(3)   E. M. Petrie, *Handbook of Adhesives & Sealants*; Mcgraw-hill, 1999.

(4)   F. Elias, M. T. Peracchia and P. Couvreur, *Handbook of Biodegradable Polymers*; CRC Press: 1998.

(5)   P. Couvreur, B. Kante, M. Roland and P. Speiser, *J. Pharm. Sci.* **1979**, *68*, 1521.

(6)   A. Graf, A. McDowell and T. Rades, *Expert Opin. Drug Del.* **2009**, *6*, 371.

(7)   J. Nicolas and P. Couvreur, *Wiley Interdiscip. Rev. Nanomed. and Nanobiotechnol.* **2009**, *1*, 111.

(8)   P. Couvreur, B. Kante, M. Roland, P. Guiot, P. Bauduin and P. Speiser, *J. Pharm. Pharmacol.* **1979**, *31*, 331.

(9)   M. G. Han, S. Kim and S. X. Liu, *Polym. Degrad. Stab.* **2008**, *93*, 1243.

(10)   D. R. Robello, T. D. Eldridge and M. T. Swanson, *J. Polym. Sci., Part A: Polym. Chem.* **1999**, *37*, 4570.

(11)   B. Ryan and G. McCann, *Macromol. Rapid Commun.* **1996**, *17*, 217.

(12)   M. G. Han and S. Kim, *Polymer* **2009**, *50*, 1270.

(13)   J. B. Kinsinger, J. R. Panchak, R. L. Kelso, J. S. Bartlett and R. K. Graham, *J. Appl. Polym. Sci.* **1965**, *9*, 429.

(14)   B. Yamada, M. Yoshioka and T. Otsu, *Makromol. Chem.* **1983**, *184*, 1025.

(15)   B. Yamada, T. Hayashi and T. Otsu, *J. Macromol. Sci. Pure Appl. Chem.* **1983**, *19*, 1023.

(16)   B. Yamada, T. Kontani, M. Yoshioka and T. Otsu, *J. Polym. Sci., Part A: Polym. Chem.* **1984**, *22*, 2381.

(17)   I. Değirmenci, V. Aviyente, V. Van Speybroeck and M. Waroquier, *Macromolecules* **2009**, *42*, 3033.

(18)   A. J. Canale, W. E. Goode, J. B. Kinsinger, J. R. Panchak, R. L. Kelso, and R. K. Graham, *J. Appl. Polym. Sci.* **1960**, *4*, 231.

(19)   S. Beuermann, M. Buback, T. P. Davis, R. G. Gilbert, R. A. Hutchinson, O. F. Olaj, G. T. Russell, J. Schweer and A. M. van Herk, *Macromol. Chem. Phys.* **1997**, *198*, 1545.

(21)   A. P. Haehnel, M. Stach, A. Chovancova, J. M. Rueb, G. Delaittre, A. M. Misske, I. Lacik and C. Barner-Kowollik, *Polym. Chem.* **2014**, *5*, 862.

(22)   Hutchinson, R. A.; Paquet, D. A.; McMinn, J. H.; Beuermann, S.; Fuller, R. E.; Jackson, C. in *5th International Workshop on Polymer reaction Engineering*, DECHEMA Monographs Vol 131, ed. K.-H. Reichert and H.-U. Moritz, VCH Verlags, Weinheim Germany, **1995**, 467.

(23)   M. Dossi, K. Liang, R. A. Hutchinson and D. Moscatelli, *J. Phys. Chem. B* **2010**, *114*, 4213.

(24)   R. A. Hutchinson, J. H. McMinn, D. A. Paquet, S. Beuermann and C. Jackson, *Ind. Eng. Chem. Res.* **1997**, *36*, 1103.

(25)   E. F. Donnelly and D. C. Pepper, *Makromol. Chem., Rapid Commun.* **1981**, *2*, 439.

(26)   N. Markova, G. Ivanova, V. Enchev and M. Simeonova, *Struct. Chem.* **2012**, *23*, 815.

(27)   S. Beuermann and M. Buback, *Prog. Polym. Sci.* **2002**, *27*, 191.

(28)   S. Beuermann, M. Buback, T. P. Davis, R. G. Gilbert, R. A. Hutchinson, A. Kajiwara, B. Klumperman and G. T. Russell, *Macromol. Chem. Phys.* **2000**, *201*, 1355.

(29)   M. Dossi and D. Moscatelli, *Macromol. React. Eng.* **2012**, *6*, 74.

(30)   E. Mavroudakis, K. Liang, D. Moscatelli and R. A. Hutchinson, *Macromol. Chem. Phys.* **2012**, *213*, 1706.

(31)   T. Fukuda, Y. D. Ma and H. Inagaki, *Macromolecules* **1985**, *18*, 17.

(32)   M. D. Zammit, M. L. Coote, T. P. Davis and G. D. Willett, *Macromolecules* **1998**, *31*, 955.

(33)   S. Beuermann and M. Buback, *Pure Appl. Chem.* **1998**, *70*, 1415.

(34)   C. Barner-Kowollik, F. Günzler and T. Junkers, *Macromolecules* **2008**, *41*, 8971.

(35)   D. A. Morrison and T. P. Davis, *Macromol. Chem. Phys.* **2000**, *201*, 2128.

(36)   M. D. Zammit, M. L. Coote, T. P. Davis and G. D. Willett, *Macromolecules* **1998**, *31*, 955.

(37)   M. L. Adams, A. Lavasanifar, G. S. Kwon, *J. Pharm. Sci.* **2003,** *92*, 1343.

(38)   L. M. Ensign, R. Cone, J. Hanes, *Adv. Drug Deliv. Rev.* **2012,** *64*, 557.

(39)   G. Fundueanu, M. Constantin, C. Stanciu, G. Theodoridis, P. Ascenzi, *J. Mater. Sci.-Mater. Med.* **2009,** *20*, 2465.

(40)   M. A. Trojer, A. Wendel, K. Holmberg, M. Nyden, *J. Colloid Interface Sci.* **2012,** *375*, 213.

(41)   R. Ferrari, Y. C. Yu, M. Morbidelli, R. A. Hutchinson, D. Moscatelli, *Macromolecules* **2011,** *44*, 9205.

(42)   M. G. Han, S. Kim, *Polymer* **2009,** *50*, 1270.

(43)   L. Zheng, C. Li, Z. Wang, J. Wang, Y. Xiao, D. Zhang, G. Guan, *Ind. Eng. Chem. Res.* **2012,** *51*, 7264.

(44)   T. K. Dash, V. B. Konkimalla, *J. Control. Release* **2012,** *158*, 15.

(45)   J. Xu, H. Yang, G. Zhang, *Macromol. Chem. Phys.* **2013,** *214*, 378.

(46)   G. A. Stahl, *J. Polym. Sci., Polym. Chem. Ed.* **1979,** *17*, 1883.

(47)   N. Grassie, B. J. D. Torrance, J. D. Fortune, J. D. Gemmell, *Polymer* **1965,** *6*, 653.

(48)   R. Siegmann, A. Jelicic, S. Beuermann, *Macromol. Chem. Phys.* **2010,** *211*, 546.

(49)   K. Liang, M. Dossi, D. Moscatelli, R. A. Hutchinson, *Macromolecules* **2009,** *42*, 7736.

(50)   M. Buback, C. H. Kurz, *Macromol. Chem. Phys.* **1998,** *199*, 2301.

Chapter 5

Polylactic Acid Macromonomer Radical Propagation Kinetics and Degradation Behavior

Preface

There were two motivations for the work performed in this Chapter. Firstly, the study of propagation kinetics for hydroxyl terminated macromonomers detailed by Chapter 4 was limited due to poor solubility of the produced comb-polymers in any solvent. As a result, I was not able to conclusively achieve my objective of assessing the propagation rate coefficient (k_p) behavior as a function of the average number of polyester units per macromonomer chain. Thus, I synthesized the new family of macromonomer materials, termed PLA$_N$EMA, whose terminal ethyl ester group ensures complete solubility of the resulting comb-polymers in the SEC eluent, THF. Secondly, for nanoparticles (NP) produced by emulsion RP of short-chain polyester macromonomers, the dependence of NP hydrolytic degradation time on the average number and type of polyester units has been well-documented. Therefore, I wanted to determine to what extent end-group functionality of PLA$_N$EMA macromonomers can be used to provide another means to tune NP degradation time for homopolymer and copolymer systems. This study is presented in manuscript format as it was recently accepted as a full paper to Reaction Chemistry & Engineering.

Abstract

Polylactic acid ethyl ester methacrylate (PLA$_N$EMA) macromonomers are synthesized with N=1, 5, 7, and 9 average number of polyester units. While propagation rate coefficients (k_p) determined by pulsed laser polymerization experiments for bulk PLA$_1$EMA and PLA$_5$EMA are not significantly different over the 40–100 °C temperature range, they are elevated by 60% compared to methyl methacrylate at 50 °C, indicating that the nature of substituents several units beyond the methacrylic group does not decisively impact bulk k_p measurements. Compared to bulk PLA$_5$EMA, the apparent k_p in 75 wt% n-butanol solution is enhanced due to hydrogen bonding, whereas in 75 wt% dimethylformamide solution it is reduced by 35% because of differences in macromonomer and solvent molar volumes. The PLA$_5$EMA macromonomers are used to produce nanoparticles (NP) by emulsion radical polymerization that degrade almost four times more slowly than NPs produced from their hydroxyl terminated macromonomer counterpart.

5.1 Introduction

Polylactic acid (PLA) is a highly versatile material produced from 100% renewable resources with an auspicious outlook for a variety of commodity applications.[1] Indeed, packaging, disposable bottles, and biomedical applications benefit from one of PLA's most notable features: hydrolysis of the polyester backbone to yield non-toxic degradation products.[2,3] Production of PLA can be accomplished via the polycondensation of lactic acid; however, difficulties associated with efficient removal of the liberated water limit the molecular weight (MW) that can be achieved by this route.[4] Thus, most approaches focus on the ring-opening polymerization (ROP) of the cyclic lactide (LA) dimer which allows for better control over PLA's MW characteristics.[5] In addition, functional ROP initiators can be implemented to impart customized features onto the final polyester material.[6-8]

When 2-hydroxyethyl methacrylate (HEMA) is used as ROP initiator, the resulting HEMA-PLA$_{2n}$ macromonomers, with average chain length $2n$ defined by the stoichiometric ratio of LA to HEMA, can be further polymerized via "grafting through" radical polymerization (RP) of

the vinyl end-group to produce comb-polymers with well-defined polyester grafts affixed to a higher MW acrylic backbone.[9-11] Such HEMA-PLA$_{2n}$ macromonomers have been employed in radical miniemulsion polymerization,[12,13] solution polymerization to make hydrogels,[14] and emulsion polymerization to produce degradable nanoparticles (NP) for drug delivery applications.[15-17] In the case of NPs, degradation time is controllable by the type and average number n (typically n=1-5) of grafted polyesters, a feature that causes distinct changes in material hydrophobicity which can be exploited for various applications.[15,18] As bulk erosion can be assumed for PLA hydrolysis of nanoscale materials,[19] degradation of the PLA grafts in NPs produced from macromonomers can be compared to the solution hydrolysis of PLA oligomers which is not only influenced by factors such as temperature and pH,[20,21] but also chain length due to the difference in reactivity of backbone and terminal esters.[22] Terminal ester hydrolysis, via preferential backbiting or chain-end scission mechanisms, is facilitated by the terminal hydroxyl group[23] and was found to be chain-length independent.[24] For backbiting (or preferential chain-end scission) to be effective, the terminal hydroxyl groups must be accessible to the aqueous environment;[20] in general, the balance of water diffusion and PLA degradation behavior depends on material dimensions and topology (e.g., surface brushes, bulk, solution) which are governed by the intended application and method of production. Thus, to efficiently produce and to better predict degradation performance of polyester macromonomer based comb-(co)polymer materials, an understanding of the underlying macromonomer RP kinetics is required to track both hydroxyl end-group and macromonomer chain length incorporation behaviors.

To date, few works have addressed the RP kinetics of methacrylate type polyester macromonomers. Although studied under limited conditions, typical methacrylate/methacrylate relative reactivity – i.e., equal addition probabilities – was demonstrated for HEMA-PLA$_{2n}$ and polycaprolactone (PCL) based HEMA-PCL$_n$ macromonomer copolymerizations with methyl methacrylate (MMA),[25-27] while another study detailing the copolymerization of styrene (ST) with

polyester methacrylate type macromonomers showed that the relative reactivity depends only on the chemical identity up to several units away from the methacryloyl end-group.[28] In terms of propagation rate behavior, the pulsed laser polymerization coupled with size exclusion chromatography (PLP-SEC) technique is the most accurate and reliable method for determining propagation rate coefficients (k_p), as is described in comprehensive detail by Beuermann and Buback.[29] The k_p is calculated according to Eqn. 5.1 where MW_i is the MW of the ith inflection point of a low-conversion PLP-generated molar mass distribution (MMD), ϕ_{mon} is the volume fraction of monomer in solution, ρ_{mon} is the monomer density, and t_0 is the time between pulses.

$$k_p = \frac{MW_i}{i \cdot \phi_{mon} \cdot \rho_{mon} \cdot t_0} \tag{5.1}$$

The IUPAC *subcommittee on "Modeling of Polymerization Kinetics and Processes"* has established family type behavior for MMA, ethyl methacrylate (EMA), *n*-butyl methacrylate (BMA), and dodecyl methacrylate (DMA),[30,31] where an increase in the length of the linear alkyl ester group correlates to an increase in the value of k_p measured for bulk monomer using the PLP-SEC technique; this trend is reported more recently to extend even up to behenyl methacrylate.[32] A similar increase in bulk k_p with increasing ester side chain length was reported for polyethylene glycol ethyl ether methacrylate (PEGEEMA, 3 PEG units) compared to EEMA (1 PEG unit),[33] although another study found no additional increase in bulk k_p for polyethylene glycol methyl ether methacrylate (PEGMA, 7-8 PEG units) at similar temperatures.[34] For the polyester macromonomer systems of interest in this study, the estimation of k_p could not be completed for hydroxyl-terminated HEMA-PCL$_3$ because of the poor solubility of the resulting comb-polymer in tetrahydrofuran (THF), the SEC eluent; nonetheless, bulk copolymerizations with up to 50 wt% MMA indicated no significant differences in copolymer propagation rate coefficient ($k_{p,cop}$) for HEMA-PCL$_n$ with average chain length $n=2$ and $n=3$.[27]

Since macromonomers are inherently viscous (some even solid at room temperature) their solution propagation behavior is also of high practical and technical importance. The influences of

65

solvent on propagation kinetics are extensive and can arise from both specific and non-specific interactions between monomer and solvent.[35] For example, at a monomer concentration of 0.8 mol·L^{-1} in n-butanol (BuOH), the k_p of BMA is enhanced by as much as 85% because of the well-documented hydrogen bond formation between hydroxyl and methacryloyl carbonyl which reduces the electron density at the double bond, making BMA more reactive towards radical addition.[36] On the other hand, differences between the molar volumes of monomer and solvent (V_{mon}–V_{sol}) can manifest as a competition for positions at the radical chain-end leading to a lower than or greater than analytical local monomer concentration and corresponding increase or decrease in apparent k_p measured by PLP-SEC, respectively.[35] Beuermann and Garcia substantiated this concept by establishing a linear relationship between V_{mon}–V_{sol} and the ratio of k_p at infinite dilution to bulk k_p (i.e., $k_{p,\infty}/k_{p,bulk}$) for a variety of monomer/solvent pairs contained within -100 cm^3·mol^{-1} $< V_{mon}$–$V_{sol} < 150$ cm^3·mol^{-1}.[37] In terms of macromonomers, this relationship was extended to PEGEEMA solution homopolymerizations in toluene (V_{mon}–$V_{sol} = 139$ cm^3·mol^{-1}) and THF (V_{mon}–$V_{sol} = 164$ cm^3·mol^{-1}), for which the apparent k_p at 25 °C in 80 vol% solvent was reduced by 32% and 53% compared to bulk, respectively.[33]

In this work, polylactic acid ethyl ester methacrylate (PLA$_N$EMA, where N average PLA units corresponds to $2n$+1 cyclic LA monomers in the ROP step because the ethyl 2-hydroxypropionate initiator fragment contributes 1 PLA unit to each macromonomer chain), was synthesized according to Scheme 5.1. As the alkyl end-group of PLA$_N$EMA ensures the resulting comb-polymer is THF soluble, the determination of macromonomer k_p is not hindered by solubility limitations, as is the case for hydroxyl-terminated HEMA-PCL$_n$ or HEMA-PLA$_{2n}$ macromonomers. Another benefit of the alkyl end-group is that PLA$_N$EMA can be copolymerized with HEMA-PLA$_{2n}$ to yield PLA-grafted comb-polymers with tunable hydroxyl group density (an important design parameter for post-polymerization modifications such as esterification reactions); however, the influence of the ethyl ester end-group on the hydrolytic degradability of PLA must be assessed.

66
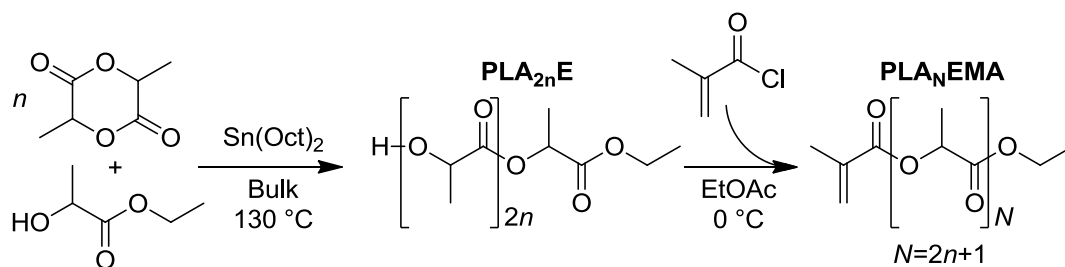
Scheme 5.1: Synthetic route for production of PLA$_N$EMA.

Therefore, this work investigates both the production and hydrolysis performance of PLA$_N$EMA-based comb-polymers. Firstly, PLA$_N$EMA homopropagation kinetics are studied in BuOH, dimethylformamide (DMF), and xylenes solutions, in addition to bulk, to examine the effects of hydrogen bonding and molar volumes on polyester macromonomer k_p. Secondly, PLA$_N$EMA macromonomers are used to produce NPs by emulsion radical polymerization in order to evaluate the influence of PLA$_N$EMA's ethyl ester end-group on the rate of NP hydrolytic degradation in comparison to NPs produced from hydroxyl-terminated HEMA-PLA$_{2n}$ macromonomers.

5.2 Experimental

Materials

All materials relevant to (macro)monomer syntheses and pulsed laser polymerization experiments are detailed by Chapters 3 and 4, respectively. The macromonomer syntheses of PLA$_1$EMA, PLA$_5$EMA, and HEMA-PLA$_5$ were performed according to the procedures detailed in Sections 3.4.1, 3.4.2, and 3.4.5 of Chapter 3, respectively.

Methyl methacrylate (MMA, 99%), ammonium persulfate (APS, >98%), *n*-butanol (BuOH, 99%), and dimethylformamide (DMF, 99.8%) were purchased from Sigma Aldrich and used as received. Xylenes (99.9%, Fisher Chemical), dichloromethane (DCM, 99.9%, Fisher Chemical), sodium dodecyl sulfate (SDS, ~99%, MP Biomedicals), chloroform-d (CDCl$_3$, 99.8% D, Sigma Aldrich), and dimethylsulfoxide-d6 (DMSO-d6, 99.9% D, Cambridge Isotope Laboratories) were used as received. All water used in this work was in-house distilled water that

was further purified (18.2 MΩ·cm) using a Millipore Synergy water purification system equipped with SynergyPak purification cartridges.

Pulsed Laser Polymerization

Low-conversion MMA, PLA$_1$EMA, and PLA$_5$EMA bulk as well as solution homopolymerizations in 75 wt% DMF, xylenes, and BuOH mixtures were conducted using the pulsed laser setup described by Chapter 4. Experiments were conducted using laser repetition rates between 5 and 50 Hz (see Table B.3-B.7 of the Appendix B for the exact operating conditions employed for each sample). The Waters SEC setup and procedure for measuring differential refractive indices (dn/dc) described in Chapter 3 were employed in this work. Parameters relevant to k_p determination are summarized by Table 5.1. The densities of MMA, PLA$_1$EMA, and xylenes were measured at temperatures between 25 and 70 °C using a Paar DMA 48 Density Meter, while the density of highly viscous PLA$_5$EMA was extrapolated from solution density measurements in xylenes, assuming volume additivity, as shown by Table B.1 in Appendix B.

Since PLA$_5$EMA is a distribution of macromonomers with an average of N=5.3 PLA units per chain, ^{1}H NMR analysis of several PLP-generated low-conversion poly(PLA$_5$EMA) comb-polymers was employed to confirm preservation of graft density into the comb-polymer (average N=5.0). SEC of low conversion polymers produced by PLP was also performed using a Viscotek

Table 5.1: Parameters for calculation of k_p from SEC analysis of PLP-generated samples of PLA$_N$EMA.

	ρ (g·mL^{-1})	[M] at 25 °C (mol·L^{-1})	dn/dc (mL·g^{-1})	Mark-Houwink parameters	
				K (10^{-5} dL·g^{-1})	a
MMA	0.9671–0.001117·T/°C	9.39	0.089[38]	9.44	0.719[39]
PLA$_1$EMA	1.0478–0.001048·T/°C	5.49	0.069	24.4	0.581
PLA$_5$EMA	1.1892–0.000956·T/°C[a]	2.46	0.055	7.52	0.647
Xylenes	0.8833–0.000876·T/°C	-	-	-	-
DMF[40]	0.9686–0.000958·T/°C[b]	-	-	-	-
BuOH[41]	0.8267–0.000809·T/°C[b]	-	-	-	-

[a] Pure species density extrapolated from xylenes solution assuming volume additivity.
[b] Independent regression of literature data.

270 max separation module with a RI, viscosity (IV), and LS (low and LALS and right angle

RALS) triple detector setup.

A set of two porous PolyAnalytik columns with an exclusion limit molecular weight of

$20 \cdot 10^6$ g·mol^{-1} was used in series at 40 °C with distilled THF as eluent at a flow rate of 1 mL·min^{-1}. The Mark-Houwink (MH) parameters for poly(PLA$_1$EMA) and poly(PLA$_5$EMA) homopolymers

in Table 5.1 were estimated as an average of the output from the IV and LS detectors (using dn/dc

summarized by Table 5.1) generated by several independent samples. The IV vs MW data for

poly(PLA$_1$EMA) and poly(PLA$_5$EMA) are included as Figure B.1 and Figure B.2 with global fits

presented in Figure B.3 of Appendix B.

5.2.1 NP Synthesis and Degradation Study

NP synthesis was carried out following a previously reported procedure with minor modification.[17]

In a 50 mL 3 neck round bottom flask equipped with condenser, 0.2 g SDS surfactant was dissolved

in 18 mL deionized water, heated to 70 °C, and further purged with nitrogen for 10 min. About 16

mg APS was dissolved in 2 mL deionized water and added to the purged solution. One gram of

macromonomer was dissolved in one gram of DCM and then the mixture was fed over one hour at

constant injection rate using syringe pump (PLA$_1$EMA was fed directly without DCM) under

constant flow of nitrogen. The reaction was allowed to proceed for one additional hour (two

additional hours for PLA$_5$EMA macromonomer systems). No coagulum was formed during the

emulsion polymerization of PLA$_1$EMA; however, a coagulum less than 8 wt% (relative to

macromonomer fed) was formed for the macromonomer systems, a result consistent with HEMA-

PLA$_5$ NP synthesis reported elsewhere.[17] While feeding the macromonomer over a one hour period

gives starved conditions for HEMA-PLA$_5$, macromonomer, droplets were observed throughout the

feeding period for the PLA$_5$EMA homopolymer and copolymer systems, an observation indicative

of the increased hydrophobicity of PLA$_N$EMA in comparison to HEMA-PLA$_5$ macromonomers.

The conversion of all systems was greater than 99% as estimated by concentrating 1 mL of latex

under constant air stream overnight and dissolving the solids in DMSO-d6 for ^{1}H NMR characterization.

The particle size distributions (PSD) for all four NP suspensions are presented in Figures B.5-B.8 where each PLA$_N$EMA (macro)monomer system exhibited a secondary peak near 4000 nm which continued to appear even after passing the latex multiple times through a 0.2 μm filter. Although less than 1% residual macromonomer was detected by ^{1}H NMR analysis of the final dried PLA$_5$EMA latex, longer reaction times as well as additional initiator and MMA shots at the end of the reaction were unsuccessful in removing the secondary peak. Despite its incomplete characterization or removal, this secondary peak accounts for less than 0.1 vol% of the PLA$_N$EMA NP systems, and therefore no further treatment was implemented. An accelerated degradation study was performed by maintaining NP latexes at 50 °C in an external water bath and periodically removing them for characterization, following procedures used previously.[42] The solution pH was measured using a Mettler Toledo SevenExcellence pH meter, while NP size and polydispersity indices (PDI) were determined with a Malvern Zetasizer Nano ZS (size range 0.3 nm –10 μm) at 25 °C with backscattering optics (173°), using a 4 mW He–Ne (633 nm) laser. All samples were measured in DTS0012 disposable cuvettes. The reported sizes represent an intensity average of at least 30 scans.

5.3 Results and Discussion

5.3.1 Bulk Homopropagation

PLP experiments were performed for bulk homopolymerizations of MMA (equivalent to PLA$_0$EMA), PLA$_1$EMA, and PLA$_5$EMA over a temperature range of 40–100 °C, with specific conditions summarized by Tables B.3, B.4, and B.6. As a highly viscous liquid, the PLA$_5$EMA macromonomer is characterized by the low-termination limit of the PLP-SEC technique;[43,44] therefore, to maximize the success of bulk PLA$_5$EMA PLP experiments, relatively low pulse repetition rates (10-33 Hz) were employed[43,44] and the total number of pulses was limited to 100.[45]

In conjunction with Tables B.4 and B.7, the MMDs and corresponding first derivative plots in Figure 5.1 demonstrate that bulk PLA$_N$EMA (both N=1 and N=5) homopolymerizations fulfil the PLP-SEC consistency criteria: at least two inflection points separated by a MW factor of 2 as well as good agreement between k_p estimations made from a minimum of two different pulse repetition rates under otherwise identical conditions.

As shown by the poly(PLA$_5$EMA) MMDs interpreted by universal calibration, the consequence of PLP experiments with lower pulse repetition rates is that higher MW polymer is produced which may exceed the calibration range of the SEC instrument; fortunately, the inflection point positions for all poly(PLA$_5$EMA) samples were well within the polyMMA calibration range such that k_p determination was not impeded. Universal calibration is applied throughout this work using MH parameters (Table 5.1) for poly(PLA$_1$EMA) and poly(PLA$_5$EMA) estimated by the Viscotek SEC (see Figure B.1 and B.2, respectively) over a MW range of approximately 25,000–160,000 g·mol^{-1} and 126,000–800,000 g·mol^{-1}, respectively. The intrinsic viscosity of the comb-like polymers at identical MW decreases as the graft length is increased from N=0 (PMMA), to N=1, and to N=5 (Figure B.3), following the trends seen for calibrations established for polyMMA to polyDMA.[46] Despite being estimated by calibrations established over a limited MW range, the k_p values for poly(PLA$_1$EMA) and poly(PLA$_5$EMA) based on the determined MH parameters are corroborated by the reasonable agreement (within 15%; see Tables B.4-B.7) with those estimated from light scattering.

In Figure 5.2, the k_p values measured for bulk PLA$_1$EMA, and PLA$_5$EMA homopolymerizations over the temperature range of 40–100 °C are compared to values measured for bulk MMA, which are within 10% of the IUPAC benchmark values.[30] Following family type behaviour,[31] the k_p for an alkyl ester methacrylate with linear ester side chain length of 5 atoms (e.g., PLA$_1$EMA), is expected to be 20% greater than $k_{p,MMA}$ at 50 °C.[32] However, the data in

71
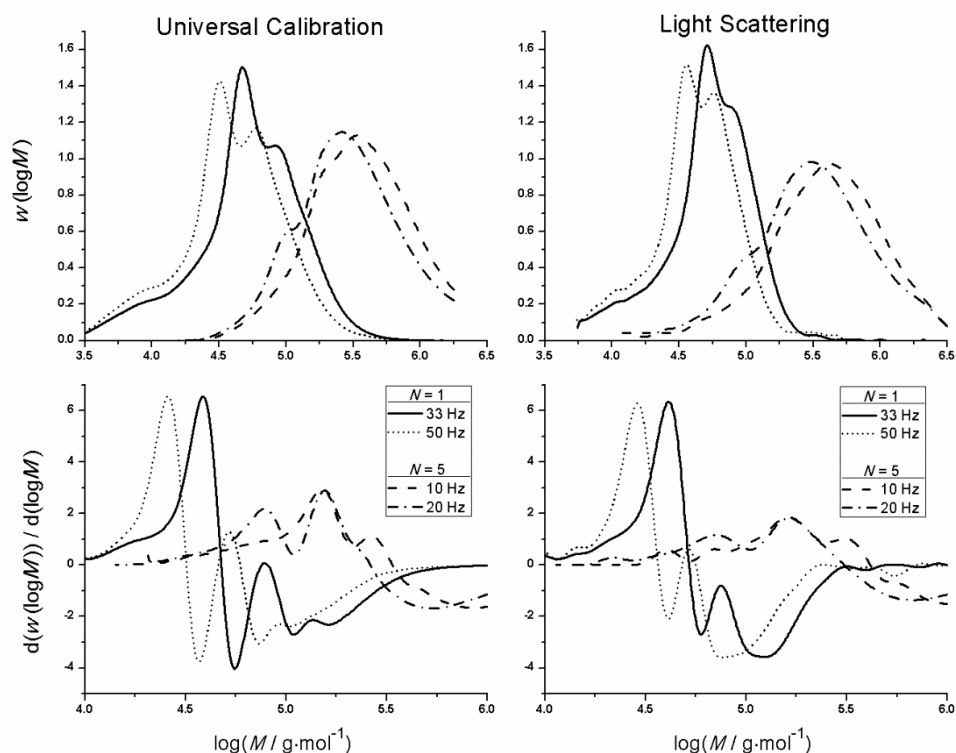
Figure 5.1: RI (left; interpreted by universal calibration) and LS (right) measures of MMDs (top) and corresponding first derivative plots (bottom) for polymer produced by PLP homopolymerization experiments of bulk PLA₁EMA (*N*=1) and PLA₅EMA (*N*=5) at 60 °C with 5 mmol·L⁻¹ DMPA, at pulse repetition rates as indicated in the legends.

Figure 5.2 show that the k_p for PLA$_1$EMA is augmented by 60% compared to $k_{p,MMA}$ at 50 °C, with the difference maintained over the complete range of temperatures studied. The structure of PLA$_1$EMA is unique in that it comprises both branched methyl groups as well as polar ester functionalities in its ester side chain. A combination of these features is thought to contribute to the comparatively elevated k_p estimate for PLA$_1$EMA at 50 °C of 952 L·mol^{-1}·s^{-1}, which is in a similar range as other diverse non-hydroxylated and non-linear heteroatom-containing methacrylates.[47-51] In particular, similar values were established for four bulky tertiary amine substituted
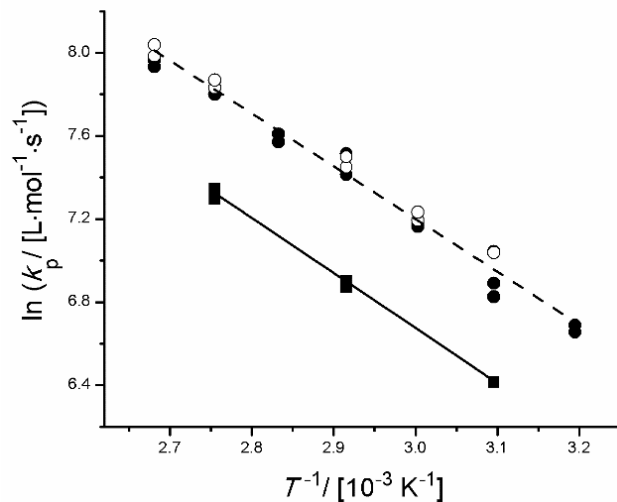
Figure 5.2: Arrhenius plot for k_p determined from bulk PLP experiments of MMA (■), PLA$_1$EMA (●), and PLA$_5$EMA (○) using universal calibration to interpret SEC output. Best fit lines for MMA (solid) and the combined $N = 1, 5$ data set (dashed) are provided.

ethylmethacrylates,[48] with the k_p of 2-(N,N-dimethylamino)ethyl methacrylate (DMAEMA) slightly higher, presumably related to its less encumbered tertiary amine, and the k_p for 3-(N,N-dimethylamino)propyl methacrylate (DMAPMAE) clearly below the proposed family behavior due to the additional methylene of its propyl spacer. Thus, an interpretation of bulk PLA$_1$EMA k_p behavior is likely rooted in the proximity of its polar and steric substituents to the methacrylic group.

In the case of the PLA$_5$EMA macromonomer, inspection of Figure 5.2 reveals that the addition of 4 more PLA units into the ester side chain does not significantly alter its bulk k_p from that of PLA$_1$EMA, certainly not to the extent that the bulk k_p was increased from MMA (N=0) to PLA$_1$EMA. Since the bulk k_p Arrhenius estimates for PLA$_1$EMA and PLA$_5$EMA in Table 5.2 encompass values typical of the linear alkyl ester methacrylate family,[30,31] a combined N=1,5 fit is justified. Thus, the chemical features of the isobutyrate bridge adjacent to the methacrylic group

73

must be solely responsible for the elevated PLA$_1$EMA k_p measurements in bulk. (As stated previously, ^{1}H NMR analysis of the low-conversion PLP-generated polymers showed that the average N of the PLA$_5$EMA macromonomer is preserved during the "grafting through" polymerization.) In other words, the presence of polar or steric groups further along the ester side chain does not decisively impact the bulk k_p of PLA$_N$EMA systems. In support of this claim, we found that polyester type, length, and end-group functionality did not contribute to the relative reactivity of various methacrylate macromonomers and ST copolymerization systems,[28] and other work showed that the influence of the N,N-dimethylamino substituent on bulk k_p is diluted from DMAEMA to DMAPMAE.[48] Furthermore, while Siegmann et al. measured a 50% increase in bulk k_p for PEGEEMA (3 PEG units) compared to EEMA (1 PEG unit) at 25 °C,[33] Smolne et al. found no further increase in the bulk k_p of PEGMA (7-8 PEG units) compared to that reported for PEGEEMA.[34] Interestingly, the values at which the PEGylated methacrylates appear to plateau (707 and 1954 L·mol^{-1}·s^{-1} at 40 and 80 °C, respectively) are close to the values measured for PLA$_1$EMA (780 and 1978 L·mol^{-1}·s^{-1} at 40 and 80 °C, respectively). Finally, we recall that the pre-exponential for k_p is largely governed by the degree to which the internal rotations of the transition state (TS) for propagation are hindered,[52] and that Buback has explained the trend of increasing bulk k_p from MMA to DMA in terms of the longer aliphatic ester side chain which can better shield the dipolar interactions between methacrylic esters, causing less friction in the TS.[53] As the addition of 4 more "frictional" dipolar esters in the ester side chain did not cause a significant change in bulk k_p for PLA$_N$EMA, it seems that the nature of the substituents several units beyond the methacrylic ester does not decisively influence k_p.

Table 5.2: Arrhenius parameters estimated for bulk PLA$_N$EMA (macro)monomers with error margins for the 95% confidence intervals.

	$k_p^{70°C}$ (L·mol^{-1}·s^{-1})	E_A (kJ·mol^{-1})	$\pm$	A (L·mol^{-1}·s^{-1})	$\pm$
MMA $N=0$	979	22.1	2.2	2.3×10^6	2.6×10^6 1.2×10^6
PLA$_1$EMA $N=1$	1744	21.6	1.6	3.1×10^6	2.3×10^6 1.3×10^6
PLA$_5$EMA $N=5$	1764	19.9	1.2	1.8×10^6	9.8×10^5 6.4×10^5
Combined $N=1,5$	-	21.1	1.3	2.7×10^6	1.5×10^6 9.8×10^5

5.3.2 Solution Homopropagation Kinetics

In order to investigate the influence of hydrogen bonding and (macro)monomer molar volume on PLA$_N$EMA homopropagation kinetics, the PLP-SEC study was extended to MMA, PLA$_1$EMA, and PLA$_5$EMA solution homopolymerizations in 75 wt% BuOH, DMF, and xylenes with conditions summarized by Tables B.3, B.5, and B.7; additional experiments with MMA and PLA$_1$EMA were conducted at an equimolar ratio of BuOH to monomer. The resulting k_p estimates at 70 °C and 90 °C are presented in Figure 5.3 and Figure B.4, respectively, to compare specific solvent influences on each system ($N=0$, 1, and 5). However, due to the marked decrease in monomer molar concentration from $N=0$ to $N=5$ at constant solvent weight fraction (see bulk monomer concentrations in Table 5.1, direct comparison of solution k_p estimates from different N are not necessarily meaningful. In the case of MMA ($N=0$), for which differences in monomer and solvent molar volumes ($V_{mon}-V_{sol}$) are not very large, there is no significant difference between the solution k_p measured in xylenes compared to bulk, the k_p is slightly elevated in DMF, and in BuOH the k_p of MMA is clearly enhanced because of the well-documented hydrogen bond formation between
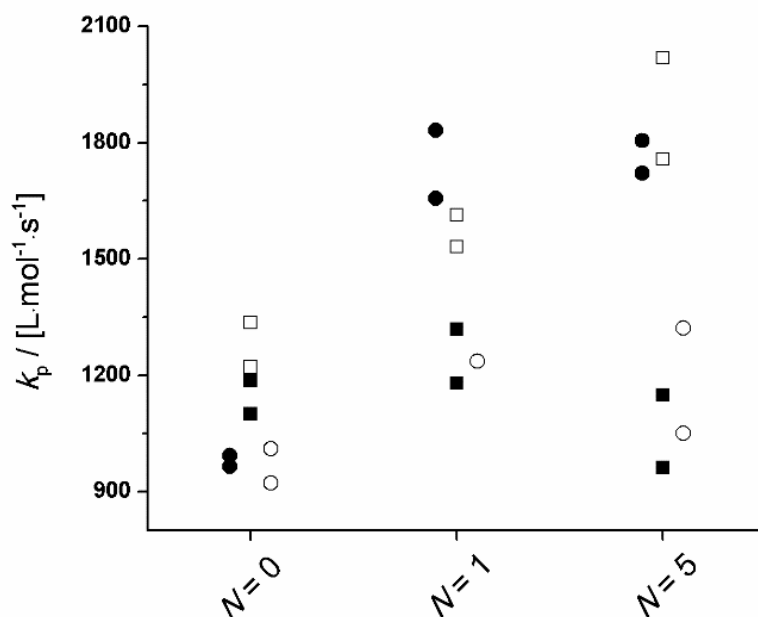
Figure 5.3: Plots for k_p of MMA, PLA$_1$EMA, and PLA$_5$EMA determined by universal calibration in bulk (●), 75 wt% xylenes (○), 75 wt% DMF (■), and 75 wt% BuOH (□) solutions at 70 °C with 5 mmol·L^{-1} DMPA.

hydroxyl and methacryloyl carbonyl which reduces the electron density at the double bond making MMA more reactive towards radical addition.[35]

The situation is different for the PLA$_1$EMA and PLA$_5$EMA systems, for which a reduction in k_p compared to bulk is measured (modest in xylenes and pronounced in DMF), even though no specific interaction between PLA$_N$EMA and either solvent is expected. This same trend in apparent k_p was reported in the PLP-SEC study of PEGEEMA in toluene ($V_{mon}-V_{sol} = 139$ cm^3·mol^{-1}) and THF ($V_{mon}-V_{sol} = 164$ cm^3·mol^{-1}),[33] solvents similar to xylenes and DMF (in terms of relative polarities and molar volumes), respectively, a result that was reconciled in terms of the previously established linear relationship between $V_{mon}-V_{sol}$ and $k_{p,\infty}/k_{p,bulk}$.[37] Although this correlation formally predicts that systems with very large $V_{mon}-V_{sol}$ (i.e., > 226 cm^3·mol^{-1}) yield negative ratios

of $k_{p,\infty}/k_{p,bulk}$, the logic can still be applied to explain the PLA$_N$EMA results: at 70 °C the molar volumes of PLA$_1$EMA (191 cm$^3 \cdot$mol^{-1}) and PLA$_5$EMA (average of 422 cm$^3 \cdot$mol^{-1}) are larger than those of DMF (81 cm$^3 \cdot$mol^{-1}) and xylenes (129 cm$^3 \cdot$mol^{-1}) such that solvent molecules outcompete (macro)monomers for positions at the reaction site, leading to a lower than analytical local (macro)monomer concentration and corresponding reduction in apparent k_p measured by PLP-SEC. The fact that there is only a small difference in the apparent k_p (measured as 75·wt% solvent) for 0.50 mol·L^{-1} PLA$_5$EMA in DMF ($V_{mon}-V_{sol}$ = 341 cm$^3 \cdot$mol^{-1}) and 1.23 mol·L^{-1} PLA$_1$EMA in DMF ($V_{mon}-V_{sol}$ = 110 cm$^3 \cdot$mol^{-1}) at 70 and 90 °C (Figure 5.3 and Figure B.4, respectively), indicates that there should exist a minimum $k_{p,\infty}/k_{p,bulk}$ which cannot be exceeded by further increases in $V_{mon}-V_{sol}$ of monomer/solvent pairings. The physical interpretation is that the volume around the chain-end radical which can be preferentially occupied by solvent molecules is finite. This reasoning is consistent with Buback's interpretation of linear alkyl acrylate homopropagation trends in toluene: a larger molar volume of the solvent (compared to monomer) allows for higher mobility of the TS structure and thus a higher k_p results from the lower entropic penalty.[53,54]

Turning now to the PLA$_N$EMA homopolymerization experiments in 75 wt% BuOH, the k_p values in Figure 5.3 are increased compared to bulk PLA$_5$EMA and slightly decreased compared to bulk for the PLA$_1$EMA system. Since the effect of hydrogen bonding on the k_p of a generic methacrylate (xMA) is known to depend on the relative concentrations of alcohol and xMA,[36,55] additional experiments were performed so that the k_p data estimated for MMA, PLA$_1$EMA, and PLA$_5$EMA in BuOH could be examined as a function of δ (molar ratio of alcohols to methacryloyl carbonyls; Eqn. 5.2) for solution homopolymerizations, as summarized at 70 °C in Table 5.3 and at 90 °C in Table B.2 of Appendix B, respectively.

$$\delta = \frac{[BuOH]}{[xMA]} \tag{5.2}$$

As δ increases from 1.0 to 4.1, the ratio of $k_{p,BuOH}/k_{p,bulk}$ for MMA increases from 1.20 to 1.31 at 70 °C, in reasonable agreement with a 10% linear increase in k_p per δ up to δ=6.1 reported for MMA

in benzyl alcohol at 30 °C.[55] A similar increase in k_p was observed at even greater dilutions (up to $\delta=11.3$) for BMA in BuOH at 70 °C,[36] as also summarized by Table 5.3. In contrast, the ratio of $k_{p,BuOH}$ to $k_{p,bulk}$ decreases for PLA$_1$EMA, as the comparison is confounded by the effect of large $V_{mon}-V_{sol}$ on apparent k_p. Thus, it is more meaningful to compare the k_p in BuOH (96 cm^3·mol^{-1}) against the k_p measured in DMF (81 cm^3·mol^{-1}) because the corresponding $V_{mon}-V_{sol}$ for these solvents in PLA$_N$EMA systems are similar.

Table 5.3: Ratio of k_p determined in BuOH to bulk or DMF at 70 °C with 5 mmol·L^{-1} DMPA at various δ for each (macro)monomer.

Monomer	δ	$\dfrac{k_{p,BuOH}}{k_{p,bulk}}$	$\dfrac{k_{p,BuOH}}{k_{p,DMF}}$
MMA	1.0	1.20	-
	4.1	1.31	1.12
BMA[36]	5.3	1.33	-
	11.3	1.47	-
PLA$_1$EMA	1.0	0.81	-
	7.5	0.90	1.26
PLA$_5$EMA	19.1	1.07	1.79

When the $k_{p,BuOH}/k_{p,DMF}$ ratios are computed, it is clear that the hydrogen bonding provided by BuOH also leads to augmented k_p for PLA$_N$EMA systems. The extent of the increase is quite significant, although the corresponding values of δ are also much higher (see Table 5.3), and the systems are complicated by the extra linkages in the methacrylate side chain: while for MMA and BMA, there is only a single methacryloyl carbonyl with which the alcohol's hydroxyl can interact, in PLA$_N$EMA systems there are $N+1$ carbonyls which can accept hydrogen bonding. As the measured increases in $k_{p,BuOH}/k_{p,DMF}$ for the limited $N=1$ and $N=5$ data sets can be reasonably accounted for by the proportionalities with δ estimated for BMA and MMA, it is unlikely that hydrogen bonding interactions with the N polyesters in the methacrylic ester side chain have any

significant intrinsic kinetic effect on PLA$_N$EMA homopropagation, in agreement with our conclusion that the substituents several units beyond the methacrylic ester do not decisively influence the bulk k_p measurements for PLA$_N$EMA. Nevertheless, the extent to which system specific enhanced k_p via hydrogen bonding between hydroxyl and methacryloyl carbonyl is diluted by the repeating esters in the PLA$_N$EMA side chain should be further investigated by controlling for δ as a function of the $N+1$ carbonyls at various temperatures. Furthermore, since $V_{mon}-V_{sol}$ is an important parameter for PLA$_N$EMA homopolymerizations, future work should include the influence of macromonomer molar volume on apparent reactivity ratios as well as $k_{p,cop}$ measurements for PLA$_N$EMA bulk copolymerizations with smaller molar volume comonomers such as MMA.

5.3.3 Nanoparticle Degradation Study

As previously mentioned, the ability to tune the degradation time of NPs produced from polyester macromonomers by specifying the average number and type of polyester units in the ROP step of the macromonomer synthesis has been demonstrated.[15,18] However, whether the rate of NP degradation can be further controlled by end-group design needs to be evaluated, since the terminal hydroxyl of HEMA-PLA$_5$ and the terminal ethyl ester of PLA$_5$EMA distinguish macromonomers with the same average chain lengths by different hydrophobicities. To investigate the effect of PLA$_N$EMA's alkyl end-group on degradation, 5 wt% NP suspensions were prepared by semi batch radical emulsion polymerizations at 70 °C with 1% SDS as surfactant using the following four (macro)monomer systems: PLA$_1$EMA, PLA$_5$EMA, HEMA-PLA$_5$, and a comonomer mixture of 50 wt% PLA$_5$EMA and 50 wt% HEMA-PLA$_5$, with PSDs presented in Figures B.5, B.6, B.7, and B.8, respectively.

An accelerated degradation test for each NP suspension was performed over several weeks at 50 °C with the progress of the degradative swelling mechanism monitored by periodically measuring the increase in average particle size, as shown in Figure 5.4; as degradation proceeds,

the NPs become more hydrophilic leading to an increase in water absorption and apparent particle size at constant polydispersity index (PDI), thus confirming that the increase in size is not due to coagulation.[15,42] The corresponding PDI values from this study summarized by Figure B.9 of Appendix B are near constant with time, only increasing slightly at the final stages of degradation to suggest the formation of a small quantity of aggregates late in the process. The important feature of the data in Figure 5.4 is the time at which the particle size begins to rapidly increase, as this indicates that the NPs have almost degraded to the final water-soluble material. For example, the rapidly increasing size of the HEMA-PLA$_5$ latex from days 7-9 leads to the complete hydrolysis of the PLA grafts by day 10 to yield a poly(HEMA) backbone (which is observed as a swollen polymer
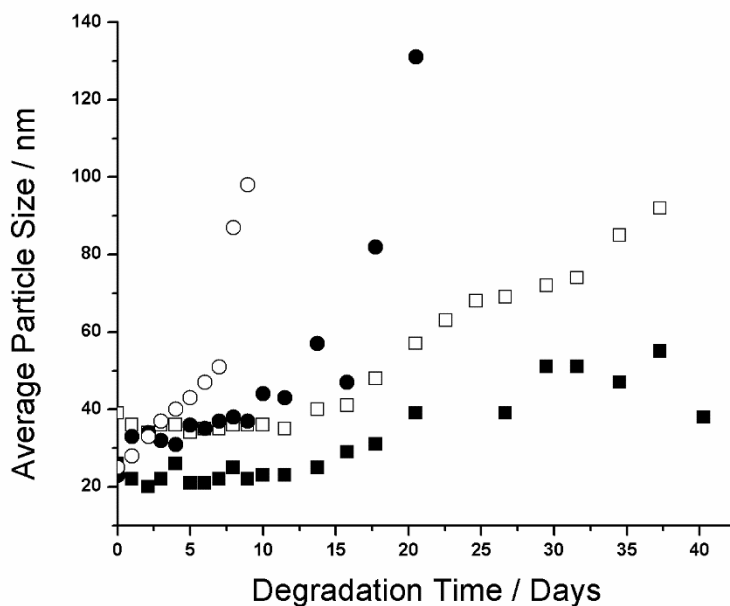
Figure 5.4: Intensity average size measurements at 25 °C for NPs produced from PLA$_1$EMA (■), PLA$_5$EMA (□), an equal mass copolymer of PLA$_5$EMA and HEMA-PLA$_5$ (●), and HEMA-PLA$_5$ (○) throughout the accelerated degradation study performed at 50 °C. Measurement standard deviations typically within 2% of the mean, but increase to 10% during final days of degradation.

at room temperature that can be dissolved upon dilution), in close agreement with an 8 day degradation time measured for very similar HEMA-PLA$_4$ NPs.[18] On the other hand, after 40 days the PLA$_5$EMA homopolymer latex has finally degraded while the PLA$_1$EMA latex is still observable.

The continual increase in NP sizes over 40 days indicates that hydrolytic degradation of the NPs produced from the hydrophobic alkyl-terminated macromonomer occurs at a much slower rate because of the added hydrophobicity of PLA$_N$EMA's ethyl ester end-group. For comparison, NPs produced from the PCL (more hydrophobic than PLA) based HEMA-PCL$_3$ macromonomer, with similar average MW as both PLA$_5$EMA and HEMA-PLA$_5$, were completely degraded after only 20 days under the same conditions.[42] Furthermore, PLA$_N$EMA's lack of terminal hydroxyl precludes preferential chain-end scission hydrolysis, where protection of oligomeric PLA hydroxyl end-groups (through esterification or acetylation) has been shown to significantly reduce the rate of hydrolysis under both acidic and basic conditions.[23,24] However, as illustrated by Scheme 5.2, any hydrolysis event in a PLA$_N$EMA chain yields a carboxyl-terminated graft. Since Codari et al. showed that preferential chain-end hydrolysis of bifunctional hydroxyl- and carboxyl- terminated oligomeric PLA can be ascribed to the increased end-group hydrophilicities,[22] the slow hydrolysis of PLA$_N$EMA NPs must be due to the initial ethyl ester protection of PLA end-groups. Consideration must also be given to the pH of the NP environment because the terminal units of the hydrolyzed PLA$_N$EMA grafts could exist as carboxylic acids or carboxylates which would certainly influence their degradability. Nevertheless, the delayed degradation (in comparison to HEMA-PLA$_5$ NPs) afforded by the initial ethyl ester protection should remain effective regardless of the pH.
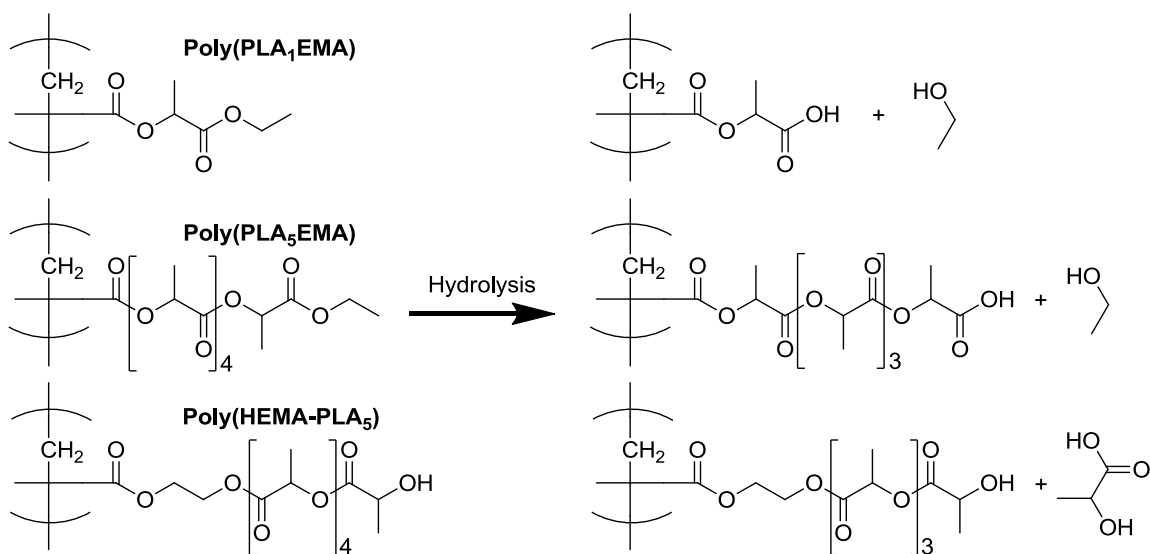
Scheme 5.2: Proposed degradation products after one hydrolysis event at the terminal grafted unit of poly(PLA₁EMA), poly(PLA₅EMA), and poly(HEMA-PLA₅) comb-polymers.

In the case of PLA_1EMA NPs, the reduction in pH after 35 days of accelerated degradation (Table B.8 of Appendix B) indicates hydrolysis of the terminal ethyl ester to release ethanol; however, minimal increases in PLA_1EMA NP size measurements to 40 days suggests that hydrolysis of the single grafted PLA unit to yield a PMAA backbone is unfavorable such that complete degradation of PLA_1EMA homopolymer will not occur over a timescale typically associated with PLA based materials. As seen in Figure 5.4, the PLA_5EMA homopolymer latex degrades more quickly than the PLA_1EMA latex; although it seems counterintuitive that complete degradation of the PLA_5EMA homopolymer was observed before that of the PLA_1EMA homopolymer, the latter has roughly 2.5 times more esters attached to the methacrylic backbone per unit mass due to the macromonomer's larger MW. In support of the notion that these units are more difficult to hydrolyze than typical ester linkages in the polyester backbone, the release of ethylene glycol was not detected at the end of the polyester graft degradation for previous HEMA-

PLA$_3$ NP degradation studies, indicating that the poly(HEMA) backbone did not degrade to PMAA.[17]

Under unbuffered degradation conditions (i.e., acidic), the choice of macromonomer end-group affords a considerable range of NP degradation times from 10 to 40 days for HEMA-PLA$_5$ and PLA$_5$EMA homopolymer latexes, respectively; when 50 wt% PLA$_5$EMA is added to the HEMA-PLA$_5$ macromonomer recipe, an intermediate NP degradation time of 23 days is achieved (Figure 5.4). This finding verifies the successful copolymerization of the two macromonomers, despite their differences in water solubility, and also demonstrates that end-group choice can be used to tune NP degradation time in acidic environments. Depending on the pH and functional timescale of the intended application, formulations could benefit by using PLA$_N$EMA as a comonomer to modify system hydrophobicity and degradation time while still maintaining the properties of a PLA based system. In addition, PLA$_N$EMA can be used to improve selectivity of post-polymerization esterification reactions through use as a comonomer spacer with hydroxyl or carboxyl functionalized monomers.

5.4 Conclusions

Polylactic acid based methacrylate (macro)monomers (PLA$_N$EMA) with N=1 and N=5 average polyester units per chain were synthesized and their homopropagation kinetics studied in bulk and solution using the PLP-SEC technique. Reasonable agreement (within 15%) was obtained for k_p estimates from low-conversion PLP samples analysed by SEC coupled with light scattering and universal calibration, validating the dn/dc and Mark-Houwink parameters measured in this work for both N=1 and N=5 comb-polymers. No significant difference between PLA$_1$EMA and PLA$_5$EMA bulk k_p estimates was detected over the temperature range of 40–100 °C, indicating that polar and steric characteristics several units beyond the methacrylic group do not decisively influence k_p. Furthermore, the apparent solution k_p values measured for both PLA$_1$EMA and PLA$_5$EMA in DMF as well as in xylenes were markedly decreased compared to bulk due to

differences in (macro)monomer and solvent molar volumes, while in BuOH the apparent k_p of both systems increased relative to in DMF because of hydrogen bonding.

PLA$_N$EMA (macro)monomers were used to produce NPs by semi batch radical emulsion polymerization. When an equal weight of PLA$_5$EMA is used as comonomer, the time for accelerated degradation at 50 °C of hydroxyl terminated HEMA-PLA$_5$ NPs is increased from 10 to 23 days, while the PLA$_5$EMA homopolymer NPs took 40 days to degrade. An explanation for the slow degradation is proposed in terms of PLA graft orientation relative to the methacrylic backbone; ethyl ester protection of poly(PLA$_N$EMA) grafts' carboxyl end-groups delays the onset of preferential chain-end hydrolysis. The ability to affect degradation time by copolymerizing PLA$_N$EMA with HEMA-PLA$_{2n}$ provides further opportunities to tune the performance characteristics of this family of degradable NPs according to specific application requirements.

5.5 References

(1)   Drumright, R. E.; Gruber, P. R.; Henton, D. E. *Adv. Mater.* **2000**, *12*, 1841.

(2)   Davachi, S. M.; Kaffashi, B. *Polym.-Plast. Tech. Eng.* **2015**, *54*, 944.

(3)   Jamshidian, M.; Tehrany, E. A.; Imran, M.; Jacquot, M.; Desobry, S. *Compr. Rev. Food Sci. Food Saf.* **2010**, *9*, 552.

(4)   Achmad, F.; Yamane, K.; Quan, S.; Kokugan, T. *Chem. Eng. J.* **2009**, *151*, 342.

(5)   Dechy-Cabaret, O.; Martin-Vaca, B.; Bourissou, D. *Chem. Rev.* **2004**, *104*, 6147.

(6)   van den Berg, S. A.; Zuilhof, H.; Wennekes, T. *Macromolecules* **2016**, *49*, 2054.

(7)   Rooney, T. R.; Gumfekar, S. P.; Soares, J. B. P.; Hutchinson, R. A. *Macromol. Mater. Eng.* **2016**, *301*, 1248.

(8)   Okuda, T.; Ishimoto, K.; Ohara, H.; Kobayashi, S. *Macromolecules* **2012**, *45*, 4166.

(9)   Kiehl, J.; Delaite, C.; Bistac, S.; Schuller, A. S.; Farge, H. *Polymer* **2012**, *53*, 694.

(10)   Hawker, C. J.; Mecerreyes, D.; Elce, E.; Dao, J.; Hedrick, J. L.; Barakat, I.; Dubois, P.; Jérôme, R.; Volksen, W. *Macromol. Chem. Phys.* **1997**, *198*, 155.

(11)   Wallach, J. A.; Huang, S. J. *Biomacromolecules* **2000**, *1*, 174.

(12)   Ishimoto, K.; Arimoto, M.; Ohara, H.; Kobayashi, S.; Ishii, M.; Morita, K.; Yamashita, H.; Yabuuchi, N. *Biomacromolecules* **2009**, *10*, 2719.

(13)   Ishimoto, K.; Arimoto, M.; Okuda, T.; Yamaguchi, S.; Aso, Y.; Ohara, H.; Kobayashi, S.; Ishii, M.; Morita, K.; Yamashita, H.; Yabuuchi, N. *Biomacromolecules* **2012**, *13*, 3757.

(14)   Lim, D. W.; Choi, S. H.; Park, T. G. *Macromol. Rapid Commun.* **2000**, *21*, 464.

(15)   Colombo, C.; Dragoni, L.; Gatti, S.; Pesce, R. M.; Rooney, T. R.; Mavroudakis, E.; Ferrari, R.; Moscatelli, D. *Ind. Eng. Chem. Res.* **2014**, *53*, 9128.

(16)   Ferrari, R.; Yu, Y.; Lattuada, M.; Storti, G.; Morbidelli, M.; Moscatelli, D. *Macromol. Chem. Phys.* **2012**, *213*, 2012.

(17)   Yu, Y.; Ferrari, R.; Lattuada, M.; Storti, G.; Morbidelli, M.; Moscatelli, D. *J. Polym. Sci. Part A: Polym. Chem.* **2012**, *50*, 5191.

(18)   Ferrari, R.; Colombo, C.; Dossi, M.; Moscatelli, D. *Macromol. Mater. Eng.* **2013**, *298*, 730.

(19)   Grizzi, I.; Garreau, H.; Li, S.; Vert, M. *Biomaterials* **1995**, *16*, 305.

(20)   Xu, L.; Crawford, K.; Gorman, C. B. *Macromolecules* **2011**, *44*, 4777.

(21)   Lazzari, S.; Codari, F.; Storti, G.; Morbidelli, M.; Moscatelli, D. *Polym. Degrad. Stab.* **2014**, *110*, 80.

(22)   Codari, F.; Lazzari, S.; Soos, M.; Storti, G.; Morbidelli, M.; Moscatelli, D. *Polym. Degrad. Stab.* **2012**, *97*, 2460.

(23)   de Jong, S. J.; Arias, E. R.; Rijkers, D. T. S.; van Nostrum, C. F.; Kettenes-van den Bosch, J. J.; Hennink, W. E. *Polymer* **2001**, *42*, 2795.

(24)   van Nostrum, C. F.; Veldhuis, T. F. J.; Bos, G. W.; Hennink, W. E. *Polymer* **2004**, *45*, 6779.

(25)   Shinoda, H.; Matyjaszewski, K. *Macromolecules* **2001**, *34*, 6243.

(26)   Eguiburu, J.; Fernandez-Berridi, M. J.; Román, J. S. *Polymer* **1996**, *37*, 3615.

(27)   Ferrari, R.; Rooney, T. R.; Lupi, M.; Ubezio, P.; Hutchinson, R. A.; Moscatelli, D. *Macromol. Biosci.* **2013**, *13*, 1347.

(28)   Rooney, T. R.; Monyatsi, O.; Hutchinson, R. A. *Macromolecules* **2017**.

(29)   Beuermann, S.; Buback, M. *Prog. Polym. Sci.* **2002**, *27*, 191.

(30)   Beuermann, S.; Buback, M.; Davis, T. P.; Gilbert, R. G.; Hutchinson, R. A.; Olaj, O. F.; Russell, G. T.; Schweer, J.; van Herk, A. M. *Macromol. Chem. Phys.* **1997**, *198*, 1545.

(31)   Beuermann, S.; Buback, M.; Davis, T. P.; Gilbert, R. G.; Hutchinson, R. A.; Kajiwara, A.; Klumperman, B.; Russell, G. T. *Macromol. Chem. Phys.* **2000**, *201*, 1355.

(32)   Haehnel, A. P.; Schneider-Baumann, M.; Hiltebrandt, K. U.; Misske, A. M.; Barner-Kowollik, C. *Macromolecules* **2013**, *46*, 15.

(33)   Siegmann, R.; Jeličić, A.; Beuermann, S. *Macromol. Chem. Phys.* **2010**, *211*, 546.

(34)   Smolne, S.; Weber, S.; Buback, M. *Macromol. Chem. Phys.* **2016**, *217*, 2391.

(35)   Beuermann, S. *Macromol. Rapid Commun.* **2009**, *30*, 1066.

(36)   Beuermann, S. *Macromolecules* **2004**, *37*, 1037.

(37)   Beuermann, S.; García, N. *Macromolecules* **2004**, *37*, 3018.

(38)   Dossi, M.; Liang, K.; Hutchinson, R. A.; Moscatelli, D. *J. Phys. Chem. B* **2010**, *114*, 4213.

(39)   Hutchinson, R. A.; McMinn, J. H.; Paquet, D. A.; Beuermann, S.; Jackson, C. *Ind. Eng. Chem. Res.* **1997**, *36*, 1103.

(40)   Bernal-García, J. M.; Guzmán-López, A.; Cabrales-Torres, A.; Estrada-Baltazar, A.; Iglesias-Silva, G. A. *J. Chem. Eng. Data* **2008**, *53*, 1024.

(41)   Bravo-Sánchez, M. G.; Iglesias-Silva, G. A.; Estrada-Baltazar, A.; Hall, K. R. *Journal of Chemical & Engineering Data* **2010**, *55*, 2310.

(42)   Ferrari, R.; Yu, Y.; Morbidelli, M.; Hutchinson, R. A.; Moscatelli, D. *Macromolecules* **2011**, *44*, 9205.

(43)   Drawe, P.; Buback, M. *Macromol. Theory Sim.* **2016**, *25*, 74.

(44)   Beuermann, S.; Paquet, D. A.; McMinn, J. H.; Hutchinson, R. A. *Macromolecules* **1996**, *29*, 4206.

(45)   Nikitin, A. N.; Lacík, I.; Hutchinson, R. A. *Macromolecules* **2016**, *49*, 9320.

(46)   Hutchinson, R. A.; Paquet, D. A.; McMinn, J. H.; Beuermann, S.; Fuller, R. E.; Jackson, C. in *5ᵗʰ International Workshop on Polymer reaction Engineering*, DECHEMA Monographs Vol 131, ed. K.-H. Reichert and H.-U. Moritz, VCH Verlags, Weinheim Germany, **1995**, 467.

(47)   Kockler, K. B.; Fleischhaker, F.; Barner-Kowollik, C. *Polym. Chem.* **2016**, *7*, 4342.

(48)   Kockler, K. B.; Fleischhaker, F.; Barner-Kowollik, C. *Macromolecules* **2016**, *49*, 8572.

(49)   Zoller, A.; Kockler, K. B.; Rollet, M.; Lefay, C.; Gigmes, D.; Barner-Kowollik, C.; Guillaneuf, Y. *Polym. Chem.* **2016**, *7*, 5518.

(50)   Haehnel, A. P.; Stach, M.; Chovancova, A.; Rueb, J. M.; Delaittre, G.; Misske, A. M.; Lacik, I.; Barner-Kowollik, C. *Polym. Chem.* **2014**, *5*, 862.

(51)   Buback, M.; Kurz, C. H. *Macromol. Chem. Phys.* **1998**, *199*, 2301.

(52)   Heuts, J. P. A.; Gilbert, R. G.; Radom, L. *Macromolecules* **1995**, *28*, 8771.

(53)   Buback, M. *Macromol. Symp.* **2009**, *275–276*, 90.

(54)   Buback, M. *Macromol. Rapid Commun.* **2015**, *36*, 1979.

(55)   O'Driscoll, K. F.; Monteiro, M. J.; Klumperman, B. *J. Polym. Sci. Part A: Polym. Chem.* **1997**, *35*, 515.

Chapter 6

Applications of Nitrogen Containing Macromonomers

Preface

The group of Dr. João Soares at the University of Alberta is developing improved techniques for oil sands tailings remediation. One of the concepts put forward was polymeric flocculants that improve sediment dewaterability by becoming more hydrophobic in response to temperature changes. Building on my experience with degradable macromonomer-based materials in the Moscatelli group, I synthesized a new cationic macromonomer whose resulting comb-polymer becomes more hydrophobic in response to hydrolysis instead of temperature. In addition, the macromonomer design allows for tunable charge density and hydrophobic content, important flocculant performance parameters, and therefore our groups have begun a collaboration testing this material for oil sands tailings remediation applications.

Since the precursor to the cationic macromonomer is the tertiary macromonomer I sought to find an application for it as well. From attending group meetings of Professor Michael Cunningham, I was familiar with some of the challenges of CO_2 switchable technologies for dispersed phase polymerization systems, namely burial of switchable groups and the relative hydrophobicity of the system. Thus, I proposed to the post doctoral associate in his group, Dr. Omar Garcia-Valdez, to investigate the effect of distancing the switchable groups from the polymer backbone using macromonomers.

This Chapter combines the proof of concept application work performed for both the cationic and tertiary amine macromonomers. The cationic flocculant work incorporates additional data for several degradation experiments not included as part of the full paper published in *Macromolecular Materials and Engineering* (2016, vol. 301, 1248-1254) in which all flocculation experiments were performed by Sarang Gumfekar at the University of Alberta. Finally, the

experimental results for the tertiary amine macromonomer CO_2-responsivity were performed by Dr. Garcia Valdez.

6.1 Quaternary Ammonium Macromonomer

Abstract

Micellar radical polymerization of a short-chain polyester macromonomer, polycaprolactone choline iodide ester methacrylate (PCL_nChMA), is used to produce a new cationic flocculant that becomes more hydrophobic in response to hydrolytic degradation. The cationic tips of the comb-like poly(PCL_3ChMA) accelerate the settling rate of oil sands tailings, while partial hydrolysis of the polyester grafts reveals the hydrophobic segments that reduce capillary suction time by 30 %. This technology combines the material properties of polyesters with the productivity of radical polymerization to make dual functional flocculants with characteristics that can be easily tuned to control flocculation performance, such as polymeric cation density, hydrophobic content, and polymer architecture.

6.1.1 Introduction

During the last 50 years of oil sands mining operations in Canada, approximately 830 million cubic meters of tailings have accumulated in ponds that cover an area of approximately 176 km^2.[1] Oil sands tailings comprise the by-product slurry from the bitumen extraction process, which is discharged as an aqueous suspension of pH 8-9 containing coarse sands, fine solids, clays, and fugitive bitumen.[2-4] These tailings ponds pose two serious environmental concerns: they hold a substantial amount of unrecovered process water, and the vast area of land they occupy cannot be reclaimed.

Typically, oil sands tailings are treated with high molecular weight (MW) water-soluble polymers that flocculate and dewater the resulting sediment.[5-8] Current polymeric flocculation technologies are centered on commercially available polyacrylamide (PAM) grades, as these exhibit reasonably high settling rates, and have been extensively employed in other industries (e.g.

paper making, mining, *etc.*).[1] However, the resulting sediments are difficult to dewater because PAM is hydrophilic and forms loosely-packed flocs.

Thus, there is the need to develop improved technology. Cationic polymers can settle the negatively charged clay species found in oil sands tailings more effectively because their quaternary ammonium groups play two roles in remediation: charge neutralization and bridging flocculation (aggregation of multiple clay particles induced by a single polymer chain).[9,10] However, an optimum cation density must be determined, as too high of a cation concentration may redisperse the clay particles;[11,12] in addition, the dewatering problem still persists. To improve sediment dewatering, other researchers are exploring the use of temperature-sensitive poly(*N*-isopropyl acrylamide) (PNIPAM) to exploit the temperature-activated hydrophilic/hydrophobic transition.[6,13,14] Although these value-added materials for the remediation of oil sands tailings offer significant promise, many associated optimization challenges remain.

Our aim is to develop a new family of dual functional flocculants that can be easily adapted to field conditions from a library of building-block materials. In this work, we present the methodology and proof of concept for a dual functional polymer with tunable cationic density for rapid settling, and modifiable polyester units that are passively degraded by hydrolysis to reveal hydrophobic segments that further expel water from the sediment. As illustrated by Scheme 6.1, comb-like high MW polymer chains are produced via the grafting through approach of new short-chain polyester cationic macromonomers, thus combining the hydrolytic degradability of polyesters with the high production rates and industrial familiarity of radical polymerization (RP).
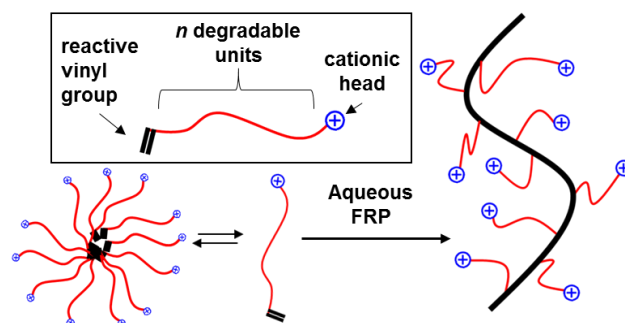
Scheme 6.1: Schematic representation of PCL$_n$ChMA micellar polymerization to achieve cationic degradable flocculants.

The simplicity and effectiveness of this approach to tune final material properties such as degradation rates by adjusting the average number n (e.g. n=2, 3, 5) of units in the polyester side chain has been demonstrated in the biomedical field for hydroxyl functionalized macromonomers.[15,16] Changing the cyclic monomer from ε-caprolactone (CL) to lactide (LA) in the bulk ring opening polymerization (ROP) step provides another means to tune degradation rates, since polycaprolactone (PCL) is more hydrophobic than polylactic acid (PLA).[15,16] For our application, the density of the polymeric cations per hydrophobic content, an important flocculating agent parameter,[17-20] is also adjusted by controlling the stoichiometric ratio of cyclic monomer to initiator in the bulk ROP step. In addition, branched architectures may be achieved by changing from a methacrylate to an acrylate macromonomer, with further control of cation density and hydrophobicity achievable through copolymerization of (meth)acrylate macromonomer with a water-soluble monomer such as acrylamide (AM).

In this work, polycaprolactone choline iodide ester methacrylate (PCL$_n$ChMA), shown in Scheme 6.2, is polymerized by RP to produce flocculants with enhanced sediment dewaterability upon hydrolysis. In situ degradation of the flocculant inside the sediment is studied for PCL$_n$ChMA of n=3, while ex situ flocculant degradation behavior is compared for both n=2 and n=3 average polyester lengths.
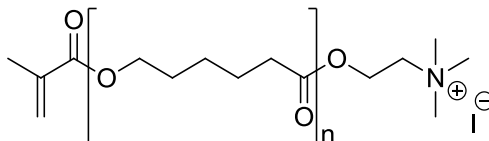
Scheme 6.2: Structure of PCL$_n$ChMA cationic macromonomer.

6.1.2 Experimental

Materials

Materials associated with PCL$_n$ChMA synthesis are detailed in Section 3.2. 2,2-azobis(2-methylpropionamidine)dihydrochloride (V-50, 97%), sodium hydroxide (NaOH, ≥97.0%), non-ionic polyacrylamide (PAM, 5-6 million Da), sodium tetraborate buffer solution pH 9.0 (borax/hydrochloric acid), and sodium deuteroxide (NaOD, 99.5% D) were purchased from Sigma Aldrich and used as received. Deuterium oxide (D$_2$O, 99.9% D, Cambridge Isotope Laboratories), deionized water (Millipore Synergy water purification system), and kaolin (Thermo Fisher Scientific) were used as received. Fluid fine tailings (FFT, 2.5 % bitumen and 41.4 % solids by mass) obtained from Syncrude Canada Ltd. were diluted to 2 wt% total solids for flocculation experiments.

Macromonomer Synthesis and Characterization

The synthesis of PCL$_n$ChMA is detailed in Section 3.3. The critical micelle concentration (CMC) for PCL$_3$ChMA in water was determined by surface tension using a Wilhelmy plate setup (TensioCAD with platinum plate EN14370).

Macromonomer Polymerization and Comb-Polymer Characterization

For flocculation experiments, 0.20 g of PCL$_3$ChMA dissolved in 1.80 g H$_2$O (containing 0.22 wt% V-50) was bubbled with nitrogen for 1 hour in a sealed 10 mL single neck round bottom flask. The solution was then heated to 85 °C for 1 hour, cooled to room temperature, and diluted with H$_2$O to achieve a stock solution concentration of 0.4 wt% poly(PCL$_3$ChMA).

For in situ ^{1}H NMR kinetic studies, 70 mg of PCL$_3$ChMA or AM was dissolved in 630 mg of D$_2$O (containing 0.22 wt.% V-50) and bubbled with nitrogen for 1 hour (done carefully in the case of PCL$_3$ChMA to avoid excessive foaming). The polymerization was performed at 50 °C inside a Bruker Avance instrument operating at 400 MHz using a previously described procedure.[22] Monomer consumption was monitored by tracking the decrease in vinyl peak integration relative to the HOD signal.

Transmission electron microscopy (TEM) images were taken on a Hitachi H-7000 instrument operating at 75 kV. To prepare the TEM images, an aqueous solution of 1.0 mg/mL polymer was deposited on a carbon coated copper grid and left for 1 minute before excess solution was removed.

Ex situ Degradation Study

A 5 wt% solution of PCL$_n$ChMA in H$_2$O, with 0.22 wt% V-50 relative to the aqueous phase, was polymerized at 85 °C for 1 hour then cooled back to room temperature and diluted to 1 wt.% using H$_2$O; one solution was prepared in this fashion with pH adjusted to 9 via addition of NaOH, with a second polymer solution prepared and buffered with pH=9. The 1 wt% poly(PCL$_n$ChMA) samples were held at 85 °C for 1 day increments then cooled to room temperature for analysis before increasing the temperature back to 85 °C. The solution pH was measured using a Mettler Toledo SevenExcellence pH meter, while size and zeta potential were determined with a Malvern Zetasizer Nano ZS (size range 0.3 nm –10 μm) at 25 °C with backscattering optics (173°), using a 4 mW He–Ne (633 nm) laser. All samples were measured in quartz cuvettes, and a universal dip cell (DTS1070) was used to measure zeta potential. The reported sizes represent an intensity average of at least 30 scans.

Separately, a 5 wt% solution of poly(PCL$_3$ChMA) in D$_2$O (with initial NaOD concentration adjusted to 10^{-5} M using NaOD) was polymerized at 85 °C using 0.22 wt% V-50 relative to D$_2$O.

The solution was diluted to 1 wt% using D_2O (with 10^{-5} M NaOD), held at 85 °C for 1 day increments, and cooled to room temperature to record the ^1H NMR spectrum at 25 °C.

In situ Sediment Dewaterability

In a typical experiment, 100 mL slurry of model tailings containing 2 wt.% kaolin clay (with pH adjusted between 8 and 9) was stirred in a 100 mL beaker using a radial impeller at 600 rpm and then a specified dose of polymeric flocculant (relative to the solids content of the slurry) was added. Stirring was continued at 600 rpm for 2 minutes and then reduced to 300 rpm for an additional 8 minutes. The slurry was then transferred to a 100 mL cylinder to allow consolidation of solid particles for 24 hours. The supernatant was decanted to collect the sediments which contained a certain amount of water, depending on the effectiveness of polymer dosage. Next, the sediments were covered with aluminum foil and held at 85 °C for 1 week to allow in situ degradation of the polymer within the sediments. Sediment capillary suction time (CST) was measured before and after the accelerated degradation test using a Triton Electronics meter (Type 319 multi-CST) with five test heads; single-radius cell heads 10 mm in diameter and Whatman filter paper #4. Three replicates per individual sample were analyzed for CST to construct error bars using an intra-sample standard deviation.

6.1.3 Results and Discussion

PCL$_n$ChMA macromonomers can be classified as tail-type polymerizable surfactants (surfmers) because they are amphiphiles that possess a cationic head and contain a vinyl group within the hydrophobic tail.[23,24] In general, the micellar structure undergoes extensive reorganization during surfmer polymerization,[25-28] and the resulting polyelectrolytes can reach high MW due to compartmentalization of the polymerizeable group.[29-31] As depicted by Scheme 6.1, PCL$_n$ChMA surfmers form micelles in aqueous solution (critical micelle concentration determined from Figure C.1 of Appendix C); the rapid consumption of 10 wt% PCL$_3$ChMA during a batch radical homopolymerization at 50 °C in D_2O was demonstrated in situ using ^1H NMR, with

90 % conversion reached almost twice as fast as AM under identical conditions (see Figure C.2 of Appendix C). The transmission electron microscopy (TEM) image of poly(PCL$_3$ChMA) produced at 50 °C, shown in Figure 6.1, indicates a non-spherical morphology with fiber-like characteristics, while preliminary MW analysis using multi-angle light scattering indicates the material has a weight-average MW of greater than 5×10^5 Da. These two characteristics are beneficial for oil sands tailings remediation because they promote bridging flocculation which ultimately improves settling performance.[10,12]
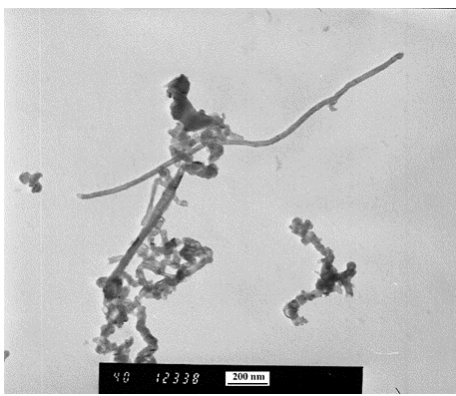
Figure 6.1: Transmission electron microscopy image of poly(PCL$_3$ChMA) synthesized at 50 °C as 10 wt% in D$_2$O with 0.22 wt% V-50 as thermal initiator. Scale bar is 200 nm.

In Figure 6.2, the performance of poly(PCL$_3$ChMA) flocculant in fluid fine tailings from the Alberta oil sands is compared to commercial PAM.[14,19,32] The better clarity of the supernatant, and compactness of the resulting sediment after only 10 minutes of settling demonstrates that poly(PCL$_3$ChMA) is a more effective flocculant than PAM due to its cationic groups. Furthermore, preliminary experiments indicate further improvement in settling behavior when poly(PCL$_2$ChMA) is employed because it has a higher density of cationic groups than poly(PCL$_3$ChMA), a feature that is independent of the overall MW. Following flocculation, poly(PCL$_3$ChMA) is expected to undergo hydrolytic degradation to reveal a more hydrophobic polymer to expel water from the
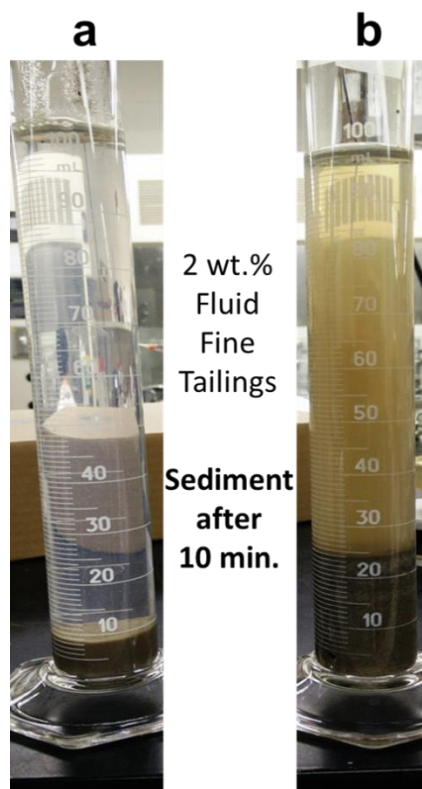
Figure 6.2: Comparison of flocculation performance for 500 ppm (a) poly(PCL₃ChMA) and (b) commercial PAM in 2 wt% fluid fine tailings after 10 minutes of sedimentation.

sediment. This important second aspect of our flocculant design is demonstrated ex situ in Figure 6.3, with full pictorial representation given by Figure C.4 of Appendix C. Visually, the poly(PCL$_3$ChMA) dispersion begins clear, progresses to cloudy after being held at 85 °C for several days, and finally becomes phase separated as a result of the partial hydrolysis of the polyester grafts as indicated by the decreasing pH in Figure 6.4; despite lack of characterization for the partial hydrolysis products, the occurrence of choline and caproic acid hydrolysis products are qualitatively supported by the ^{1}H NMR spectra in Figure C.3 of Appendix C. Although the pH of the H$_2$O used as diluent was initially adjusted to 9 via addition of NaOH, the pH corresponding to 0 days in Figure 6.4 is roughly 7 due to minor hydrolysis of PCL$_3$ChMA during polymerization (1-2 mol%), as suggested by ^{1}H NMR in Figure C.3 of Appendix C. The decrease in pH with increased degradation time is accompanied by an increase in poly(PCL$_3$ChMA) dispersion size. Since choline

units should be most susceptible to cleavage by hydrolysis, and the zeta potential measurements in Figure C.5 of Appendix C demonstrate that cationic stabilization is maintained throughout the degradation process, the increase in dispersion size and large polydispersity indices (Table C.1 of Appendix C) must be attributed to an aggregation mechanism which compensates for the increased interfacial area resulting from loss of stabilizing groups. Also included in Table C.1 are the dispersion size measurements for the accelerated hydrolysis of poly(PCL$_2$ChMA) which demonstrate that flocculant ex situ degradability can be tuned from 6 to 9 days by increasing the average number of polyesters in PCL$_n$ChMA from $n=2$ to $n=3$. Finally, while the complete hydrolysis of the polyester grafts should yield a water-soluble polymethacrylic acid backbone, no change in the precipitated material was observed after more than 1 month at 85 °C. Thus it is the partial degradation of the PCL grafts which distinguishes poly(PCL$_3$ChMA) hydrolysis product from those of other cationic flocculants, such as copolymers of 2-(acryloyloxyethyl)trimethylammonium chloride (choline acrylate), whose hydrolysis would yield water-soluble polyacrylic acid repeat units.
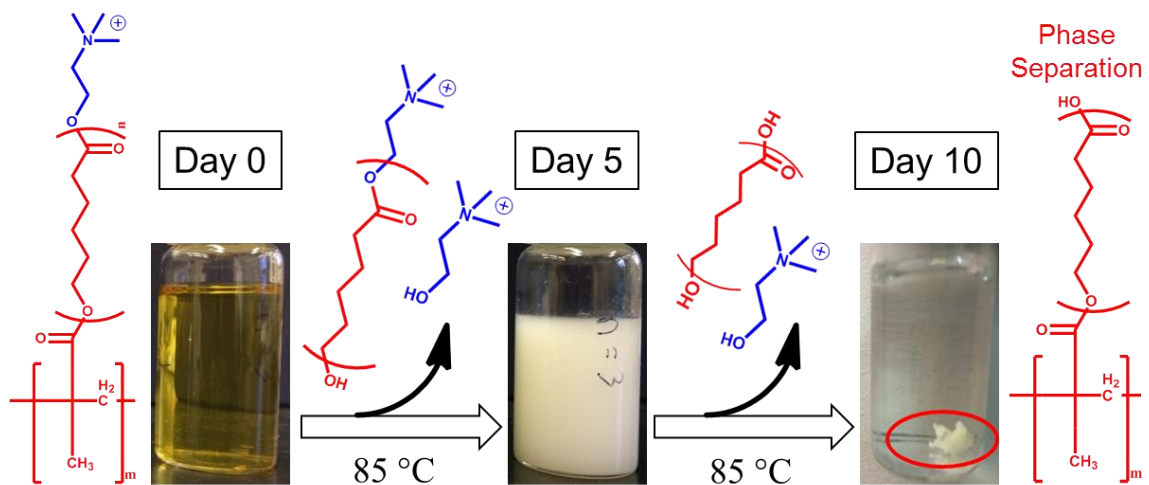
Scheme 6.3: Accelerated hydrolytic degradation test at 85 °C of 1 wt% poly(PCL$_3$ChMA) in H$_2$O with initial pH of 9 with expected degradation product. Samples were cooled to room temperature for visual documentation.

As a lower limit to the ex situ dewatering performance, the accelerated degradation of poly(PCL$_3$ChMA) was also performed in pH=9 buffer solution, where the carboxylate form of the partially degraded graft PCL spacers should predominate. Indeed, zeta potential measurements in Figure C.5 of Appendix C indicate that after one day of degradation the material becomes and remains a polyanion stabilized by carboxylates groups. Moreover, the increase in partially degraded poly(PCL$_3$ChMA) dispersion size (Figure C.6 of Appendix C) and narrowing of polydispersity indices (Table C.2 of Appendix C) with increased degradation time can be attributed to a swelling mechanism.[15,16] While hydrophobic fragments are continually released with pH maintained at 9, the number of carboxylates on the polyanion remains constant, resulting in a more hydrophilic
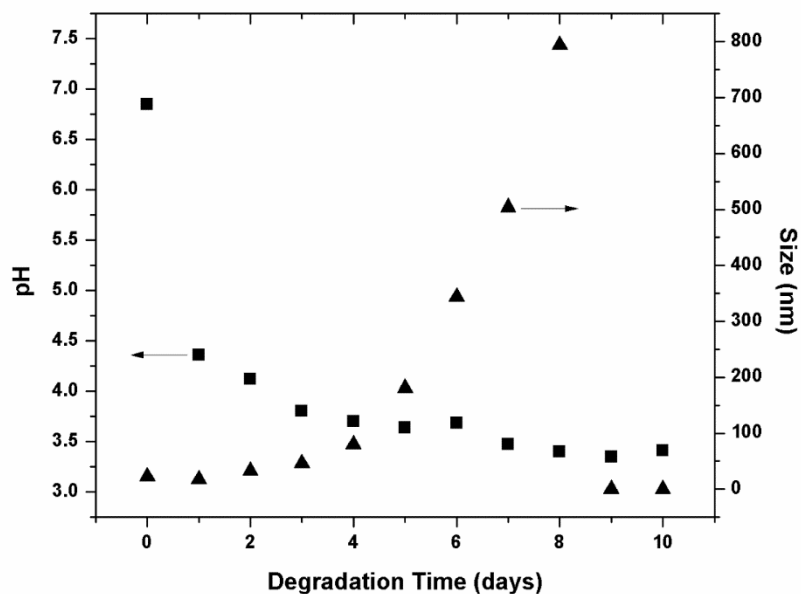
Figure 6.3: Evolution of intensity average size (▲) and pH (■) during ex situ accelerated hydrolytic degradation of 1 wt% poly(PCL$_3$ChMA) in H$_2$O at 85 °C. Samples were cooled to room temperature for measurement. Standard deviations for the size measurements are within 2% of the mean.

polymer. Given that the oil sands are only mildly alkaline (pH roughly 8-9) and that the pK_a of a similar weak polyacid such as polymethacrylic acid is 6–7,[33] one hydrolysis event per graft is sufficient to lower the pH of a sediment from 9 to below 7, under which conditions a significant amount of non-ionized partially degraded PCL grafts will exist and a dewatering effect should be observed.

The ex situ degradation study could be used as a preliminary indicator for the in situ poly(PCL$_3$ChMA) enhanced dewaterability performance, but the differences in micro-environment are not fully understood. During ex situ poly(PCL$_3$ChMA) degradation the polymer is free in solution until it precipitates, whereas in situ it is confined within the sediment. Thus, capillary suction time (CST) was used to quantify the effect of poly(PCL$_3$ChMA) degradation on the in situ dewaterability of a 2 wt.% kaolin clay model tailings sediment. Since oil sands tailings contain various clays whose physicochemical properties play an important role in determining flocculant performance,[10] the dominant clay component, kaolin, was chosen as a model to widely represent the oil sands tailings and to minimize the system complexity. Furthermore, non-ionic PAM was chosen as control because significant amide hydrolysis is not expected under these accelerated degradation conditions, and any such hydrolysis would yield water-soluble acrylic acid repeat units. As shown in Figure 6.5, the CST of poly(PCL$_3$ChMA) sediments is roughly one third that of PAM generated sediments. In addition, accelerated degradation conditions led to a 30 % reduction in CST for the sediments produced using 500 ppm poly(PCL$_3$ChMA), whereas the change in CST was negligible for the 0 and 500 ppm PAM controls. Under field conditions, the enhanced dewaterability of poly(PCL$_3$ChMA) will be significantly slower than the accelerated conditions chosen in this work; similar hydroxyl functionalized short-chain PCL-based materials exhibited total degradation at room temperature after 6 months.[15] However, only partial hydrolytic degradation of poly(PCL$_n$ChMA) is required to cleave the cationic components and elicit its hydrophobic transition. To decrease the time required for the onset of enhanced dewatering, lactide
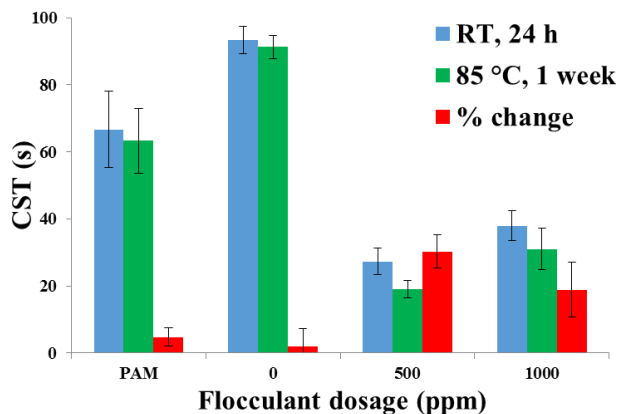
Figure 6.4: CST measurements for 2 wt% kaolin sediments as well as % change in CST measurements after 1 week of accelerated degradation at 85 °C for poly(PCL₃ChMA) flocculant with 0 and 500 ppm PAM included as controls. Error bars represent intra-sample standard deviation from triplicates runs.

could be selected in the ROP step to produce PLA macromonomers whose hydrolytic degradation rates are significantly faster than PCL.[34]

Although the change in final material properties following hydrolysis of polyesters has been well-documented,[35,36] poly(PCL₃ChMA) is, to the best of our knowledge, the first reported polymeric material specifically designed to become more hydrophobic in response to hydrolysis for application in oil sands tailings remediation. Moreover, the increased dewaterability of poly(PCL₃ChMA) is advantageous because it does not depend on the input of external energy to trigger a hydrophilic to hydrophobic transition (in contrast to PNIPAM-based flocculants), and the polyester hydrolysis byproducts are widely regarded as biodegradable.[37]

6.1.4 Conclusions

In this work, we have presented the methodology and proof of concept for the production of a new family of cationic polyester macromonomers, termed polycaprolactone choline iodide ester methacrylate (PCL$_n$ChMA), which become more hydrophobic in response to hydrolysis. Using

micellar radical polymerization of these macromonomers, we combined the material properties of polyesters with the productivity of radical polymerization to generate dual functional comb-like polymeric flocculants, poly(PCL$_3$ChMA), with tunable charge density for rapid settling, and hydrolytically degradable grafts that reveal hydrophobic segments which further expel water from the sediment. A significantly clearer supernatant and more compact sediment was achieved when poly(PCL$_3$ChMA) was used to flocculate fluid fine tailings from the Alberta oil sands compared to commercial polyacrylamide flocculant. In addition, we demonstrated that partial hydrolytic degradation of poly(PCL$_3$ChMA) causes up to a 30 % reduction in capillary suction time (a measure of sediment permeability) for a kaolin model tailings sediment. Preliminary experiments indicate that flocculants produced from PCL$_n$ChMA with average n=2 instead of n=3 polyester units settle tailings more rapidly and reduce the ex situ degradation time from 9 to 6 days.

Thus, our future studies will systematically vary the value of n and the polyester type (PCL and PLA) to produce macromonomers with both methacrylate and acrylate functionality. Via macromonomer copolymerization with acrylamide, we will then correlate the properties of the resulting polymer (degree of branching, cationic density, hydrophobicity, and copolymer sequence distribution) with flocculation and degradation performance.

6.2 Tertiary Amine Macromonomer

6.2.1 Introduction

Cellulose nanocrystals (CNC) are biorenewable materials whose unique physical and mechanical properties have attracted the attention of many researchers.[38-44] The majority of CNC research has focused on its incorporation into new products (e.g., as a reinforcing agent in polymer-based composites). However, it is difficult to disperse CNC in most hydrophobic polymer matrices because its surface is considerably hydrophilic due to the high concentration of hydroxyls and charged surface sulphate half-esters (up to 0.5–2% in sulphur content) that are a result of CNC production using sulfuric acid.[45]

In addition, the possibility to reversibly transition a material from hydrophobic to hydrophilic using CO_2 as stimulus has also attracted much attention recently. For example, in the presence of water and CO_2, carbonic acid is formed which can protonate the tertiary amine bearing repeat units of a polymer, causing the polymer chains to become more hydrophilic. Then, purging the system with N_2, Ar, or air displaces the dissolved CO_2, causing the carbonic acid equilibrium to shift which results in deprotonation of the amines and returns the polymer to its neutral and hydrophobic state.[46-47]

Many CO_2 switchable polymer systems make use of monomers such as 2-(*N, N* dimethylamino)ethyl methacrylate (DMAEMA), whose tertiary amine is in close proximity to the polymeric backbone after polymerization. A potential shortcoming is that the "switched off" state of poly(DMAEMA) is relatively hydrophilic (in comparison to the homopolymer of 2-(*N, N* diethylamino)ethyl methacrylate, for example) and that the switchable groups may become buried inside the polymer, making it difficult for carbonic acid to access them. Thus, the central premise of this work is to attach the pH responsive macromonomers, polycaprolactone 2-(*N,N*-dimethylamino)ethyl ester methacrylate (PCL$_n$DeMA; for *n*=2 and 3), shown in Scheme 6.3, to CNC in order to investigate the effect of switchable group distance from the backbone on the
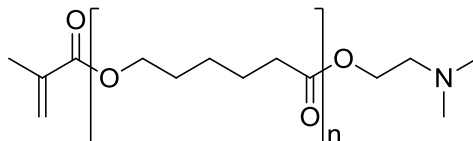
Scheme 6.4: Chemical structure of PCL$_n$DeMA pH responsive macromonomers.

dispersability of CNC in aqueous media using CO_2 as pH trigger. It should be noted that DMAEMA corresponds to PCL$_n$DeMA with $n=0$, and therefore the effect of the PCL grafts is also to increase the system's hydrophobicity per switchable group.

6.2.2 Experimental

The materials required for the synthesis of PCl$_2$DeMA and PCl$_3$DeMA are detailed in Section 3.2 with corresponding syntheses performed according to Section 3.3. CNC, provided by FPInnovations, was prepared at FPInnovations pilot plant (Pointe-Claire, QC) using sulphuric acid hydrolysis of a commercial bleached softwood Kraft pulp. BlocBuilder® (N-(2-methylpropyl)-N-(1-diethylphosphono-2,2-imethylpropyl)-O-(2- carboxylprop-2-yl) hydroxylamine (BB, 99%) was used as received from Arkema. CNC-macroalkoxyamine was synthesized following a previously reported procedure.[38,39]

Dr. Omar Garcia-Valdez performed all grafting reactions, characterizations, and CO_2-responsivity evaluations using procedures documented elsewhere.[38,39] Briefly, PCL$_2$DeMA and PCL$_3$DeMA were grafted from the CNC surface by nitroxide mediated polymerization (NMP) with respective yields of 35 and 40 wt% (relative to CNC) as determined by elemental analysis. Inside a 50 mL 3-neck round bottom flask equipped with pH meter probe and dispersion tube, the products CNC-*g*-PCL$_2$DeMA and CNC-*g*-PCL$_3$DeMA were dispersed in deionized water (1 mg·mL^{-1}). Then, the dispersion was bubbled with either CO_2 or N_2 until the pH measurement was stable (at least 1 hour), and then samples were extracted for ζ-potential determination. This cycle was repeated several times to demonstrate the reversibility of the process.

6.2.3 Results and Discussion

The presence of polymeric tertiary amines covalently linked to the CNC surface enables CNC to become protonated (hydrophilic surface) in the presence of carbonic acid (i.e., CO_2 conditions) to form a stable dispersion, or deprotonated (hydrophobic surface) in the absence of carbonic acid (i.e., N_2 conditions) to form an unstable dispersion that aggregates. Ideally, CO_2/N_2 cycles can be used to trigger CNC to reversibly form a stable dispersion or to aggregate.

Figure 6.6 shows the ζ-potential values vs pH for CNC-*g*-PCL$_2$DeMA and CNC-*g*-PCL$_3$DeMA dispersions under alternating CO_2/N_2 atmospheres. In the presence of CO_2, the ζ-potential for CNC-*g*-PCL$_2$DeMA ranges from 34-38 mV (pH~3.9-4.4), forming stable dispersions, while under N_2 the ζ-potential decreased to 3.3-7.20 mV (pH=8.9-9.2), resulting in destabilization of the dispersion and the formation of aggregates (confirmed visually). On the other hand, although a poor ζ-potential of 19-22 mV (pH~3.1-3.2) was reached under CO_2, the CNC-*g*-PCL$_3$DeMA dispersion was effectively aggregated under N_2 (ζ-potential of 3.2-4.5 mV). These observations could be attributed to two factors. Firstly, given that a similar weight fraction of polymer was grafted to the CNC surface for both *n*=2 and *n*=3 macromonomers (35 and 40 wt% relative to CNC), the total concentration of tertiary amines (switchable groups) is more than 20% lower for the PCL$_3$DeMA system (MW$_{avg}$=499 g·mol^{-1}) than for the PCL$_2$DeMA system (MW$_{avg}$=385 g·mol^{-1}) because of differences in macromonomer average MWs. The second reason could be that the increased hydrophobicity of PCL$_3$DeMA system cannot be adequately stabilized by the available density of switchable groups. Nevertheless, it is clear that the CNC-*g*-PCL$_2$DeMA provides better dispersion and CO_2 switchable properties.
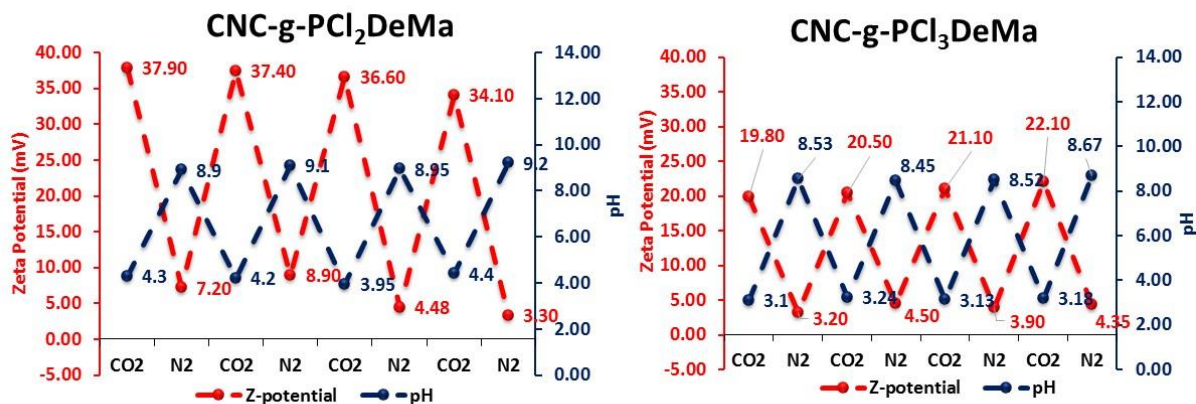
Figure 6.5: ζ-potential versus pH of CNC-*g*-PCL₂DeMA (left) and CNC-*g*-PCL₃DeMA (right) under CO_2/N_2.

It is also important to compare the CO_2-responsivity of CNC-*g*-PCL₂DeMA to that of CNC-*g*-DMAEMA, the system which corresponds to PCLₙDeMA with *n*=0 and whose synthesis was previously reported.[39] In the case of CNC-*g*-DMAEMA (roughly 53 wt% polymer relative to CNC), the ζ-potential under CO_2 was in the range of 30-31 mV (pH~3.9), indicating a stable dispersion, while under N_2 the ζ-potential decreased to 1.6-2.0 mV (pH=9.23). In comparison, the CNC-*g*-PCL₂DeMA system reaches a significantly higher ζ-potential under CO_2 to form a more stable dispersion despite having a considerably lower content of grafted polymer (35 wt%). Assuming that in isolation the individual tertiary amines of poly(DMAEMA) and poly(PCL₂DeMA) have similar pK_{aH}, the better protonation of CNC-*g*-PCL₂DeMA might be attributed to better accessibility of the switchable groups (which are farther from the polymeric backbone) or the more hydrophobic character afford by the PCL spacers.

6.2.4 Conclusions

Two new CNC-based materials with CO_2 (pH)-responsive properties were synthesized via NMP using tertiary amine functionalized macromonomers PCLₙDeMA with both *n*=2 and *n*=3. The

resulting comb-polymer grafted-CNC dispersions (i.e., CNC-*g*-PCL$_2$DeMA and CNC-*g*-PCL$_3$DeMA) exhibited CO$_2$-responsivity and full reversibility, demonstrating that when protonated, the grafted polymer allows the CNC surface to transition from a hydrophilic to a hydrophobic state in response to CO$_2$/N$_2$ triggers. The length of the side chain of PCL$_2$DeMA or PCL$_3$DeMA plays an important role controlling the density of tertiary amines on the CNC surface (and therefore the CO$_2$-responsivity) as well as the system hydrophobicity. In comparison to CNC-*g*-DMAEMA produced using the common monomer DMAEMA (i.e., PCL$_n$DeMA with *n*=0), the CNC-g-PCL$_2$DeMA produces dispersions with higher stability despite having a lower content of grafted polymer.

6.3 References

(1)   Vedoy, D. R. L.; Soares, J. B. P. *Can. J. Chem. Eng.* **2015**, *93*, 888.

(2)   Klein, C.; Harbottle, D.; Alagha, L.; Xu, Z. *Can. J. Chem. Eng.* **2013**, *91*, 1427.

(3)   Botha, L.; Soares, J. B. P. *Can. J. Chem. Eng.* **2015**, *93*, 1514.

(4)   Kasperski, K. L.; Mikula, R., J. *Elements* **2011**, *7*, 387.

(5)   Beier, N.; Wilson, W.; Dunmola, A.; Sego, D. *Can. Geotech. J.* **2013**, *50*, 1001.

(6)   Li, H.; P., O. S. J.; Franks, G. V. *AIChE J.* **2009**, *55*, 2070.

(7)   Hogg, R. *Int. J. Miner. Process.* **2000**, *58*, 223.

(8)   Demoz, A.; Mikula, R. J. *J. Environ. Eng.* **2012**, *138*, 129.

(9)   Gregory, J.; Barany, S. *Adv. Colloid Interface Sci.* **2011**, *169*, 1.

(10)   Wang, C.; Harbottle, D.; Liu, Q.; Xu, Z. *Miner. Eng.* **2014**, *58*, 113.

(11)   Long, J.; Li, H.; Xu, Z.; Masliyah, J. H. *AIChE J.* **2006**, *52*, 371.

(12)   Li, H.; Long, J.; Xu, Z.; Masliyah, J. H. *Can. J. Chem. Eng.* **2008**, *86*, 177.

(13)   Sakahara, S.; Yagi, S.; Iizawa, T. *Sep. Purif. Technol.* **2011**, *80*, 148.

(14)   O'Shea, J.; Tallón, C. *Sep. Purif. Technol.* **2011**, *82*, 167.

(15)   Ferrari, R.; Yu, Y.; Morbidelli, M.; Hutchinson, R. A.; Moscatelli, D. *Macromolecules* **2011**, *44*, 9205.

(16)   Colombo, C.; Dragoni, L.; Gatti, S.; Pesce, R. M.; Rooney, T. R.; Mavroudakis, E.; Ferrari, R.; Moscatelli, D. *Ind. Eng. Chem. Res.* **2014**, *53*, 9128.

(17)   Yang, Z.; Shang, Y.; Lu, Y.; Chen, Y.; Huang, X.; Chen, A.; Jiang, Y.; Gu, W.; Qian, X.; Yang, H.; Cheng, R. *Chem. Eng. J.* **2011**, *172*, 287.

(18)   Yang, Z.; Wu, H.; Yuan, B.; Huang, M.; Yang, H.; Li, A.; Bai, J.; Cheng, R. *Chem. Eng. J.* **2014**, *244*, 209.

(19)   Wang, L.; Wang, J.; Zhang, S.; Chen, Y.; Yuan, S.; Sheng, G.; Yu, H. *Sep. Purif. Technol.* **2009**, *67*, 331.

(20)   Zheng, H.; Sun, Y.; Zhu, C.; Guo, J.; Zhao, C.; Liao, Y.; Guan, Q. *Chem. Eng. J.* **2013**, *234*, 318.

(21)   Warneke, J.; Wang, Z.; Zeller, M.; Leibfritz, D.; Plaumann, M.; Azov, V. A. *Tetrahedron* **2014**, *70*, 6515.

(22)   Preusser, C.; Hutchinson, R. A. *Macromol. Symp.* **2013**, *333*, 122.

(23)   Jaeger, W.; Bohrisch, J.; Laschewsky, A. *Prog. Polym. Sci.* **2010**, *35*, 511.

(24)   Joynes, D.; Sherrington, D. C. *Polymer* **1996**, *37*, 1453.

(25)   Hamid, S.; Sherrington, D. *J. Chem. Soc., Chem. Commun.* **1986**, 936.

(26)   Cochin, D.; Zana, R.; Candau, F. *Macromolecules* **1993**, *26*, 5765.

(27)   Chatjaroenporn, K.; Baker, R. W.; FitzGerald, P. A.; Warr, G. G. *J. Colloid Interface Sci.* **2009**, *336*, 449.

(28)   FitzGerald, P. A.; McDonald, D. M.; Warr, G. G. *Soft Matter* **2013**, *9*, 2711.

(29)   Cochin, D.; Candau, F.; Zana, R. *Macromolecules* **1993**, *26*, 5755.

(30)   FitzGerald, P. A.; Chatjaroenporn, K.; Zhang, X.; Warr, G. G. *Langmuir* **2011**, *27*, 11852.

(31)   FitzGerald, P. A.; Warr, G. G. *Adv. Colloid Interface Sci.* **2012**, *179–182*, 14.

(32)   Franks, G. V.; O'Shea, J.; Forbes, E. *AIChE J.* **2014**, *60*, 2940.

(33)   Izumrudov, V. A.; Kharlampieva, E.; Sukhishvili *Biomacromolecules* **2005**, *6*, 1782.

(34)   Yu, Y.; Ferrari, R.; Lattuada, M.; Storti, G.; Morbidelli, M.; Moscatelli, D. *J. Polym. Sci., Part A: Polym. Chem.* **2012**, *50*, 5191.

(35)   Geng, Y.; Discher, D. E. *J. Am. Chem. Soc.* **2005**, *127*, 12780.

(36)   Kumari, A.; Yadav, S. K.; Yadav, S. C. *Colloids Surf. B* **2010**, *75*, 1.

(37)   Shah, A. A.; Hasan, F.; Hameed, A.; Ahmed, S. *Biotechnol. Adv.* **2008**, *26*, 246.

(38)   Roeder, R. D.; Garcia-Valdez, O.; Whitney, R. A.; Champagne, P.; Cunningham, M. F. *Polym. Chem.*, **2016**, *7*, 6383.

(39)   Garcia-Valdez, O.; Brescacin, T.; Arredondo, J.; Bouchard, J.; Jessop, P. G.; Champagne, P.; Cunningham, M. F. *Submitted to Polym. Chem.*

(40)   Brown, E. E.; Hu, D.; Abu Lail, N.; Zhang, X. *Biomacromolecules*, **2013**, *14*, 1063.

(41)   Eichhorn, S.; Dufresne, A.; Aranguren, M.; Marcovich, N.; Capadona, J.; Rowan, S.; Weder, C.; Thielemans, W.; Roman, M.; Renneckar, S.; *J. Mater. Sci.*, **2010**, *45*, 1.

(42)   Klemm, D.; Kramer, F.; Moritz, S.; Lindström, T.; Ankerfors, M.; Gray, D.; Dorris, A. *Angew. Chem.*, Int. Ed., **2011**, *50*, 5438.

(43)   Peng, B.; Dhar, N.; Liu, H.; Tam, K. *Can. J. Chem. Eng.*, **2011**, *89*, 1191.

(44)   Xiang, C.; Taylor, A. G.; Hinestroza, J. P.; Frey, M. W. *J. Appl. Polym. Sci.*, **2013**, *127*, 79.

(45)   Araki, J.; Wada, M.; Kuga, S.; Okano, T. *Colloids Surf., A*, **1998**, *142*, 75.

(46)   Darabi, A.; Jessop, P. G.; Cunningham, M. F. *Chem. Soc. Rev.*, **2016**, *45*, 4391.

(47)   Cunningham, M. F.; Jessop, P. G. *Eur. Polym. J.*, **2016**, *76*, 208.

Chapter 7

Pulsed Laser Studies of Cationic Reactive Surfactant Radical Propagation

Preface

The cationic macromonomers used to produce flocculants for oil sands tailings remediation (Chapter 6) possess many desirable features: tunable charge density and enhanced sediment dewaterability in response to hydrolysis. As their application development progresses, a better understanding of the radical polymerization kinetics that govern the material's production is required to more systematically correlate polymer structure to flocculant performance. In 2015 I was fortunate to spend 4 months in Dr. Igor Lacík's lab at the Polymer Institute of the Slovak Academy of Sciences where I benefitted from his expertise in aqueous phase size exclusion chromatography and pulsed laser polymerization (PLP). The kinetic study that I performed in Dr. Lacík's lab is particularly exciting because it represents the first application of PLP to a self-assembled monomer system. In addition, this work also includes kinetic studies of cationic macromonomer copolymerization with acrylamide, a common comonomer in polymeric flocculants. This work is being prepared for publication and is therefore presented in manuscript format.

Abstract

Pulsed laser polymerization coupled with size exclusion chromatography was implemented to study the radical homopropagation kinetics of the cationic tail-type reactive surfactant, polycaprolactone choline iodide ester methacrylate (PCL_nChMA) with $n=2$ average polyester units, at 5, 10, and 20 wt% in H_2O at 25, 50, 70, and 85 °C. Due to PCL_2ChMA compartmentalization, the reaction locus changes with temperature, and the corresponding saturated macromonomer concentrations ($[M]$) cannot easily be determined. Thus, depending on temperature, the products of propagation rate coefficient (k_p) and $[M]$ exhibit a combination of bulk and aqueous homopropagation behaviors. Since propagation at 25 °C is predominantly compartmentalized, a minimum k_p is estimated as 863 ± 95 $L \cdot mol^{-1} \cdot s^{-1}$, assuming bulk $[M]$. (Macro)monomer composition drifts for batch acrylamide (AM)/PCL_nChMA micellar copolymerizations, with $n=2$ and 3, at 5 and 10 wt% in D_2O at 50 °C are adequately represented by the reactivity ratios estimates $r_{AM}=0.31\pm0.03$ and $r_{PCL3ChMA}=8.79\pm0.38$.

7.1 Introduction

Polyelectrolytes are unique among polymers because their ionic character allows them to participate in long-range Coulombic interactions which can be exploited for many applications.[1] In particular, cationic polyelectrolytes (i.e., polycations) find uses in diverse areas as flocculants,[2,3] as anti-microbial devices,[4] and in gene therapy.[5] In many cases, the density of cations as well as the hydrophobic content of the polyelectrolyte are important parameters which need to be carefully designed in order to control performance.[6] The density of cations along the polyelectrolyte backbone can be tuned via aqueous radical copolymerization of a cationic monomer with non-ionic hydrophilic monomers such as acrylamide (AM),[7,8] while the hydrophobic content may be adjusted via a technique known as micellar radical polymerization (MRP).[9] In MRP, the hydrophobic monomer may be solubilized in an appropriate surfactant solution, or a reactive surfactant (surfmer) may be polymerized.[10-12]

In the former version of MRP, the copolymers are produced with blocky hydrophobic microdomains whose lengths depend on the intrinsic reactivity of the hydrophobic/hydrophilic comonomers as well as the so-called micellar effect in which the reactivity of the hydrophobic monomer is enhanced due to its compartmentalization.[13] The micellar effect extends to surfmer polymerization, as above their critical micelle concentration (CMC) surfmers form micelles which give rise to elevated polymerization rates and high molecular weight (MW) materials,[14] whereas polymerizations below the CMC are very inefficient.[15] The large MWs produced by surfmer MRP can be explained in part by the high local concentration of compartmentalized polymerizable groups, but also by the observation that preservation of micelle structure after polymerization is highly unlikely because the rate of surfmer exchange between micelles is much faster than the rate of radical propagation.[16,17] In other words, despite continuous nucleation and dynamic reorganization of the system, surfmer MRP is similar to emulsion radical polymerization in that a saturated monomer concentration inside the growing particle is maintained by monomer diffusion from a reservoir.

Indeed, for the MRP of cationic tail-type surfmer, ω-methacryloyloxyundecyltrimethylammonium bromide (MUTAB), with concentration twice its CMC at 25 °C, Chatjaroenpron et al. showed by small-angle neutron scattering (SANS) that the presence of unpolymerized MUTAB micelles and a constant concentration of free aqueous MUTAB were maintained up to ≈50% conversion, confirming that poly(MUTAB) micelles grow at the expense of the unpolymerized ones.[18] In terms of morphology, unpolymerized and fully polymerized MUTAB micelles are spheroidal (i.e., geometries with long and short radii ranging roughly from 10-100 Å and 10-20 Å, respectively), while at intermediate conversions rod-like mixed polymer/monomer micelles (with length and cross-section radius ranging roughly from 200-3000 Å and 10-30 Å, respectively) coexist in dynamic equilibrium with unpolymerized micelles.[18-20] The structures of poly(MUTAB) systems are also sensitive to environmental factors, responding

111

dynamically and reversibly to temperature, counterion, and salt addition.[21] Furthermore, as suggested by Hamid and Sherrington,[22] cationic tail-type surfmers, such as MUTAB, can adopt a "looped" or "hairpin" conformation where both cationic head and polar methacrylate tail reside at the micelle/water interface. The extent to which the methacrylate group partitions to the micelle/water interface instead of the micelle core depends on conditions like temperature and counterion,[23] and it could be that its radical propagation behavior is different at the two sites. Although many works have recently been devoted to understanding the self-assembly behaviors of surfmers,[21] there are currently no studies to estimate individual propagation rate coefficients (k_p) for these intricate surfmer systems.

The pulsed-laser polymerization coupled with size exclusion chromatography (PLP-SEC) technique is the most reliable and accurate method to evaluate k_p and is described by Beuermann and Buback in comprehensive detail.[24] The product of k_p and monomer concentration, $[M]$, is estimated according to Eqn. 7.1, where L_i is the length of a polymer chain, as measured by SEC, that survived i dark periods during a low-conversion PLP experiment, and t_0 is the time between pulses.

$$\frac{L_i}{t_0} = i \cdot k_p[M] \qquad (\textbf{7.1})$$

The IUPAC *subcommittee on "Modeling of Polymerization Kinetics and Processes"* has benchmarked Arrhenius parameters that describe family behavior for the bulk k_p of methyl methacrylate (MMA) and other alkyl ester methacrylates,[25,26] where an increase in linear length of the ester side chain correlates with an increase in bulk k_p. However, the study of aqueous propagation kinetics is not as straightforward due to the added complexities of aqueous phase SEC analysis,[27] and significant solvent effects on k_p.[28] For example, entropic reasons dictate that the k_p for non-ionized water-soluble monomers increases sharply towards low monomer concentrations,[29-36] while fully ionized monomers, such as methacrylic acid (MAA), exhibit a modest decrease in k_p towards more dilute monomer systems.[37,38]

To date, the successful application of PLP-SEC to a cationic monomer system has not been reported. The main challenge is the ionic repulsion in the system which significantly reduces the probability of termination of growing polycations, and therefore restricts the PLP technique to a narrow range of operating conditions known as the so-called low-termination limit (LTL).[39-41] Thus, Kattner et al. recently developed a new technique, which combines a single laser initiated pulse with time resolved electron paramagnetic resonance (SP–PLP–EPR), to measure the k_p of 20 wt% [2-(methacryloyloxyl)ethyl] trimethylammonium chloride (TMAEMC) in D_2O to be 3,500 $L \cdot mol^{-1} \cdot s^{-1}$ at 60 °C.[42] Furthermore, although PLP-SEC has been implemented in heterogeneous systems to deduce the local styrene concentration compartmentalized in microemulsion droplets,[43] latex particles,[44,45] and vesicle structures,[46] PLP-SEC has not yet been applied to estimate k_p for a self-assembled reactive surfactant system. In this work, the PLP-SEC technique is applied for the first time to a cationic and reactive surfactant system using the recently described macromonomer, polycaprolactone choline iodide ester methacrylate (PCL$_n$ChMA),[47] which is a tail-type surfmer whose structure is shown in Scheme 7.1.
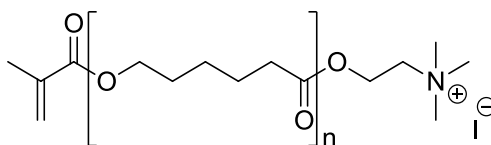
Scheme 7.1: Chemical structure of PCL$_n$ChMA.

7.2 Experimental

Materials

Materials relevant to PCL$_n$ChMA syntheses are detailed in Section 3.2. Formic acid (FA, 98.0-100%), dimethylformamide (DMF, 99.8%) acrylamide (AM, ≥99%), sodium chloride (NaCl, ≥99.0%), 2,2-dimethoxy-2-phenylacetophenone (DMPA, 99%), and 2,2-azobis(2-methylpropionamidine) dihydrochloride (V-50, 97%) were purchased from Sigma Aldrich and used as received. Lithium bromide (LiBr, 99+% for analysis, anhydrous, Acros), lithium phenyl-

2,4,6-trimethylbenzoylphosphinate (LiTPO, synthesized by R. Liska group Institute of Applied Synthetic Chemistry, Vienna University of Technology, Austria) and deuterium oxide (D_2O, 99.9% D, Cambridge Isotope Laboratories) were used as received. Ultrapure pure water was obtained from Ultrapure Water System NW Series (Heal Force Bio-Meditech Holdings, Ltd., China).

Macromonomer Characterizations

The syntheses of PCL_nChMA (for n=2 and n=3) macromonomers were performed according to Section 3.2 with ^{1}H NMR for PCL_2ChMA provided as Figure D.1 of Appendix D.

As shown in Figure D.2 of Appendix D, the solid PCL_2ChMA salt was dissolved at various weight fractions in DMF, and the solution densities were measured between temperatures of 25 and 70 °C using a Paar DMA 48 Density Meter. Assuming volume additivity, the densities of the PCL_2ChMA salt were extrapolated at each temperature (Table D.1 of Appendix D), and subsequently fit by linear regression as summarized by Table 7.1. The critical micelle concentrations (CMC) of PCL_nChMA macromonomers in H_2O solutions were determined by surface tension measurements (Figures D.4 and D.10 of Appendix D) using a Wilhelmy plate setup (TensioCAD with platinum plate EN14370).

The particle size distributions (PSD) and polydispersity indices (PDI) for 10 wt% PCL_2ChMA dispersions in H_2O were determined with a Malvern Zetasizer Nano ZS (size range 0.3 nm −10 μm) at 25 and 70 °C with backscattering optics (173°), using a 4 mW He–Ne (633 nm) laser. All samples were measured in DTS0012 disposable cuvettes. The reported sizes represent an intensity average of at least 30 scans.

Pulsed Laser Polymerization

Stock solutions of 5, 10, and 20 wt% macromonomer in H_2O were prepared by stirring overnight with 10 mmol·L^{-1} LiTPO (relative to H_2O) or 10 mmol·L^{-1} DMPA (relative to macromonomer). As previously described,[35] PLPs were carried out using an excimer laser (ExciStar XS 500, Coherent, Inc.) operated at 351 nm and equipped with corona preionization and an all-solid-state-pulser. Pulse

repetition rates from 5-50 Hz were used at a laser energy of 3 mJ/pulse. The polymerizations were carried out in a 110 OS cell (Hellma GmbH & Co. KG, Germany) of 10 mm path length. The cell was filled with 1 mL solution, sealed with a PTFE stopper, and subjected to polymerization. The beam expander BXUV-10.0-3X (CVI Melles Griot, USA) was placed between the laser and the cell to extend the beam such as to homogeneously illuminate the solution. Prior to applying the laser pulses, the macromonomer solutions were thermostated for 10 minutes (at 25, 50, 70, or 85 °C) before insertion of the cell into the thermostated metallic cell holder where the laser pulses were applied. No significant hydrolysis of the macromonomer (or resulting polymer) is expected during the timeframe of a PLP experiment under these conditions.[47] After pulsing, the reaction mixture was poured into a vial containing a few crystals of hydroquinone monomethyl ether to suppress post-polymerization. The comb-polymer was isolated by dialysis using SpectraPor tubing with a molar mass cutoff at 3500 Da (Spectra/Por 6, Spectrum Laboratories, Inc., Compton, CA), freeze-dried using a Mini-Lyotrap (LTE Scientific, Greenfield, UK), and then conversion was determined by gravimetry. The iodide counterions of the comb-polymers are sensitive to UV degradative reactions and therefore the samples were stored in the dark at 4 °C.

Size Exclusion Chromatography

For SEC analysis of the PLP generated comb-polymers, an aqueous eluent of 0.3 M formic acid with 0.3 wt% LiBr was selected to ensure good solubility of the cationic polymers and to provide sufficient screening of polyelectrolyte charges. The samples were dissolved in the eluent at concentrations of 2 mg·mL^{-1} by stirring for 24-48 hours and filtered via a 0.45 μm nylon membrane filter (Millex-HN, Millipore, Ireland) prior to injections on the columns. SEC was performed using a column setup consisting of PSS Novema MAX 8×50 mm guard and three PSS Novema MAX 8x300 mm 100 + 1000 + 3000 Å columns with 10 μm particle size, which was positioned in the column heater at 40 °C. The flow rate of 1.0 mL·min^{-1} was controlled by using ethylene glycol as the flow marker. 100 μL of polymer solution at the concentration of 1 to 3 mg·mL^{-1} of eluent was

injected. A Waters SEC setup (degasser, 515 pump, column heater, differential RI detector 2410, autosampler 717) with SLD 7000 MALLS detector (Polymer Standards Service, Mainz, Germany) was used. The PSS WinGPC®UniChrom (Polymer Standards Service, Mainz, Germany) software was employed for data acquisition and evaluation. The differential refractive index values, dn/dc, were determined by integration of the RI signals from injection of five poly(PCL$_n$ChMA) solutions with concentrations of 0.1–10.0 mg·mL^{-1} using WinGPC®UniChrom software. The dn/dc values for poly(PCL$_2$ChMA) and poly(PCL$_3$ChMA) summarized by Table 7.1 demonstrate that the dn/dc becomes independent of backbone as well as graft MW. An effective calibration was established using nine narrow pullulan standards between 180–830,000 g·mol^{-1} (Polymer Laboratories, UK), while pullulan of 113,000 g·mol^{-1} was used as isotropic scatterer to calibrate the MALLS detector.

Table 7.1: Monomer and polymer parameters relevant to k_p determination by PLP-SEC.

		Monomer		Polymer
	n	ρ (g·mL^{-1})	CMC^b (mmol·L^{-1})	dn/dc^c (mL·g^{-1})
PCL$_2$ChMA	2.0	$-0.0006 \cdot T/°C+1.3181^a$	1.5	0.114
PCL$_3$ChMA	3.2	-	0.51[47]	0.117
Pullulan	-	-	-	0.136

^{a} Extrapolated from DMF solutions assuming volume additivity.
^{b} measured at room temperature.
^{c} determined in 0.3 M formic acid with 0.3 wt% LiBr aqueous eluent.

The SEC traces from the RI detector in Figure D.5 of Appendix D do not show any significant concentration dependence, which verifies the appropriateness of the current SEC setup to separate poly(PCL$_n$ChMA) samples exclusively based on size. MALLS data are only reported if good agreement between at least 2 injections of the same sample is achieved – the SEC traces from the MALLS detector in Figure D.6 of Appendix D (summarized by Table D.3) show good reproducibility for samples injected at a minimum of 1.86 mg·mL^{-1}. As summarized by Table D.4 of Appendix D, inflection points from MALLS are correlated to the effective pullulan calibration by a factor of 1.83±0.08.

Macromonomer Copolymerization Study

All AM/PCL$_n$ChMA copolymerizations were performed in D$_2$O (containing 0.22 wt% V-50 initiator) at 50 °C following a previously described procedure for in situ ^{1}H NMR,[48] using a Bruker Avance instrument operating at 400 MHz. (Macro)monomer solutions, with initial AM content of $f_{AM,0}$=0, 0.1, 0.5, 0.9, and 1.0, were prepared at 5 or 10 wt% concentrations relative to D$_2$O and carefully bubbled with N$_2$ for at least 1 hour prior to polymerization. Monomer composition was monitored by comparing the vinyl peak intensity for AM to that of PCL$_n$ChMA, while conversion was determined via the sum of both (macro)monomers' vinylic integrations relative to the HOD signal as a function of time. The monomer composition drift as a function of conversion data was used to estimate Terminal Model reactivity ratios via the integrated Mayo-Lewis equation implemented by Predici software.[48]

7.3 Results and Discussion

7.3.1 Pulsed Laser Polymerization

Initial PCL$_3$ChMA aqueous homopolymerization PLP-SEC experiments performed at 50 °C with pulse repetition rates of 33 and 50 Hz yielded molar mass distributions (MMD) whose corresponding 1st derivative plots did not exhibit inflection points characteristic of the PLP technique. This shortcoming is related to the relatively high viscosity associated with PCL$_3$ChMA (average MW of 641 g·mol^{-1}), making it a LTL PLP system in which operating conditions that lead to successful k_p determination are limited.[39,41] Therefore, PLP-SEC experiments for aqueous homopolymerizations of PCL$_2$ChMA, whose lower average MW of 527 g·mol^{-1} facilitates improved termination relative to PCL$_3$ChMA, were performed at 25, 50, 70, and 85 °C with specific reaction conditions summarized by Tables D.5, D.6, D.7, and D.8, respectively. It should be noted that PCL$_2$ChMA is a distribution of macromonomers (Figure A.12 of Appendix A), with number average n=2.0 polyester units, that contains up to 10 mol% TMAEMI (as determined by ^{1}H NMR in Figure D.1).

Figure 7.1 demonstrates that PCL$_2$ChMA homopropagation can be controlled by laser pulsing at various pulse repetition rates and temperatures. However, a significant fraction of chains are terminated prior to the arrival of the subsequent laser pulse giving rise to a peak with inflection point near 35,000 g·mol^{-1}, as indicated by D on the 1st derivative plots in Figure 7.1. The location of inflection point D does not shift according to pulse repetition rate, and only slightly decreases to lower MW at higher temperatures – although the origin of D is unknown, it could indicate the relevance of possible chain transfer to monomer reactions, which were deemed significant for several other cationic surfmer polymerization systems.[15] Inflection point D often obstructs the identification of PLP generated primary inflection point, L_1, such that the ratio of secondary to primary inflection points, L_2/L_1, is frequently less than 2.0; at 30 Hz, L_1 is completely overlapped by D, and therefore L_2 is used to evaluate PCL$_2$ChMA PLP experiments performed at relatively low pulse repetition rates in this study, consistent with previous work.[36] Since determination of the macromonomer concentration at the reaction site, [M], is not straightforward for PCL$_2$ChMA aqueous homopolymerizations, the PLP-SEC experiments are evaluated in terms of $k_p \cdot [M]$ in Tables D.5-D.8 of Appendix D, with k_p estimated from the L_2 position.
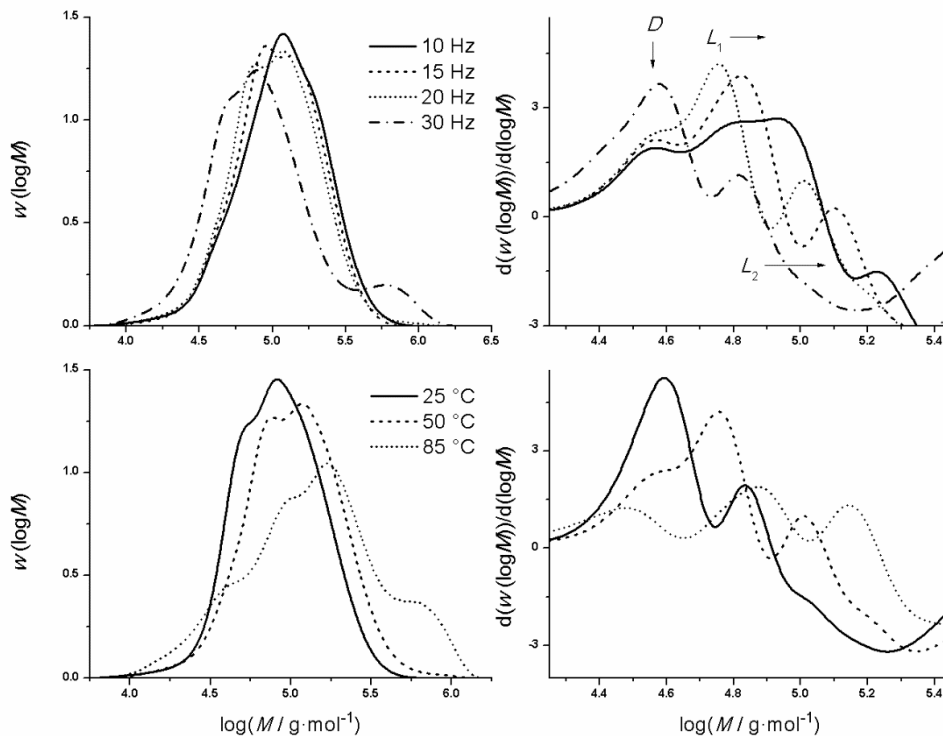
Figure 7.1: MMDs (left) and corresponding 1st derivative plots (right) according to pullulan calibration for PLP-SEC experiments of 10 wt% PCL$_2$ChMA at 50 °C and variable pulse repetition rate (top) as well as 10 wt% PCL$_2$ChMA at 20 Hz and variable temperature (bottom). Inflection point labelled _D_ corresponds to the length of chain terminated by unknown mechanism.

The particle size distributions for 10 wt% macromonomer aqueous solutions at 25 and 70 °C, shown by Figure D.3 of Appendix D, are evidence of PCL$_2$ChMA compartmentalization, where the bimodal intensity scattering indicates that PCL$_2$ChMA micelles may have non-spherical geometries.[49] In addition, the dispersion parameters summarized by Table D.2 highlight the dynamic nature of the system; in particular, the decreasing scattering intensity towards higher
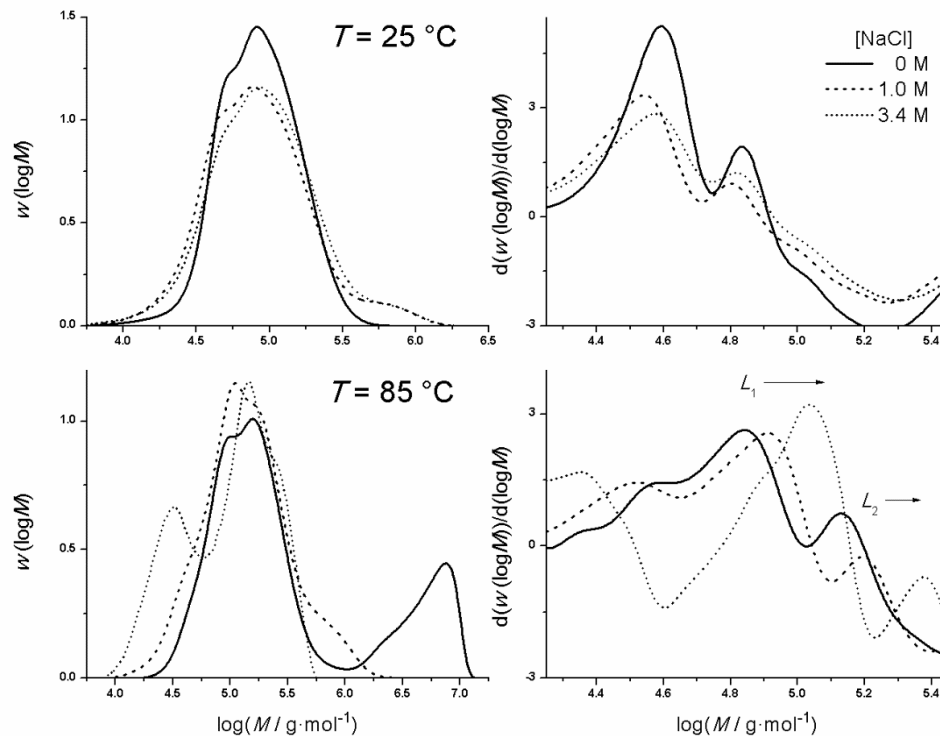
Figure 7.2: MMDs (left) and corresponding 1st derivative plots (right) according to pullulan calibration for PLP-SEC experiments of 10 wt% PCL$_2$ChMA at 25 °C (top) and 85 °C (bottom) with NaCl concentrations of 0 M (solid line), 1.0 M (dashed line), and 3.4 M (dotted line) performed at 20 Hz.

temperatures indicates increased PCL$_2$ChMA aqueous solubility. Thus, it is likely that the location of the reaction site (aqueous or compartmentalized) changes with temperature such that determination of [M] is not trivial. For compartmentalized systems, the aqueous phase monomer concentration is governed by the CMC; if aqueous phase propagation is dominant, addition of salt to lower the CMC should result in a commensurate reduction in $k_p \cdot [M]$ measured by PLP-SEC. To test this hypothesis, PLP experiments were performed with 0, 1.0, and 3.4 M NaCl, as shown by Figure 7.2. While addition of 3.4 M NaCl reduces the CMC of PCL$_2$ChMA at 25 °C by

approximately one order of magnitude (see Figure D.4 of Appendix D), the concentration of NaCl has no significant effect on the PLP MMDs at this temperature, certainly not to an extent that would be expected for a ten-fold reduction in aqueous macromonomer concentration. Although the L_1 positions in the 25 °C MMDs in Figure 7.2 are likely overlapped by peak D (as was the case for MMD of the 50 °C sample performed at 30 Hz in Figure 7.1), the L_2, from which $k_p \cdot [M]$ estimations are made, are plainly unobstructed. Therefore it can be safely assumed that propagation occurs predominantly inside the compartmentalized phase at 25 °C. In support of this claim, Figure 7.3 shows no significant change in secondary inflection point location when LiTPO (high aqueous solubility) or DMPA (low aqueous solubility) is used as photoinitiator at 25 °C, indicating that chains initiated in the aqueous phase quickly nucleate unpolymerized PCL$_2$ChMA micelles, and then continue propagation in the compartmentalized phase. In addition, the negligible differences in PLP structure up to 28% conversion at 25 °C (see Figure 7.4) suggest that the compartmentalized propagation occurs at constant macromonomer concentration, for if the PCL$_2$ChMA concentration at the reaction site were not constant, a different k_p measured by PLP-SEC would be expected towards higher conversions since the proportion of solvent to monomer molecules is directly related to the relative mobility of the transition state (TS) for propagation.[28] Therefore, it is reasonable to assume that during polymerization at 25 °C (and up to at least 28% conversion), an equilibrium, or saturated, PCL$_2$ChMA concentration at the compartmentalized reaction site is maintained via macromonomer diffusion from unpolymerized micelles.[14,17,18]
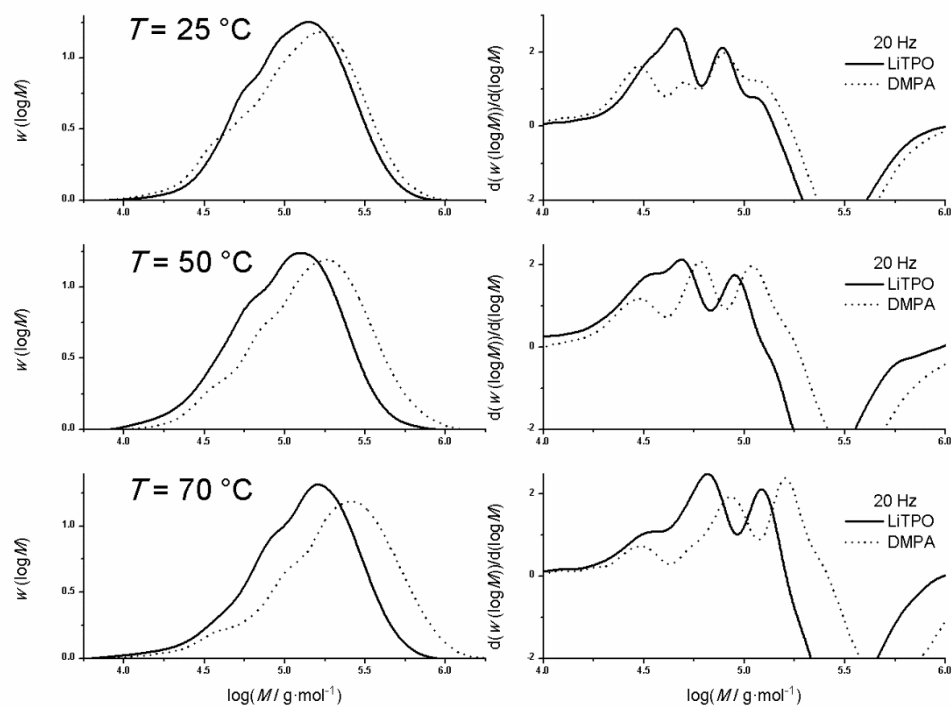
Figure 7.3: MMDs (left) and corresponding 1st derivative plots (right) according to pullulan calibration for 20 wt% PCL$_2$ChMA PLP-SEC experiments performed at 25 (top), 50 (centre), and 70 °C (bottom) with 20 Hz and 10 mmol·L^{-1} LiTPO or DMPA as photoinitiator.

Determining the reaction site of PCL$_2$ChMA homopropagation at elevated temperatures is more complicated. Recalling that the macromonomer aqueous solubility increases with temperature and that PCL$_2$ChMA comprises a distribution of macromonomers with up to 10 mol% TMAEMI (Figures A.12 and D.1, respectively), distinct aqueous phase propagation is plausible. Indeed, at 50 and 70 °C, the inflection points for PLP MMDs shown in Figure 7.3 are shifted to higher MW when DMPA is used as photoinitiator instead of LiTPO. This indicates that higher temperatures afford enhanced aqueous solubility of the oligomers initiated in the aqueous phase such that the growing chain can spend more time outside the compartmentalized phase (where $k_P \cdot [M]$ must be different

122
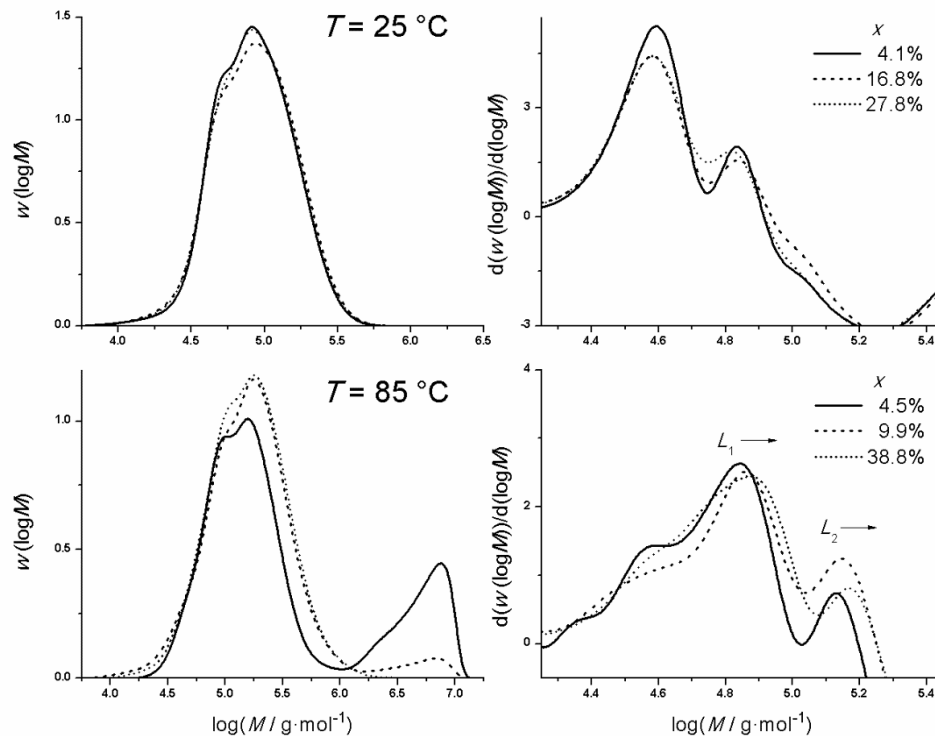
Figure 7.4: MMDs (left) and corresponding 1ˢᵗ derivative plots (right) according to pullulan calibration for PLP-SEC experiments of 10 wt% PCL₂ChMA at 25 °C (top) and 85 °C (bottom) and variable monomer conversions.

than inside the micelle) before being terminated at the next laser pulse. Additional evidence for aqueous propagation at elevated temperatures is exhibited by the 85 °C PLP MMDs in Figure 7.2, where greater NaCl concentrations lead to higher MW inflection points and thus greater values of $k_p \cdot [M]$. Assuming a predominantly aqueous propagation at 85 °C, this could be attributed to the measured effect of ionic strength to decrease the E_A for k_p of partially and fully ionized methacrylic acid aqueous homopropagation systems.[37]

Also in Figure 7.2, the secondary (non-PLP) peaks in the 85 °C MMDs shift from log$M$=7.0 towards log$M$=5.7 and then to log$M$=4.5 with increasing NaCl concentration. As these peaks comprise chains whose terminations were not controlled by laser pulsing, the shift to lower MWs may reflect the ability of NaCl to better screen ionic repulsions between macroradicals so as to increase the probability of termination in the aqueous phase. Finally, the slight increase in inflection point MW towards higher conversions at 85 °C (Figure 7.4) follows the homopropagation behavior expected for aqueous non-ionized monomer systems.[28,33,36]

While it is clear that aqueous propagation of PCL$_2$ChMA must be taken into consideration at elevated temperatures, the relative extents of propagation in the aqueous and compartmentalized phases cannot be determined from the current data set. Furthermore, micellar radical copolymerization studies of hydrophobic monomers with water-soluble comonomers demonstrated that the growing chain can alternate between reaction sites such that the two modes of propagation cannot be considered exclusively.[9] Thus, as detailed by Eqn. 7.2, an appropriate treatment of the L_i values measured by PLP-SEC would account for both the aqueous and compartmentalized phase $k_p \cdot [M]$ contributions as a chain-end radical lifetime-weighted average, where t_0 is the time between successive laser pulses, t_{aq} and $t_0 - t_{aq}$ are the chain-end radical mean lifetimes (during t_0) in the aqueous and compartmentalized phases, respectively.

$$\frac{L_i}{t_0} = k_p[M] = k_p^{aq}[M]_{aq}\left(\frac{t_{aq}}{t_0}\right) + k_p^{comp.}[M]_{comp.}\left(\frac{t_0 - t_{aq}}{t_0}\right) \qquad (7.2)$$

Without knowledge of the extent to which the locus of polymerization changes or the corresponding aqueous and compartmentalized macromonomer concentrations, the treatment detailed by Eqn. 7.2 cannot be applied, and therefore the $k_p \cdot [M]$ values, plotted vs weight fraction macromonomer in Figure 7.5, must be interpreted individually at each temperature. We recall that for aqueous systems in general, as monomer content increases relative to H$_2$O, there is a modest increase in k_p for fully ionized monomers,[37] and a strong decrease in k_p for non-ionized monomers.[33] Since propagation at 25 °C was determined to be predominantly compartmentalized with a
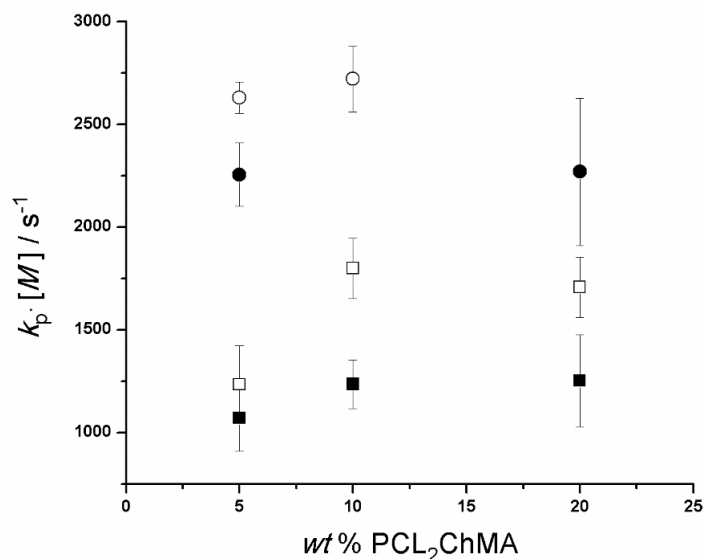
Figure 7.5: Product of k_p and [M], determined from secondary inflection points of PLP-SEC MMDs with pullulan calibration, as a function of initial PCL$_2$ChMA weight fraction relative to H$_2$O at 25 (■), 50 (□), 70 (●), and 85 °C (○). Error bars represent standard deviations.

saturated macromonomer concentration (up to at least 28% conversion), it is no surprise that the measured $k_p \cdot$[M] values are invariant with macromonomer content relative to H$_2$O, similar to a bulk polymerization system.

In contrast to the situation at 25 °C, the $k_p \cdot$[M] measured for 5 wt% PCL$_2$ChMA at 50 °C is markedly lower than at 10 and 20 wt%, which is indicative of aqueous phase contributions to the value. If the measured increase from 5 to 10 wt% was due simply to an increasing monomer concentration, a commensurate increase from 10 to 20 wt% would also be expected, but is not observed. In addition to the fact that the $k_p \cdot$[M] values measured at 10 and 20 wt% are roughly the same, a significant amount of PCL$_2$ChMA is still compartmentalized at 50 °C meaning that both aqueous and compartmentalized macromonomer concentrations are saturated. Therefore, the increase in $k_p \cdot$[M] from 5 to 10 wt% likely reflects a true increase in k_p, which is a characteristic

feature of fully ionized MAA propagation kinetics.[37] At 50 °C, the aqueous solubility of the cationic monomer TMAEMI, which comprises up to 10 mol% of the macromonomer and whose iodide counterion makes it a relatively hydrophobic ion pair, is substantially increased, such that the 50 °C behavior in Figure 7.5 can be interpreted as a combination of TMAEMI aqueous propagation and PCL$_2$ChMA compartmentalized propagation, as described by Eqn. 7.2.

Based on the limited data sets at 70 and 85 °C, there is no clear trend in $k_p \cdot [M]$ with macromonomer weight fraction, an indication that the effect of TMAEMI to decrease $k_p \cdot [M]$ at lower macromonomer weight fraction (i.e., 5 wt%) is counterbalanced by the contribution of another component in the aqueous phase (e.g., a non-ionized monomer whose k_p increases upon dilution). At 70 and 85 °C, the aqueous solubilities of the low MW oligomers (individual $n=1$ or $n=2$ chains) in the PCL$_2$ChMA macromonomer distribution (Figure A.12) are significant. Since the quaternary ammonium groups of PCL$_n$ChMA oligomers are separated from their methacryloyl carbonyl by n CL spacers, their aqueous propagation kinetics are expected to be similar to non-ionic MAA: increased k_p towards more dilute monomer concentrations and invariance of k_p with the ionic strength of the solution.[37] This interpretation is consistent with the increasing inflection point MW towards higher conversions documented for the PLP experiments performed at 85 °C (Figure 7.4), which reflect the greater mobility of the TS facilitated by higher water to monomer ratios.[28]

The $k_p \cdot [M]$ estimates from 10 and 20 wt% PCL$_2$ChMA homopolymerizations at temperatures between 25 and 85 °C are summarized by the Arrhenius plot in Figure 7.6. Assuming bulk monomer concentrations at each temperature, as would exist in a micelle in the absence of polymer, the minimum k_p ($k_{p,min}$) can be estimated in order to calculate an activation energy of 11.6 kJ·mol^{-1} which is well below the values for bulk MMA (22.4 kJ·mol^{-1})[25] and aqueous non-ionized MAA (mean value of 15.6 kJ·mol^{-1}),[33] yet in a similar range as 5-40 wt% fully ionized MAA systems (12.4-8.0 kJ·mol^{-1}).[37] However, without temperature dependent information about
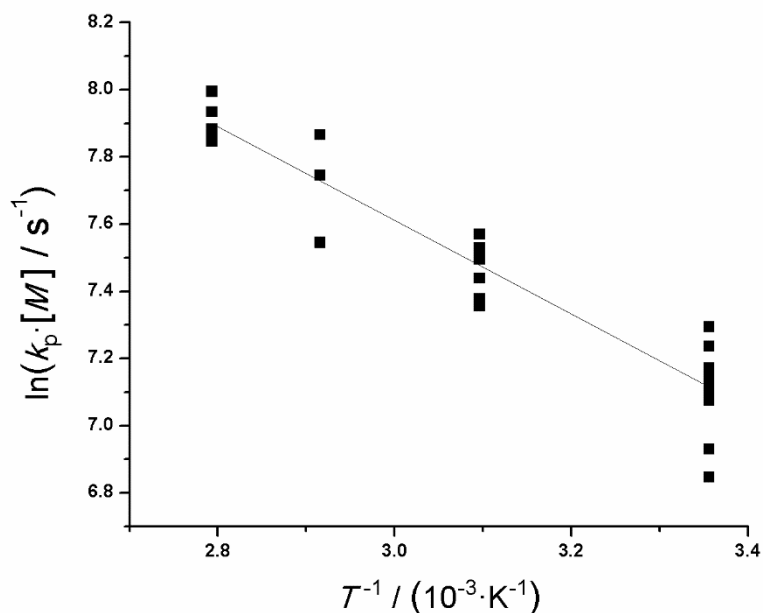
Figure 7.6: Arrhenius plot for the product of k_p and [M], determined from secondary inflection points of PLP-SEC MMDs with pullulan calibration, for 10 and 20 wt% PCL$_2$ChMA experiments performed at temperatures between 25 and 85 °C.

saturated macromonomer concentrations or extents of aqueous and compartmentalized polymerization loci, a meaningful interpretation of PCL$_2$ChMA Arrhenius parameters cannot be established.

Nevertheless, the invariance at 25 °C of $k_p \cdot$[M] to NaCl concentration, monomer conversion, and initiator type justifies the implementation of bulk macromonomer concentration to calculate a $k_{p,min}$ at this temperature. The ratios of $k_p \cdot$[M] estimated by MALLS and pullulan calibrations in Table D.5 of Appendix D are in good agreement with the 1.8 proportionality established in Table D.4 such that an absolute value for $k_{p,min}$ of PCL$_2$ChMA at 25 °C is calculated as 863±95 L·mol^{-1}·s^{-1} from the MALLS output of 11 samples. As comparison for PCL$_2$ChMA, whose average MW is 527 g·mol^{-1}, PLP-SEC studies of other high MW methacrylates, such as polyethylene glycol methyl ether methacrylate (PEGMA, $M_n \approx 500$ g·mol^{-1}) and behenyl

methacrylate (BeMA, 366 g·mol^{-1}), estimated bulk k_p values at 25 °C of 515 and 635 L·mol^{-1}·s^{-1}, respectively.[36,50] The assumption of bulk macromonomer concentration to yield $k_{p,min}$ is a limiting case; more realistically, the saturated macromonomer concentration could be up to 50-60% of the bulk value with the presence of polymer in the micelles, as measured for MMA in poly(MMA) at room temperature,[51] meaning that the k_p for PCL$_2$ChMA at 25 °C could be as much as 2-3 times the values for PEGMA or BeMA, and thus among the highest reported bulk methacrylate k_p values. Such an elevated methacrylate k_p could be inflated by a different propagation behavior for the TMAEMI fraction in the compartmentalized phase. Alternatively, it could be that the elevated estimate for bulk k_p is a feature of the micellar environment in which the "looped" or "hairpin" conformation adopted by tail-type cationic surfmers[22,23] causes the methacrylate groups at the micelle/water interface to propagate more rapidly than those buried in the micellar core.

7.3.2 Macromonomer Copolymerization

The PLP-SEC investigations highlighted the complexities of PCL$_2$ChMA homopropagation kinetics, and therefore batch experiments were performed to shed more light on the intricacies of PCL$_n$ChMA MRP. Furthermore, since a greater diversity of material properties can be achieved through surfmer copolymerization with water soluble comonomers,[9] the batch studies were extended to AM copolymerization. Using the in situ ^{1}H NMR technique,[48,52] monomer conversion and composition drift were monitored during batch radical (co)polymerizations of PCL$_n$ChMA and acrylamide (AM) in D$_2$O at 50 °C with initial monomer concentrations of 5 and 10 wt% for PCL$_3$ChMA as well as 10 wt% for PCL$_2$ChMA systems. Strong evidence for PCL$_n$ChMA compartmentalized propagation is demonstrated by the respective conversion profiles in Figures D.7, D.8, and D.9 of Appendix D, in which greater than 90% conversion is reached more rapidly for PCL$_n$ChMA homopropagation than any of the AM homopropagation or copolymerization systems.

In contrast to AM copolymerizations with the acrylate analog of TMAEMC[53] or ionized acrylic acid,[52] the monomer composition drift profiles for 5 and 10 wt% AM/PCL$_3$ChMA systems, presented in Figure 7.7, show no dependence on the initial monomer concentration relative to D$_2$O. Although this behavior was also documented for AM copolymerization with non-ionized acrylic acid,[48] in this case it is more likely attributed to PCL$_n$ChMA compartmentalization during its micellar radical copolymerization. Using both AM/PCL$_3$ChMA data sets in Figure 7.7, the integrated Mayo-Lewis approach was implemented to estimate monomer reactivity ratios of r_{AM}=0.31±0.03 and $r_{PCL3ChMA}$=8.79±0.38; these values, which also adequately fit the AM/PCL$_2$ChMA composition drift data, indicate preferential PCL$_n$ChMA incorporation at all compositions.

Previous studies on the incorporation behavior of small amounts of hydrophobic monomer (1-3 mol%) during micellar radical copolymerization with hydrophilic monomers ascertained that the reaction mechanism is governed by the intrinsic monomer reactivity ratios as well as the micellar effect (high monomer concentration within micelles in conjunction with rapid monomer exchange between micelles).[13] Therefore, it is likely that these reactivity ratios estimated for AM/PCL$_3$ChMA copolymerization represent apparent rather than intrinsic values. The copolymerization of AM with methyl methacrylate (MMA), whose polymerizable group is the same as that of PCL$_n$ChMA, has reported reactivity ratios in dioxane (r_{AM}=0.90 and r_{MMA}=5.53) and in cyclohexanone (r_{AM}=0.65 and r_{MMA}=8.75).[54] Despite potential different solvent effects between organic and aqueous environments, the AM/MMA systems indicate an inherent tendency for preferential methacrylate incorporation also seen for AM/PCL$_3$ChMA, independent of the micellar effect.
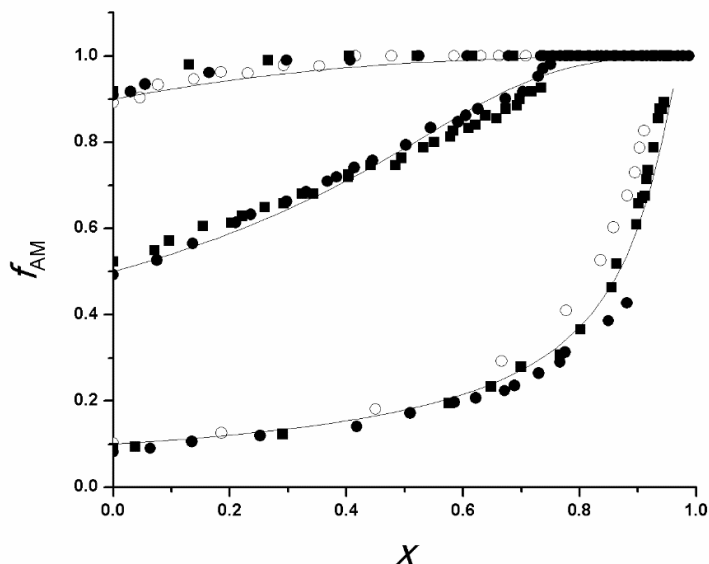
Figure 7.7: Monomer composition drift plots for AM/PCL$_n$ChMA copolymerizations at 5 wt% ($n=3$; ■) and 10 wt% ($n=3$; ● and $n=2$; ○) in D$_2$O performed at 50 °C with 0.22 wt%V-50 as initiator. Solid lines represent Terminal Model reactivity ratios $r_{AM}=0.31$ and $r_{surfmer}=8.79$.

It is interesting to note that monomer consumption for $f_{AM,0}=0.5$ copolymerizations (Figures D.7 and D.8) is markedly slower than for either of the homopropagation systems, and as summarized by Table D.9, the $f_{AM,0}=0.5$ systems exhibit the longest inhibition times. Two considerations are presented to better understand the slow copolymerization of equimolar (macro)monomers concentrations (i.e., $f_{AM,0}=0.5$), the situation in which the opportunity for cross-propagation is highest. The estimates of $r_{AM}=0.31$ and $r_{surfmer}=8.79$ indicate that an AM macroradical will preferentially add a PCL$_n$ChMA dissolved in the aqueous phase. Since a subsequent cross-propagation with AM is improbable, the macroradical will prefer to add more PCL$_n$ChMA units (albeit at a slow rate because the aqueous PCL$_n$ChMA concentration is significantly lower than that of AM) until the macroradical is hydrophobic enough to enter a micelle to continue PCL$_n$ChMA homopropagation. It follows that it is both kinetically and

130

thermodynamically unfavorable for the growing compartmentalized poly(PCL$_n$ChMA) chain to add a hydrophilic AM from the aqueous phase, and therefore an elevated rate of PCL$_n$ChMA compartmentalized homopropagation continues, at the expense of PCL$_n$ChMA micelle reservoirs. Given that the saturated aqueous concentration of PCL$_n$ChMA is the same for all $f_{AM,0}$ compositions, the high fraction of AM-PCL$_n$ChMA macroradicals produced in the aqueous phase must be responsible for the slow rate of conversion in the $f_{AM,0}$=0.5 system. In AM-rich systems ($f_{AM,0}$=0.9) the PCL$_n$ChMA micelles are quickly depleted such that AM homopropagation can ensue, while in AM-poor systems ($f_{AM,0}$=0.1), the ratio of aqueous PCL$_n$ChMA to AM concentrations is highest such that fewer AM-PCL$_n$ChMA relative to PCL$_n$ChMA-PCL$_n$ChMA macroradicals are produced in the aqueous phase, where it is thermodynamically more favorable for the latter to enter a micelle.

In support of the above interpretation of AM/PCL$_n$ChMA copolymerization, it could be that the initial equimolar amount of AM reduces the aqueous PCL$_3$ChMA concentration such that macroradicals cannot grow large (or hydrophobic) enough to enter a micelle before being terminated in the aqueous phase. However, as shown in Figure D.10, neither the surface activity nor the CMC of PCL$_3$ChMA at room temperature are significantly different in 1 wt% AM aqueous solution (the concentration of AM at the beginning of a 10 wt% $f_{AM,0}$=0.5 copolymerization) than in pure H$_2$O. On the other hand, at concentrations above its CMC, PCL$_3$ChMA suspensions in 1 wt% AM aqueous solutions were observed to become cloudy after several hours at room temperature, as indicated by the increased particle sizes presented in Figure D.11. Since PCL$_3$ChMA solutions are stable in 3.4 M NaCl solutions, it is unlikely that the observed increase in size for 1 wt% AM solutions is caused by aggregation resulting from screening of the PCL$_3$ChMA cationic groups. Instead, a specific interaction between AM's primary amide and PCL$_3$ChMA's polyester carbonyls could be responsible for increasing the hydrophilicity of PCL$_3$ChMA micelles, swelling them with H$_2$O, and making entry of a growing chain more difficult.

131

7.4 Conclusions

The PLP-SEC technique was implemented to measure $k_p \cdot [M]$ for 5, 10, and 20 wt% PCL$_2$ChMA in H$_2$O at 25, 50, 70, and 85 °C. At 25 °C, the inflection point locations of the PLP MMDs were unchanged with conversions up to 28%, NaCl concentrations up to 3.4 M, or photoinitiator type (LiTPO and DMPA: high and low aqueous solubilities, respectively), whereas the MMD inflection points from PLP produced at 85 °C were sensitive to all these parameters. These findings indicate that PCL$_2$ChMA propagation is predominantly compartmentalized inside the micelles at a saturated macromonomer concentration at 25 °C, whereas at 85 °C the aqueous phase $k_p \cdot [M]$ contributions are significant.

The L_i measured by PLP-SEC at 50, 70, and 85 °C contain contributions from both aqueous and compartmentalized $k_p \cdot [M]$ which should be averaged according to the mean lifetime of a macroradical in the aqueous and compartmentalized phases, respectively. However, the extent to which the locus of polymerization changes as well as the corresponding macromonomer concentrations in the aqueous and compartmentalized phases are unknown. Therefore, the PLP MMDs are evaluated as overall $k_p \cdot [M]$ values at each temperature. At 50 °C, the significant increase in $k_p \cdot [M]$ measured from 5 to 10 wt% macromonomer in H$_2$O is reconciled in terms a strong aqueous contribution from the cationic monomer TMAEMI (which comprises up to 10 mol% of the PCL$_2$ChMA distribution), a behavior previously documented for fully ionized MAA.[37] The values of $k_p \cdot [M]$ measured at 70 and 85 °C are even more difficult to interpret, and are thought to comprise contributions from compartmentalized macromonomer, aqueous TMAEMI propagation, and aqueous propagation of low-MW PCL$_n$ChMA oligomers.

Compartmentalized macromonomer propagation can be safely assumed at 25 °C, and therefore using the bulk PCL$_2$ChMA concentration, the $k_{p,min}$ is calculated as 863 ± 95 L·mol^{-1}·s^{-1} at 25 °C, a value quite elevated in comparison to those of other large MW methacrylates such as PEGMA or BeMA. In reality, the true k_p would be even higher when the equilibrium concentration

of swollen PCL_2ChMA at the reaction site is take into account. Such an elevated k_p measurement could be explained by the "looped" or "hairpin" conformation known to occur with other cationic tail-type surfmers,[22,23] where the methacrylate groups at the micelle/water interface and buried in the micellar core could have different reactivities.

Lastly, in situ ^{1}H NMR was used to track monomer composition drift during batch PCL_nChMA copolymerizations with AM performed at 50 °C in D_2O. The integrated Mayo-Lewis approach was implemented to estimate reactivity ratios $r_{AM}=0.31\pm0.03$ and $r_{PCL3ChMA}=8.79\pm0.38$ which adequately represent monomer composition drifts for initial overall (macro)monomer concentrations of 5 and 10 wt% for both $n=2$ and $n=3$ macromonomers. An explanation for the markedly slow rates of conversion in the $f_{AM,0}=0.5$ copolymerizations is proposed in terms of the high fraction of $AM-PCL_nChMA$ macroradicals (relative to the low saturated aqueous concentration of PCL_nChMA) which do not favorably cross propagate with AM, and can only become hydrophobic enough to enter a PCL_nChMA micelle via addition of a PCL_nChMA unit in the aqueous phase.

7.5 References

(1)   Jaeger, W.; Bohrisch, J.; Laschewsky, A. *Prog. Polym. Sci.* **2010**, *35*, 511.

(2)   Vedoy, D. R. L.; Soares, J. B. P. *Can. J. Chem. Eng.* **2015**, *93*, 888.

(3)   Wang, C.; Harbottle, D.; Liu, Q.; Xu, Z. *Miner. Eng.* **2014**, *58*, 113.

(4)   Sharma, S. K.; Chauhan, G. S.; Gupta, R.; Ahn, J.-H. *J. Mater. Sci. Mater. Med.* **2009**, *21*, 717.

(5)   Kuo, C.-H.; Leon, L.; Chung, E. J.; Huang, R.-T.; Sontag, T. J.; Reardon, C. A.; Getz, G. S.; Tirrell, M.; Fang, Y. *J. Mater. Chem. B* **2014**, *2*, 8142.

(6)   Wever, D. A. Z.; Picchioni, F.; Broekhuis, A. A. *Prog. Polym. Sci.* **2011**, *36*, 1558.

(7)   González García, G.; Kreft, T.; Alb, A. M.; de la Cal, J. C.; Asua, J. M.; Reed, W. F. *J. Phys. Chem. B* **2008**, *112*, 14597.

(8)   Losada, R.; Wandrey, C. *Macromolecules* **2009**, *42*, 3285.

(9)   Candau, F.; Selb, J. *Adv. Colloid Interface Sci.* **1999**, *79*, 149.

(10)   Stähler, K.; Selb, J.; Candau, F. *Mater. Sci. Eng., C* **1999**, *10*, 171.

(11)   Summers, M.; Eastoe, J. *Adv. Colloid Interface Sci.* **2003**, *100–102*, 137.

(12)   Joynes, D.; Sherrington, D. C. *Polymer* **1996**, *37*, 1453.

(13)   Lacík, I.; Selb, J.; Candau, F. *Polymer* **1995**, *36*, 3197.

(14)   Cochin, D.; Zana, R.; Candau, F. *Macromolecules* **1993**, *26*, 5765.

(15)   Hamid, S. M.; Sherrington, D. C. *Polymer* **1987**, *28*, 332.

(16)   Cochin, D.; Candau, F.; Zana, R. *Macromolecules* **1993**, *26*, 5755.

(17)   Hamid, S.; Sherrington, D. *J. Chem. Soc., Chem. Commun.* **1986**, 936.

(18)   Chatjaroenporn, K.; Baker, R. W.; FitzGerald, P. A.; Warr, G. G. *Langmuir* **2010**, *26*, 11715.

(19)   Chatjaroenporn, K.; Baker, R. W.; FitzGerald, P. A.; Warr, G. G. *J. Colloid Interface Sci.* **2009**, *336*, 449.

(20)   FitzGerald, P. A.; McDonald, D. M.; Warr, G. G. *Soft Matter* **2013**, *9*, 2711.

(21)   FitzGerald, P. A.; Warr, G. G. *Adv. Colloid Interface Sci.* **2012**, *179–182*, 14.

(22)   Hamid, S. M.; Sherrington, D. C. *Polymer* **1987**, *28*, 325.

(23)   FitzGerald, P. A.; Chatjaroenporn, K.; Zhang, X.; Warr, G. G. *Langmuir* **2011**, *27*, 11852.

(24)   Beuermann, S.; Buback, M. *Prog. Polym. Sci.* **2002**, *27*, 191.

(25)   Beuermann, S.; Buback, M.; Davis, T. P.; Gilbert, R. G.; Hutchinson, R. A.; Olaj, O. F.; Russell, G. T.; Schweer, J.; van Herk, A. M. *Macromol. Chem. Phys.* **1997**, *198*, 1545.

(26)   Beuermann, S.; Buback, M.; Davis, T. P.; Gilbert, R. G.; Hutchinson, R. A.; Kajiwara, A.; Klumperman, B.; Russell, G. T. *Macromol. Chem. Phys.* **2000**, *201*, 1355.

(27)   Lacík, I.; Stach, M.; Kasák, P.; Semak, V.; Uhelská, L.; Chovancová, A.; Reinhold, G.; Kilz, P.; Delaittre, G.; Charleux, B.; Chaduc, I.; D'Agosto, F.; Lansalot, M.; Gaborieau, M.; Castignolles, P.; Gilbert, R. G.; Szablan, Z.; Barner-Kowollik, C.; Hesse, P.; Buback, M. *Macromol. Chem. Phys.* **2015**, *216*, 23.

(28)   Buback, M. *Macromol. Symp.* **2009**, *275–276*, 90.

(29)   Stach, M.; Lacík, I.; Kasák, P.; Chorvát, D.; Saunders, A. J.; Santanakrishnan, S.; Hutchinson, R. A. *Macromol. Chem. Phys.* **2010**, *211*, 580.

(30)   Stach, M.; Lacík, I.; Chorvát, D.; Buback, M.; Hesse, P.; Hutchinson, R. A.; Tang, L. *Macromolecules* **2008**, *41*, 5174.

(31)   Lacík, I.; Beuermann, S.; Buback, M. *Macromolecules* **2003**, *36*, 9355.

(32)   Beuermann, S.; Buback, M.; Hesse, P.; Kukučková, S.; Lacık, I. *Macromol. Symp.* **2007**, *248*, 41.

(33)   Beuermann, S.; Buback, M.; Hesse, P.; Lacík, I. *Macromolecules* **2006**, *39*, 184.

(34)   Lacík, I.; Beuermann, S.; Buback, M. *Macromolecules* **2001**, *34*, 6224.

(35)   Lacík, I.; Chovancová, A.; Uhelská, L.; Preusser, C.; Hutchinson, R. A.; Buback, M. *Macromolecules* **2016**, *49*, 3244.

(36)   Smolne, S.; Weber, S.; Buback, M. *Macromol. Chem. Phy.* **2016**, *217*, 2391.

(37)   Lacík, I.; Učňová, L.; Kukučková, S.; Buback, M.; Hesse, P.; Beuermann, S. *Macromolecules* **2009**, *42*, 7753.

(38)   Beuermann, S.; Buback, M.; Hesse, P.; Kukučková, S.; Lacık, I. *Macromol. Symp.* **2007**, *248*, 23.

(39)   Beuermann, S.; Paquet, D. A.; McMinn, J. H.; Hutchinson, R. A. *Macromolecules* **1996**, *29*, 4206.

(40)   Vana, P.; Yee, L. H.; Davis, T. P. *Macromolecules* **2002**, *35*, 3008.

(41)   Drawe, P.; Buback, M. *Macromol. Theory Simul.* **2016**, *25*, 74.

(42)   Kattner, H.; Drawe, P.; Buback, M. *Macromol. Chem. Phys.* **2015**, *216*, 1737.

(43)   Manders, B. G.; Van Herk, A. M.; German, A. L.; Sarnecki, J.; Schomäcker, R.; Schweer, J. *Makromol. Chem.-Rapid* **1993**, *14*, 693.

(44)   Schweer, J.; van Herk, A. M.; Pijpers, R. J.; Manders, B. G.; German, A. L. *Macromol. Symp.* **1995**, *92*, 31.

(45)   van Herk, A. M.; de Brouwer, H.; Manders, B. G.; Luthjens, L. H.; Hom, M. L.; Hummel, A. *Macromolecules* **1996**, *29*, 1027.

(46)   Jung, M.; van Casteren, I.; Monteiro, M. J.; van Herk, A. M.; German, A. L. *Macromolecules* **2000**, *33*, 3620.

(47)   Rooney, T. R.; Gumfekar, S. P.; Soares, J. B. P.; Hutchinson, R. A. *Macromol. Mater. Eng.* **2016**, *301*, 1248.

(48)   Preusser, C.; Hutchinson, R. A. *Macromol. Symp.* **2013**, *333*, 122.

(49)   da Silva, G. C.; Rossi, C. G. F. T.; Dantas Neto, A. A.; Dantas, T. N. C.; Fonseca, J. L. C. *Colloids Surf., A* **2011**, *377*, 35.

(50)   Haehnel, A. P.; Schneider-Baumann, M.; Hiltebrandt, K. U.; Misske, A. M.; Barner-Kowollik, C. *Macromolecules* **2013**, *46*, 15.

(51)   Gardon, J. L. *J. Polym. Sci. Part A: Polym. Chem.* **1968**, *6*, 2859.

(52)   Preusser, C.; Ezenwajiaku, I. H.; Hutchinson, R. A. *Macromolecules* **2016**, *49*, 4746.

(53)   Cuccato, D.; Storti, G.; Morbidelli, M. *Macromolecules* **2015**, *48*, 5076.

(54)   Kaim, A.; Oracz, P. *Polymer* **1997**, *38*, 2221.

Chapter 8

Polyester Macromonomer Copolymerization Kinetics with Styrene

Preface

Given the diversity of monomers available, there is significant impetus in the polymerization kinetics community to establish generalized family type behaviors for copolymerization systems. Therefore, it is important to investigate how the copolymerization of methacrylate macromonomers compares to the family behaviors already established for common methacrylate systems. In Chapters 5 and 6, it was demonstrated that the polyester type, length, and end-group functionality give rise to important comb-polymer properties. Therefore, this Chapter focuses on the effect of macromonomer polyester type, length, and end-group functionality on its solution copolymerization kinetics with styrene. In addition, the copolymerization behaviors are examined in terms of the solvent and hydrogen bonding effects that are well-documented for common (meth)acrylate systems. This work has been published as a full paper in *Macromolecules* (2017, vol 50, 784-795) for which the majority of the ^{1}H NMR experiments were performed by co-author Otlaatla Monyatsi under my guidance. Details of the macromonomer syntheses and characterizations have been extracted to Chapter 3 to improve the continuity and readability of the thesis.

Abstract

Short-chain polyester methacrylate macromonomers with alkyl, tertiary amine, carboxyl, and hydroxyl end-group functionalities are synthesized by ring-opening polymerization and subsequent modification. Monomer conversion and composition drift during batch radical copolymerizations of (macro)monomer with styrene are tracked using the in situ ^{1}H NMR technique in both polar and non-polar deuterated solvents at 80 °C. For experiments with initial methacrylate molar fraction $f_{xMA} = 0.2$, the effects of end-group functionality, solvent, and hydrogen bonding on relative reactivity are pronounced for monomeric analogs of the macromonomers. However, the polyester spacers significantly dilute these effects in macromonomer copolymerization, as polyester type, length, and end-group functionality did not influence copolymerization kinetics. Instead, the chemical identity up to several units from the methacryloyl group is the most important indicator of macromonomer relative reactivity.

8.1 Introduction

The utility of graft polymers to modify or replace existing materials with tailored architectures is well-documented.[1,2] To that end, grafting through macromonomer polymerization is particularly attractive, as the user may specify well-defined graft properties in the macromonomer synthesis step, and then efficiently impart these features onto the comb-polymer product.[3] For example, acrylic-type macromonomers combine the productivity of radical polymerization (RP) with the properties of polyesters,[4-6] polyethylene glycols,[7,8] polyvinylidene fluorides,[9] and polyurethanes[10] to make high molecular weight (MW) materials with easily tunable degradation time,[11,12] charge density,[13] lower critical solution temperature (LCST),[14] *etc*. Moreover, through macromonomer copolymerization a greater diversity of materials is accessible, thus necessitating the understanding of RP kinetics to facilitate the design and prediction of their end-use properties.

Nowadays, elucidation of kinetic parameters in the complex RP scheme is greatly assisted by tools such as pulsed laser polymerization coupled with size exclusion chromatography (PLP-

SEC) to study propagation kinetics,[15-18] quantum chemical simulation to estimate a variety of rate coefficients,[19-22] electron paramagnetic resonance (EPR) spectroscopy to determine radical structure and to follow termination kinetics,[23-26] and in situ proton nuclear magnetic resonance (^{1}H-NMR) spectroscopy as an efficient means to simultaneously track monomer conversion and comonomer/copolymer composition.[27-29] The cumulative aim of these specialized techniques is a complete kinetic description for each polymerization system, as has been established for certain acrylic solution copolymerizations,[30,31] such that simulations can support the accurate prediction of structure/property relationships for new and existing monomer systems. These systematic studies have revealed generalized kinetic trends based on monomer structure so that, for example, copolymer composition can be described as follows: methacrylate/methacrylate copolymerizes with equal monomer addition probabilities,[32-34] methacrylate/acrylate yields methacrylate-rich copolymer,[35] while methacrylate/styrene tends towards a more alternating structure.[36-38] However, deviations from these generalizations occur when monomers capable of hydrogen bonding, such as 2-hydroxyethyl methacrylate (HEMA), are introduced to the (co)polymerization system.[39-43]

The monomer reactivity ratios r_1 and r_2 which describe copolymer composition and sequence distribution are frequently estimated from the Mayo-Lewis relationship (Eqn. 8.1) by measuring the instantaneous molar composition of low-conversion copolymer (F_1) produced from monomer mixtures with different initial molar composition (f_1).

$$F_1 = \frac{r_1 f_1^2 + f_1 f_2}{r_2 f_2^2 + 2 f_1 f_2 + r_1 f_1^2} \qquad (\textbf{8.1})$$

Unfortunately, the study of macromonomer copolymerization is more difficult due to the inherently low molar concentration and high viscosity of the macromonomers as well as the associated difficulties in properly isolating low-conversion copolymer. Thus, most macromonomer reactivity studies employ the Jaacks method to partially circumvent these issues; by maintaining a large excess of comonomer M_1 relative to macromonomer M_2, the relative consumption of M_1 to M_2

reduces to Eqn. 8.2 such that a plot of the integrated expression, Eqn. 8.3, should be linear with slope r_1.[44]

$$\frac{F_1}{F_2} = \frac{d[M_1]}{d[M_2]} = r_1 \frac{[M_1]}{[M_2]} \tag{8.2}$$

$$\log \frac{[M_1]_t}{[M_1]_0} = r_1 \log \frac{[M_2]_t}{[M_2]_0} \tag{8.3}$$

Despite its simplicity, the Jaacks method is only appropriate for systems in which $r_1 \cdot$ and r_2 support the conditions $r_1 \frac{[M_1]}{[M_2]} \gg 1$ and $r_2 \frac{[M_2]}{[M_1]} \ll 1$, while estimation of the macromonomer reactivity ratio, r_2, is usually limited to that of a low-MW model compound. Moreover, the condition of excess comonomer limits the Jaacks method to f_1 rich mixtures, which may not capture solvent or hydrogen bonding effects that are most pronounced at intermediate compositions in a Mayo-Lewis plot.[40,41]

Meijs and Rizzardo reviewed many copolymerization systems analyzed by the Jaacks method and identified the chemical nature of the polymerizable group as the primary factor affecting macromonomer reactivity.[45] Indeed, family-type behavior is generally observed with methacryloyl-terminated polyester macromonomers; copolymer composition from low-conversion bulk methyl methacrylate (MMA) and polycaprolactone macromonomer (HEMA-PCL) copolymerizations was well-represented by reactivity ratios near unity, albeit over a limited macromonomer molar composition range.[46] In addition, for polylactic acid macromonomer (HEMA-PLA) solution copolymerizations analyzed by the Jaacks method, Eguiburu et al. measured $r_{MMA} = 1.01$,[47] while Shinoda and Matyjaszewski measured $r_{MMA} = 1.09 \pm 0.05$ for RP in contrast to $r_{MMA} = 0.57 \pm 0.02$ measured for atom transfer radical polymerization.[6] Although the authors proposed that the latter result suggests that the inherent reactivity of HEMA-PCL/MMA is comparable to HEMA/MMA, the discrepancy is more likely attributed to a fundamental incongruency of the Jaacks method and controlled radical polymerization.[48]

In this work, several short-chain methacryloyl-terminated polyester macromonomers with similar average MW yet different end-group functionalities – alkyl, tertiary amine, hydroxyl, and

carboxyl – were synthesized by ring opening polymerization (ROP) and subsequent modification, with the structures shown in Scheme 8.1. The average number of polyester units (n) per macromonomer, specified by the stoichiometric ratio of cyclic monomer to initiator in the ROP step, controls the hydrolytic degradability

PLA$_5$EMA

PLA$_1$EMA

PCL$_3$DeMA

DMAEMA

HEMA-PLA$_5$

HEMA

HEMA-PCL$_3$

GMA

HEMA-PCL$_3$-PR

***n*-BMA**

HEMA-PCL$_3$-COOH

HEMA-COOH
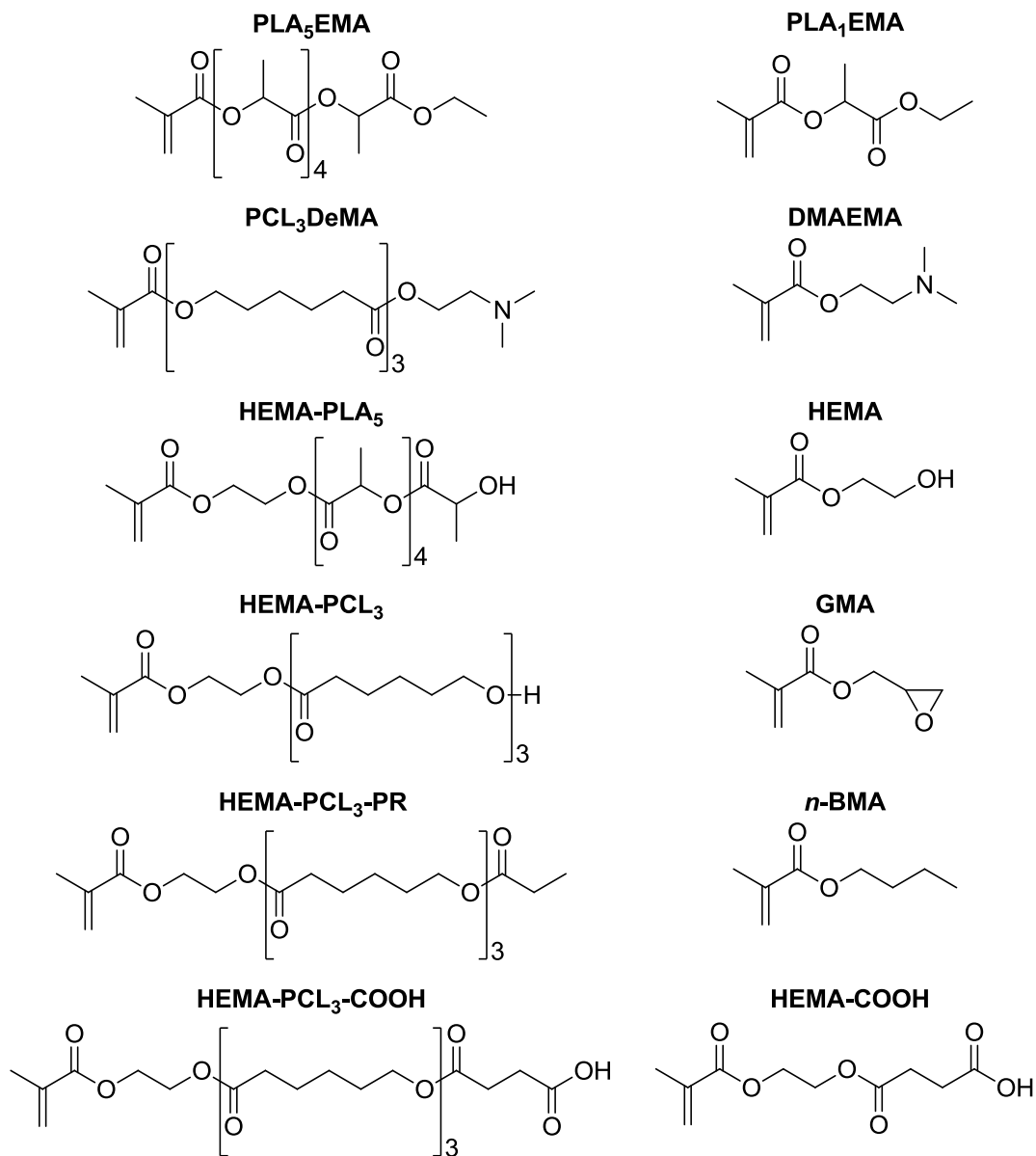
Scheme 8.1: Structures of methacrylate polyester macromonomers synthesized and studied in this work along with monomeric analogs corresponding to end-group functionality (except for the HEMA-PCL$_3$/GMA and HEMA-PCL$_3$-PR/BMA pairs).

and functional group density of the final comb-polymer material. Using in situ ^{1}H NMR, the aim of this work is to clarify trends in macromonomer copolymer composition behavior in terms of polyester side chain type, length, and end-group functionality as well as to further investigate solvent and hydrogen bonding effects documented for monomeric systems. To achieve this aim, Scheme 8.1 also summarizes the monomeric analogs (in terms of end-group functionality) investigated alongside their corresponding macromonomers; the monomer 2-ethoxy-1-methyl-2-oxoethyl methacrylate (herein termed PLA$_1$EMA) was also synthesized as it is not commercially available.

8.2 Experimental

The materials, syntheses, and characterizations for PLA$_N$EMA (for N=1 and N=5), PCL$_3$DeMA, HEMA-PLA$_5$, HEMA-PCL$_3$, HEMA-PCL$_3$-PR, and HEMA-PCL$_3$-COOH are detailed in Chapter 3. Glycidyl methacrylate (GMA, 97%), n-butyl methacrylate (BMA, 99%), 2-(dimethylamino)ethyl methacrylate (DMAEMA, 98%), 2-hydroxyethyl methacrylate (HEMA, 97%), mono-2-(methacryloyloxy)ethyl succinate (HEMA-COOH, ≥95.0%), styrene (ST, ≥99%), and 2,2'-azobis(2-methylpropionitrile) (AIBN, 98%) were purchased from Sigma Aldrich and used as received. Dimethylsulfoxide-d6 (DMSO-d6, 99.9% D, Cambridge Isotope Laboratories), and toluene-d8 (99.5% D, Cambridge Isotope Laboratories) were used as received.

For in situ ^{1}H NMR methacrylate/styrene copolymerization kinetics studies, 35 mg AIBN was added to 200 mg of monomer mixture (with methacrylate molar fraction specified as 0.2, 0.5, or 0.8), dissolved in 765 mg of toluene-d8 or DMSO-d6, and the solution was bubbled with nitrogen for 20 minutes. Polymerizations were performed at 80 °C with 0.6 mL solution inside a Bruker Avance instrument operating at 400 MHz using a previously described procedure.[27] At 3.5 wt% initiator content, the duration of a typical experiment was 4 hours due to low polymerization rates for these particular methacrylate/styrene copolymerization conditions.[36]

8.3 Results and Discussion

8.3.1 Copolymerization Technique Validation

The in situ ^{1}H NMR technique was chosen as the method to study structure-reactivity trends as it conveniently provides monomer composition drift measurements throughout batch radical copolymerizations without having to isolate, purify, and re-dissolve copolymer samples. The main requirement of the technique is that the two monomers exhibit distinct vinylic signals up to high conversion. For this reason, styrene (ST) was selected as the comonomer for methacrylate (xMA) copolymerizations; in addition, the data can be compared to an extensive study of the effect of solvent on the polymerization of ST with n-butyl methacrylate (BMA), glycidyl methacrylate (GMA) and 2-hydroxyethyl methacrylate (HEMA) conducted using copolymer vs comonomer composition data measured in low-conversion experiments.[40] Monomer composition data is collected as a function of molar conversion (x) in order to estimate reactivity ratios using the integrated Mayo-Lewis equation, given by Eqn. 8.4, where f_1 and x are determined from the ^{1}H-NMR signals and F_1 is calculated according to Eqn. 8.1. The accuracy and reproducibility of this approach has been validated for various aqueous copolymerization systems up to 40 wt% solids content.[27-29]

$$\frac{df_1}{dx} = \frac{f_1 - F_1}{1 - x} \qquad (8.4)$$

The copolymerization of BMA and ST was selected as a model system to verify the accuracy and sensitivity of in situ ^{1}H NMR in non-polar 80 wt% toluene-d8 and polar 80 wt% DMSO-d6 solutions. Figure E.1 of Appendix E illustrates the relevant peaks of typical BMA/ST ^{1}H NMR spectra, both before polymerization and at high conversion, used to calculate monomer molar composition and conversion. The resulting conversion vs time profile, monomer composition drift vs conversion, and cumulative copolymer composition (F_1^{cum}, given by Eqn. 8.5) vs conversion are presented in Figure 8.1 for three different initial BMA fractions, with predictions calculated using literature bulk BMA/ST reactivity ratios included for comparison.[52]

143

$$\frac{df_1}{dx} = \frac{f_1 - F_1}{1 - x} \tag{8.5}$$

The non-linear parameter estimation capabilities of PREDICI software were implemented to estimate BMA/ST reactivity ratios from the comonomer composition drift data in both toluene-d8 and DMSO-d6, with estimated values summarized by Table 8.1.

Table 8.1: Summary of xMA/ST reactivity ratio estimations.

System	Conditions	r_{xMA}	r_{ST}	Method
BMA/ST	Bulk[52]	0.42 ± 0.03	0.61 ± 0.03	Low-conv. copolymer
	80 wt% toluene-d8	0.494 ± 0.004	0.777 ± 0.003	in situ ^{1}H NMR
	80 wt% DMSO-d6	0.499 ± 0.005	0.538 ± 0.002	in situ ^{1}H NMR
HEMA/ST	Bulk[53]	0.49	0.27	
	50 v% toluene[40]	1.09 ± 0.18	0.23 ± 0.02	Low-conv. copolymer
	50 v% DMF[40]	0.53 ± 0.10	0.45 ± 0.03	

In the previous study, the *r* values estimated from low-conversion BMA/ST bulk experiments also provided a good description of the copolymer composition measured in toluene and dimethylformamide (DMF) solutions.[40] A different conclusion is reached when examining the monomer composition drifts (center plots in Figure 8.1) from the in situ ^{1}H NMR experiments; the predicted curve starts to deviate from the experimental data in both toluene-d8 and DMSO-d6 at intermediate to high conversions. However, the copolymer content drifts (F_1^{cum} in bottom plots) calculated from these experiments are reasonably well-represented when using the same bulk *r* values.

The *r* values estimated from the in situ ^{1}H NMR monomer composition data (Table 8.1) provide an improved representation of the change in f_1 vs. conversion in Figure 8.1. However, the Mayo-Lewis curves generated with these DMSO and toluene-specific *r* values result in very similar representations of instantaneous copolymer composition compared to the literature bulk values, as demonstrated in Figure 8.2A. Thus it can be concluded that tracking monomer composition by
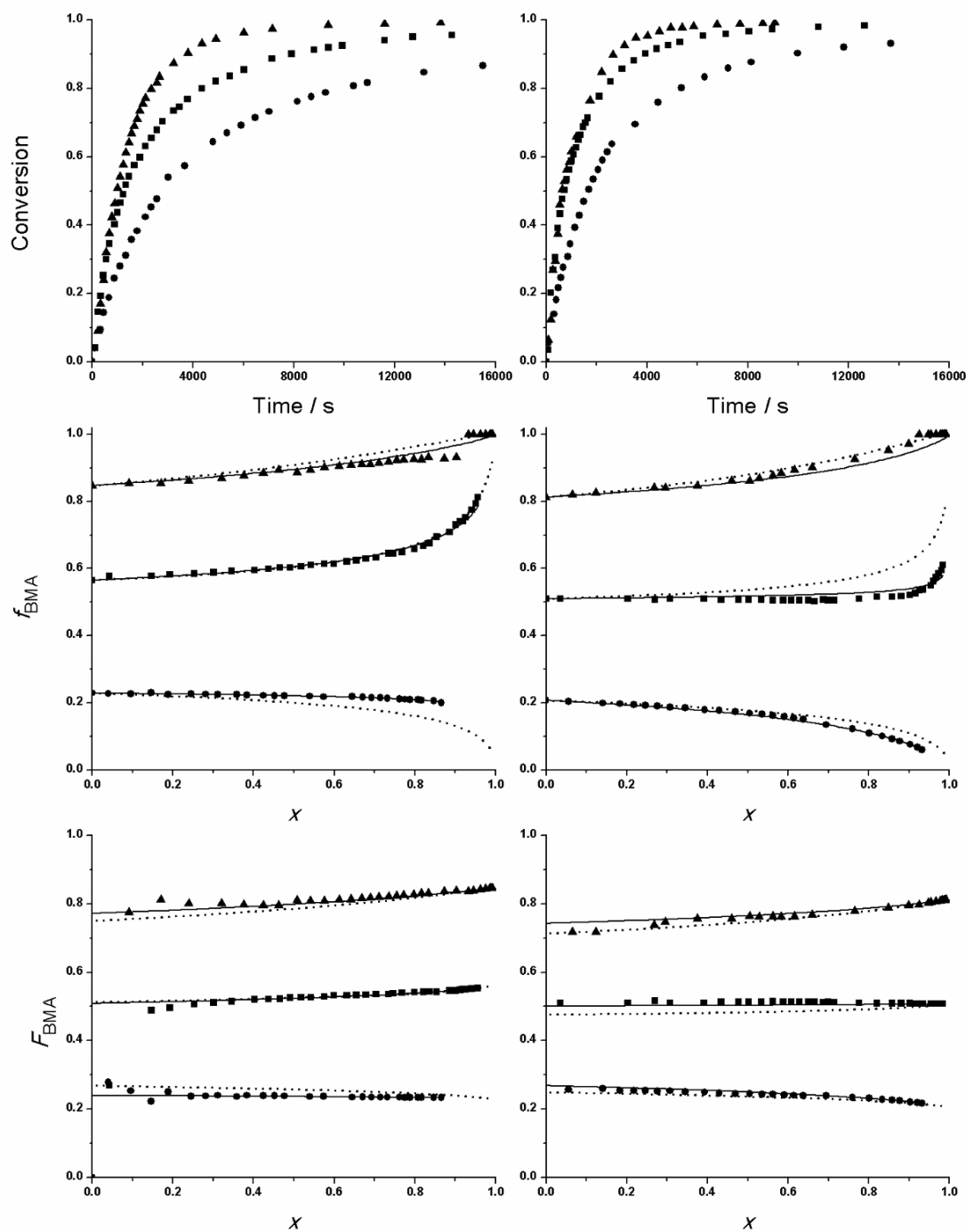
Figure 8.1: Overall monomer conversion vs time (top), as well as monomer composition (center) and cumulative copolymer content (bottom) vs conversion plots for BMA/ST copolymerizations performed at 80 °C in 80 wt% toluene-d8 (left) and 80 wt% DMSO-d6 (right) with $f_{BMA,0}$ = 0.2 (●), 0.5 (■), and 0.8 (▲). Respective fits PREDICI (solid line) compared to predictions (dotted line) using literature bulk BMA/ST reactivity ratios r_{BMA} = 0.42 and r_{ST} = 0.61[52] determined from low-conversion copolymer composition analyses.
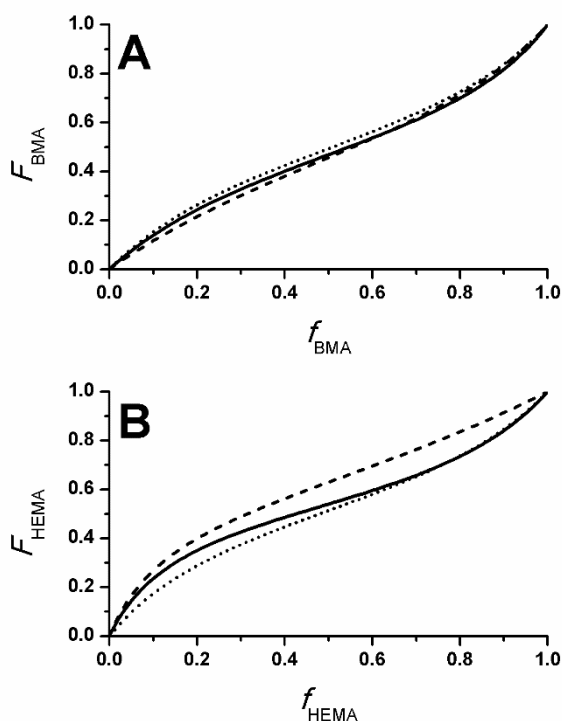
Figure 8.2: Mayo-Lewis plots for BMA/ST (panel A) copolymerization generated using literature bulk reactivity ratios measured by low-conversion copolymer composition analysis in bulk (solid line) as well as reactivity ratios fitted by in situ ^{1}H NMR in 80 wt% toluene-d8 (dashed line) and 80 wt% DMSO-d6 (dotted line). HEMA/ST (panel B) Mayo-Lewis plots are reproduced using literature reactivity ratios measured by low-conversion copolymer composition analysis in bulk (solid line), 50 v% toluene (dashed line), and 50 v% DMF (dotted line) solutions. See Table 8.1 for *r* values.

in situ ^{1}H NMR coupled with the integrated Mayo-Lewis approach is a more sensitive method than low conversion copolymer composition analysis for detecting precise differences in macromonomer structure/reactivity relationships.

The negligible (or very minor) influence of solvent on BMA/ST copolymer composition was contrasted to that of HEMA/ST in the previous low-conversion study.[40] To demonstrate this point, Figure 8.2B plots the instantaneous HEMA/ST copolymer composition calculated using the best-fit reactivity ratios from that work, as summarized by Table 8.1. Unlike BMA/ST, significant differences in copolymer composition were seen for the three systems, a result explained in terms

of hydrogen bonding interactions between HEMA monomers that are disrupted in the polar solvent DMF to reduce the HEMA fraction incorporated, and are amplified in toluene, leading to increased HEMA incorporation into the copolymer.

To investigate this difference further, the methacrylate composition drifts for BMA/ST and HEMA/ST are contrasted in DMSO-d6 and toluene-d8 using the in situ ^{1}H NMR technique, where Figure 8.3A plots the four curves. To gain the most information from minimal experiments and to provide a basis for comparison of the macromonomer systems, all xMA/ST copolymerizations throughout this work were conducted at a single initial composition, $f_{xMA,0} = 0.2$; at this value, the differences in instantaneous copolymer composition between BMA/ST and HEMA/ST in toluene
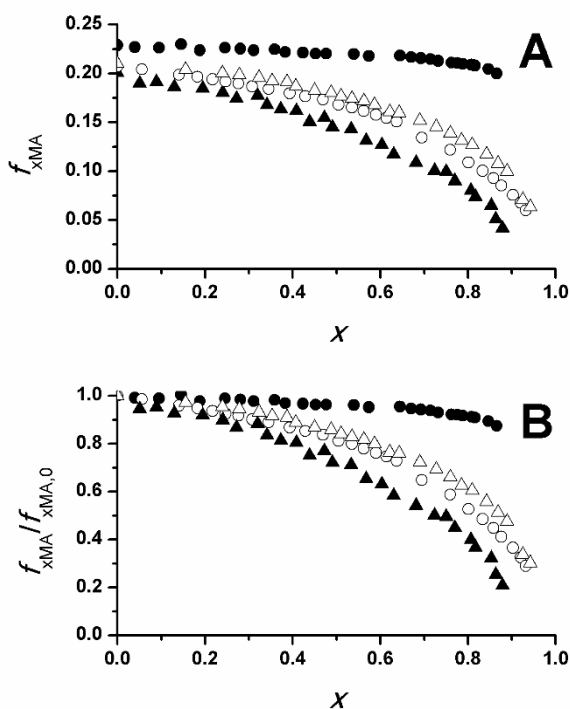
Figure 8.3: Monomer composition drifts (panel A) and corresponding monomer composition drifts normalized by $f_{xMA,0}$ (panel B) for ST copolymerizations with $f_{xMA,0} = 0.2$ for BMA (circles) and HEMA (triangles) in 80 wt% toluene-d8 (closed symbols) and 80 wt% DMSO-d6 (open symbols) performed at 80 °C with 3.5 wt% AIBN.

is pronounced and the disruption of hydrogen bonding in HEMA/ST by DMF is obvious, as seen by an examination of the Mayo-Lewis plots in Figure 8.2. As the initial composition $f_{xMA,0}$ could vary by as much as 10 % due to experimental error or differences in macromonomer average MW (target versus measured), the monomer composition drifts have been normalized by initial $f_{xMA,0}$, as shown in Figure 8.3B. Normalizing the composition drift provides a clearer picture of the enhanced incorporation of HEMA compared to BMA in toluene-d8 due to its increased relative reactivity caused by hydrogen bonding, while in DMSO-d6, a hydrogen bond disrupting solvent, there is a clear reduction in HEMA consumption rate towards that of BMA. These reactivity trends are in good agreement with those reported in the previous low-conversion study.[40] Also noteworthy is the increased relative reactivity of BMA in the more polar DMSO-d6 solvent compared to in toluene-d8, despite the similarities in their Mayo-Lewis plots (Figure 8.2A). Lastly, it is noted that the sensitivity of these observations to solvent concentration was verified by replicate experiments performed at 60 wt% solvent that are summarized by Figures E.2 and E.3 of Appendix E, which also include the plots of overall monomer conversion. It was found that the overall rate of conversion was higher for HEMA/ST than BMA/ST in toluene-d8, in agreement with previous kinetic investigations. However, the two systems were less differentiated in DMSO-d6 due to the reduction of HEMA reactivity in the polar solvent. Decreasing solvent content from 80 to 60 wt% had a greater impact on HEMA incorporation rate than BMA, also in agreement with previous work.

8.3.2 Monomeric Reactivity

In addition to the hydrolytic degradability of polyesters, the macromonomer end-group functionality (e.g., alkyl, tertiary amine, carboxyl, hydroxyl) provides tunable properties to the end-use performance of the comb-polymer product. The density of functional groups in the final material is affected by the number of degradable units in the macromonomer synthesis step (i.e., the value of n) as well as by comonomer selection and mole fraction; however, it may be that n

148

could also influence the reactivity of the macromonomer during copolymerization. Thus, to specifically investigate the structure/reactivity relationship associated with end-group functionality, the monomeric analogs of each macromonomer (i.e., $n = 0$ or 1 bearing the same end-group functionalities) were copolymerized with ST in both 80 wt% toluene-d8 and 80 wt% DMSO-d6 solutions. The normalized composition drifts are presented in Figure 8.4 such that each plot shows the respective drift in methacrylate mole fraction in both solvents relative to the composition drifts found for BMA and HEMA when copolymerized with ST in toluene-d8 under identical conditions with $f_{xMA,0} = 0.2$ and 80 wt% solvent.

In toluene-d8, all of the functional methacrylates studied are consumed more rapidly than BMA, the only monomer that does not contain an electronegative atom nor any degree of steric hindrance in its ester side chain. The enhanced relative reactivity of HEMA is rivalled only by PLA$_1$EMA and HEMA-COOH, while GMA and DMAEMA demonstrate intermediate relative reactivities. In DMSO-d6, the consumption profiles of HEMA and HEMA-COOH systems are reduced compared to in toluene-d8 due to the disruption of hydrogen bonding in the polar solvent, whereas the relative reactivities of the remaining monomers are all increased in DMSO-d6 compared to toluene-d8. To emphasize this final observation, the plots in Figure 8.4 are reorganized according to solvent in Figure E.4 of Appendix E, with corresponding conversion plots in Figure E.5, to show that even for non-hydrogen bonding monomers, the spread in consumption profiles is significantly reduced going from toluene-d8 to DMSO-d6. The tighter grouping suggests that the reduced ST reactivity seen in polar solvents[40] has a larger impact on the relative reactivities of $f_{xMA,0} = 0.2$ copolymerizations in DMSO-d6 than does specific features of the methacrylate comonomer.

GMA is a familiar monomer whose increased reactivity towards ST radicals, similar to that of HEMA,[36,53] is supported by elevated bulk k_p measurements compared to linear alkyl methacrylates,[39,54] with $k_{p,GMA}$ 60% higher than $k_{p,BMA}$ at 25 °C despite their identical MW. However, Siegmann et al. found no significant deviation from linear alkyl methacrylate family type
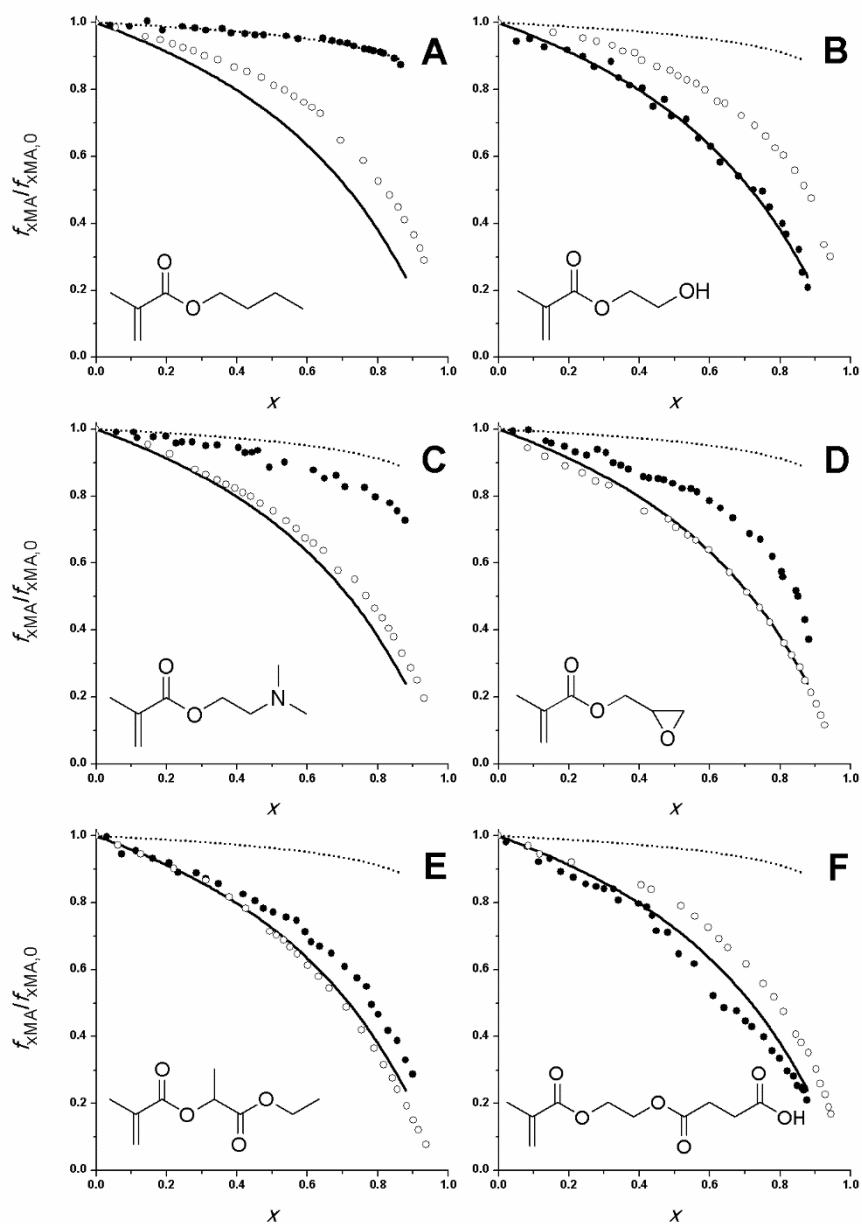
Figure 8.4: Normalized monomer composition drifts for ST copolymerizations with $f_{xMA,0}$ = 0.2 for BMA (panel A), HEMA (panel B), DMAEMA (panel C), GMA (panel D), PLA$_1$EMA (panel E), and HEMA-COOH (panel F) in 80 wt% toluene-d8 (solid circles) and 80 wt% DMSO-d6 (open circles) performed at 80 °C with 3.5 wt% AIBN. Best fit lines for HEMA/ST (solid line) and BMA/ST (dotted line) in 80 wt% toluene-d8 are provided as visual guide.

behavior for poly(ethylene glycol) ethyl ether methacrylate (PEGEEMA, with three linear ether linkages in the ester side chain); compared to BMA, the k_p of PEGEEMA was measured to be 30% higher at 25 °C,[55] in close agreement with the 40% increase relative to BMA for an alkyl methacrylate of similar MW, dodecyl methacrylate (DMA).[16] Indeed, when DMSO-d6 is employed to negate the effect of HEMA hydrogen bonding, the relative reactivity of HEMA is less than that of GMA (see Figure E.4 of Appendix E), even though both methacrylates contain an electronegative oxygen atom at the same position in their ester side chains. Therefore, it is more likely that the enhanced reactivity of GMA towards ST radicals is attributed to the steric nature of its cyclic side chain; consistent with this observation, the k_p for four cyclic ester methacrylates was measured to be 16% higher than linear DMA, regardless of the size of the cyclic ester group.[54]

The tertiary amine functionalized monomer, DMAEMA, shows mildly increased incorporation compared to BMA in both toluene-d8 and DMSO-d6, a result supported by elevated k_p measurements for several methacrylates containing tertiary amines.[56,57] Surprisingly, although PLA₁EMA is not capable of hydrogen bonding due to its ethyl ester end-group functionality, it is consumed almost as rapidly as HEMA in toluene-d8. Among the monomers studied, the isobutyrate bridge is a feature unique to PLA₁EMA that must cause its enhanced reactivity; even though structure/reactivity trends in methacrylates and acrylates are not necessarily interchangeable, Dervaux et al. measured the k_p of 1-ethoxyethyl acrylate, a monomer with a methacryloyl bridge similar in structure to that of PLA₁EMA, to be almost 50 % greater than butyl acrylate (BA) at 40 °C.[58] On the other hand, Soykan and Erol found 2-(4-tert-butylphenoxy)-2-oxo-ethyl methacrylate (TBPOEMA) to be less reactive towards ST than alkyl methacrylates ($r_{\text{TBPOEMA}} = 0.35 \pm 0.20$ and $r_{\text{ST}} = 1.22 \pm 0.43$ in DMSO),[59] while a significant reduction in k_p for two pairs of carbamate acrylates was measured when the ethyl bridge was replaced with an isopropyl one.[60] The other consumption profile comparable to HEMA in toluene-d8 is that of HEMA-COOH, whose reactivity is also facilitated by hydrogen bonding; in DMSO-d6 without hydrogen bonding, the slightly faster

151

consumption of HEMA-COOH compared to HEMA copolymerization (see also Figure E.5 of Appendix E) might be attributed to the bulkiness of the mono-succinate ester in its methacrylate ester side chain. Given all these structural considerations a conclusive explanation for xMA/ST monomer consumption behavior cannot be proposed, but it should be noted that the most rapidly consumed methacrylates are not strictly linear in their ester side chain.

8.3.3 Macromonomer Reactivity

The monomer composition drifts in toluene-d8 for each end-functional group pair, monomer and macromonomer, are presented in Figure 8.5. Best fit lines for both BMA/ST and HEMA/ST composition drifts in toluene-d8 are included in each plot, to provide a reference for the paired experiments that were performed with $f_{xMA,0} = 0.2$ and subsequently normalized by $f_{xMA,0}$. For the tertiary amine terminated pair, the monomer (DMAEMA) relative consumption is significantly enhanced compared to the macromonomer during copolymerization with ST, the latter curve even slightly more azeotropic than BMA. Therefore, although it is unclear whether a steric or polar effect is responsible, the enhanced reactivity of DMAEMA must be related to the proximity of its tertiary amine to the methacryloyl group. In spite of the polarity associated with its average of three polyester units and pendant tertiary amine, inspection of the structure of PCL_3DeMA macromonomer near the methacryloyl group reveals its similarity to BMA which is manifested by their similar relative reactivities. The consumption profiles for the PLA_nEMA pair are very similar ($n = 1$ vs $n = 5$), indicating that the MW of the ester side chain does not affect the reactivity of the xMA/ST system, a result supported by n-alkyl methacrylate/ST copolymer composition family behavior.[36] Although functionalized with an alkyl end-group, the PLA_nEMA consumption profiles are more similar to that of HEMA than BMA. Thus, the rapid PLA_nEMA incorporations are more likely attributed to their equivalent and distinct isobutyrate bridges rather than their end-group functionality; however, the relative importance of the methyl group adjacent to the methacryloyl moiety and the proximity and/or the orientation of the ester functionality on the copolymerization

152
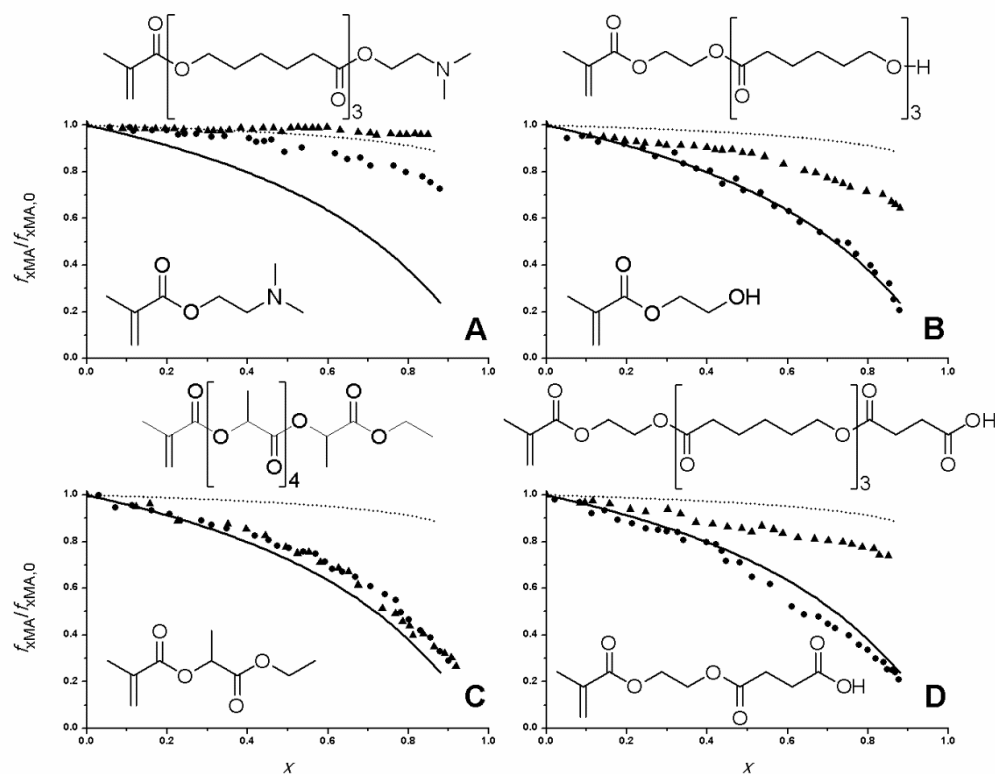
Figure 8.5: Normalized composition drifts for ST copolymerizations with $f_{xMA,0} = 0.2$ for macromonomer (triangles) and monomer (circles) pairs in 80 wt% toluene-d8 with amine (panel A), hydroxyl (panel B), alkyl (panel C), and carboxyl (panel D) end-group functionalities. Best fit lines for HEMA/ST (solid line) and BMA/ST (dotted line) in 80 wt% toluene-d8 are provided as visual guides.

behavior cannot yet be determined. The remaining hydroxyl and carboxyl terminated (macro)monomer pairs, shown in Figure 8.5, demonstrate the same behavior: while the relative reactivities of the macromonomer systems are higher than BMA, they do not attain the hydrogen bonding dependent increased reactivity of their monomeric analogs.

The increased reactivity of HEMA compared to alkyl methacrylates in both bulk and toluene is currently explained by hydrogen-bonding between hydroxyl and methacryloyl carbonyl groups that draws electron density away from the double bond, making the monomer more reactive to radical addition.[42] Since the ratio of carbonyl to hydroxyl (i.e., hydrogen bond acceptors to

153

donors) is 1:1 for HEMA and 4:1 for HEMA-PCL$_3$, it follows that the effect of hydrogen bonding on macromonomer reactivity should still be noticeable during its copolymerization with ST, albeit diluted. If diluted hydrogen bonding is responsible for increased methacrylate consumption in HEMA-PCL$_3$/ST, elimination of the hydroxyl group should reduce its reactivity towards that of BMA/ST, as was evidenced in Figure 8.5 (panel A) for copolymerization of the tertiary amine macromonomer, PCL$_3$DeMA. To test this hypothesis, the hydroxyl group of HEMA-PCL$_3$ was end-capped by reaction with propionyl chloride to yield HEMA-PCL$_3$-PR (see Scheme 8.1), whose relative consumption profile when copolymerized with ST is compared in Figure 8.6 to other macromonomers.
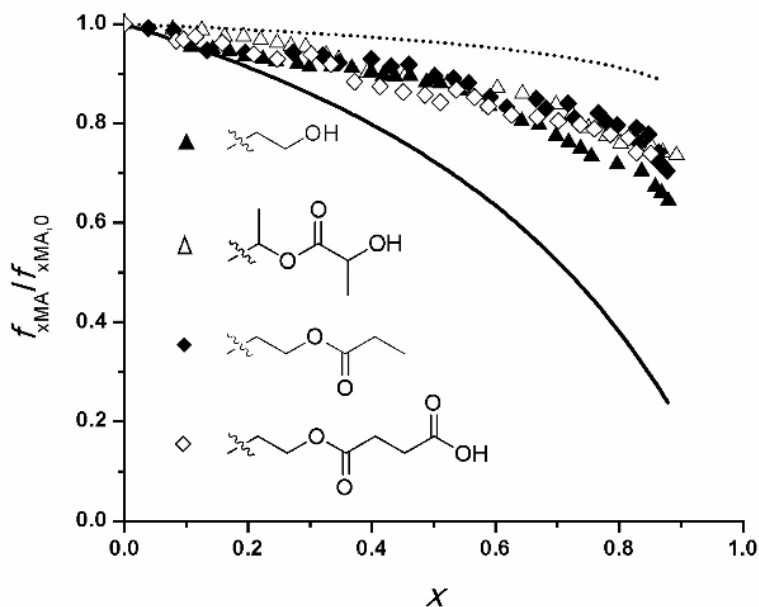
Figure 8.6: Normalized macromonomer composition drift for ST copolymerizations with
$f_{xMA,0} = 0.2$ **for HEMA-PCL$_3$ (▲), HEMA-PLA$_5$ (△), HEMA-PCL$_3$-COOH (◆), and HEMA-**
PCL$_3$-PR (◇) in 80 wt% toluene-d8. Best fit lines for HEMA/ST (solid line) and BMA/ST
(dotted line) in 80 wt% toluene-d8 are provided as visual guides.

154

Comparison of the macromonomer composition drifts in Figure 8.6 and their corresponding conversion profiles in Figure E.6 of Appendix E indicates no significant difference between any of the hydrogen bonding capable macromonomers or the HEMA-PCL$_3$-PR derivative. Since the HEMA-PCL$_3$-PR macromonomer drift did not reduce to the BMA profile, it is more likely that the ester moiety, separated from the methacryloyl group by an ethyl bridge, has a greater impact on HEMA-PCL$_3$/ST copolymerization behavior than hydrogen bonding arising from the pendant alcohol, in stark contrast to monomeric systems.[41,43] Also shown in Figure 8.6 is data for the PLA-based hydroxyl functionalized macromonomer, HEMA-PLA$_5$, with average MW comparable to that of HEMA-PCL$_3$ but a carbonyl to hydroxyl ratio of 6:1. The similar consumption profile supports the assertion that the relative comonomer reactivities are not specific features of polyester type.

The mitigated impact of hydrogen bonding on macromonomer incorporation is supported by our previous composition measurements for low-conversion HEMA-PCL$_3$/MMA copolymer produced in bulk with $f_{macromonomer} \leq 0.66$, which showed no significant deviation from the diagonal indicating equal relative reactivity of MMA and the macromonomer[46] in agreement with other HEMA-PLA/MMA solution copolymerizations.[6,47] In addition, while only HEMA and HEMA-COOH exhibited reduced consumption behavior in DMSO-d6 because of hydrogen bond disruption, HEMA-PCL$_3$ consumption was augmented in DMSO-d6 relative to toluene-d8 (see of Appendix E), a result consistent with all non-hydrogen bonding monomers studied in this work. Altogether, these results indicate that hydrogen bonding is not an important consideration for predicting polyester macromonomer copolymer composition from solution copolymerizations in toluene or DMSO solvents.

The finding that the (n+1) carbonyls of HEMA-PCL$_n$ and HEMA-PLA$_n$ drastically dilute the effects of hydrogen bonding on copolymer composition enriches our understanding of organic solution radical copolymerization for hydroxyl-bearing acrylic monomers. According to this

155

finding, the effects of hydrogen bonding should also be diluted for hydroxyl-bearing (meth)acrylate copolymerizations by the carbonyls of their alkyl (meth)acrylate comonomers. However, the opposite was found for several different acrylic copolymerization systems in which the hydroxyl-bearing monomer was instead preferentially incorporated,[41,43] an effect that can be exacerbated by increased concentration of toluene or xylenes in solution.[40,43] Thus, the observed kinetic behavior cannot be explained solely by the increased monomer reactivity via hydrogen bonding with the monomeric carbonyl group; specific associations between monomer and repeat units on the growing chain should also be considered. For example, Noguchi and Kuzuya substantiated through experiment and simulation that enhanced methacrylic acid (MAA) incorporation in MAA/ST copolymerization in dilute benzene solution could be represented by an intrachain reaction of chain-end radical with MAA monomers hydrogen-bonded to MAA repeat units in the macroradical.[61] Therefore, future copolymerization investigations of hydroxyl-bearing (meth)acrylates, such as HEMA, could benefit from analogous consideration of monomer association to explain their peculiar trends in copolymer composition.

Finally, the composition drifts are reorganized in Figure 8.7 to illustrate the macromonomer structure/reactivity relationship in solution copolymerization with ST. The copolymer molar mass distributions and MW averages for these macromonomer/ST systems are in the same range as BMA/ST and HEMA/ST copolymers produced at identical experimental conditions (Figure E.8 and Table E.1 of Appendix E). For copolymerizations in 80 wt% toluene-d8, the effects of hydrogen bonding, macromonomer average MW, polyester type, and end-group functionality were not measurable. Rather, the chemical identity, up to several units away from the methacryloyl polymerizable group, was the most significant indicator of the composition drift and relative reactivity. Since the complete investigation of BMA/ST solution copolymerizations by in situ ^{1}H NMR yielded reactivity ratios in reasonable agreement with bulk literature values, it can be safely assumed that the macromonomer/ST composition drifts obtained in toluene-d8 give a

156

reasonable representation of their chemically-controlled bulk reactivity trends. However, the extent to which macromonomer structure impacts consumption behavior must still be quantified through in situ ^{1}H NMR experiments at additional $f_{xMA,0}$ and subsequent estimation of the respective macromonomer/ST reactivity ratios. Furthermore, our understanding of the macromonomer structure/reactivity relationship would benefit from homopropagation rate information as well as copolymer propagation rate coefficient ($k_{p,cop}$) measurements using pulsed-laser techniques.
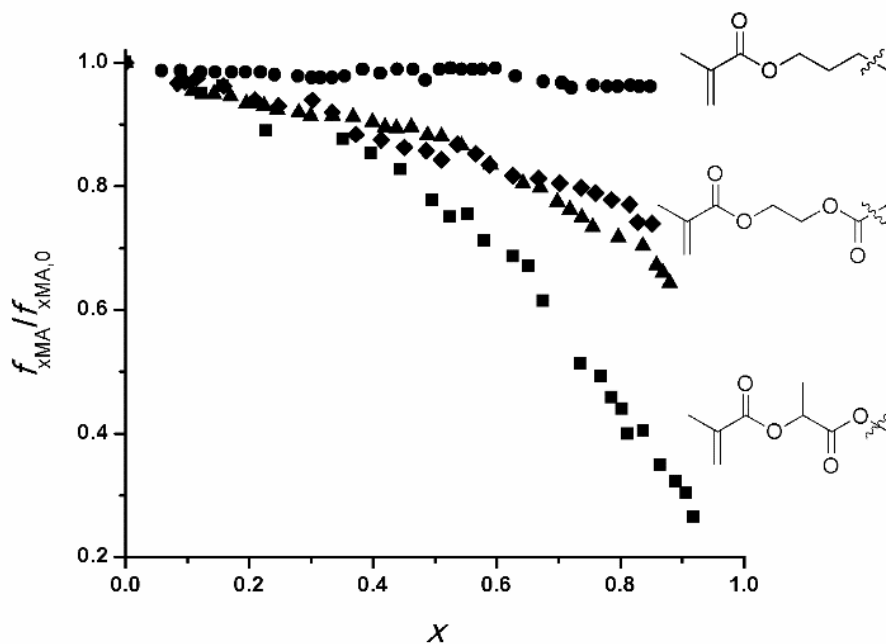
Figure 8.7: Summary of normalized macromonomer composition drifts for ST copolymerizations with $f_{xMA,0}$ = 0.2 for PLA$_5$EMA (■), PCL$_3$DeMA (●), HEMA-PCL$_3$ (▲), and HEMA-PCL$_3$-COOH (◆) at 80 °C in 80 wt% toluene-d8 with 3.5 wt% AIBN.

8.4 Conclusions

Several short-chain polyester methacrylate-type macromonomers with different end-group functionalities (alkyl, tertiary amine, carboxyl, hydroxyl) were synthesized through ring opening polymerization and subsequent modification. To investigate the relationship between macromonomer structure and reactivity, the kinetics of macromonomer/ST batch radical copolymerizations at 80 °C were studied in 80 wt% toluene-d8 and 80 wt% DMSO-d6 solutions using the in situ ^{1}H NMR technique. Traditionally, macromonomer reactivity is studied by the Jaacks method in which the condition of excess comonomer may negate composition ranges where kinetic features such as hydrogen bonding are pronounced. Thus, the ability of the in situ ^{1}H NMR technique to capture the effect of hydrogen bonding was demonstrated for HEMA/ST copolymerization, while the accuracy and sensitivity was verified for the model system, BMA/ST, in both solvents.

Composition drifts for the copolymerization of monomers (bearing the same end-functionality as their macromonomer pair) conducted with $f_{xMA,0}$ = 0.2 showed increased methacrylate consumption relative to BMA, depending on hydrogen bonding capabilities as well as steric hindrance or polarity of the ester side chain. However, the effects of end-group functionality were rendered insignificant by the polyester spacers in macromonomer/ST copolymerization such that under the conditions studied in this work, hydrogen bonding, end-group functionality, polyester type and average number of units did not contribute to macromonomer reactivity. Rather, the chemical identity up to several units away from the methacryloyl group is the most important consideration for predicting macromonomer/ST copolymerization behavior, where the isobutyrate bridge of PLA$_5$EMA led to the most rapid methacrylate consumption.

8.5 References

(1)   Bhattacharya, A.; Misra, B. N., *Prog. Polym. Sci.* **2004,** *29* (8), 767-814.

(2)   Carlmark, A.; Larsson, E.; Malmström, E., *Eur. Polym. J.* **2012,** *48* (10), 1646-1659.

(3)   Ito, K., *Prog. Polym. Sci.* **1998,** *23* (4), 581-620.

(4)   Ishimoto, K.; Arimoto, M.; Okuda, T.; Yamaguchi, S.; Aso, Y.; Ohara, H.; Kobayashi, S.; Ishii, M.; Morita, K.; Yamashita, H.; Yabuuchi, N., *Biomacromolecules* **2012,** *13* (11), 3757-3768.

(5)   Hawker, C. J.; Mecerreyes, D.; Elce, E.; Dao, J.; Hedrick, J. L.; Barakat, I.; Dubois, P.; Jérôme, R.; Volksen, W., *Macromol. Chem. Phys.* **1997,** *198* (1), 155-166.

(6)   Shinoda, H.; Matyjaszewski, K., *Macromolecules* **2001,** *34* (18), 6243-6248.

(7)   Capek, I., *Adv. Colloid Interface Sci.* **2000,** *88* (3), 295-357.

(8)   Neugebauer, D.; Zhang, Y.; Pakula, T., *J. Polym. Sci. Part A: Polym. Chem.* **2006,** *44* (4), 1347-1356.

(9)   Guerre, M.; Ameduri, B.; Ladmiral, V., *Polym. Chem.* **2016,** *7* (2), 441-450.

(10)   Zhang, H.; Duan, L.; Chen, L.; Huang, H., *J. Appl. Polym. Sci.* **2007,** *103* (3), 1992-1999.

(11)   Ferrari, R.; Yu, Y.; Morbidelli, M.; Hutchinson, R. A.; Moscatelli, D., *Macromolecules* **2011,** *44* (23), 9205-9212.

(12)   Yu, Y.; Ferrari, R.; Lattuada, M.; Storti, G.; Morbidelli, M.; Moscatelli, D., *J. Polym. Sci. Part A: Polym. Chem.* **2012,** *50* (24), 5191-5200.

(13)   Rooney, T. R.; Gumfekar, S. P.; Soares, J. B. P.; Hutchinson, R. A., *Macromol. Mater. Eng.* **2016**, *301* (10), 1248-1254.

(14)   Lutz, J.-F., *J. Polym. Sci. Part A: Polym. Chem.* **2008,** *46* (11), 3459-3470.

(15)   Buback, M.; Gilbert, R. G.; Hutchinson, R. A.; Klumperman, B.; Kuchta, F.-D.; Manders, B. G.; O'Driscoll, K. F.; Russell, G. T.; Schweer, J., *Macromol. Chem. Phys.* **1995,** *196* (10), 3267-3280.

(16)   Beuermann, S.; Buback, M.; Davis, T. P.; Gilbert, R. G.; Hutchinson, R. A.; Kajiwara, A.; Klumperman, B.; Russell, G. T., *Macromol. Chem. Phys.* **2000,** *201* (12), 1355-1364.

(17)   Beuermann, S.; Buback, M., *Prog. Polym. Sci.* **2002,** *27* (2), 191-254.

(18)   Buback, M., *Macromol. Symp.* **2009,** *275–276* (1), 90-101.

(19)   Zhang, G.; Konstantinov, I. A.; Arturo, S. G.; Yu, D.; Broadbelt, L. J., *J. Chem. Theory Comput.* **2014,** *10* (12), 5668-5676.

(20)   Rooney, T. R.; Mavroudakis, E.; Lacik, I.; Hutchinson, R. A.; Moscatelli, D., *Polym. Chem.* **2015,** *6* (9), 1594-1603.

(21)   Mavroudakis, E.; Cuccato, D.; Moscatelli, D., *Polymers* **2015,** *7* (9), 1483.

(22)   Abreu, C. M. R.; Mendonça, P. V.; Serra, A. C.; Noble, B. B.; Guliashvili, T.; Nicolas, J.; Coote, M. L.; Coelho, J. F. J., *Macromolecules* **2016,** *49* (2), 490-498.

(23)   Kattner, H.; Drawe, P.; Buback, M., *Macromol. Chem. Phys.* **2015,** *216* (16), 1737-1745.

(24)   Barth, J.; Buback, M.; Barner-Kowollik, C.; Junkers, T.; Russell, G. T., *J. Polym. Sci. Part A: Polym. Chem.* **2012,** *50* (22), 4740-4748.

(25)   Barth, J.; Buback, M., *Macromol. React. Eng.* **2010,** *4* (5), 288-301.

(26)   Barth, J.; Buback, M.; Hesse, P.; Sergeeva, T., *Macromol. Rapid Commun.* **2009,** *30* (23), 1969-1974.

(27)   Preusser, C.; Hutchinson, R. A., *Macromol. Symp.* **2013,** *333* (1), 122-137.

(28)   Cuccato, D.; Storti, G.; Morbidelli, M., *Macromolecules* **2015,** *48* (15), 5076-5087.

(29)   Preusser, C.; Ezenwajiaku, I. H.; Hutchinson, R. A., *Macromolecules* **2016,** *49* (13), 4746-4756.

(30)   Wang, W.; Hutchinson, R. A., *Macromol. React. Eng.* **2008,** *2* (3), 199-214.

(31)   Wang, W.; Hutchinson, R. A., A comprehensive kinetic model for high-temperature free radical production of styrene/methacrylate/acrylate resins. *AIChE J.* **2011,** *57* (1), 227-238.

(32)   Faraguna, F.; Vidović, E.; Jukić, A., *Polym. Int.* **2015,** *64* (10), 1497-1504.

(33)   Grassie, N.; Torrance, B. J. D.; Fortune, J. D.; Gemmell, J. D., *Polymer* **1965,** *6* (12), 653-658.

(34)   Zoller, A.; Kockler, K. B.; Rollet, M.; Lefay, C.; Gigmes, D.; Barner-Kowollik, C.; Guillaneuf, Y., *Polym. Chem.* **2016,** *7* (35), 5518-5525.

(35)   Buback, M.; Feldermann, A.; Barner-Kowollik, C.; Lacík, I., *Macromolecules* **2001,** *34* (16), 5439-5448.

(36)   Wang, W.; Hutchinson, R. A., *Macromolecules* **2008,** *41* (23), 9011-9018.

(37)   Fukuda, T.; Ma, Y. D.; Inagaki, H., *Macromolecules* **1985,** *18* (1), 17-26.

(38) O'Driscoll, K. F.; Kale, L. T.; Rubio, L. H. G.; Reilly, P. M., *J. Polym. Sci. Polym. Chem. Ed.* **1984,** *22* (11), 2777-2788.

(39) Buback, M.; Kurz, C. H., *Macromol. Chem. Phys.* **1998,** *199* (10), 2301-2310.

(40) Liang, K.; Hutchinson, R. A., *Macromolecules* **2010,** *43* (15), 6311-6320.

(41) Liang, K.; Rooney, T. R.; Hutchinson, R. A., *Ind. Eng. Chem. Res.* **2013,** *53* (18), 7296-7304.

(42) Beuermann, S., *Macromol. Rapid Commun.* **2009,** *30* (13), 1066-1088.

(43) Schier, J. E. S.; Hutchinson, R. A., *Polym. Chem.* **2016,** *7* (27), 4567-4574.

(44) Jaacks, V., *Makromol. Chem.* **1972,** *161* (1), 161-172.

(45) Meijs, G. F.; Rizzardo, E., *J. Macromol. Sci., Rev. Macromol. Chem.* **1990,** C*30* (3-4), 305-377.

(46) Ferrari, R.; Rooney, T. R.; Lupi, M.; Ubezio, P.; Hutchinson, R. A.; Moscatelli, D., *Macromol. Biosci.* **2013,** *13* (10), 1347-1357.

(47) Eguiburu, J.; Fernandez-Berridi, M. J.; Román, J. S., *Polymer* **1996,** *37* (16), 3615-3622.

(48) Zapata-González, I.; Hutchinson, R. A.; Matyjaszewski, K.; Saldívar-Guerra, E.; Ortiz-Cisneros, J., *Macromol. Theory Simul.* **2014,** *23* (4), 245-265.

(49) Lupi, M.; Colombo, C.; Frapolli, R.; Ferrari, R.; Sitia, L.; Dragoni, L.; Bello, E.; Licandro, S. A.; Falcetta, F.; Ubezio, P.; Bigini, P.; Salmona, M.; D'Incalci, M.; Morbidelli, M.; Moscatelli, D., *Nanotechnology* **2014,** *25* (33), 335706

(50) Colombo, C.; Dragoni, L.; Gatti, S.; Pesce, R. M.; Rooney, T. R.; Mavroudakis, E.; Ferrari, R.; Moscatelli, D., *Ind. Eng. Chem. Res.* **2014,** *53* (22), 9128-9135.

(51) Ferrari, R.; Pecoraro, C. M.; Storti, G.; Moscatelli, D., *RSC Adv.* **2014,** *4* (25), 12795-12804.

(52) Li, D.; Li, N.; Hutchinson, R. A., *Macromolecules* **2006,** *39* (13), 4366-4373.

(53) Liang, K.; Dossi, M.; Moscatelli, D.; Hutchinson, R. A., *Macromolecules* **2009,** *42* (20), 7736-7744.

(54) Beuermann, S.; Buback, M.; Davis, T. P.; García, N.; Gilbert, R. G.; Hutchinson, R. A.; Kajiwara, A.; Kamachi, M.; Lacík, I.; Russell, G. T., *Macromol. Chem. Phys.* **2003,** *204* (10), 1338-1350.

(55) Siegmann, R.; Jeličić, A.; Beuermann, S., *Macromol. Chem. Phys.* **2010,** *211* (5), 546-562.

(56)   Haehnel, A. P.; Stach, M.; Chovancova, A.; Rueb, J. M.; Delaittre, G.; Misske, A. M.; Lacik, I.; Barner-Kowollik, C., *Polym. Chem.* **2014,** *5* (3), 862-873.

(57)   Kockler, K. B.; Fleischhaker, F.; Barner-Kowollik, C., *Polym. Chem.* **2016,** *7* (26), 4342-4351.

(58)   Dervaux, B.; Junkers, T.; Schneider-Baumann, M.; Du Prez, F. E.; Barner-Kowollik, C., *J. Polym. Sci. Part A: Polym. Chem.* **2009,** *47* (23), 6641-6654.

(59)   Soykan, C.; Erol, I., *J. Polym. Res.* **2004,** *11* (1), 53-63.

(60)   Barner-Kowollik, C.; Bennet, F.; Schneider-Baumann, M.; Voll, D.; Rolle, T.; Facke, T.; Weiser, M.-S.; Bruder, F.-K.; Junkers, T., *Polym. Chem.* **2010,** *1* (4), 470-479.

(61)   Noguchi, A.; Kuzuya, M., *Macromol. Chem. Phys.* **2001,** *202* (7), 1021-1030.

Chapter 9

A Systematic Approach for Modeling the Influence of Hydrogen Bonding on Radical Copolymerization Kinetics

Preface

The observation that the effect of hydrogen bonding on reactivity was significantly diluted in the polyester macromonomer copolymerization with styrene prompted me to probe more deeply into the topic. This chapter outlines a framework for interpreting the radical copolymerization kinetics of hydroxyl-bearing monomers in organic solution copolymerization, presenting the motivations and considerations that underlie this new approach. Although more speculative in nature, the approach developed using kinetic Monte Carlo simulations seems promising, as it adequately represents the variations in copolymerization behavior with solvent choice for several hydroxyl-bearing monomer systems important to the automotive coatings industry.

9.1 Introduction

The influence of hydrogen bonding (HB) in organic solution n-alkyl ester acrylic propagation kinetics has been documented for many systems. Currently, this influence is understood as an association between donor hydroxyl and (meth)acryloyl carbonyl group which reduces the electron density around the double bond making it more reactive towards radical addition, as is reflected by an increase in propagation rate coefficient (k_p).[1] The hydroxyl group may be provided externally by an alcohol solvent, as summarized by Table 9.1, or provided internally by a hydroxyl-bearing monomer, as summarized by Table 9.2. Furthermore, the effect of HB on organic solution k_p for (meth)acrylic monomers can also be disrupted by solvents such as dimethylformamide (DMF) or tetrahydrofuran (THF).[2]

The influence of HB on k_p is known to be concentration dependent,[1,3] where 50 vol% n-butanol (BuOH) is sufficient to increase the k_p of n-butyl methacrylate (BMA) or n-butyl acrylate (BA) by 30% compared to the bulk value. In addition, HB is responsible for the elevated bulk k_p of hydroxyl-bearing monomers, such as 2-hydroxyethyl methacrylate (HEMA), hydroxypropyl methacrylate (HPMA), and ethyl-α-hydroxymethacrylate (EHMA) compared to their alkyl analogs. However, what is not clear is how HB influences radical copolymerization propagation kinetics, in particular the copolymer composition behavior.

Scheme 9.1 illustrates why the current understanding of HB in copolymer propagation kinetics is inadequate. The parameter δ, defined as the ratio of HB donors to acceptors (i.e., ratio of hydroxyl to carbonyl groups), is introduced to qualitatively track HB dilution. For HEMA homopolymerization δ=1, whereas δ=1/4 for the homopolymerization of hydroxyl terminated polycaprolactone (PCL) macromonomer with average 3 PCL units (HEMA-PCL$_3$). In a recent methacrylate (xMA) and styrene (ST) copolymerization study, solution copolymerizations in toluene-d8 showed that the elevated relative reactivity of xMA, exhibited by the HEMA/ST system,

Table 9.1: Influence of externally provided HB by HB donating solvents on acrylic k_p.
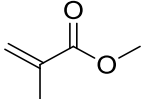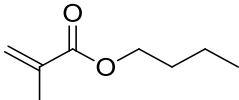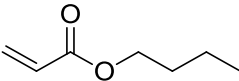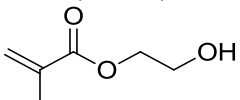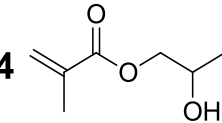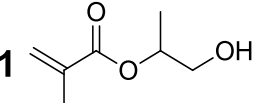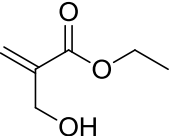
Monomer	Increase in k_p in alcohol solvent	Conditions
methyl methacrylate (MMA)	$$\frac{k_{p,app}}{k_{p,bulk}} = 0.1 \cdot \frac{[BzOH]}{[MMA]} + 1$$	For $\frac{[BzOH]}{[MMA]} \leq 6.08$ at 30 °C[3]

n-butyl methacrylate (BMA)	[BMA] (L·mol^{-1}·s^{-1})	E_A (kJ·mol^{-1})	A (10^6 L·mol^{-1}·s^{-1})	n-butanol (0–80°C)[1]
	Bulk	23.0	4.52	
	1.5	20.4	2.41	
	0.8	20.5	2.77	

| n-butyl acrylate (BA) | $$\frac{k_{p,app}}{k_{p,bulk}} = 1.2$$ | 50 vol% n-butanol at 50 °C[4] |

Table 9.2: Influence of internally provided HB by hydroxyl-bearing monomers on acrylic k_p.

Monomer	k_p (L·mol^{-1}·s^{-1})				Conditions
		Solvent			
	Bulk	Disruptor	Promoter	Inert	
2-hydroxyethyl methacrylate (HEMA)	1201	n.d.	973 (n-butanol)	n.d.	50 vol% mon. 22 °C[5]
hydroxypropyl methacrylate (HPMA) **4** **1**	1211	720 (2.77 M in THF)	1170 (3.04 M in BzOH)	1350 (2.69 M in Toluene)	57 wt% mon. at 40 °C[6]
Ethyl a-hydroxymethacrylate (EHMA)	n.d.	580 (1.82 M in THF)	647 (1.72 M in propan-1-ol)	1635 (1.79 M toluene)	75 wt% mon. at 15 °C[7]

was significantly reduced for HEMA-PCL$_3$/ST.[8] In fact, the relative xMA consumption of HEMA-PCL$_3$ was unchanged even when its hydroxyl group was end-capped with propionate ester, which suggests that at $\delta=1/4$, the influence of HB is so dilute that its effect on radical copolymerization kinetics is negligible.

Alternatively, the parameter δ can be diluted by copolymerizing HEMA with alkyl (meth)acrylate comonomers, such as BMA. For bulk copolymerizations with $\delta<1$ (all points along a Mayo-Lewis curve), hydroxyl-bearing monomers such as HEMA and 2-hydroxyethyl acrylate (HEA) unexpectedly demonstrate self-promoting behavior compared to their copolymerizations in DMF (where all HB effects are negated), a result found for HEMA/BMA,[9] HEMA/BA,[9] and HEA/BMA.[10] Thus, increased monomer reactivity facilitated by HB-induced reduction of electron density at the double bond cannot solely account for this peculiar self-promoting behavior of hydroxyl-bearing monomers, nor can it account for the exacerbation of this self-promoting behavior in non-specific interacting solvents (e.g., xylenes, toluene) documented for HEMA/ST[11] and HEA/BMA.[10]

Similar self-promoting behavior, which increases in dilute non-interacting solvent, was documented for the radical copolymerization of methacrylic acid (MAA) and ST in which δ would be unity; Noguchi and Kuzuya substantiated through experiment and model that enhanced MAA incorporation could be represented by an intrachain reaction of chain-end radical with MAA monomers hydrogen-bonded to MAA repeat units in the growing chain.[12] In benzene solution, MAA dimer associations are highly favorable,[12] while in the aqueous environment the association between H$_2$O and MAA molecules is preferred such that MAA dimers do not play a significant role in aqueous phase propagation kinetics.[13] Therefore, by adapting the model proposed by Noguchi and Kuzuya, the aim of this work is to explain both composition and rate behavior for HEMA and HEA copolymerization systems in terms of increased reaction probabilities instead of intrinsically different kinetic rate coefficients.
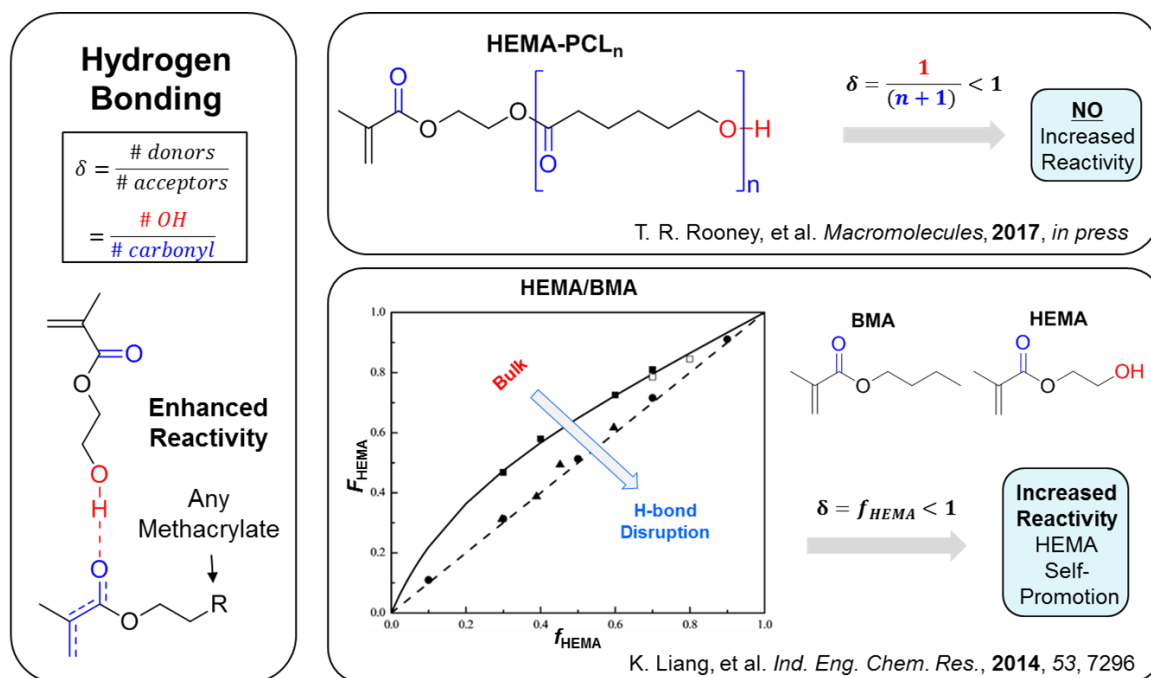
Scheme 9.1: Schematic representation of the inconsistencies in the influence hydrogen bonding in radical copolymerization kinetics.

9.2 Model Development

9.2.1 Monomer Types

A comprehensive model for hydroxyl monomers in organic solution copolymerization must describe the influence of internally- (monomer) and externally- (solvent) induced HB in terms of both composition and rate for a variety of hydroxyl functionalized (meth)acrylate (co)polymerization systems. Moreover, feasible experiments should be recommended to estimate minimal new parameters. The set of possible monomers existing in bulk, non-specific interacting solvents, or HB promoting/disrupting solvents is summarized by Scheme 9.2. The HEMA/BMA system is used as example (can be readily interchanged with HEA as well as other BA or other non-hydroxyl bearing comonomers), where * denotes a HB promoted monomer with increased reactivity and + denotes a dimer species.
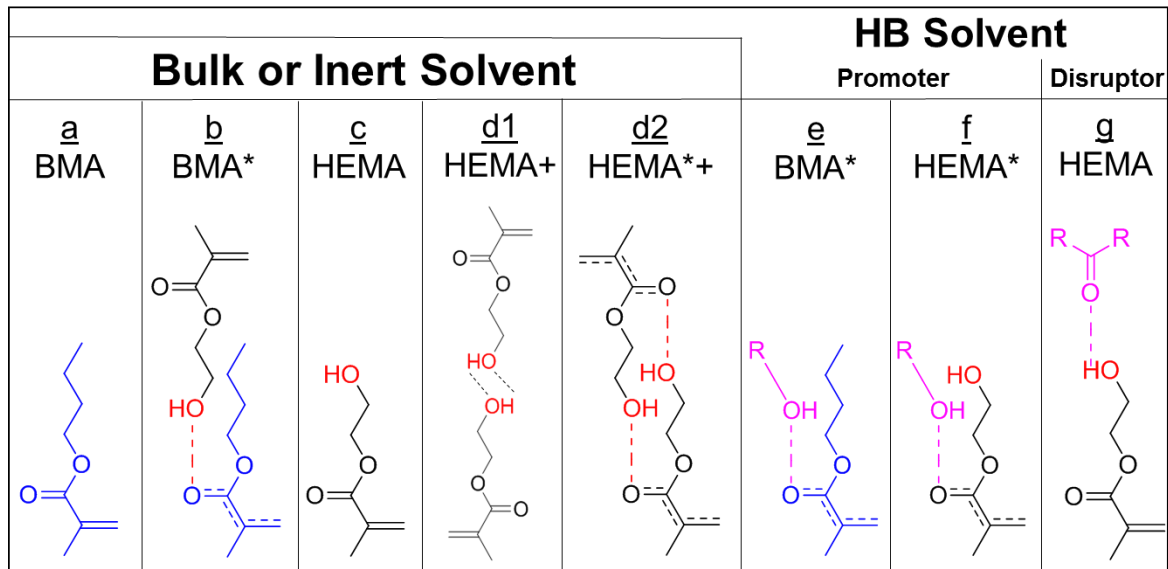
Scheme 9.2: All possible monomer types in a HEMA/BMA system with internally or externally provided hydrogen bonding (HB).

Both the hydroxyl and carbonyl substituents of HEMA can accept HB, while only the hydroxyl can donate HB. Infrared (IR) spectroscopy of bulk HEMA shows no free –OH groups; rather they coexist as OH…OH aggregate, OH…OH dimer, or C=O…OH associations.[14] For HEMA solutions in CCl$_4$ below 1 mol% HEMA there exists mostly free HEMA but also C=O…OH and OH…OH interactions that show no concentration dependence, whereas MeOH molecules become isolated under the same conditions. This observation provides strong evidence for intermolecular HEMA dimer structures of two types as shown by cases (d1) and (d2) in Scheme 2, noting that the latter could not be distinguished from a proposed quasi intramolecular ring structure. In addition, IR measurements of dry polyHEMA (minimal water content) showed that under ambient conditions roughly 47% of –OH groups are engaged in C=O…OH interactions while the remaining 53% contribute to the OH…OH interactions; above the polyHEMA glass transition temperature (T_g; ~80 °C), the latter associations are increasingly dissociated and replaced by the former.[15] This is an indication that the nature of HB and dimer formation in HEMA monomers can change significantly at elevated temperatures.

According to Scheme 9.2, in bulk or in non-specific interacting solvents (e.g., xylenes or toluene), BMA can exist on its own (a) or it can be promoted to BMA* (b) via HB with a free HEMA monomer (c). In bulk, HEMA can exist as HEMA+ (d1) or HEMA*+ (d2) where the former does not result in a promoted HEMA monomer whereas the latter yields a HEMA dimer with increased reactivity. In a non-specific interacting solvent, the free HEMA monomer can exist (c) in addition to the dimer configurations (d1) and (d2). In alcohol solution (HB promoter), the dimer structures (d1) and (d2) should be disrupted and most methacrylates should be promoted, such that BMA* (e) and HEMA* (f) predominate (with equal reactivities) over the free monomers (a) and (c), whose reactivities are also equal. Finally, in a HB disrupting solvent such as DMF, the dimer structures (d1) and (d2) should be disrupted to yield only non-promoted methacrylates (a) and (g) which copolymerize with equal reactivity.

9.2.2 Approach to Copolymer Composition

The central premise is that the systematic variations in copolymer composition observed for hydroxyl-bearing (meth)acrylates with solvent choice is not an intrinsic kinetic effect. Rather, these HB monomers have the same reactivity as their non-functional analogues but their reaction probabilities are increased by contributions from dimer associations between free monomer and HB repeat units already incorporated into a growing chain, as illustrated by Scheme 9.3. Therefore, the kinetic parameters obtained in HB disrupting solvents (e.g., DMF or THF) should be used as the basis to model each system. By extension, this premise should also apply to the measurement of propagation rate coefficients for both homopolymerization and copolymerization systems (see Section 9.4).

It is assumed that the equilibria which govern HEMA dimers (d1) and (d2) also describe the corresponding HB repeat unit and unreacted HB monomer interactions. In addition, while both HEMA dimers (d1) and (d2) coexist (certainly below the T_g), for the purpose of simplicity and demonstrating proof of concept, only HEMA dimer case (d1) is considered in this work because

169
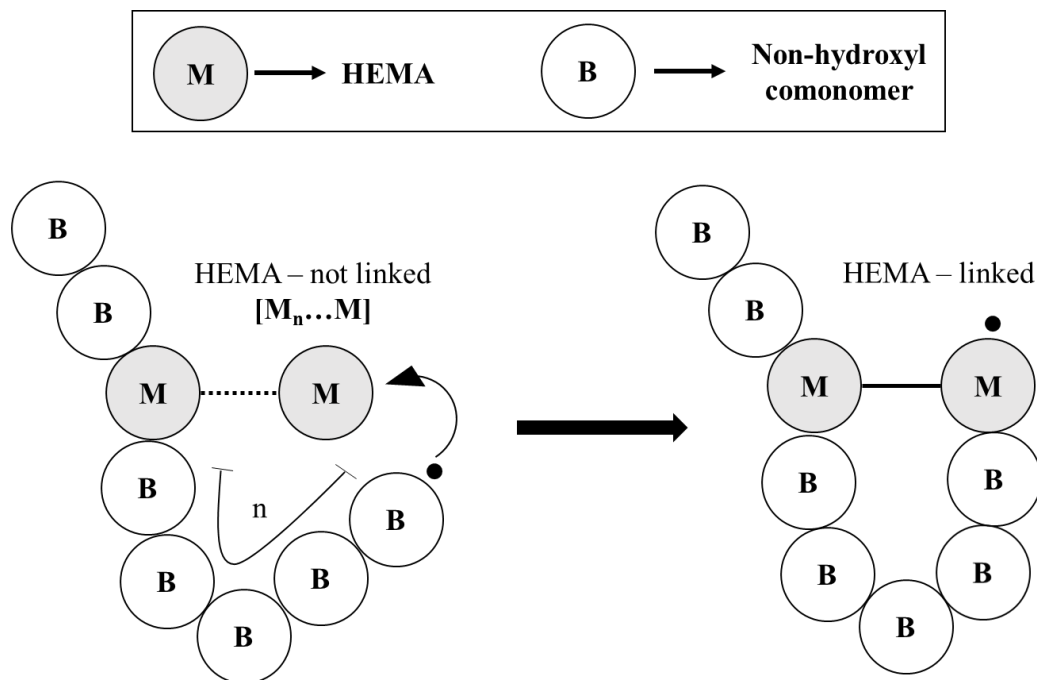
Scheme 9.3: Schematic representation of intramolecular HEMA propagation reaction between chain-end radical and HEMA monomer "stuck" to a HEMA unit in the growing polymer chain.

(d2) requires knowledge of the true promoted methacrylate $k^*_{p,xMA}$, a value which is not yet available (see Section 9.4.3 for experiments to deduce). However, case (d2) can readily be incorporated into a kinetic Monte Carlo simulation following the same methodology to describe increased reaction probabilities that is implemented for case (d1). Finally, although HEMA-polyBMA or BMA-polyHEMA associations can exist, they are ignored because their interactions should be weaker compared to (d1) or (d2) HB types, and the net change in copolymer composition resulting from their combined considerations would be near zero.

By adapting the model originally put forth by Noguchi and Kuzuya for MAA/ST copolymerization,[12] the kinetic basis for the approach depicted by Scheme 9.3 is captured by Equations 9.1 – 9.6, where M is HEMA monomer, B is non-hydroxyl monomer (e.g., ST, BMA,

BA, etc.) and $M_n...M$ is a HEMA monomer stuck to a polyHEMA unit in the growing chain. Equations 9.7 and 9.8 emphasize the implementation of reactivity ratios in HB disrupting solvent (e.g., DMF), which approach unity for xMA/xMA copolymerizations.

$$M \bullet + B \quad \overset{k_{12}}{\rightarrow} \quad B \bullet \tag{9.1}$$

$$M \bullet + M \quad \overset{k_{11}}{\rightarrow} \quad M \bullet \tag{9.2}$$

$$M \bullet + M_n...M \quad \overset{k_{1n}}{\rightarrow} \quad M \bullet \tag{9.3}$$

$$B \bullet + B \quad \overset{k_{22}}{\rightarrow} \quad B \bullet \tag{9.4}$$

$$B \bullet + M \quad \overset{k_{21}}{\rightarrow} \quad M \bullet \tag{9.5}$$

$$B \bullet + M_n...M \quad \overset{k_{2n}}{\rightarrow} \quad M \bullet \tag{9.6}$$
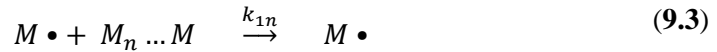
$$r_1 = \frac{k_{11}}{k_{12}} \rightarrow \qquad \frac{k_{1n}}{k_{12}} = \frac{k_{11}}{k_{12}} \quad \therefore \ r_{1n} = r_1 \tag{9.7}$$

$$r_2 = \frac{k_{22}}{k_{21}} \rightarrow \qquad \frac{k_{22}}{k_{2n}} = \frac{k_{22}}{k_{21}} \quad \therefore \ r_{2n} = r_2 \tag{9.8}$$

$$[M_n...M] = \alpha \cdot n^\beta \tag{9.9}$$

The feature which gives rise to the increased reaction probability of hydroxyl-bearing monomers is the dependence of the effective HEMA concentration stuck to polyHEMA in the growing chain, $[M_n...M]$, on the distance (n) from the chain-end radical. The relationship was carefully approximated by Noguchi and Kuzuya for the MAA/ST system based on experimental measurements. In this work, as shown by Figure 9.1, the expression for $[M_n...M]$ as a function of n is reproduced and simplified according to Equation 9.9 such that only two parameters are required per system (α, β). The parameters α=10.3 mol·L^{-1} and β=-2.18, which were fitted to the MAA/ST measurements, are used throughout this work.

The following assumptions about the effective concentration of HEMA dimers stuck to polyHEMA units in the growing chain, $[M_n...M]$, are carried over from the Noguchi and Kuzuya:

171

1. $M_n...M$ can only react if $n \geq 5$.

2. Once $M_n...M$ has reacted it becomes permanently linked to its intramolecular pair such that both HEMA units become inactive.

3. $M_n...M$ has the same reactivity as M (Equations 9.7 and 9.8).

Assumption 1 pertains to the length of the shortest α,ω-alkanedioic acid, $HOOC(CH_2)_nCOOH$, capable of forming a stable intramolecular HB,[12] and therefore it seems reasonable that a HEMA stuck to a polyHEMA unit in the growing chain can only react for $n \geq 5$ as long as the growing chain is not exceedingly rigid compared to a MAA/ST chain. In addition, assumption 2 should apply to HEMA as extensive intra- and inter- HB between polyHEMA chains has been documented by IR.[15] Thus, from Eqns. 9.1-9.9, the reaction probabilities detailed by Eqns. 9.10-9.15 can be implemented in a kinetic Monte Carlo Model, capable of tracking incorporated HEMA positions.
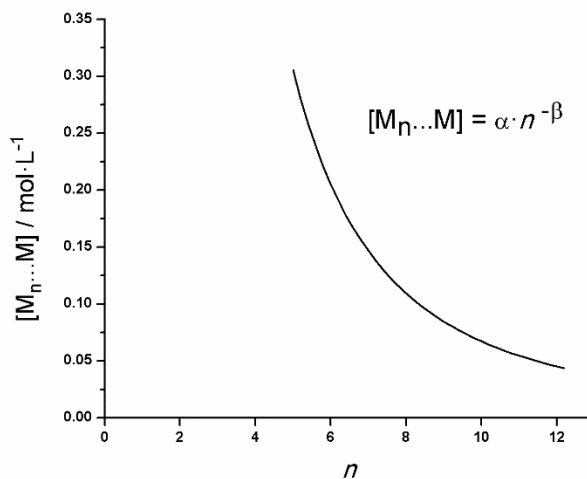
Figure 9.1: Representation of effective MAA concentration stuck to polyMAA units in a growing chain, [$M_n...M$], as a function of n, the distance from the chain-end radical. Data taken from MAA/ST copolymerization system to construct simplified expression with α=10.3 mol·L^{-1} and β=2.18.[12]

$$P_{12} = \frac{[B]}{([M] + \sum[M_n \ldots M]) \cdot r_1 + [B]} \tag{9.10}$$

$$P_{11} = \frac{[M] \cdot r_1}{([M] + \sum[M_n \ldots M]) \cdot r_1 + [B]} \tag{9.11}$$

$$P_{1n} = \frac{[M_n \ldots M] \cdot r_1}{([M] + \sum[M_n \ldots M]) \cdot r_1 + [B]} \tag{9.12}$$

$$P_{22} = \frac{[B] \cdot r_2}{[M] + \sum[M_n \ldots M] + [B] \cdot r_2} \tag{9.13}$$

$$P_{21} = \frac{[M]}{[M] + \sum[M_n \ldots M] + [B] \cdot r_2} \tag{9.14}$$

$$P_{2n} = \frac{[M_n \ldots M]}{[M] + \sum[M_n \ldots M] + [B] \cdot r_2} \tag{9.15}$$

9.3 Results

9.3.1 Outline

Concerning the instantaneous copolymer composition of hydroxyl-bearing (meth)acrylate systems, there is currently no cohesive explanation in the literature for the three peculiar behaviors, listed below, which are evidenced by HEMA/ST, HEA/BMA, HEMA/BMA, and HEMA/BA. These behaviors are caused by HB because in DMF (HB disruptor) solution copolymerizations, the Mayo-Lewis plots for these hydroxyl-bearing monomer systems approach those of their alkyl (meth)acrylate analogues. Thus, the objective of this section is to demonstrate that these peculiar behaviors are caused by increased reaction probabilities of the hydroxyl-bearing monomers instead of intrinsic differences in kinetic rate coefficients, and that the observed solution copolymerization behaviors can be described in terms of a gradient from "turning off" to "turning on" HB.

1. For HEA/BMA,[10] HEMA/BMA,[9] and HEMA/BA[9] why is the hydroxyl-bearing (meth)acrylate preferentially incorporated (compared to non-hydroxyl analogue) even though all the comonomers are also capable of accepting HB at their methacryloyl carbonyl

(presumably to reduce electron density at the double bond making them more reactive towards radical addition)?

2. In the HEMA/ST[11] and HEA/BMA[10] systems, why is the preferential hydroxyl-bearing monomer incorporation, exhibited in bulk, exacerbated in increasingly dilute solutions of non-interacting solvents (e.g., xylenes, toluene)?

3. xMA/acrylate copolymerizations are known to produce xMA-rich copolymers.[16] Why do bulk and solution HEA/BMA[10] copolymerization systems generate copolymers increasingly enriched by acrylates?

Kinetic Monte Carlo simulations to stochastically produce low-conversion Mayo-Lewis plots are performed by implementing Eqns. 9.10-9.15 in MATLAB using each system's experimentally determined reactivity ratios in the HB disrupting solvent, DMF. The exception is HEMA/ST, where the reactivity ratios for its non-hydroxyl analog, BMA/ST, are used instead, as the observed k_p reduction of ST in DMF[11,17] cannot be easily decoupled from the ability of DMF to negate HB in HEMA. The representation for [M_n…M], given by Eqn. 9.9, assumes only dimer (d1) types (i.e., non-promoted dimers – no enhanced reactivity) and uses α=10.3 mol·L^{-1} and β=-2.18, the value fitted to the MAA/ST measurements from another work.[12] For each initial monomer composition of each system, a single chain with degree of polymerization 1500 is simulated and its copolymer composition is compared in Figures 9.2-9.5 to the experimentally determined low-conversion copolymer composition estimates reproduced as curves using literature reactivity ratios.

9.3.2 Simulation Results

The scenario in which HB is "turned off" (i.e., in DMF) in the HEMA/ST system is given by the copolymer composition simulation at bulk conditions (~9 M) shown in Figure 9.2A, where the effective concentration of HEMA dimers, [M_n…M] is very small in comparison to the analytical monomer concentration, [M]$_{analytic}$ = [M]+[B], and therefore the corresponding intramolecular dimer reaction probabilities, Eqns. 9.12 and 9.15, are insignificant compared to the four classic

174

Terminal Model propagation steps, Eqns. 9.10, 9.11, 9.13, and 9.14. The tightness of the simulation results to the literature bulk BMA/ST curve demonstrates that the kinetic Monte Carlo simulation size (1500 iterations) is sufficient to accurately represent copolymer composition.

Since the effective dimer concentration is only determined by distance from chain-end radical (n) as well as the (α, β) pair, the scenarios in which HB is present are simulated by artificially diluting the overall analytical monomer concentration such that $[M_n...M]$ becomes larger relative to $[M]_{analytic} = [M]+[B]$, and consequently the reaction probabilities Eqns. 9.12 and 9.15 become more significant. Note that the term artificial is applied because the (α, β) pair has not been optimized for this system and therefore does not accurately represent the absolute value of $[M_n...M]$. The effect of "turning on" HB via HEMA dimer intrachain propagation is seen in Figure 9.2B, where an artificial $[M]_{analytic} = 0.005$ M roughly matches the copolymer composition curve for bulk HEMA/ST. When $[M]_{analytic}$ is further diluted to 0.001 M (i.e., further "turning on" HB), Figure 9.2C yields the HEMA/ST curve in 25 vol% toluene copolymer composition. Finally, when the case of infinite dilution is considered (i.e., when $[M_n...M] >> [M]_{analytic}$) the 50 vol% toluene curve is reproduced in Figure 9.2D. This result is very promising since a Density Functional Theory (DFT) study found that the radical propagation transition state (TS) geometries for HEMA/ST copolymerizations in bulk and toluene are similar, and therefore the authors were unable to computationally reproduce the experimentally determined Mayo-Lewis plot for toluene solution copolymerization.[18]

The limiting condition of infinite dilution implies that when a HEMA dimer is incorporated into the growing chain by a classical Terminal Model propagation step (Eqn. 9.11 or 9.14), there is a 100% probability that once $n = 5$, the "stuck" HEMA monomer will perform an intrachain reaction with chain-end radical (Eqn. 9.12 or 9.15). In other words, towards infinitely dilute conditions, every HEMA incorporated into the growing chain will result will in the incorporation of another HEMA unit. This notion is supported by the concentration independent C=O...OH and
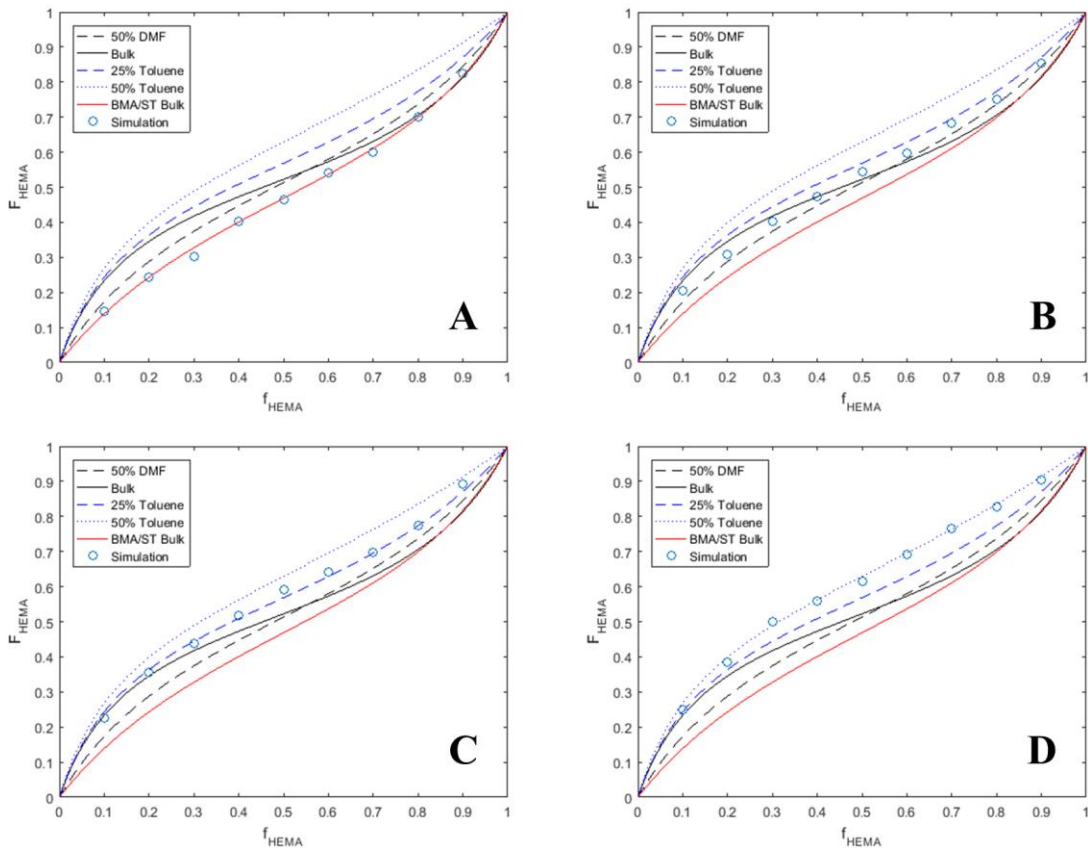
Figure 9.2: Simulated Mayo-Lewis plots for HEMA/ST systems using bulk BMA/ST reactivity ratios (r_{xMA}=0.42 and r_{ST}=0.61)[19] for overall analytical concentrations corresponding to bulk (panel A), 0.005 M (panel B), 0.001 M (panel C), and infinite dilution (panel D). Experimentally determined literature reactivity ratios for HEMA/ST[11] in bulk (solid black), 50 vol% DMF (dashed black), 25, and 50 vol% toluene (dashed and dotted blue, respectively) as well as bulk BMA/ST (solid red) are reproduced as lines labelled according to the insets.

OH…OH interactions measured by IR for HEMA as less than 1 mol% in CCl$_4$, which indicate the presence of HEMA dimers even under very dilute conditions.[14]

The same methodology (as HEMA/ST) is applied to the anomalous HEA/BMA system in which HB and solvent effects manifest as deviations from the well-documented family behavior for xMA/acrylate copolymerizations to produce methacrylate-rich copolymers.[10]– When HB is "turned off" under bulk conditions (~9 M), the simulation provides a good fit to the HEA/BMA in 50 vol% DMF curve calculated using literature reactivity ratios (Figure 9.3A), confirming the adequacy of a 1500 iteration simulation size to represent instantaneous copolymer composition.

Then, the overall analytical monomer concentration is artificially diluted such that $[M_n \ldots M]$ becomes larger relative to $[M]_{\text{analytic}} = [M]+[B]$. The effect of "turning on" HB via HEA dimer intrachain propagation is seen in Figure 9.3B, where an artificial $[M]_{\text{analytic}} = 0.002$ M roughly matches the copolymer composition curve for bulk HEA/BMA. At the limit of infinite dilution (i.e., when $[M_n \ldots M] \gg [M]_{\text{analytic}}$) the 50 vol% butyl propionate (Bpi; a weak HB disruptor) curve is reproduced in Figure 9.3C. These results are particularly promising since they provide a basis to explain the counterintuitive increasingly acrylate-rich copolymers produced from xMA/acrylate copolymerizations.

However, it is clear from Figure 9.3C that under the condition of infinite dilution, the simulation cannot adequately match the copolymer composition data for HEA/BMA in 50 vol% xylenes; i.e., even if the (α, β) pair is properly optimized for HEA/BMA copolymers, the simulation will never extend to the 50 vol% xylenes composition curve using the reactivity ratios measured for HEA/BMA in 50 vol% DMF. Alternatively, as shown by Figure 9.3D, the xylenes curve can be roughly matched at infinite dilution using bulk HEA/BMA reactivity ratios. Although the usage of experimentally determined bulk reactivity ratios as the basis for the kinetic Monte Carlo simulation probably has no physical meaning, it demonstrates that in addition to contributing increased reaction probabilities, some of the dimers must also have inherently increased reactivity. In other words, to fully describe the HEA/BMA system both dimer cases (d1) and (d2) must be considered, where their coexistence can be inferred from IR measurements of HEMA solutions below 1 mol% in CCl_4.[14] Of course, an estimation for the relative amounts of (d1) and (d2) is required (a good preliminary approximation would be 47% and 53%, respectively, estimated for dry polyHEMA HB interactions[15]), as well as knowledge of the HB promoted rate coefficients, $k^*_{\text{p,xMA}}$, r^*_1, and r^*_2 (see Section 9.4.3), to implement dimer case (d2).
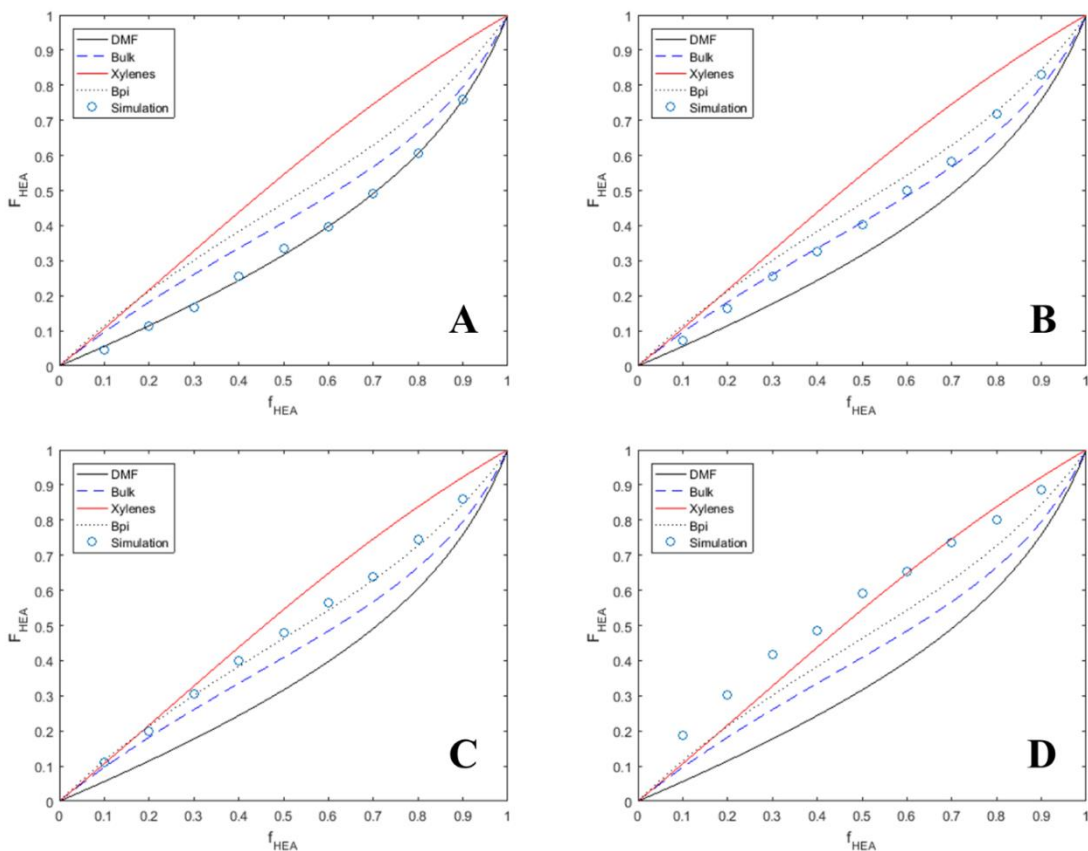
Figure 9.3: Simulated Mayo-Lewis plots for HEA/BMA systems using HEA/BMA reactivity ratios in 50 vol% DMF (rHEA=0.31 and rBMA=1.38)10 for overall analytical concentrations corresponding to bulk (panel A), 0.002 M (panel B), and infinite dilution (panel C), while bulk HEA/BMA reactivity ratios (r_{HEA}=0.37 and r_{BMA}=0.98)[10] are also implemented at infinite dilution (panel D) Experimentally determined literature reactivity ratios for HEA/BMA in bulk (dashed blue), 50 vol% DMF (solid black), 50 vol% xylenes (solid red), and 50 vol% Bpi (dotted black) are reproduced as lines labelled according to the insets.

Next, the HEMA/BMA and HEMA/BA copolymer composition simulations, shown by Figures 9.4 and 9.5, respectively, are considered together because their reactivity ratios were only experimentally determined in DMF, BuOH and in bulk.[9] Using the respective reactivity ratios measured in DMF (HB disruptor) under conditions of infinite dilution, the simulation adequately captures the shapes of both bulk HEMA/BMA and bulk HEMA/BA copolymer composition curves (Figures 9.4B and 9.5B, respectively), confirming the importance of increased hydroxyl-bearing monomer reaction probabilities via HB-facilitated dimer (d1) interactions in these systems. Since

178

experimental copolymer composition data in non-interacting solvents such as toluene or xylenes is unavailable, the approach adopted for the HEA/BMA system is implemented to predict the curves for HEMA/BMA and HEMA/BA in xylenes, as shown by Figures 9.4D and 9.5D, respectively, using bulk reactivity ratios as the basis for the kinetic Monte Carlo simulations. The purpose of the predictions in Figures 9.4D and 9.5D is to demonstrate how the shape of the respective Mayo-Lewis plots could change depending on the relative extents of dimer cases (d1) and (d2). Again, the bulk reactivity ratios are probably not physically meaningful, and therefore $k^*_{p,xMA}$, r^*_1, and r^*_2 (see Section 9.4.3) must be estimated.
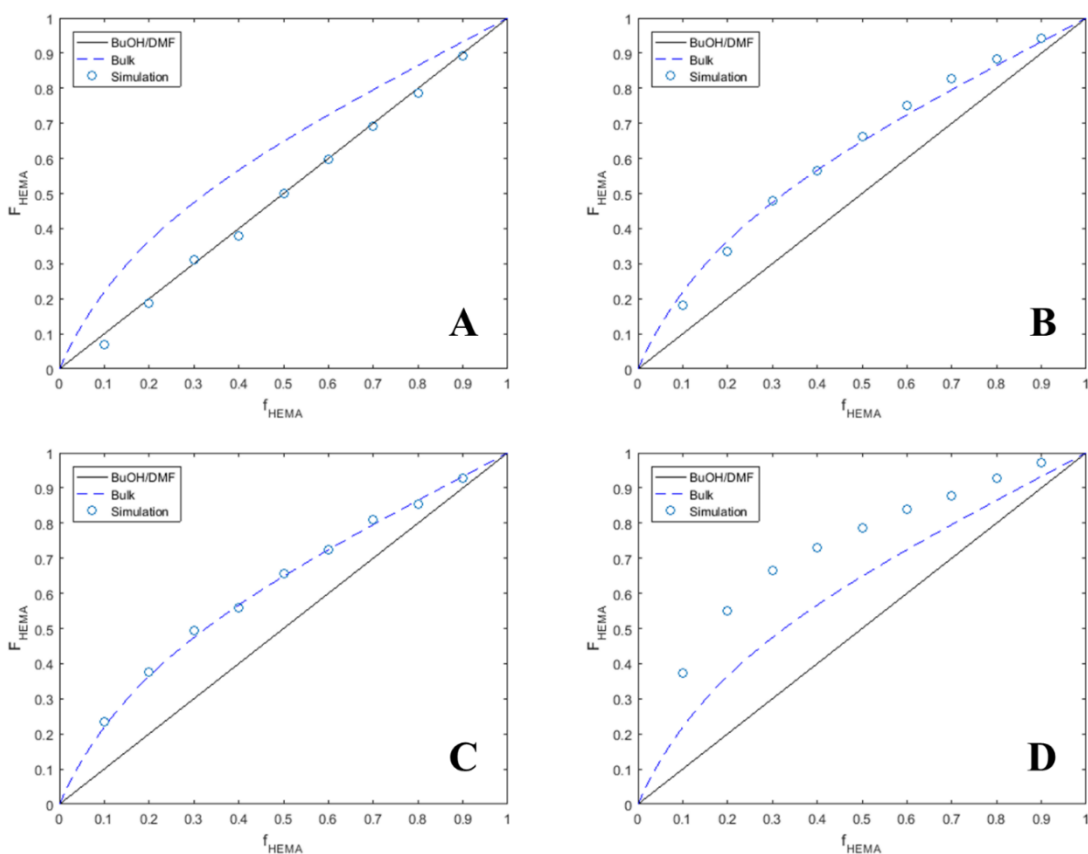
Figure 9.4: Simulated Mayo-Lewis plots for HEMA/BMA systems using HEMA/BMA reactivity ratios in 50 vol% DMF or 50 vol% BuOH (r_{xMA}=1 and r_{xMA}=1)[9] for overall analytical concentrations corresponding to bulk (panel A) and infinite dilution (panel B), while bulk HEMA/ BMA reactivity ratios (r_{HEMA}=1.49 and r_{BMA}=0.35)[9] are also implemented in bulk (panel C) and at infinite dilution (panel D). Experimentally determined literature reactivity ratios for HEMA/BMA in bulk (dashed blue) as well as 50 vol% DMF or 50 vol% BuOH (solid black) are reproduced as lines labelled according to the insets.
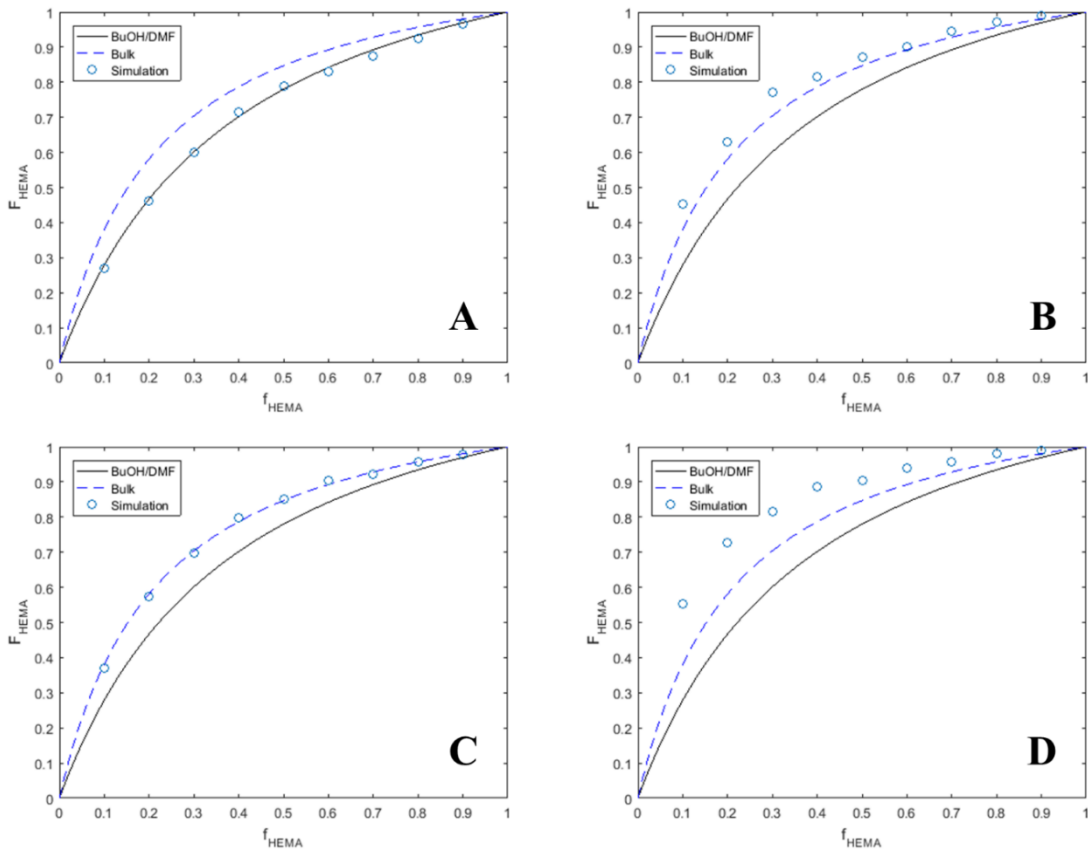
Figure 9.5: Simulated Mayo-Lewis plots for HEMA/BA systems using HEMA/BA reactivity ratios in 50 vol% DMF or 50 vol% BuOH (r_{xMA}=3.57 and r_{BA}=0.29)[9] for overall analytical concentrations corresponding to bulk (panel A) and infinite dilution (panel B), while bulk HE MA/BA reactivity ratios (r_{HEMA}=5.54 and r_{BA}=0.18)[9] are also implemented in bulk (panel C) and at infinite dilution (panel D). Experimentally determined literature reactivity ratios for HEMA/BA in bulk (dashed blue) as well as 50 vol% DMF or 50 vol% BuOH (solid black) are reproduced as lines labelled according to the insets.

By considering the four examples presented in Figures 9.2-9.5, it becomes apparent how changing from non-interacting solvent (e.g., toluene or xylenes), to weak HB disruptor (Bpi) or to bulk, and then to strong HB disruptor (DMF) represents a gradient of "turning off" HB in the systems. Under infinitely dilute conditions, the effect of dimers (d1) is to double the number of hydroxyl-bearing monomers incorporated into the chain. However, from the HEA/BMA system it is clear that dimers (d2) with enhanced reactivity must also be considered in addition to (d1), and that copolymer composition experiments for HEMA/BMA and HEMA/BA in toluene or xylenes

must still be performed. Once the relative amounts of (d1) and (d2) for each system are estimated by IR, the (α, β) pair can be optimized such that the simulated copolymer composition curves match the experiment at the correct analytical monomer concentrations (i.e., simulations without the need for artificially diluting monomer concentrations). As shown by Figure 9.6, preliminary work has already begun to use an optimized (α, β) pair to represent the HEMA/ST Mayo-Lewis plot in 25 vol% toluene using the real monomer concentrations.
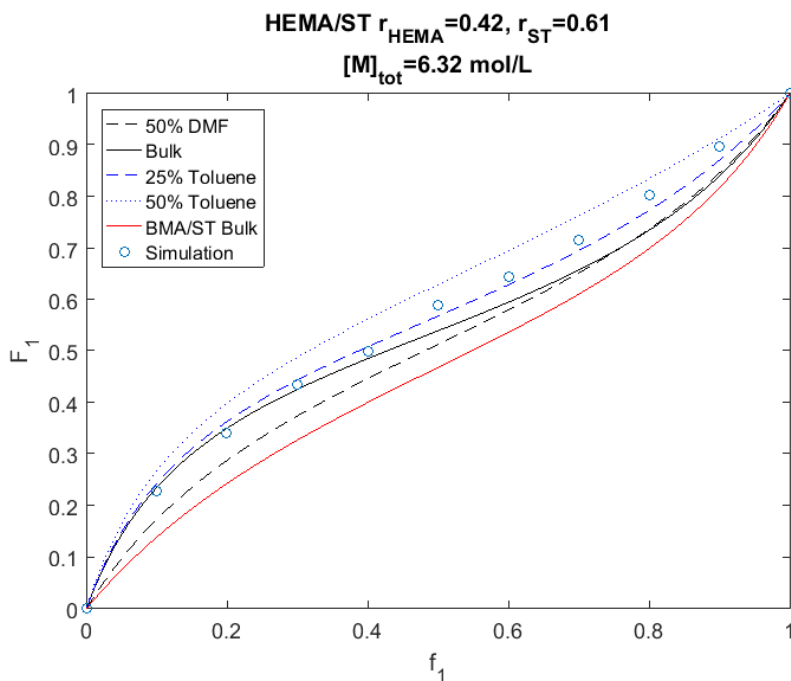
Figure 9.6: Simulation results for HEMA/ST in 25 vol% toluene with optimized α=2569 mol·L⁻¹ and β=-1.65.

Since the effective dimer concentration is independent of analytic monomer concentration, it is expected that during batch radical copolymerizations the influence of the intrachain reaction probabilities (Eqns. 9.12 and 9.15) will increase in significance towards high conversions. During monomer starved feed semi-batch operation the analytic monomer concentration is purposefully kept low and therefore Eqns. 9.12 and 9.15 should be significant throughout the entire reaction, especially towards high conversions when the total reaction volume has increased. However, under

industrially relevant high temperature conditions (i.e., $T>100$ °C) the extent of HB in organic solution will diminish, and the nature of HB between HEMA monomers (i.e., d1 or d2) will change, as significant dissociation of OH…OH and discontinuous increase of C=O…OH interactions were documented above the T_g of polyHEMA.[15]

9.4 Propagation Rate Coefficient Measurements

The approach detailed by Eqns. 9.10-9.15 builds on the premise that the experimentally observed preferential incorporation rates of HB monomers are caused by their increased reaction probabilities instead of intrinsically different propagation rate coefficients. Since this approach adequately reproduces the shapes of the Mayo Lewis plots for several acrylic copolymerization systems in Section 9.3, the methodology should be extended to include new interpretations of k_p and $k_{p,cop}$ values determined by PLP-SEC, where L is the measured chain length of the first inflection point of a low-conversion PLP-generated molar mass distribution (MMD), and t_0 is the specified time between pulses.

$$L_{measured} = k_{p,cop} \cdot [M_{overall}] \cdot t_0$$

At a glance, the addition of the effective HEMA dimer concentration to the overall monomer concentration $[M_{overall}]$ will reduce the estimation for $k_{p,cop}$ compared to the traditional calculation where only the analytical monomer concentration is employed. This implies that the true $k_{p,cop}$ for the system is less than currently estimated.

$$k_{p,cop,overall}(with\ dimer) < k_{p,cop}(analytic)$$

In general, a low-conversion copolymer from PLP-SEC should be interpreted as a sum of its parts such that the $k_{p,cop}$ can be determined for system specific monomer concentrations.

$$L_{measured} = L_{intramolecular} + L_{analytic} \qquad \textbf{(9.16)}$$

$$L_{measured} = \left(k_{p,cop}[M_n \dots M]_{avg} + k_{p,cop}[M] + k_{p,cop}[B]\right) \cdot t_0$$

$$k_{p,cop} = \frac{L_{measured}/t_0}{[M_n \dots M]_{avg} + [M] + [B]}$$

182

where $[M_n\ldots M]_{avg}$ is the time and chain length averaged effective dimer concentration. The following sections will explore the application of Eqn. 9.16 to different bulk and solution copolymerization systems which contain HB monomers.

9.4.1 Hydrogen Bond Disrupting Solvent

For HPMA in equimolar THF almost all of the C=O…OH associations disappeared.[2] Therefore it can be safely assumed that in ≥50 vol% DMF solutions there will be no C=O…OH such that all HB associations are negated (a and g situations in Scheme 9.2) and the estimated $k_{p,cop}$ will be similar to that expected for a typical non-hydroxyl x(M)A/x(M)A bulk copolymerization system (assuming minimal differences in monomer and solvent molar volumes[20]).

$$[M_{overall}] = [M_{analytic}] + [B_{analytic}]$$
$$L_{measured} = k_{p,cop} \cdot t_0 \cdot ([M_{analytic}] + [B_{analytic}])$$

9.4.2 Hydrogen Bond Promoting Solvent

According to the Raman spectrum of 1.6 mol·L^{-1} BMA in BuOH the C=O…OH intensity is significantly less than that of the non-associated C=O.[1] As such, it is unlikely that the reactivity of all BMA monomers in the system is enhanced. On the other hand, in terms of copolymer composition, low-conversion copolymerizations of HEA/BMA,[10] HEMA/BMA,[9] and HEMA/BA[9] in only 50 vol% BuOH were able to reduce the hydroxyl monomer's reactivity towards that of its alkyl analog (or its reactivity in HB disrupting solvent DMF). Therefore, since copolymer composition was described in Section 3 by intramolecular dimer reactions, it is assumed that in at least 50 vol% BuOH solutions the $[M_n\ldots M]$ contribution to $[M_{overall}]$ is negligible.

$$[M_{overall}] = [M_a] + [B_c] + [M *_f] + [B *_e]$$
$$= [M_{analytic}] + [B_{analytic}]$$
$$\gamma = \frac{[M *_f] + [B *_e]}{[M *_f] + [B *_e] + [M_a] + [B_c]} \qquad (9.17)$$

where γ is the fraction of monomers which are promoted by HB and can be estimated by quantitative IR measurements of BMA at different concentrations in BuOH. Overall, Eqn. 9.17 implies the [$M_{overall}$] will be the same in both BuOH and DMF. Therefore, any difference in $k_{p,cop}$ measured between these solvents must be a true intrinsic kinetic feature – a monomer promoted by HB should have an elevated k^*_p whose estimation is detailed by Section 9.4.3. Indeed, under similar conditions, a higher $k_{p,cop}$ was measured in BuOH compared to DMF for HEMA/BMA,[9] HEMA/BA,[9] and BMA/ST[11] but not for HEA/BMA.[10] Perhaps in the latter case, the effect of BuOH to promote the reactivity of BMA is small in comparison to the k_p of any acrylate (at least one order of magnitude difference), especially when no more than a 30% increase in k_p was measured for BMA in 50 vol% BuOH.

9.4.3 Promoted Propagation Rate Coefficient k^*_p Determination

The ability of alcohol solvent to increase the k_p of a methacrylate (xMA) is known to be concentration dependent.[3] According to the Raman spectrum of 1.6 mol·L^{-1} BMA in BuOH (which corresponds to roughly 5 BuOH molecules per BMA molecule) the intensity of the non-associated C=O peak is clearly greater than that of associated C=O peak.[1] Therefore, an equilibrium must exist which describes the concentration of methacrylates [xMA] with regular reactivity compared to that of the methacrylates with promoted reactivity [xMA*] such that the measured k_p values in BuOH are interpreted as $k^*_{p,cop}$ for a xMA/xMA* copolymerization system (keeping in mind that estimation of cross-propagations is not trivial because the effect of alcohol on macroradical species is unknown and cannot be ignored).

$$BuOH + xMA \xrightleftharpoons{K_{eq,xMA}} xMA^*$$
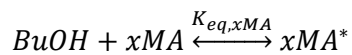
$$[xMA^*] + [xMA] = [xMA_0]$$

$$[xMA^*] + [BuOH] = [BuOH_0]$$

The ratio of hydroxyl to carbonyl in the system must be explicitly taken into account; the parameter δ is specified while γ can be measured by spectroscopic techniques.

$$\delta = \frac{[BuOH_0]}{[xMA_0]}$$

$$\gamma = \frac{[xMA^*]}{[xMA_0]} = \frac{Intensity\ of\ associated\ C = O}{Total\ C = O\ intensity}$$

Thus, the following expression is developed to estimate the HB equilibrium for MMA in BuOH.

$$K_{eq,xMA} = \frac{\gamma}{(\delta - \gamma)(1 - \gamma)} \qquad \textbf{(9.18)}$$

Even if Eqn. 9.18 cannot be simplified to establish the relationship, the individual measurements are still critical. Very crudely one can see how for small γ, a plot of γ vs δ would appear linear as was observed for the MMA in benzyl alcohol system up to δ=6.1.[3]

The influence of BuOH on the xMA monomer to reduce electron density at the double bond is clear, but how the external alcohol influences the chain-end macroradical remains unclear. Therefore the system is treated as a copolymerization according to the Terminal Model (no penultimate unit effects expected for xMA/xMA* systems), where r^*_1 is the reactivity of a non-promoted monomer and r^*_2 is the reactivity of a promoted monomer:

$$xMA \bullet + \ xMA^* \quad \xrightarrow{k^*_{12}} \quad xMA^* \bullet$$

$$xMA \bullet + \ xMA \quad \xrightarrow{k_{11}} \quad xMA \bullet$$

$$xMA^* \bullet + \ xMA^* \quad \xrightarrow{k^*_{22}} \quad xMA^* \bullet$$

$$xMA^* \bullet + \ xMA \quad \xrightarrow{k^*_{21}} \quad xMA \bullet$$
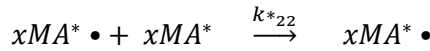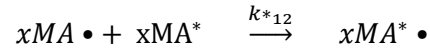
$$r^*_1 = \frac{k_{11}}{k^*_{12}}$$

$$r^*_2 = \frac{k^*_{22}}{k^*_{21}}$$

The main limiting assumption is that the interaction between BuOH and chain-end radical can also be described by $K_{eq,xMA}$ i.e., that the interaction is the same as it is for xMA monomer and BuOH. In the limiting case where the interaction of BuOH with chain-end radical has no impact on propagation, we can expect that $k^*_{21} \rightarrow k_{11}$ and $k^*_{22} \rightarrow k^*_{12}$ such that $r^*_2 = r^{*-1}_1$. The k_p measured

185

for BuOH solution homopolymerizations ($k_{p,xMA/BuOH}$) at different δ can be used to extrapolate the true value for $k^*_{p,xMA}$ as the $k^*_{p,22}$ end-point with known bulk $k_{p,11}$ xMA.

$$k_{p,MMA/BuOH}(\delta) = \frac{r *_1 \cdot f_1^2 + 2f_1\gamma + r *_2 \cdot \gamma^2}{\left(\frac{r *_1 \cdot f_1}{k_{p,11}}\right) + \left(\frac{r *_2 \cdot \gamma}{k^*_{p22}}\right)}$$

$$f_1 = \frac{xMA}{xMA + xMA^*} = (1-\gamma)$$

However, r^*_1 and r^*_2 are required, with values estimated from the Mayo-Lewis relationship.

$$1 - F^*_2 = F_1 = \frac{r *_1 \cdot f_1^2 + f_1\gamma}{r *_1 \cdot f_1^2 + 2f_1\gamma + r *_2 \cdot \gamma^2}$$

In this scenario, F^*_2 represents the instantaneous "copolymer" composition of xMA*, added through a promoted HB interaction. However, since monomers 1 and 2 are identical, it would be impossible to measure F^*_2 from a low-conversion polymer by spectroscopic techniques. Therefore, F^*_2 must be inferred from the length of dead polymer chain (L_i) formed from very specific PLP-SEC experiments.

$$L_i = i \cdot k_p \cdot [xMA] \cdot t_0$$

For xMA homopolymerizations at identical concentrations in different solvents, the L_i measured by SEC should reflect the different k_p for the solvent systems. Therefore, under identical molar concentrations, the L_i measured for xMA in BuOH compared to the L_i measured for xMA in toluene (solvent for which no specific interactions are expected with xMA) should be proportional to the number of additional xMA units added because of HB in the systems. Note that BuOH and toluene solvents are selected for MMA so as to avoid any effects of differences in monomer and solvent molar volumes on apparent k_p measured by PLP-SEC.[20] The experiments could enter very low concentration ranges and therefore low pulse repetition rates are recommended to produce polymers large enough for reliable measurement by SEC.

$$F *_2 = \frac{L_i([MMA], BuOH) - L_i([MMA], toluene)}{L_i([MMA], BuOH)}$$

186

9.5 Implications for Hydroxyl-Bearing Monomer k_p

As no free OH stretching was detected by IR for bulk HEMA,[14] it is reasonable to propose the existence of HEMA dimers; the adequacy of the approach to explain copolymer composition in Section 9.3 provides extra justification. According to Eqn. 9.16, the $L_{measured}$ from PLP-SEC experiments of HEMA, HPMA, and EMHA homopropagations should therefore contain contributions from intramolecular dimer reactions, which implies that the k_p evaluated for these homopropagations systems will be lower than the currently reported bulk values (see Table 9.2) that are significantly elevated compared to their alkyl methacrylates analogues.[5,6]

The activation energy reported for the k_p of 1.5 mol·L^{-1} BMA in BuOH of 20.4 kJ·mol^{-1} is significantly lower than that of bulk BMA homopropagation (23.0 kJ·mol^{-1}), indicating that the interaction between hydroxyl and methacryloyl carbonyl reduces electron density at the double bond (making it more reactive towards radical addition) has an enthalpic origin.[1] Therefore, if the only role of the hydroxyl and methacryloyl carbonyl interaction is to increase the double bond's reactivity towards radical addition, a reduction in activation energy should also be expected for bulk homopropagations of hydroxyl-bearing monomers. However, the reported activation energy for HEMA of 21.9 ± 1.5 kJ·mol^{-1} is close to the IUPAC value for BMA of 22.9 4 kJ·mol^{-1}.[21] Furthermore, the value of k_p for HEMA in 36-50 vol% BuOH was reduced by as much as 17% compared to bulk at 20 °C,[5] which could be an indication that HB with BuOH is disrupting the formation of HEMA dimers, leading to a lower [M$_{eff}$] and consequently lower k_p measured by PLP-SEC.

In the case of EHMA, the results must be interpreted with caution because it is difficult to decouple depropagation effects which are common for bulky α-substituted acrylic monomers.[22] Nonetheless, k_p measurements for EHMA solution homopolymerizations at similar concentrations can be safely compared: at 15 °C in 75 wt% THF (HB disruptor), propan-1-ol (HB promoter), and toluene (non-specific interactions), the k_p was measured to be 585, 647, and 1635 L·mol^{-1}·s^{-1},

respectively.[7] This trend could be interpreted as follows: in THF, there is no HB such that EHMA propagation is similar to its alkyl analog, in propan-1-ol the EHMA dimers are disrupted by solvent but hydroxyl association with methacryloyl carbonyl promotes EHMA reactivity compared to its alkyl analog, while in toluene the HB interactions are not significantly disrupted such that the effective concentration of EHMA dimers is elevated compared to the analytical free EHMA concentration (which is diluted in toluene solution).

Finally, the k_p of HPMA was reduced by about 40% in THF (HB disruptor) compared to bulk, while the k_p in both BuOH and toluene solutions was not significantly different from bulk.[6] These results confirm the importance of HB in HPMA homopropagation to yield a bulk k_p elevated compared to its alkyl methacrylate analog, but they do not indicate that dimers have any role in the system. It could be that dimer formation in HPMA is not favorable because of its branched ester side chain structure.

9.6 Conclusions and Future Work

Kinetic Monte Carlo simulations that utilize Eqns. 9.10-9.15 are implemented to explore the premise that the peculiar copolymer composition behaviors exhibited in hydroxyl-bearing monomer bulk and solution copolymerizations are caused by increased reaction probabilities arising from HB-facilitated dimer species, rather than by of intrinsically different kinetic propagation rate coefficients. Through consideration of only (d1) dimer types (without enhanced reactivity), the shapes for almost all of the experimentally determined bulk and solution Mayo-Lewis plots can be adequately reproduced using reactivity ratios determined in DMF (HB disruptor) for HEMA/ST, HEA/BMA, HEMA/BMA, and HEMA/BA systems. However, the Mayo-Lewis plot for HEA/BMA in 50 vol% xylenes could only be reproduced if HEA dimers with increased reactivity (compared to the DMF reactivity ratios) are considered, implying that (d2) dimers must also be considered. Moving forwards, the extent of (d1) and (d2) dimers must be estimated by IR measurements such that the (α, β) pair can be optimized for each system in order to describe the

peculiar copolymer composition in terms of overall analytical monomer concentrations. As shown by Figure 9.6, preliminary work has already begun to use an optimized (α, β) pair to represent the HEMA/ST Mayo-Lewis plot in 25 vol% toluene using the real monomer concentrations.

Building on the copolymer composition simulation results, several expressions are developed to reinterpret the apparent $k_{p,cop}$ estimations made by PLP-SEC for HB disrupting, HB promoting, and non-specific interacting solvents. A higher effective monomer concentration caused by intrachain hydroxyl-bearing monomer reactions implies that $k_{p,cop}$ in bulk or non-specific interacting solvents (e.g., toluene or xylenes) is lower than the reported values. Furthermore, the impact of HB (to reduce electron density at the monomeric double bond) on k_p is considered, and a set of experiments that explicitly accounts for the amount of HB donors and acceptors in a system is proposed to estimate the reactivity ratios r^*_1 and r^*_2 for non-promoted and promoted monomers, respectively, as well as the true homopropagations rate coefficient for a HB promoted monomer, k^*_p. Eventually, the goal is to apply these new interpretations of kinetic parameters in HB systems to model copolymerization behavior, including polymer molar mass distributions, of starved-feed semi batch reactions.

9.7 References

(1)   Beuermann, S. *Macromolecules* **2004**, *37*, 1037.

(2)   Beuermann, S. *Macromolecular Rapid Communications* **2009**, *30*, 1066.

(3)   O'Driscoll, K. F.; Monteiro, M. J.; Klumperman, B. *Journal of Polymer Science Part A: Polymer Chemistry* **1997**, *35*, 515.

(4)   Liang, K.; Hutchinson, R. A. *Macromolecular Rapid Communications* **2011**, *32*, 1090.

(5)   Buback, M.; Kurz, C. H. *Macromolecular Chemistry and Physics* **1998**, *199*, 2301.

(6)   Beuermann, S.; Nelke, D. *Macromolecular Chemistry and Physics* **2003**, *204*, 460.

(7)   Morrison, D. A.; Davis, T. P. *Macromolecular Chemistry and Physics* **2000**, *201*, 2128.

(8)   Rooney, T. R.; Monyatsi, O.; Hutchinson, R. A. *Macromolecules* **2017**, in press, DOI: 10.1021/acs.macromol.6b02297.

(9)   Liang, K.; Rooney, T. R.; Hutchinson, R. A. *Industrial & Engineering Chemistry Research* **2013**, *53*, 7296.

(10)   Schier, J. E. S.; Hutchinson, R. A. *Polym. Chem.* **2016**, *7*, 4567.

(11)   Liang, K.; Hutchinson, R. A. *Macromolecules* **2010**, *43*, 6311.

(12)   Noguchi, A.; Kuzuya, M. *Macromolecular Chemistry and Physics* **2001**, *202*, 1021.

(13)   Beuermann, S.; Buback, M.; Hesse, P.; Lacík, I. *Macromolecules* **2006**, *39*, 184.

(14)   Morita, S.; Kitagawa, K.; Ozaki, Y. *Vibrational Spectroscopy* **2009**, *51*, 28.

(15)   Morita, S. *Frontiers in Chemistry* **2014**, *2*.

(16)   Buback, M.; Feldermann, A.; Barner-Kowollik, C.; Lacík, I. *Macromolecules* **2001**, *34*, 5439.

(17)   Coote, M. L.; Davis, T. P. *European Polymer Journal* **2000**, *36*, 2423.

(18)   Furuncuoglu Ozaltn, T.; Dereli, B.; Karahan, O.; Salman, S.; Aviyente, V. *New Journal of Chemistry* **2014**, *38*, 170.

(19)   Li, D.; Li, N.; Hutchinson, R. A. *Macromolecules* **2006**, *39*, 4366.

(20)   Beuermann, S.; García, N. *Macromolecules* **2004**, *37*, 3018.

(21)   Beuermann, S.; Buback, M.; Davis, T. P.; Gilbert, R. G.; Hutchinson, R. A.; Kajiwara, A.; Klumperman, B.; Russell, G. T. *Macromolecular Chemistry and Physics* **2000**, *201*, 1355.

(22)   Szablan, Z.; Stenzel, M. H.; Davis, T. P.; Barner, L.; Barner-Kowollik, C. *Macromolecules* **2005**, *38*, 5944.

Chapter 10

Conclusions and Recommendations

10.1 Conclusions

"Grafting through" radical polymerization (RP) of short-chain polyester macromonomers produces comb-polymers whose hydrolytic degradability depends on the type and length of polyester in the macromonomer. Chapter 3 of this work details the synthesis of four new short-chain polyester methacrylate macromonomers with alkyl, tertiary amine, quaternary ammonium, and carboxyl end-group functionalities produced by ring opening polymerization (ROP) of ε-caprolactone or lactide. The utility of the alkyl, tertiary amine and quaternary ammonium end-groups in comb-polymers was demonstrated through proof of concept application development.

As described by Chapter 5, the alkyl terminated macromonomers were used to make nanoparticles (NP) through emulsion radical polymerization (RP) that degraded about four times more slowly than NPs produced from hydroxyl terminated macromonomers with an equivalent average number of polyesters per chain. In addition, NPs produced at an equal mass ratio of alkyl and hydroxyl terminated macromonomers exhibited an intermediate degradation time. Thus, it was demonstrated that end-group functionality is another design parameter that can be used tune comb-polymer degradation behavior.

In Chapter 6, comb-polymers produced from cationic macromonomers were used as flocculants to provide rapid settling of Alberta oil sands tailings. The macromonomer design enables the user to specify comb-polymer charge density and hydrophobic content, two parameters important to flocculant performance. Another feature of these flocculants is that following sedimentation, partial hydrolysis of the grafts reveals hydrophobic segments which further expel water from the sediment – the dewaterability of a kaolin sediment was improved by 30% after flocculant degradation. Furthermore, preliminary experiments demonstrated that the

macromonomer average chain length plays a significant role in both settling behavior and the time required for polymer degradation. Also in Chapter 6, tertiary amine macromonomers were used to modify cellulose nanocrystals (CNC) to be pH responsive using CO_2/N_2 as triggers to reversibly disperse/aggregate the dispersions. It was demonstrated that the quality of polymer grafted CNC dispersion is influenced by the density of tertiary amine groups and relative hydrophobicity afforded by the macromonomer design.

In order to facilitate efficient synthesis of new materials, the rest of the thesis describes the application of specialized kinetic techniques to the study of RP kinetics of these macromonomers and associated systems. Chain-growth kinetics of two biomedically relevant copolymerization systems were studied in Chapter 4: bulk methyl methacrylate (MMA) and *n*-butyl cyanoacrylate (BCA) as well as bulk MMA and hydroxyl terminated HEMA-PCL$_n$ macromonomers. The notoriously rapid BCA anionic polymerization was successfully suppressed in order to confirm its strongly alternating nature with MMA. Composition-averaged copolymer propagation rate coefficients ($k_{p,cop}$) could be as much as twice the value for MMA homopropagation, $k_{p,MMA}$, while the $k_{p,BCA}$ is estimated to be roughly half the value for $k_{p,MMA}$ at 50 °C. Although the kinetic studies for MMA/HEMA-PCL$_n$ were limited by poor solubility of the HEMA-PCL$_n$ comb-polymers in any solvent, it was safely concluded that systems up to 50 wt% macromonomer content copolymerize with equal addition probabilities and that there is no significant difference in $k_{p,cop}$ when the average polyester length in the macromonomer side chain is increased from $n=2$ to $n=3$.

Chapter 5 also includes a PLP kinetics study of the alkyl terminated macromonomers, PLA$_N$EMA, which could be studied over a wider composition range than HEMA-PCL$_n$ because of the improved solubility of the resulting comb-polymers. While the bulk k_p for PLA$_N$EMA is elevated compared to MMA over the temperature range of 40-100 °C, increasing the average number of polyester units in the methacrylic ester side chain from $N=1$ to $N=5$ does not result in any further increase in k_p. Furthermore, because of the large molar volume of macromonomers in

comparison to solvent molecules, the macromonomer k_p measured in non-interacting solvents, such as xylenes, were significantly lower than the corresponding bulk k_p values.

Chapter 7 presents the first reported PLP study of radical homopropagation kinetics for a self-assembled monomer system, the cationic macromonomer PCL_2ChMA. Due to the dynamic nature of micellar systems, it is difficult to determine the locus of polymerization as well as the corresponding macromonomer concentrations as a function of temperature. Depending on temperature, the PLP results indicate features of both bulk and aqueous homopropagation. At 25 °C the system is predominantly compartmentalized; assuming bulk macromonomer concentration, a minimum k_p is estimated as 863 ± 95 L·mol^{-1}·s^{-1}, a value that is in the same range (albeit slightly elevated) compared to those for bulk alkyl methacrylates with similar ester side chain lengths. The results indicate that there may be different propagation behaviors for compartmentalized methacrylate groups partitioned to the micelle/water interface compared to those buried in the micelle core.

The impact of polyester type, length, and end-group functionality on macromonomer radical copolymerization with styrene was systematically investigated in Chapter 8, with results interpreted in terms of hydrogen bonding and solvent effects. It was determined that the most important factor that dictates macromonomer relative consumption is the chemical nature up to several units away from the methacrylic ester. In addition, the effect of hydrogen bonding on the RP kinetics of hydroxyl terminated HEMA-PCL$_n$ macromonomers is significantly diluted by the n PCL spacers.

The observed dilution of hydrogen bonding effects on macromonomer copolymer composition behavior prompted the development of a kinetic Monte Carlo model (Chapter 9) to describe the peculiar copolymer composition behavior documented for hydroxyl-bearing (meth)acrylates such as 2-hydroxyethyl methacrylate (HEMA) that demonstrate preferential incorporation relative to their corresponding alkyl analogs, depending on choice of solvent. The

kinetic Monte Carlo model builds on the premise that this preferential incorporation results from the increased reaction probability associated with an intrachain reaction of chain-end radical with HEMA hydrogen-bonded to HEMA repeat units in the macroradical. The preliminary simulation results are promising, as they capture the systematic progression in the Mayo-Lewis curves with solvent choice and concentration for several different hydroxyl-containing copolymerization systems.

10.2 Recommendations

The synthetic strategies developed in this work to produce methacrylate functionalized macromonomers can be easily modified to produce the analogous acrylate macromonomers with the same alkyl, tertiary amine, quaternary ammonium, and carboxyl end-group functionalities such that an even greater range of material properties can be accessed, as an acrylic polymer backbone will be more hydrophilic and exhibit greater chain mobility than the corresponding methacrylic polymer. Since the k_p for an acrylate is at least an order of magnitude greater than its analogous methacrylate, the production of higher molecular weight (MW) comb-polymer materials can be expected.

The kinetic study in Chapter 5 revealed that the solution k_p value measured for PLA$_N$EMA is sensitive to the difference in macromonomer and solvent molar volumes. Thus, it would be interesting to investigate to what extent the difference in molar volumes affects macromonomer bulk and solution copolymerization kinetics. In addition, with reference to the macromonomer/styrene copolymerization study performed in Chapter 8, it would be interesting to investigate whether the structure/reactivity trends documented for the methacrylate macromonomers also extend to acrylate macromonomer copolymerization systems.

The work in Chapter 6 demonstrated that flocculants produced from the PCL$_n$ChMA family of cationic macromonomers efficiently settle oil sands tailings, and that the resulting sediment is further consolidated following comb-polymer degradation. Another feature of the

poly(PCL_nChMA) flocculant design is that important performance parameters, such as charge density and hydrophobic content, are defined in the macromonomer synthesis step. In contrast, in order to precisely define the charge density or hydrophobic content of flocculants produced from more common monomers such as 2-(methacryloyloxy)ethyl trimethylammonium chloride (TMAEMC), a sophisticated understanding of their exceedingly complicated aqueous (co)polymerization kinetics is required. Thus, as summarized by **Error! Reference source not ound.**, the next step involves comparing different TMAEMC and PCL_2ChMA formulations to systematically study the relationship between comb-polymer structure and flocculation performance (both in terms of settling and enhanced dewaterability following polymer degradation), a study that is already underway in cooperation with the group of Dr. João Soares at the University of Alberta. The performance of poly(TMAEMC-*co*-AM) and poly(PCL_2ChMA-*co*-AM) copolymers, whose molar charge densities are diluted compared to the respective homopolymers, is also being studied to provide performance comparisons for charge density dilution (on a mass basis) by hydrophobic content as well as charge density dilution by hydrophilic comonomer. In addition, the settling performance of flocculants produced from the acrylate analog of PCL_nChMA should be compared to the methacrylate version, while flocculants prepared from cationic polylactic acid macromonomers should be investigated to increase the rate of comb-polymer hydrolysis in situ. If a macromonomer with the required performance can be identified, developing a deeper knowledge of its radical micellar (co)polymerization behavior will facilitate scale-up and further optimization of the polymer structure.
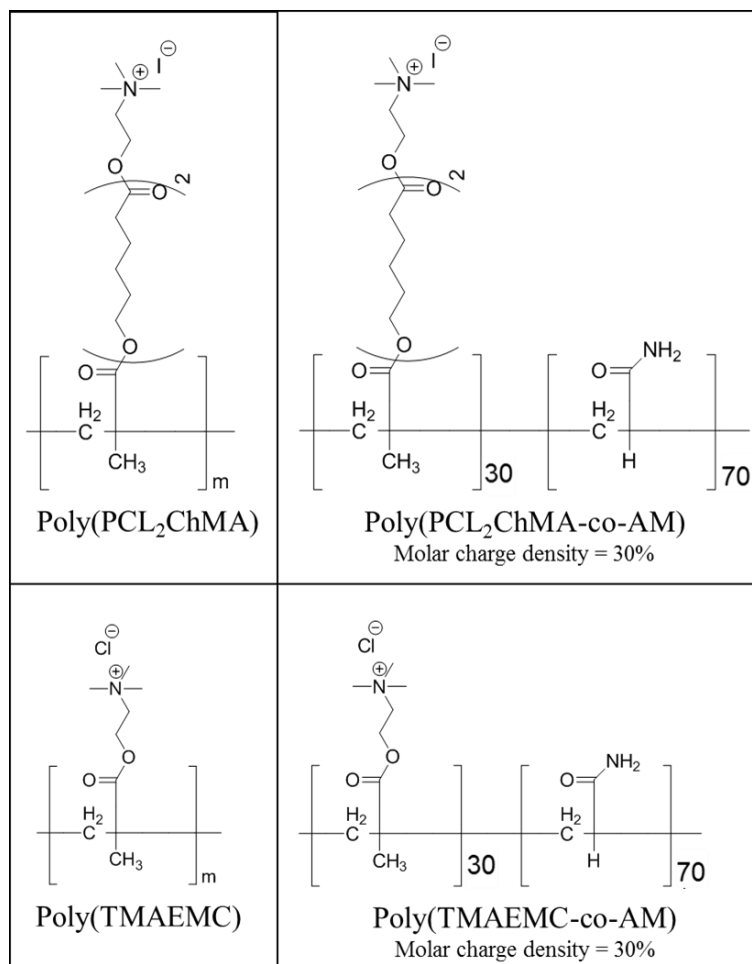
Scheme 10.1: Comparison of structures for PCL₂ChMA and TMAEMC homopolymers with identical molar charge density as well as respective AM copolymers with 30% molar charge density.

Appendix A

Supporting Information for Chapter 3

Macromonomer Syntheses

PLA₁EMA

Figure A.1: ¹H NMR spectrum with peak assignment for PLA₁EMA in CDCl₃ at 25 °C.

PLA₁EMA ¹H-NMR (CDCl₃, 400 MHz) with integrations relative to Peak S: δ = 6.19 ppm (s, 1.0H, R), δ = 5.62 ppm (s, 1.0H, S), δ = 5.10 ppm (q, 0.95H, E), δ = 4.20 ppm (q, 2.0H, F), δ = 1.96 ppm (s, 3.0H, Q), δ = 1.52 ppm (d, 3.0H, D), δ = 1.26 ppm (t, 3.0H, G).

PLA₅

Figure A.2: ¹H NMR spectrum with peak assignment for PLA₅E in CDCl₃ at 25 °C.

PLA₅E ¹H-NMR (CDCl₃, 400 MHz) with integrations relative to Peak T: δ = 5.29–5.07 ppm (m, 4.5H, E), δ = 5.03 ppm (q, 0.5H, X), δ = 4.35 ppm (q, 1.0H, T), δ = 4.30–4.13 ppm (m, 2.4H, F+F'+T'), δ = 1.68 ppm (d, 0.9H, Y), δ = 1.62–1.56 ppm (m, 10.5H, D), δ = 1.54–1.47 ppm (m, 6.8H, D'), δ = 1.42 ppm (d, 0.6H, D''), δ = 1.33–1.24 ppm (m, 3.6H, G+G').

$$n = \frac{\int E + \int T}{T} = \frac{4.7 + 1}{1} = 5.5$$

$$\%LA_{conv.} = \frac{\int E}{\int X + \int E} = \frac{4.5}{0.3 + 4.5} \times 100\% = 94\%$$

PLA₅EMA

Figure A.3: ¹H NMR spectrum with peak assignment for PLA₅EMA in CDCl₃ at 25 °C.

PLA₅EMA ¹H-NMR (CDCl₃, 400 MHz) with integrations relative to Peak S: δ = 6.20 ppm (s, 1.0H, R), δ = 5.63 ppm (s, 1.0H, S), δ = 5.26–5.06 ppm (m, 5.3H, E), δ = 4.19 ppm (q, 2.0H, F), δ = 1.96 ppm (s, 3.0H, Q), δ = 1.68–1.54 ppm (m, 12.9H, D), δ = 1.51 ppm (d, 3.0H, D'), δ = 1.27 ppm (t, 3.0H, G).

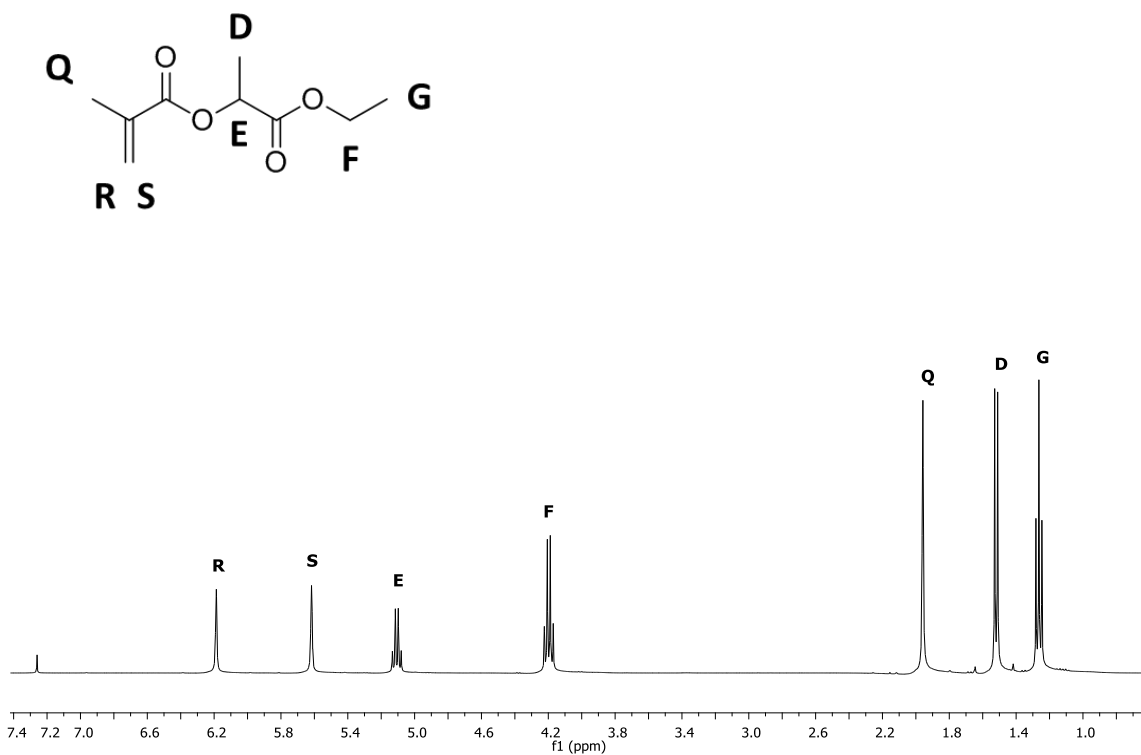$$n = \frac{\int E}{\int S} = \frac{5.3}{1} = 5.3$$

PCL₃De

Figure A.4: ¹H NMR spectrum with peak assignment for PCL₃De in CDCl₃ at 25 °C.

PCL₃De ¹H-NMR (CDCl₃, 400 MHz) with integrations relative to Peak J: δ = 4.23 ppm (t, 0.4H, CL), δ = 4.17 ppm (t, 2.0H, F), δ = 4.06 ppm (m, 4.0H, A), δ = 3.64 ppm (t, 2.0H, J), δ = 2.64 ppm (t, 0.4H, CL), δ = 2.56 ppm (t, 2.0H, G), δ = 2.44–2.24 ppm (m, 12.3H, E+K), δ = 1.86 ppm (m, 0.4H, CL), δ = 1.71–1.51   ppm (m, 13.2, B+D), δ = 1.46–1.33 ppm (m, 6.2 H, C).

$$n = \frac{\int J + \int A}{\int J} = \frac{2.0 + 4.0}{2.0} = 3.0$$

$$\%CL_{conv.} = \frac{\int J + \int A}{\int J + \int A + \int CL} = \frac{2.0 + 4.0}{2.0 + 4.0 + 0.4} \times 100\% = 94\%$$
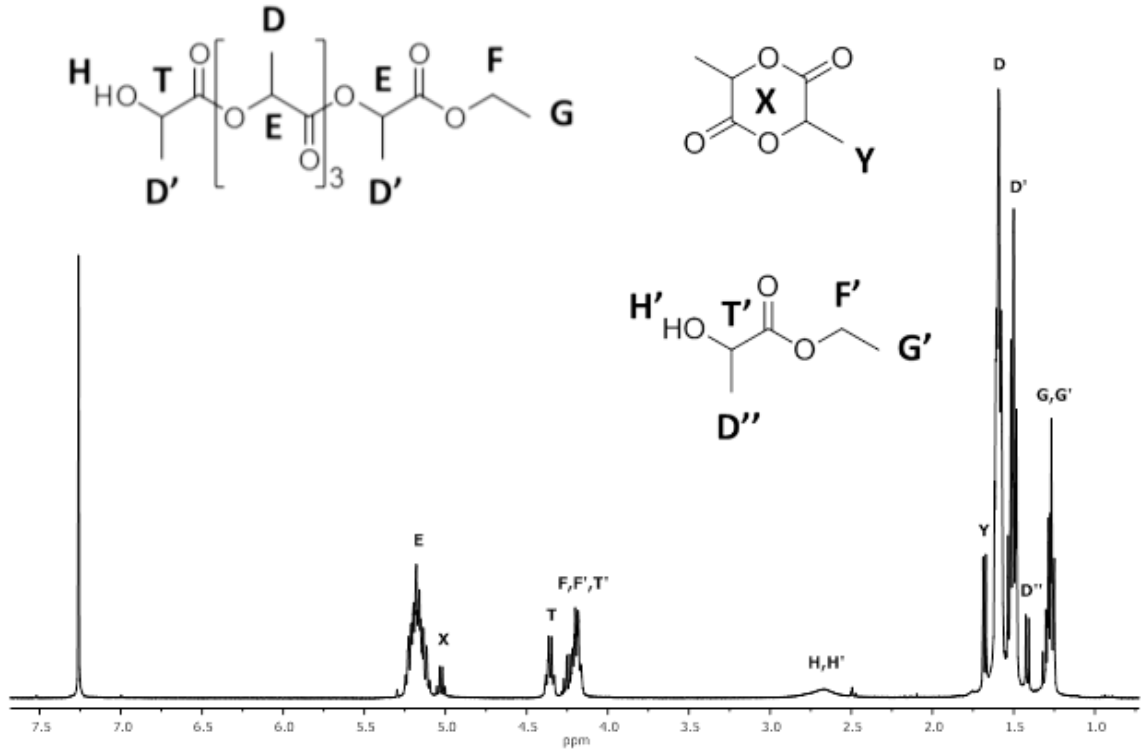
PCL₃DeMA
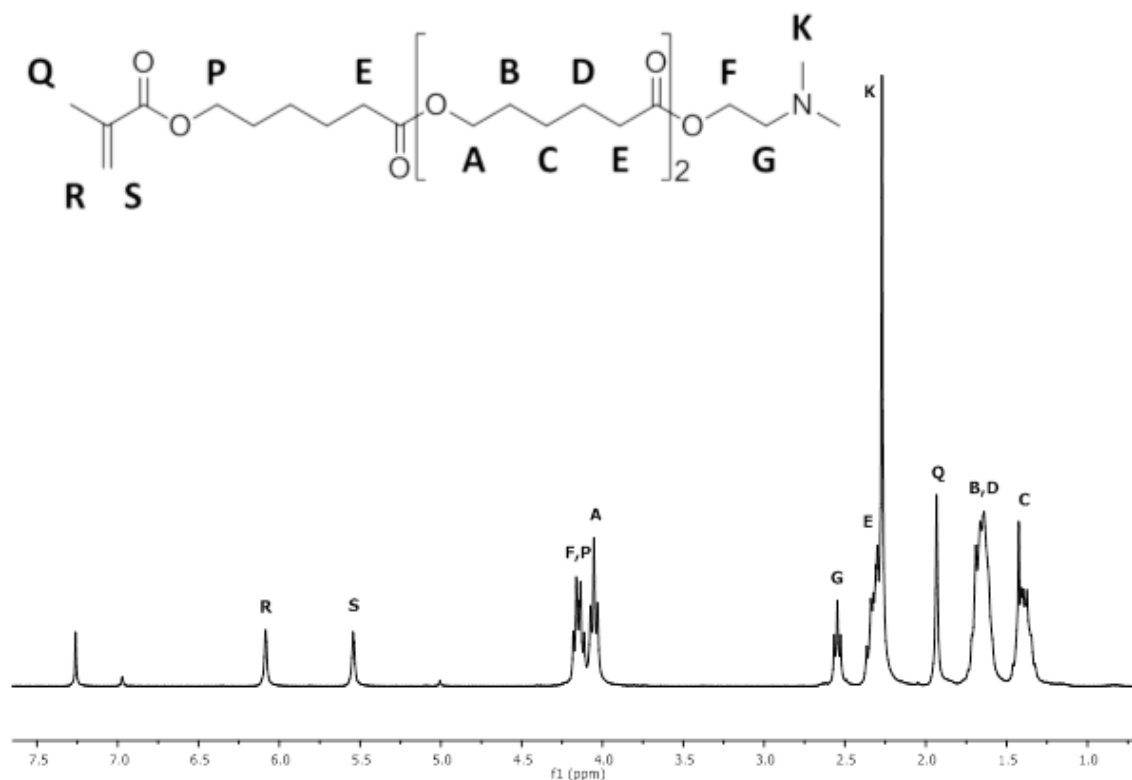
Figure A.5: ¹H NMR spectrum with peak assignment for PCL₃DeMA in CDCl₃ at 25 °C.

PCL₃DeMA ¹H-NMR (CDCl₃, 400 MHz) with integrations relative to Peak S: δ = 6.09 ppm (s, 1.0H, R), δ = 5.54 ppm (s, 1.0H, S), δ = 4.19–4.10 ppm (m, 4.0H, F+P), δ = 4.05 ppm (t, 4.1H, A), δ = 2.55 ppm (t, 2.0H, G), δ = 2.38–2.24 ppm (m, 12.4H, E+K), δ = 1.93 ppm (s, 3.0H, Q), δ = 1.70–1.52 ppm (m, 12.8H, B+D), δ = 1.45–1.31 ppm (m, 6.4H, C).

$$n = \frac{\frac{\int (A + F, P) - \int G}{2}}{\int S} = \frac{\frac{8.1 - 2}{2}}{1} = 3.05$$
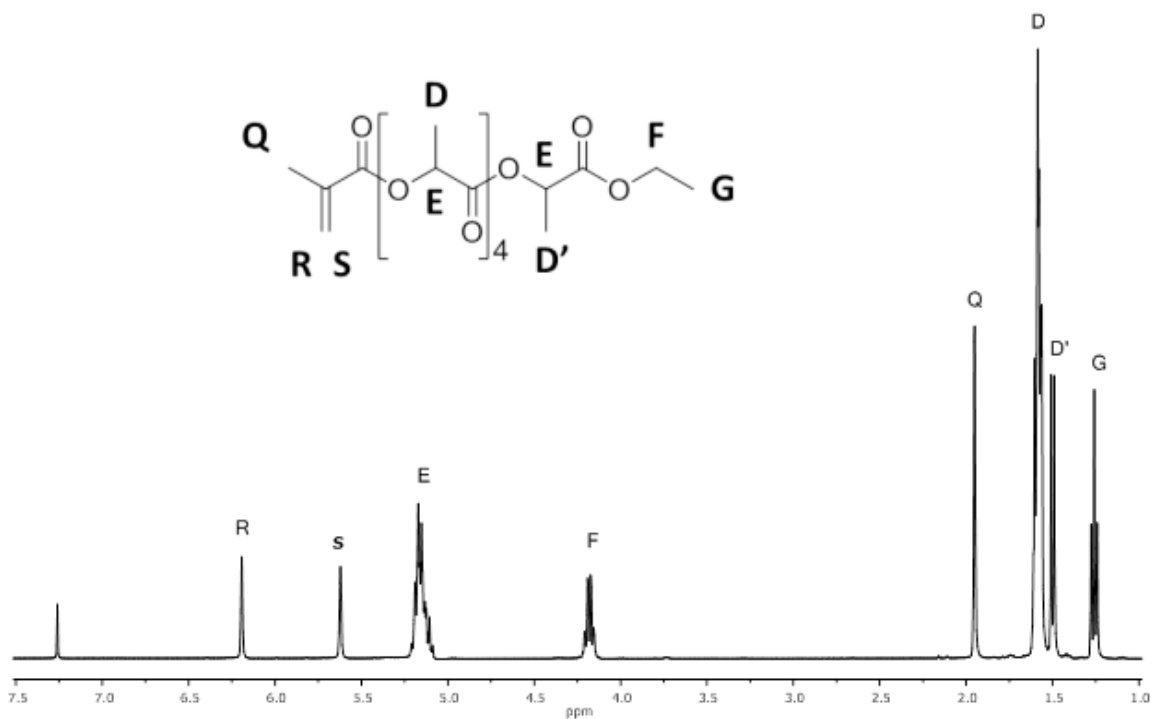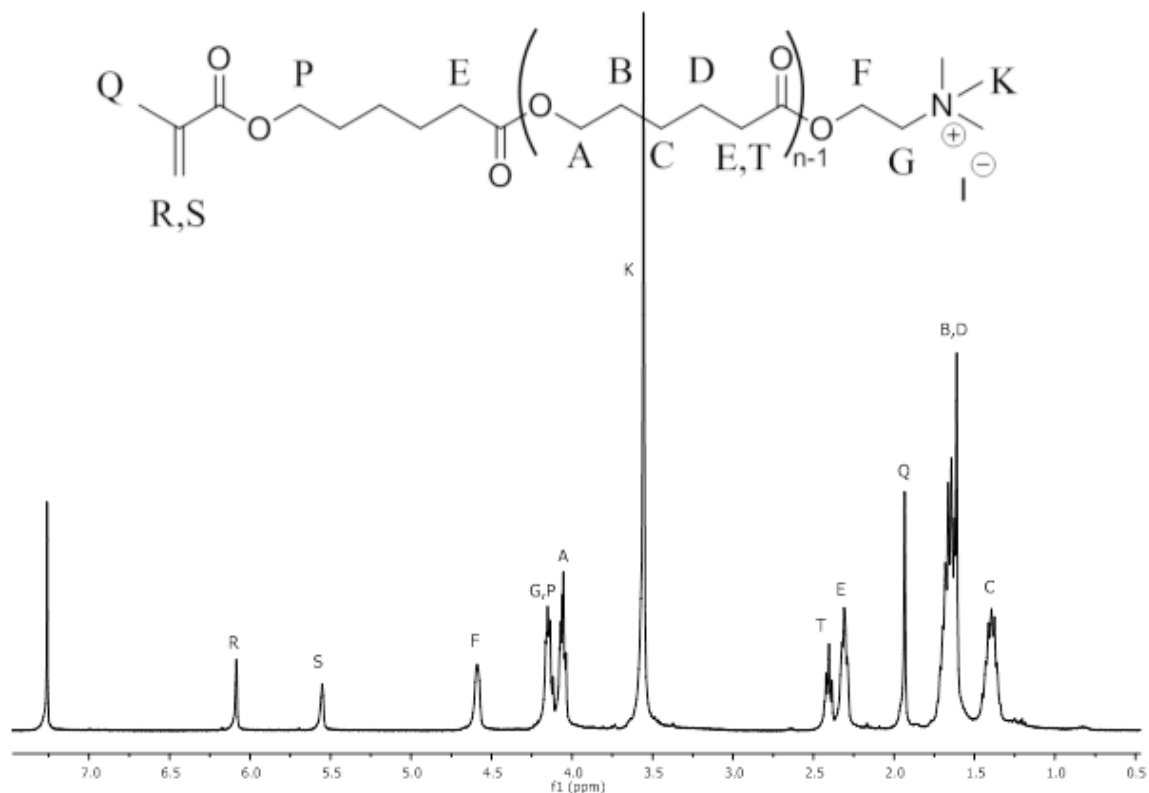
PCL₃ChMA

Figure A.6: ¹H NMR spectrum with peak assignment for PCL₃ChMA in CDCl₃ at 25 °C.

PCL₃ChMA ¹H-NMR (CDCl₃, 400 MHz) with integrations relative to Peak S: δ = 6.08 ppm (s, 1.0H, R), δ = 5.54 ppm (s, 1.0H, S), δ = 4.59 ppm (t, 2.1H, F), δ = 4.19–4.10 ppm (m, 4.1H, G+P), δ = 4.05 ppm (t, 4.1H, A), δ = 3.56 ppm (s, 9.2H, K), δ = 2.40 ppm (t, 2.0H, T), δ = 2.30 ppm (t, 4.0H, E), δ = 1.93 ppm (s, 3.0H, Q), δ = 1.70–1.52 ppm (m, 12.4H, B+D), δ = 1.45–1.31 ppm (m, 6.1H, C).

$$n = \frac{Integral\ (E+T)/2}{Integral\ (S)} = \frac{(4.0+2.0)/2}{1.0} = 3.0$$
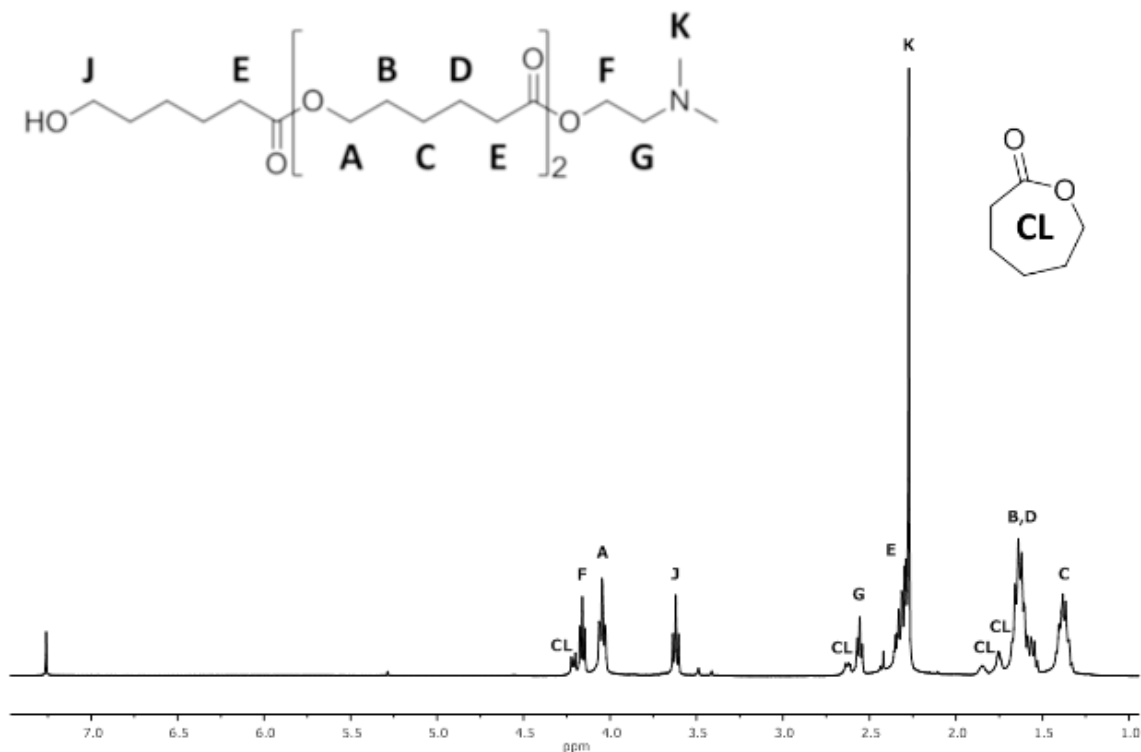
HEMA-PLA₅

Figure A.7: ¹H NMR spectrum with peak assignment for HEMA-PLA₅ in CDCl₃ at 25 °C.

HEMA-PLA₅ ¹H-NMR (CDCl₃, 400 MHz) with integrations relative to Peak S: δ = 6.12 ppm (s, 1.0H, R), δ = 5.25–5.10 ppm (m, 4.3H, E), δ = 5.03 ppm (q, 0.2H, X), δ = 4.43 ppm (q, 1.0H, A), δ = 4.35 ppm (s, 4.0H, F), δ = 1.94 ppm (s, 3.0H, Q), δ = 1.68 ppm (d, 0.6H, Y), δ = 1.63–1.45 ppm (m, 16.0, D,B).

$$n = \frac{\int E + \int A}{\int S} = \frac{4.3 + 1}{1} = 5.3$$

$$\%LA_{conv.} = \frac{\int E + \int A}{\int E + \int A + \int X} = \frac{4.3 + 1}{4.3 + 1 + 0.2} \times 100\% = 96\%$$

HEMA-PCL₃
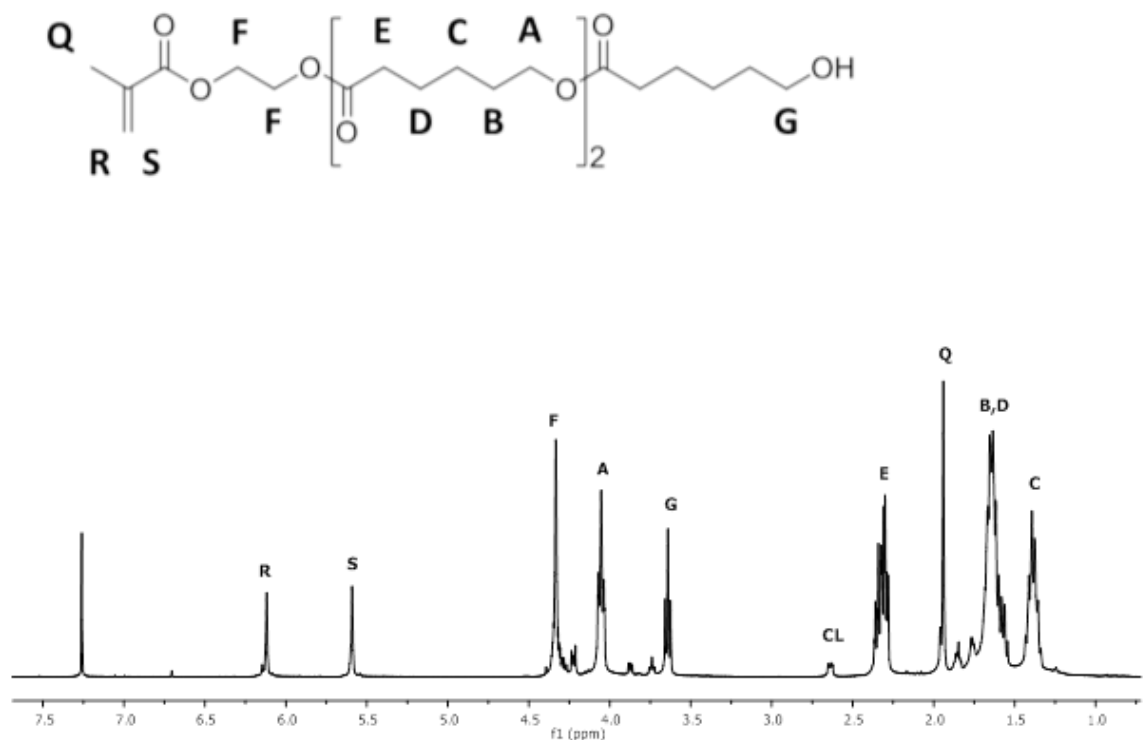
Figure A.8: ^{1}H NMR spectrum with peak assignment for HEMA-PCL$_3$ in CDCl$_3$ at 25 °C.

HEMA-PCL$_3$ ^{1}H-NMR (CDCl$_3$, 400 MHz) with integrations relative to Peak S: $\delta = 6.12$ ppm (s, 1.0H, R), $\delta = 5.59$ ppm (s, 1.0H, S), $\delta = 4.33$ ppm (s, 4.0H, F), $\delta = 4.05$ ppm (t, 4.6H, A), $\delta = 3.64$ ppm (t, 2.0H, G), $\delta = 2.65$ ppm (t, 0.4H, CL), $\delta = 2.40$–2.25 ppm (m, 6.6H, E), $\delta = 1.94$ ppm (s, 3.0H, Q), $\delta = 1.70$–1.54 ppm (m, 14.4H, B,D), $\delta = 1.44$–1.32 ppm (m, 6.7H, C).

$$n = \frac{\frac{\int E}{2}}{\int S} = \frac{6.6/2}{1} = 3.3$$

$$\% \, CL_{conv.} = \frac{\int E}{\int E + \int CL} = \frac{6.6}{6.6 + 0.4} \times 100\% = 94\%$$

HEMA-PCL₃-PR
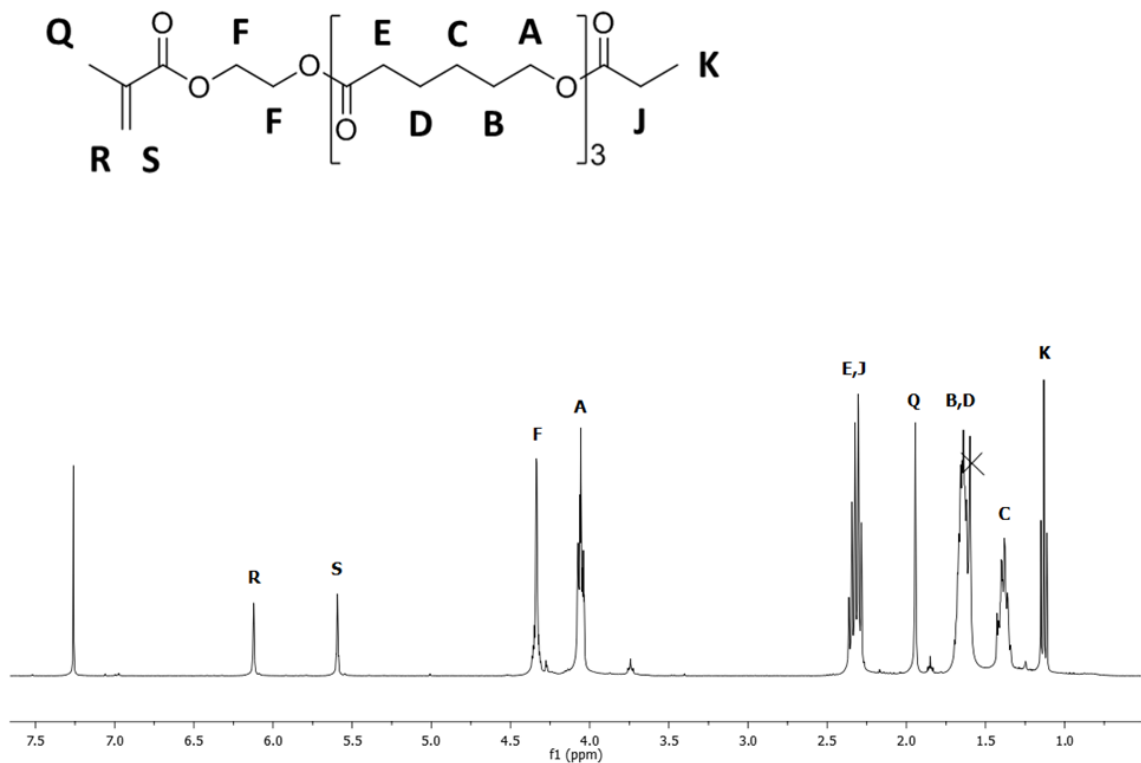
Figure A.9: ¹H NMR spectrum with peak assignment for HEMA-PCL₃-PR in CDCl₃ at 25 °C.

HEMA-PCL$_3$-PR ¹H-NMR (CDCl$_3$, 400 MHz) with integrations relative to Peak S: δ = 6.12 ppm (s, 1.0H, R), δ = 5.59 ppm (s, 1.0H, S), δ = 4.34 ppm (s, 4.0H, F), δ = 4.06 ppm (t, 6.6H, A), δ = 2.40–2.26 ppm (m, 8.6H, E+J), δ = 1.94 ppm (s, 3.0H, Q), δ = 1.70–1.54 ppm (m, N/A, B+D+H$_2$O), δ = 1.44–1.32 ppm (m, 7.4H, C), δ = 1.44–1.32 ppm (t, 3.0H, K).

$$n = \frac{\frac{\int (E,J) - 2}{2}}{\int S} = \frac{\frac{8.6 - 2}{2}}{1} = 3.3$$
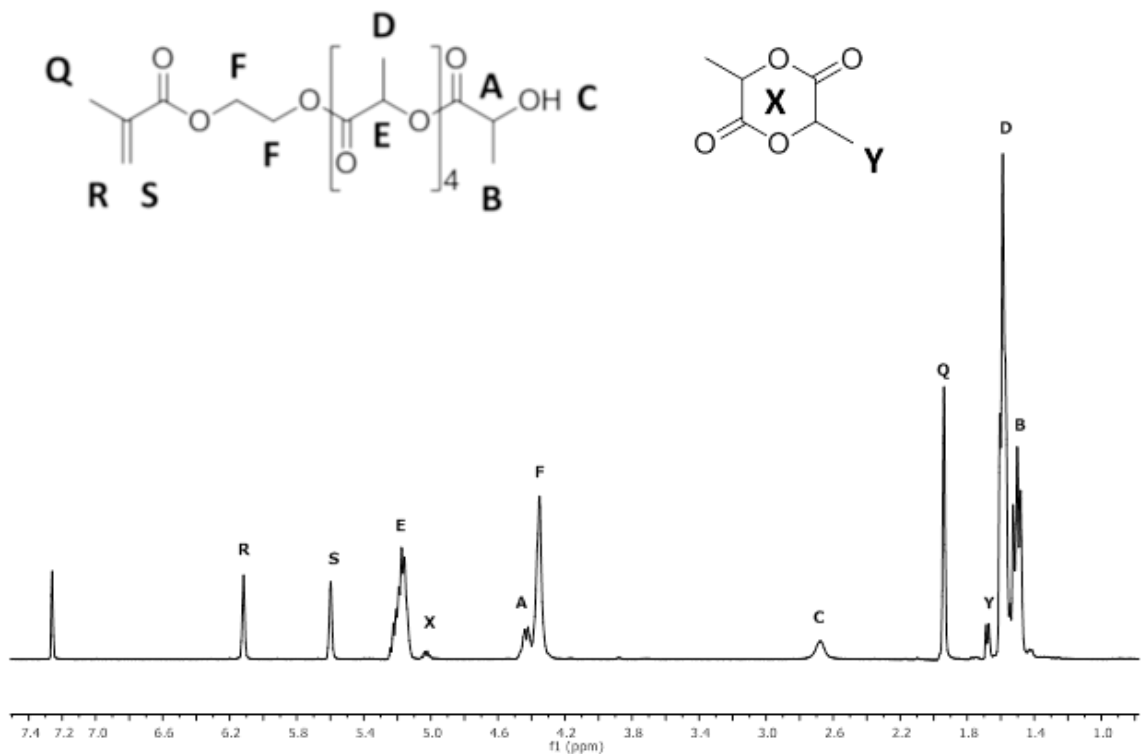
HEMA-PCL₃-COOH
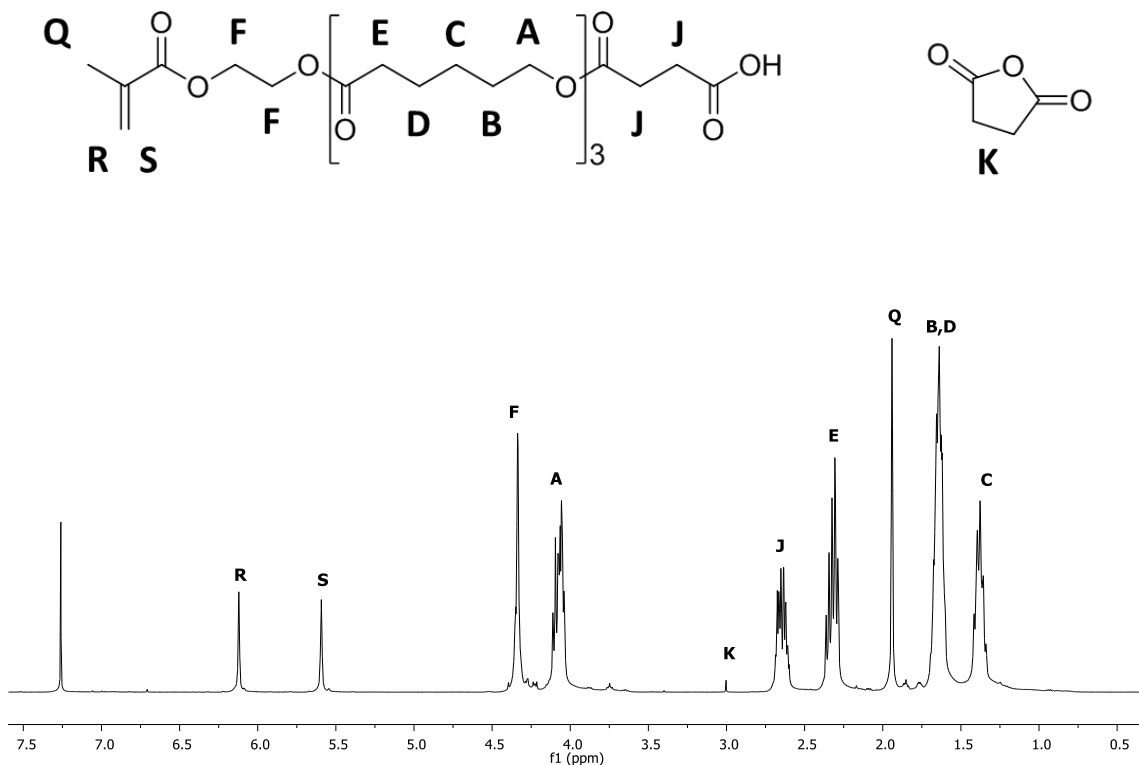
Figure A.10: ^{1}H NMR spectrum with peak assignment for HEMA-PCL₃-COOH in CDCl₃ at 25 °C.

HEMA-PCL₃-COOH ^{1}H-NMR (CDCl₃, 400 MHz) with integrations relative to Peak S: δ = 6.12 ppm (s, 1.0H, R), δ = 5.59 ppm (s, 1.0H, S), δ = 4.34 ppm (s, 4.0H, F), δ = 4.14–3.97 ppm (m, 6.7H, A), δ = 3.00 ppm (s, 0.03H, K), δ = 2.71–2.57 ppm (m, 4.4H, J), δ = 2.40–2.22 ppm (m, 6.7H, E), δ = 1.94 ppm (s, 3.0H, Q), δ = 1.70–1.54 ppm (m, 13.2H, B,D), δ = 1.44–1.32 ppm (m, 6.7H, C).

$$n = \frac{\frac{\int E}{2}}{\int S} = \frac{6.7/2}{1} = 3.35$$

Macromonomer Syntheses – SEC

PLA$_N$EMA

Table A.1: Characterization summary for PLA$_N$EMA (macro)monomer syntheses.

	LA conversion (%)	Yield (%)	N	
			Target	^{1}H NMR
PLA$_1$EMA	-	67	1	1
PLA$_5$EMA	94	77	5	5.3
PLA$_7$EMA	91	74	7	7.1
PLA$_9$EMA	97	62	9	9.5
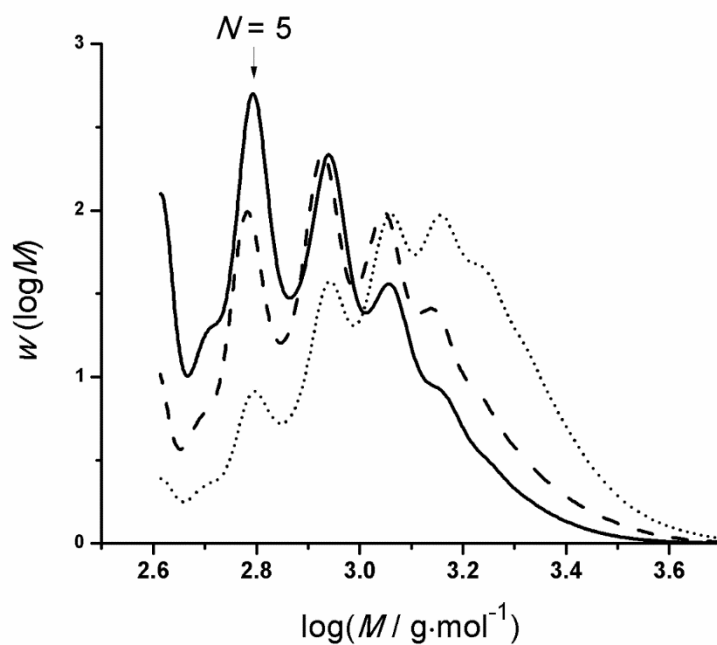
Figure A.11: MMDs measured by SEC in THF and analyzed as PMMA equivalents for PLA$_N$EMA macromonomers N=5 (solid line), N=7 (dashed line), and N=9 (dotted line).

PCL$_n$DeMA

Table A.2: Characterization summary for PCL$_n$DeMA (macro)monomer syntheses.

	CL conversion (%)	Yield (%)	N	
			Target	^{1}H NMR
PCL$_2$DeMA	94	74	2	2.0
PCL$_3$DeMA	94	76	3	3.0
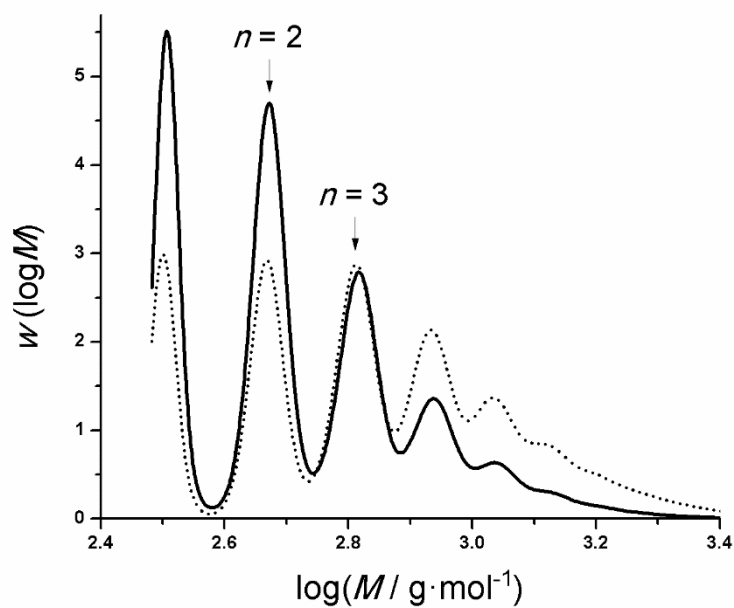
Figure A.12: MMDs for PCL$_2$DeMA (solid line) and PCL$_3$DeMA (dotted line) measured in PMMA equivalents by SEC with THF as eluent.

Macromonomer Comparison – Weight Basis
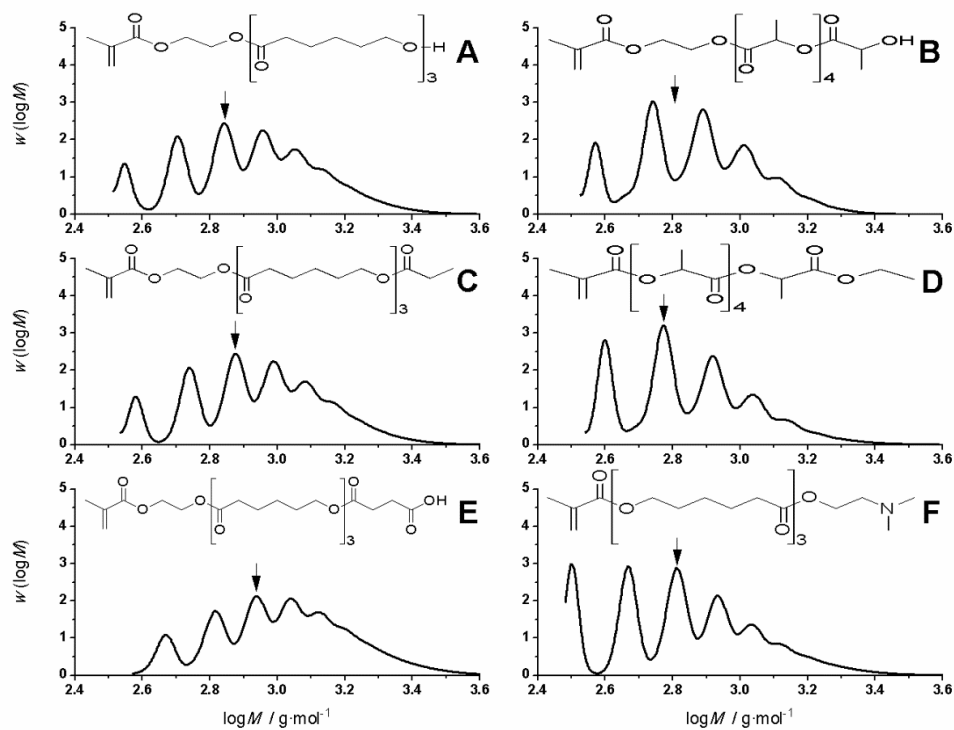
Figure A.13: MMDs measured by SEC in THF and analyzed as PMMA equivalents for HEMA-PCL$_3$ (panel A), HEMA-PLA$_5$ (panel B), HEMA-PCL$_3$-PR (panel C), PLA$_5$EMA (panel D), HEMA-PCL$_3$-COOH (panel E), and PCL$_3$DeMA (panel F). Arrows indicate expected location of target macromonomer chain length.

Macromonomer Comparison – Number Basis
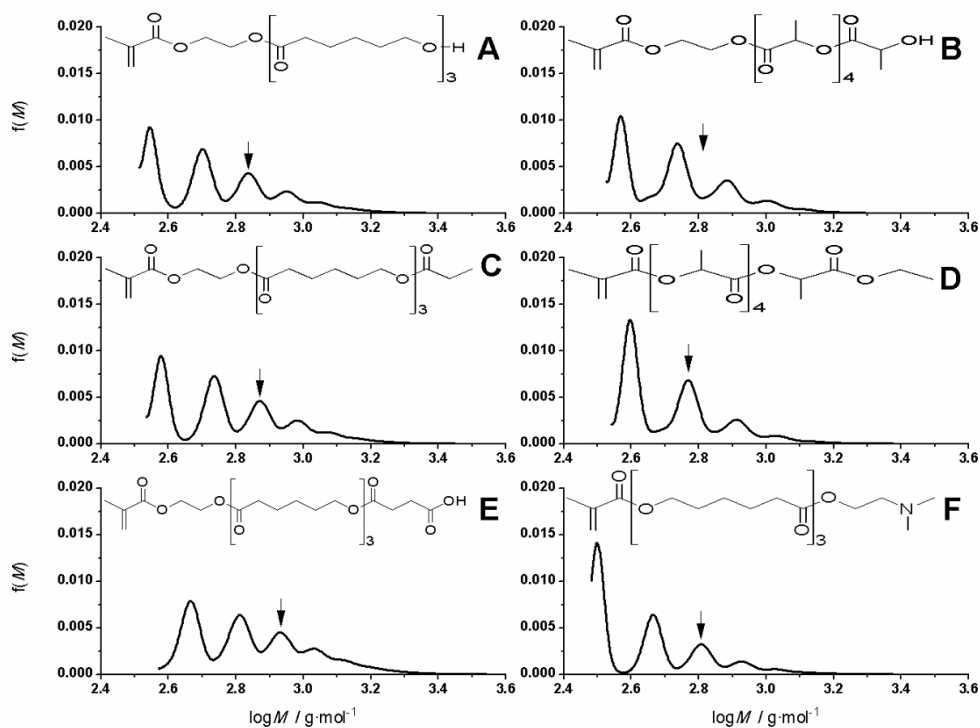
Figure A.14: Number distributions (normalized by area) measured by SEC in THF and analyzed as PMMA equivalents for HEMA-PCL$_3$ (panel A), HEMA-PLA$_5$ (panel B), HEMA-PCL$_3$-PR (panel C), PLA$_5$EMA (panel D), HEMA-PCL$_3$-COOH (panel E), and PCL$_3$DeMA (panel F). Arrows indicate expected location of target macromonomer chain length.

Appendix B

Supporting Information for Chapter 5: Polylactic Macromonomer Radical Propagation Kinetics and Degradation Behavior

Macromonomer and Comb-Polymer Characterization

Table B.1: Xylenes solution density measurements used to extrapolate density of PLA$_5$EMA assuming volume additivity.

T (°C)	Weight fraction PLA$_N$EMA				
	0.0	0.12	0.25	0.50	1.0 (extrapolated)
	ρ_{mix} (g·mL^{-1})				
25	0.8615	0.8896	0.9217	0.9908	1.165
50	0.8394	0.8677	0.8996	0.9680	1.142
70	0.8221	0.8495	0.8812	0.9491	1.122

$$\left(\frac{1}{\rho_{mix}}\right) = \left(\frac{1}{\rho_{xylenes}}\right) + w_{PLA_NEMA} \cdot \left(\frac{1}{\rho_{PLA_NEMA}} - \frac{1}{\rho_{xylenes}}\right)$$
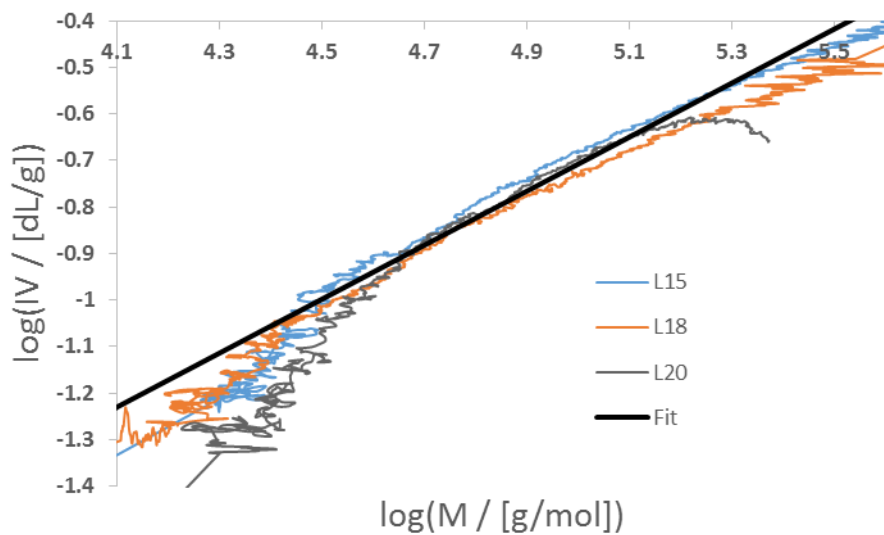
Figure B.1: Mark-Houwink analysis for poly(PLA₁EMA). Fit performed by linear regression between log$M$=4.4 and log$M$=5.2 for three independent samples.
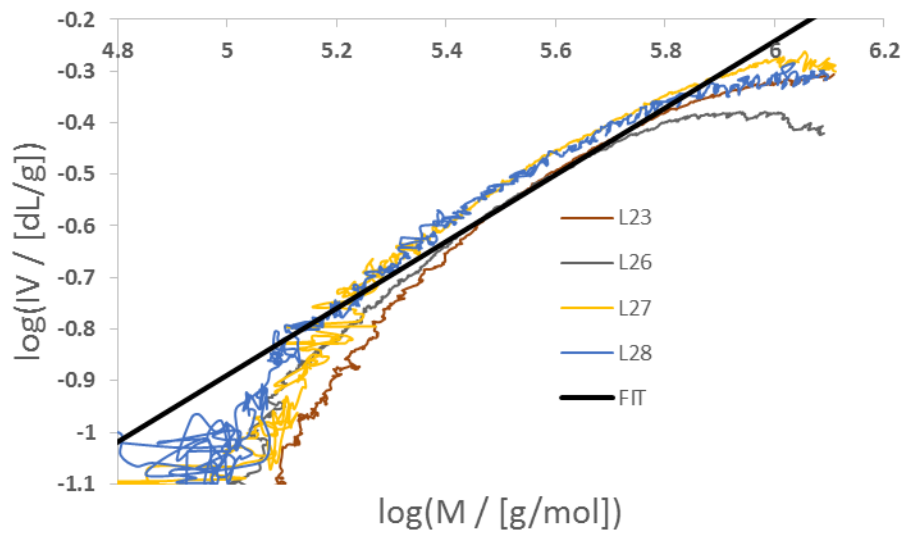
Figure B.2: Mark-Houwink analysis for poly(PLA₅EMA). Fit performed by linear regression between log$M$=5.1 and log$M$=5.9 for four independent samples.
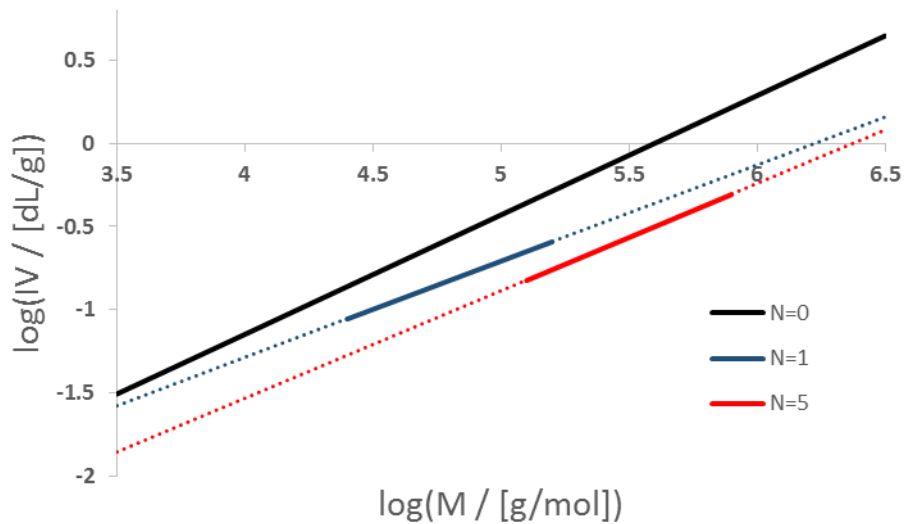
Figure B.3: Intrinsic viscosity as a function of molecular weight for PMMA (*N*=0), poly(PLA₁EMA), and poly(PLA₅EMA). The solid lines indicate fitted regions while the dotted lines represent extrapolations of the respective fits.

Pulsed Laser Polymerization Homopropagation Kinetic Study
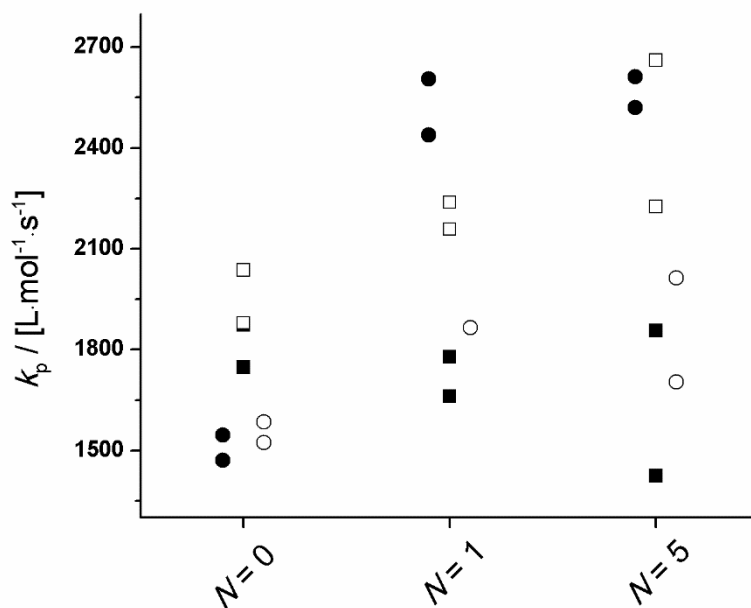
Figure B.4: Plots for k_p of MMA, PLA$_1$EMA, and PLA$_5$EMA determined by universal calibration in bulk (●), 75 wt% xylenes (○), 75 wt% DMF (■), and 75 wt% BuOH (□) solutions at 90 °C with 5 mmol·L^{-1} DMPA.

Table B.2: Ratio of k_p determined in BuOH to bulk/DMF at 90 °C with 5 mmol·L^{-1} DMPA at various δ for each (macro)monomer.

Monomer	δ	$\dfrac{k_{p,BuOH}}{k_{p,bulk}}$	$\dfrac{k_{p,BuOH}}{k_{p,DMF}}$
MMA	4.1	1.30	1.08
BMA[1]	5.3	1.26	-
	11.3	1.40	
PLA$_1$EMA	7.5	0.87	1.28
PLA$_5$EMA	19.1	0.95	1.49

Table B.3: PLP conditions and results for MMA (N=0) homopolymerizations with [DMPA]=5 mmol·L^{-1} and 4.0 mJ/pulse.

T (°C)	Solvent (wt.%)	ϕ_{xMA}	[M] (mol·L^{-1})	Pulse Repetition Rate (Hz)	Pulse Time	Conv (%)	RI M$_1$ (g·mol^{-1})	RI M$_2$/M$_1$	RI k_p from M$_1$ (L·mol^{-1}·s^{-1})	LS M$_1$ (g·mol^{-1})	LS M$_2$/M$_1$	LS k_p from M$_1$ (L·mol^{-1}·s^{-1})	$k_{p,LS}/k_{p,RI}$
50	Bulk	1	9.11	33	0:30	3.1	16,600	1.94	601	-	-	-	-
50	Bulk	1	9.11	50	0:17	1.9	11,100	1.96	610	10,500	1.88	579	0.95
50	75% Xyl	0.23	2.14	5	5:00	3.4	25,500	1.99	595	37,800	1.20	882	1.48
50	75% Xyl	0.23	2.14	10	3:00	4.7	13,600	1.95	636	18,100	1.69	844	1.33
70	Bulk	1	8.89	33	0:17	1.3	26,000	1.95	965	-	-	-	-
70	Bulk	1	8.89	50	0:14	2.8	17,700	1.95	993	-	-	-	-
70	43% BuOH	0.53	4.75	20	0:18	1.7	27,200	1.97	1146	36,100	2.02	1521	1.33
70	43% BuOH	0.53	4.75	33	0:15	1.4	17,300	1.95	1202	18,400	2.26	1278	1.06
70	75% DMF	0.25	2.25	5	4:00	5.7	49,400	2.02	1100	54,300	2.00	1209	1.10
70	75% DMF	0.25	2.25	10	3:00	6.2	26,600	1.97	1185	31,400	1.86	1398	1.18
70	75% BuOH	0.22	1.99	5	3:00	6.9	48,600	2.09	1221	58,800	1.33	1475	1.21
70	75% BuOH	0.22	1.99	10	2:00	4.7	26,600	2.00	1336	27,900	1.97	1402	1.05
70	75% Xyl	0.24	2.09	5	5:00	13.3	38,600	2.18	922	39800	1.85	950	1.03
70	75% Xyl	0.24	2.09	10	3:30	9.0	21,200	1.95	1011	22,100	1.81	1054	1.04
90	Bulk	1	8.67	33	0:18	1.8	38,600	2.00	1471	43,800	2.13	1666	1.13
90	Bulk	1	8.67	50	0:13	1.5	26,800	1.94	1546	24,900	2.21	1436	0.93
90	75% DMF	0.25	2.20	10	2:00	5.9	38,400	2.07	1747	43,400	1.94	1974	1.13
90	75% DMF	0.25	2.20	20	1:00	5.3	20,600	1.96	1873	22,300	2.02	2034	1.09
90	75% BuOH	0.22	1.95	10	2:00	6.3	36,600	2.06	1879	39,800	1.96	2044	1.09
90	75% BuOH	0.22	1.95	20	0:50	3.7	19,800	1.98	2036	19,300	2.24	1983	0.97
90	75% Xyl	0.24	2.05	10	2:00	4.4	31,200	2.08	1523	39,500	1.30	1926	1.27
90	75% Xyl	0.24	2.05	20	1:00	6.9	16,200	1.97	1584	18,100	1.50	1769	1.12

Table B.4: PLP conditions for PLA$_N$EMA (N=1) bulk homopolymerizations with [DMPA]=5 mmol·L^{-1} and 3.5 mJ/pulse.

T (°C)	Solvent (wt.%)	ϕ_{xMA}	[M] (mol·L^{-1})	Pulse Repetition Rate (Hz)	Pulse Time	Conv (%)	M$_1$ (g·mol^{-1})	M$_2$/M$_1$	k_p from M$_1$ (L·mol^{-1}·s^{-1})	M$_1$ (g·mol^{-1})	M$_2$/M$_1$	k_p from M$_1$ (L·mol^{-1}·s^{-1})	$k_{p,LS}/k_{p,RI}$
40	Bulk	1	5.40	33	0:40	1.8	23,700	2.02	777	25,700	1.83	843	1.09
40	Bulk	1	5.40	50	0:30	1.6	16,100	2.00	802	22,700	1.67	1128	1.41
50	Bulk	1	5.35	33			27,800	2.18	921	27,200	2.31	903	1.04
50	Bulk	1	5.35	50			19,600	2.02	983	18,400	2.14	925	0.94
60	Bulk	1	5.29	33	0:43	2.4	38,600	2.03	1292	41,100	1.83	1378	1.07
60	Bulk	1	5.29	50	0:33	1.8	25,800	2.02	1311	28,900	1.80	1468	1.12
70	Bulk	1	5.23	33			48,900	2.10	1656	-	-	-	-
70	Bulk	1	5.23	50			33,900	1.96	1832	-	-	-	-
80	Bulk	1	5.18	33	0:33	2.0	56,600	2.12	1939	62,200	1.72	2130	1.10
80	Bulk	1	5.18	50	0:22	2.0	38,900	2.05	2016	48,000	1.63	2488	1.23
90	Bulk	1	5.12	33			70,500	2.20	2439	-	-	-	-
90	Bulk	1	5.12	50			49,700	2.10	2606	-	-	-	-
100	Bulk	1	5.06	33	0:36	2.9	79,500	2.05	2784	90,800	1.61	3177	1.14
100	Bulk	1	5.06	50	0:26	2.7	54,300	2.11	2877	56,000	1.91	2968	1.03

Table B.5: PLP conditions for PLA$_N$EMA (N=1) solution homopolymerizations with [DMPA]=5 mmol·L^{-1} and 4.0 mJ/pulse.

T (°C)	Solvent (wt.%)	ϕ_{xMA}	[M] (mol·L^{-1})	Pulse Repetition Rate (Hz)	Pulse Time	Conv (%)	SEC Results						$k_{p,LS}/k_{p,RI}$
							RI			LS			
							M$_1$ (g·mol^{-1})	M$_2$/M$_1$	k_p from M$_1$ (L·mol^{-1}·s^{-1})	M$_1$ (g·mol^{-1})	M$_2$/M$_1$	k_p from M$_1$ (L·mol^{-1}·s^{-1})	
70	Bulk	1	5.23	33			48,900	2.10	1656	-	-	-	-
70	Bulk	1	5.23	50			33,900	1.96	1832	-	-	-	-
70	28% BuOH	0.67	3.51	20	0:45	1.7	44,700	2.27	1369	50,800	1.81	1556	1.14
70	28% BuOH	0.67	3.51	33	0:50	2.0	29,100	2.05	1469	29,200	1.74	1474	1.00
70	75% DMF	0.24	1.23	5	3:00	1.0	49,900	2.43	1318	48,600	1.81	1123	0.98
70	75% DMF	0.24	1.23	10	2:00	0.9	27,100	2.18	1179	-	-	-	-
70	75% BuOH	0.21	1.09	5	2:30	-	62,200	2.35	1531	57,300	1.81	1409	0.92
70	75% BuOH	0.21	1.09	10	2:00	1.4	32,800	2.13	1613	-	-	-	-
70	75% Xyl	0.22	1.15	5	3:00	0.3	20,300	-	-	-	-	-	-
70	75% Xyl	0.22	1.15	10	2:00	0.4	26,400	2.26	1236	-	-	-	-
90	Bulk	1	5.12	33			70,500	2.20	2439	-	-	-	-
90	Bulk	1	5.12	50			49,700	2.10	2606	-	-	-	-
90	75% DMF	0.24	1.21	10	2:00	0.9	37,300	2.37	1660	46,000	1.66	2047	1.23
90	75% DMF	0.24	1.21	20	1:00	0.9	20,000	2.06	1777	-	-	-	-
90	75% BuOH	0.21	1.07	10	2:00	1.8	42,900	2.24	2158	41,100	2.05	2067	0.96
90	75% BuOH	0.21	1.07	20	1:00	1.6	22,300	2.08	2238	22,200	1.89	2236	1.00
90	75% Xyl	0.22	1.12	10	2:00	0.9	19,400	-	-	-	-	-	-
90	75% Xyl	0.22	1.12	20	0:50	0.6	19,500	2.12	1865	-	-	-	-

Table B.6: PLP conditions for PLA$_N$EMA (N=5) bulk homopolymerizations with [DMPA]=5 mmol·L^{-1} and 2.5 mJ/pulse. Italicized data not used in Arrhenius fitting or any further analyses.

T (°C)	Solvent (wt.%)	ϕ_{xMA}	[M] (mol·L^{-1})	Pulse Repetition Rate (Hz)	Pulse #	Conv (%)	M$_1$ (g·mol^{-1})	M$_2$/M$_1$	k_p from M$_1$ (L·mol^{-1}·s^{-1})	M$_1$ (g·mol^{-1})	M$_2$/M$_1$	k_p from M$_1$ (L·mol^{-1}·s^{-1})	$k_{p,LS}/k_{p,RI}$
							SEC Results						
							RI			LS			
50	Bulk	1	2.41	10	100	4.5	130,700	1.60	1145	142,200	1.64	1246	1.09
50	Bulk	1	2.41	20	100	3.7	65,000	2.14	1139	53,600	3.05	939	0.83
60	Bulk	1	2.39	10	100	2.3	150,600	1.77	1331	162,600	1.91	1436	1.08
60	Bulk	1	2.39	20	100	3.5	78,400	1.99	1385	71,600	2.29	1265	0.91
70	*Bulk*	*1*	*2.37*	*10*	*100*	*4.2*	*175,800*	*1.71*	*1336*	*220,800*	*1.88*	*1967*	*1.26*
70	Bulk	1	2.37	20	100	3.1	96,600	1.85	1721	107,200	2.06	1909	1.11
70	Bulk	1	2.37	33	100	2.8	61,400	2.04	1806	55,200	2.61	1623	0.90
90	*Bulk*	*1*	*2.33*	*10*	*100*	*2.8*	*232,800*	*1.98*	*2110*	*276,700*	*1.95*	*2508*	*1.19*
90	Bulk	1	2.33	20	100	2.2	139,900	1.77	2520	164,100	1.81	2974	1.18
90	Bulk	1	2.33	33	100	1.8	87,300	1.91	2612	99,500	2.07	2978	1.14
100	Bulk	1	2.31	20	100	2.0	160,500	1.85	2934	179,500	1.92	3149	1.12
100	Bulk	1	2.31	33	100	1.5	102,500	1.85	3093	105,000	2.01	3167	1.02

Table B.7: PLP conditions for PLA$_N$EMA (*N*=5) solution homopolymerizations with [DMPA]=5 mmol·L^{-1} and 3.0 mJ/pulse.

T (°C)	Solvent (wt.%)	ϕ_{xMA}	[M] (mol·L^{-1})	Pulse Repetition Rate (Hz)	Pulse Time	Conv (%)	SEC Results						$k_{p,LS}/k_{p,RI}$
							RI			LS			
							M$_1$ (g·mol^{-1})	M$_2$/M$_1$	k_p from M$_1$ (L·mol^{-1}·s^{-1})	M$_1$ (g·mol^{-1})	M$_2$/M$_1$	k_p from M$_1$ (L·mol^{-1}·s^{-1})	
70	Bulk	1	2.37	20	0:05	3.1	96,600	1.85	1721	107,200	2.06	1909	1.11
70	Bulk	1	2.37	33	0:03	2.8	61,400	2.04	1806	55,200	2.61	1623	0.90
70	75% DMF	0.21	0.50	5	3:30	3.6	45,500	1.90	961	40,000	2.05	844	0.88
70	75% DMF	0.21	0.50	10	2:15	2.2	27,200	1.78	1149	23,400	1.88	989	0.86
70	75% BuOH	0.19	0.44	5	3:30	2.7	73,400	2.05	1757	70,300	2.05	1683	0.96
70	75% BuOH	0.19	0.44	10	2:15	3.1	42,200	1.88	2018	36,700	1.97	1758	0.87
70	75% Xyl	0.20	0.46	5	3:30	7.3	46,200	1.94	1050	43,100	1.95	977	0.93
70	75% Xyl	0.20	0.46	10	2:30	5.6	29,100	1.75	1322	28,000	1.70	1271	0.96
90	Bulk	1	2.33	20	0:05	2.2	139,900	1.77	2520	164,100	1.81	2974	1.18
90	Bulk	1	2.33	33	0:03	1.8	87,300	1.91	2612	99,500	2.07	2978	1.14
90	75% DMF	0.21	0.49	10	2:00	2.7	33,100	1.73	1424	27,700	1.87	1182	0.84
90	75% DMF	0.21	0.49	20	1:00	2.1	21,600	1.68	1856	17,900	1.79	1539	0.83
90	75% BuOH	0.19	0.43	10	2:00	3.7	45,500	1.93	2225	39,100	2.09	1910	0.86
90	75% BuOH	0.19	0.43	20	1:00	2.7	27,200	1.79	2661	22,200	1.91	2168	0.86
90	75% Xyl	0.20	0.46	10	2:00	2.0	36,700	1.80	1703	31,100	1.82	1439	0.85
90	75% Xyl	0.20	0.46	20	1:00	1.6	21,700	1.80	2013	22,500	1.77	2085	1.04

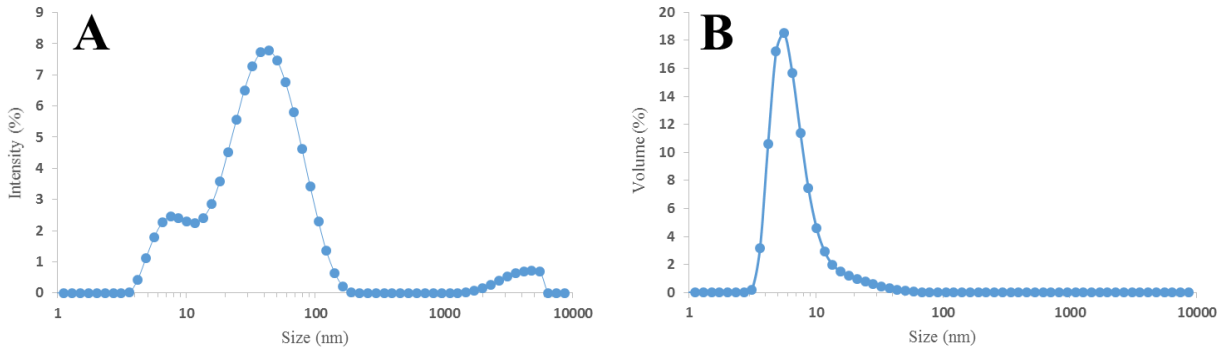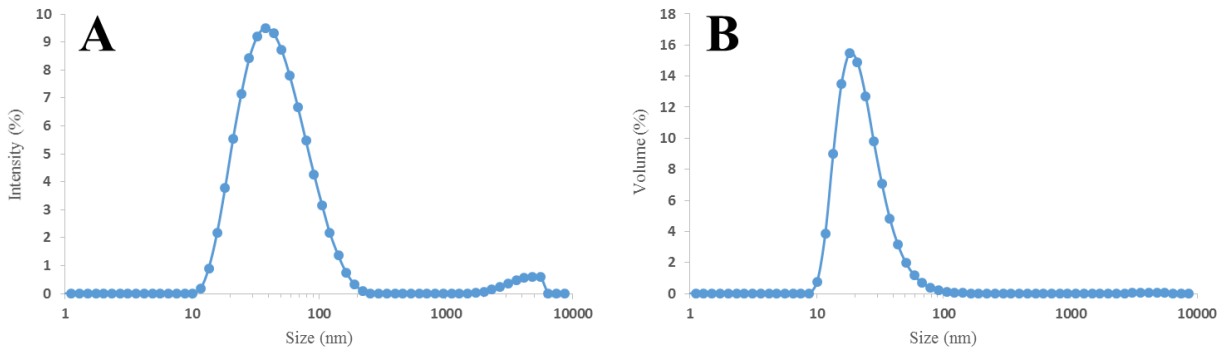# Nanoparticle Degradation Study

Figure B.5: Intensity (A) and volume (B) particle size distributions measured at 25 °C on day 0 of the accelerated degradation study of the 5 wt% latex produced from PLA$_1$EMA with 1% SDS as surfactant.
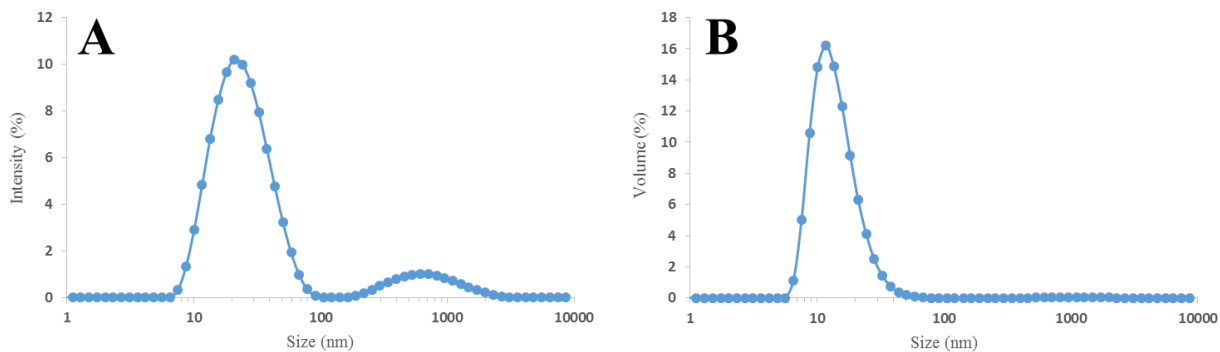

Figure B.6: Intensity (A) and volume (B) particle size distributions measured at 25 °C on day 0 of the accelerated degradation study of the 5 wt% latex produced from PLA$_5$EMA with 1% SDS as surfactant.

Figure B.7: Intensity (A) and volume (B) particle size distributions measured at 25 °C on day 0 of the accelerated degradation study of the 5 wt% latex produced from an equal mass macromonomer mixture of PLA$_5$EMA and HEMA-PLA$_5$ with 1% SDS as surfactant.
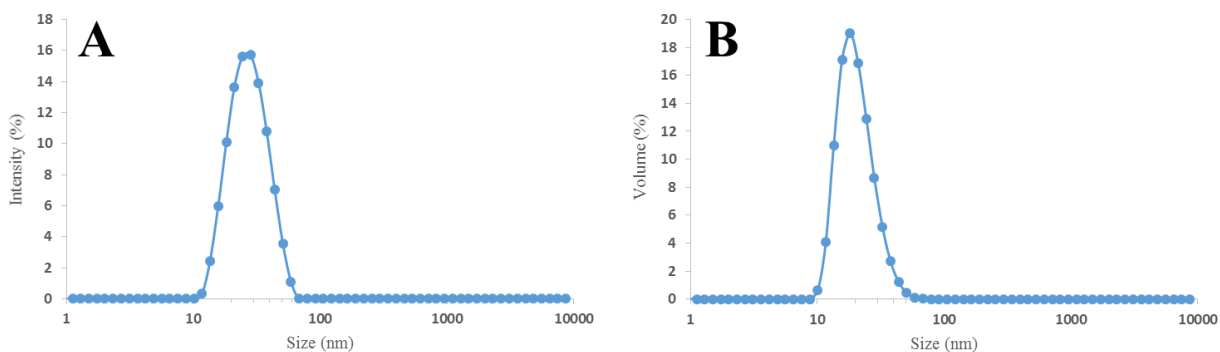

Figure B.8: Intensity (A) and volume (B) particle size distributions measured at 25 °C on day 0 of the accelerated degradation study of the 5 wt% latex produced from HEMA-PLA$_5$ with 1% SDS as surfactant.

Table B.8: pH measurements of latex taken at room temperature throughout the accelerated NP degradation study performed at 50 °C.

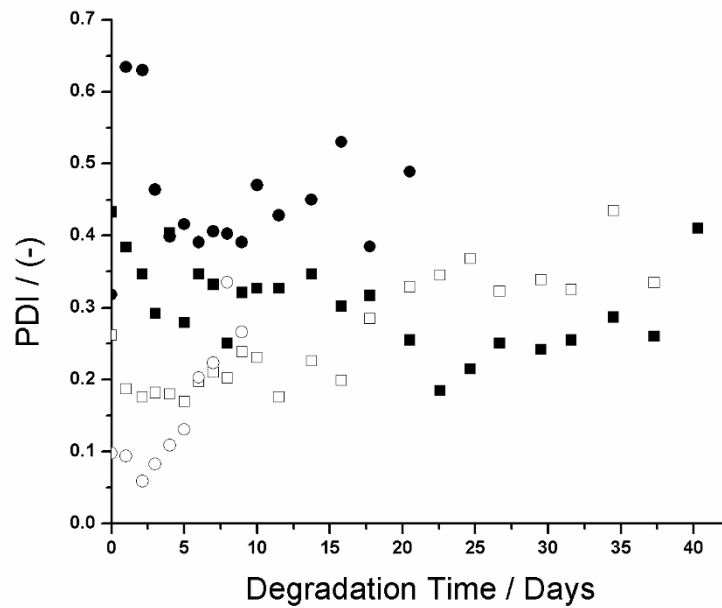| Degradation Time (days)	*pH* of 5 wt% latex	
	PLA$_1$EMA	PLA$_5$EMA
0	6.8	6.4
34.5	2.8	2.1

Figure B.9: Polydispersity indices (PDI) measured at 25 °C for NPs produced from PLA$_1$EMA (■), PLA$_5$EMA (□), an equal mass copolymer of PLA$_5$EMA and HEMA-PLA$_5$ (●), and HEMA-PLA$_5$ (○) throughout the accelerated degradation study at 50 °C. Measurement standard deviations are typically within 5% of the mean, but increase to as much as 30% during the final days of degradation.

References

(1)   Beuermann, S. *Macromolecules* **2004**, *37*, 1037.

Appendix C

Supporting Information: Applications of Nitrogen Containing Macromonomers
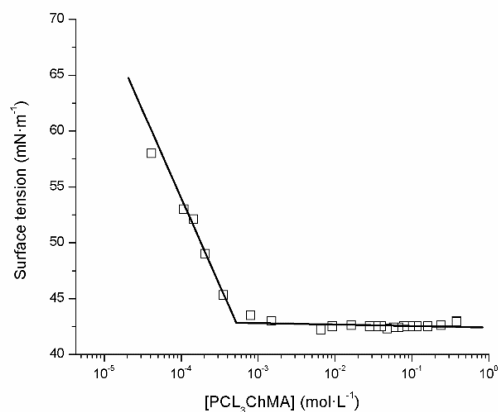
PCL₃ChMA Characterization and Homopolymeriztion

Figure C.1: Surface tension measurements used to determine critical micelle concentration of PCL₃ChMA in water at 19 °C as 5.1·10⁻⁴ mol·L⁻¹. Surface tension of water was measured as 73.7 mN·m⁻¹.
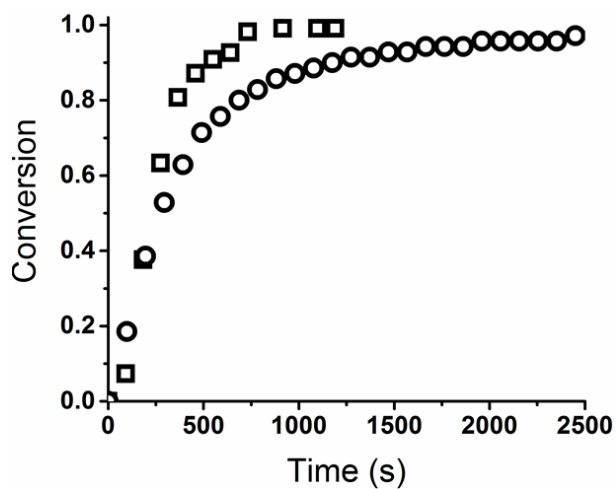

Figure C.2: Conversion profiles from in situ ¹H NMR batch homopolymerization of 10 wt% PCL₃ChMA (□) and AM (○) in D₂O with 0.22 wt% V-50 at 50 °C.
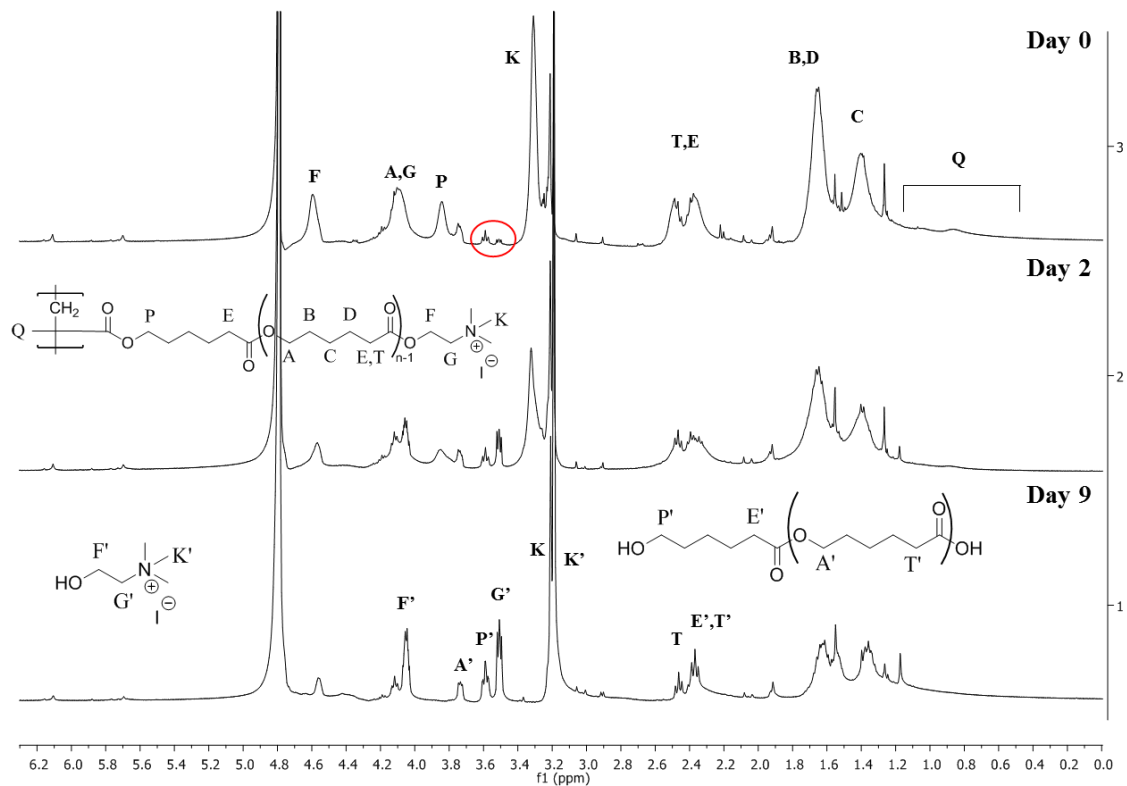
Degradation Study

Figure C.3: Select ^{1}H NMR spectra of 1 wt% poly(PCL₃ChMA) in D₂O recorded at 25 °C at 1 day increments of an accelerated degradation test at 85 °C. Peak assignments for proposed degradation products are provided.
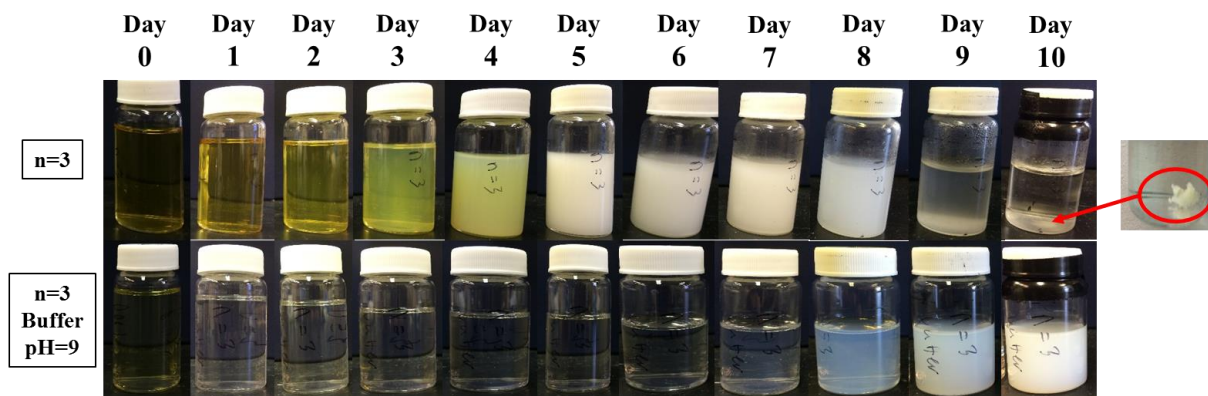

Figure C.4: Pictorial evolution of accelerated hydrolytic degradation test of 1 wt% poly(PCL₃ChMA) in H₂O (top) and in pH=9 buffer solution (bottom).

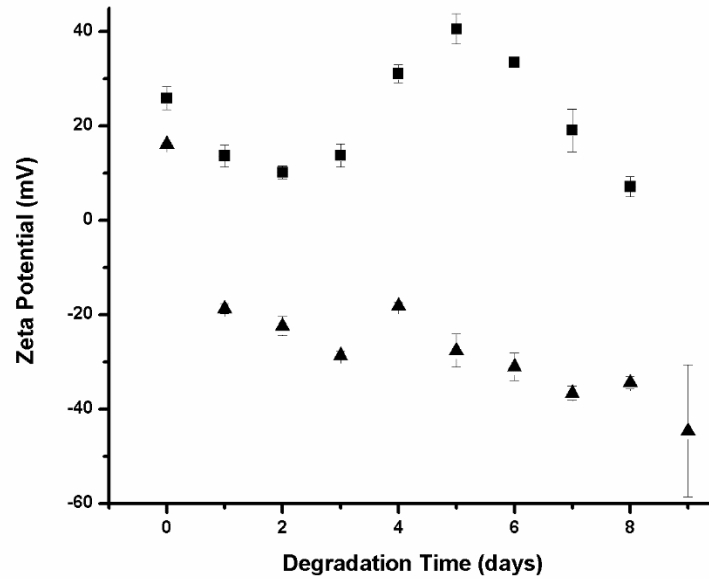**Figure C.5: Evolution of zeta potential during accelerated hydrolytic degradation test at 85 °C of 1 wt% poly(PCL₃ChMA) solution in H₂O (■) and buffer solution with pH=9 (▲). Error bars represent standard deviatons.**
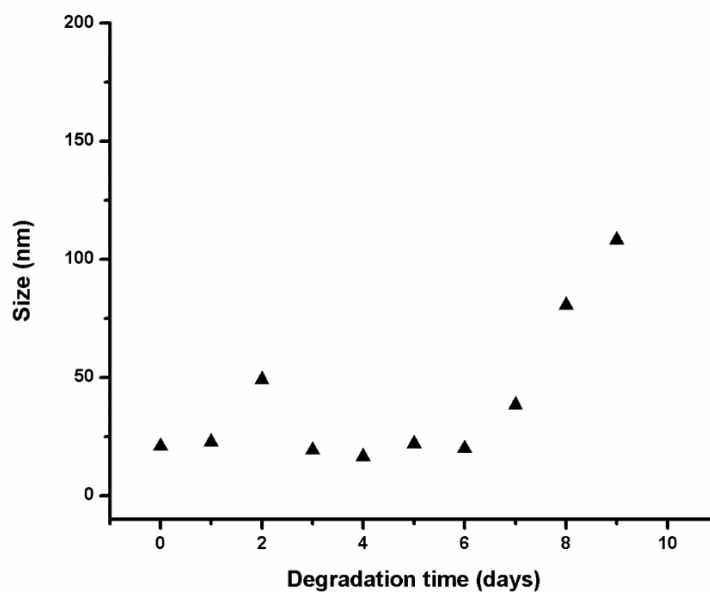
Figure C.6: Intensity average size for 1 wt% poly(PCL$_3$ChMA) in buffer solution with pH=9 throughout accelerated degradation test at 85 °C. Measurement standard deviations are typically within 2% of the mean.

Table C.1: Summary of intensity average size data from dynamic light scattering for 1 wt% poly(PCL$_n$ChMA) in H$_2$O throughout accelerated degradation test at 85 °C reported with standard deviations.

Degradation time (days)	z-avg. (nm)		PDI (-)	
	n=2	*n*=3	*n*=2	*n*=3
0	42±2.9	22±2.0	0.19±0.06	0.27±0.04
1	32±3.4	17±0.2	0.30±0.09	0.19±0.01
2	22±0.2	33±0.8	0.24±0.01	0.22±0.01
3	40±0.4	46±0.2	0.09±0.02	0.13±0.00
4	88±0.7	79±0.6	0.14±0.01	0.16±0.01
5	523±0.9	181±1.3	0.24±0.03	0.23±0.01
6	-	344±1.7	-	0.35±0.01
7	-	504±3.9	-	0.22±0.01
8	-	794±16.4	-	0.23±0.01

Table C.2: Summary of intensity average size data from dynamic light scattering for 1 wt% poly(PCL$_n$ChMA) in pH=9 buffer solution throughout accelerated degradation test at 85 °C reported with standard deviations.

Degradation time (days)	z-avg. (nm)		PDI (-)	
	n=2	n=3	n=2	n=3
0	29±1.0	21±0.6	0.24±0.02	0.31±0.01
1	87±12.0	23±0.5	0.19±0.06	0.39±0.05
2	64±28	49±11.0	0.21±0.05	0.17±0.02
3	29±8.1	19±0.3	0.32±0.16	0.39±0.01
4	61±18.5	17±0.2	0.14±0.01	0.32±0.03
5	33±10.7	22±7.4	0.31±0.17	0.30±0.10
6	20±2.4	20±0.6	0.29±0.06	0.36±0.03
7	-	39±1.0	-	0.28±0.00
8	20±1.1	81±0.8	0.39±0.017	0.24±0.01
9	234±33.9	108±0.3	0.31±0.01	0.08±0.01
10	112±21.6	124±0.5	0.21±0.02	0.02±0.01

Appendix D

Supporting Information for Chapter 7: Pulsed Laser Studies of Cationic Reactive Surfactant Radical Propagation Kinetics
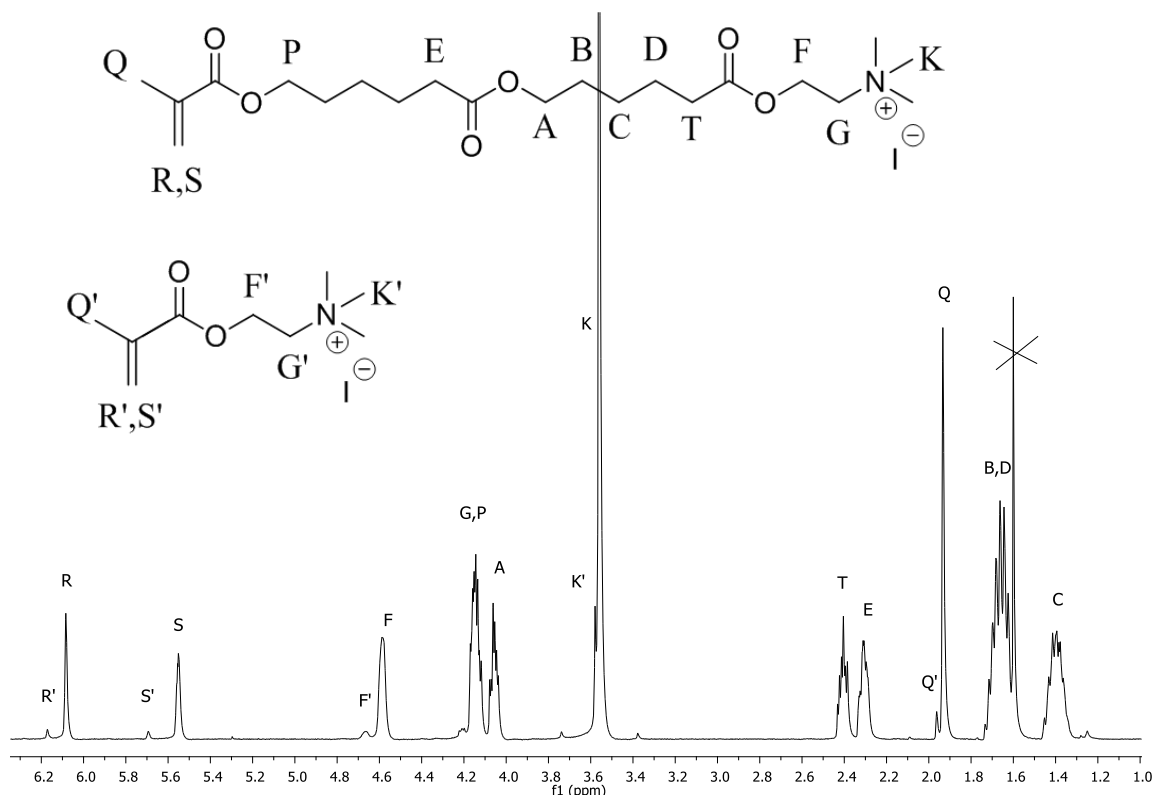
Macromonomer Characterizations

Figure D.1: ^{1}HNMR spectrum and peak assignment for PCL$_2$ChMA in CDCl$_3$ at 25 °C.

PCL$_2$ChMA ^{1}H-NMR (CDCl$_3$, 400 MHz) with integrations relative to Peak (S+S'): δ = 6.17 ppm (s, 0.1H, R'), δ = 6.09 ppm (s, 0.9H, R), δ = 5.70 ppm (s, 0.1H, S'), δ = 5.56 ppm (s, 0.9H, S), δ = 4.67 ppm (t, 0.2H, F'), δ = 4.59 ppm (t, 1.8H, F), δ = 4.23–4.11 ppm (m, 4.0H, G+P), δ = 4.06 ppm (t, 2.0H, A), δ = 3.57 ppm (s, -, K'), δ = 3.56 ppm (s, 9.0H, K+K'), δ = 2.45–2.37 ppm (t, 2.0H, T), δ = 2.36–2.27 ppm (t, 2.0H, E), δ = 1.97 ppm (s, -, Q'), δ = 1.94 ppm (s, 3.0H, Q+Q'), δ = 1.74–1.61 ppm (m, 8.0H, B+D), δ = 1.47–1.33 ppm (m, 4.0H, C).

$$n = \frac{Integral\ (E+T)/2}{Integral\ (S+S\prime)} = \frac{(2.0+2.0)/2}{1.0} = 2.0$$
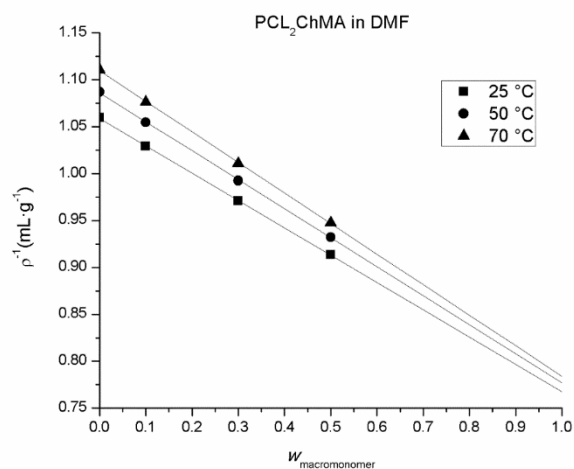
Figure D.2: Reciprocal densities measured for different weight fractions of PCL₂ChMA in DMF solution at various temperatures.

$$\left(\frac{1}{\rho_{mix}}\right) = \left(\frac{1}{\rho_{DMF}}\right) + w_{PCL_2ChMA} \cdot \left(\frac{1}{\rho_{PCL_2ChMA}} - \frac{1}{\rho_{DMF}}\right)$$

Table D.1: Extrapolated PCL₂ChMA densities from DMF solution density measurements at various temperatures, assuming volume additivity.

T (°C)	ρ (g·mL^{-1})
25	1.303
50	1.287
70	1.276
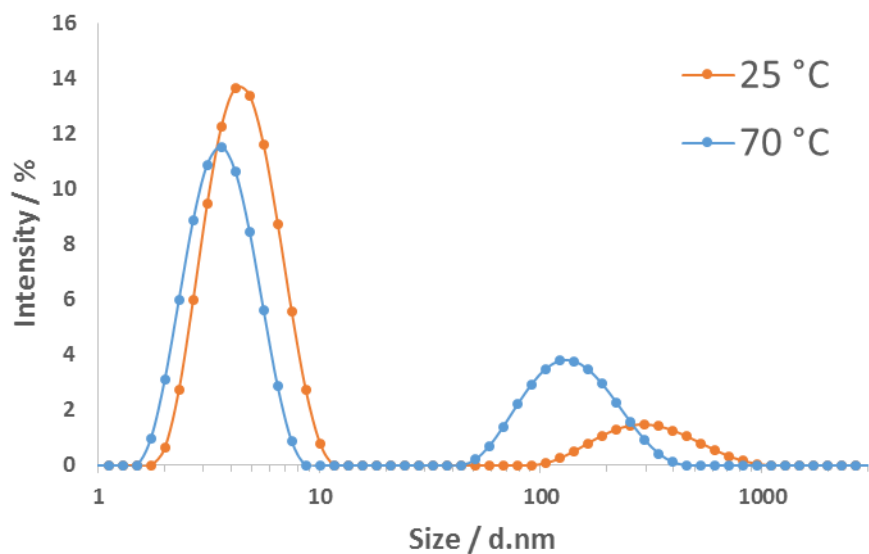
Figure D.3: Particle size distributions for 10 wt% PCL₂ChMA in H₂O at 25 and 70 °C.

Table D.2: Particle size distribution characterizations for 10 wt% PCL₂ChMA in H₂O shown in Figure D.3.

T (°C)	z-avg. (d.nm)	PDI	Scattering Intensity[a] (kcps)
25	5.0 ± 0.1	0.24 ± 0.01	324
70	11.4 ± 0.4	0.29 ± 0.01	177

[a] Attenuator level 9
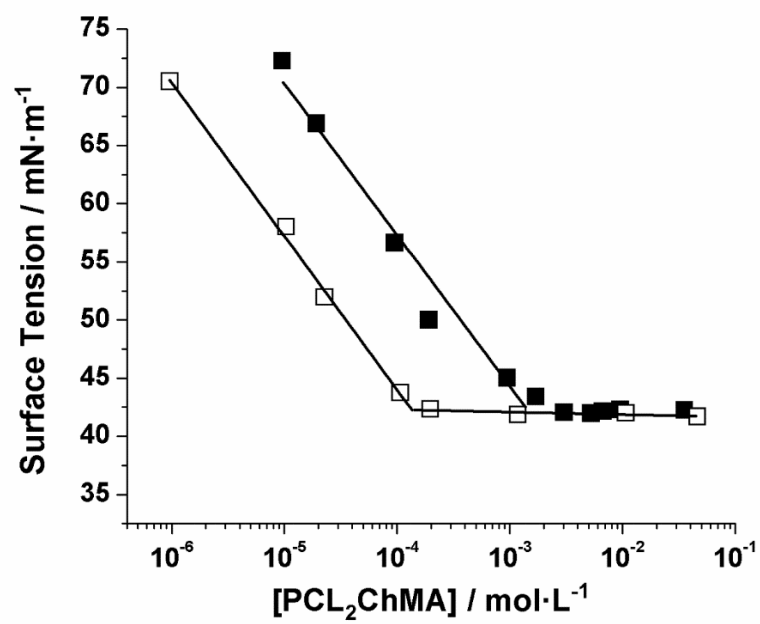
Figure D.4: Surface tension measurements for PCL$_2$ChMA at room temperature in pure H$_2$O (■) and 3.4 M NaCl (□) solutions.

PLP-SEC
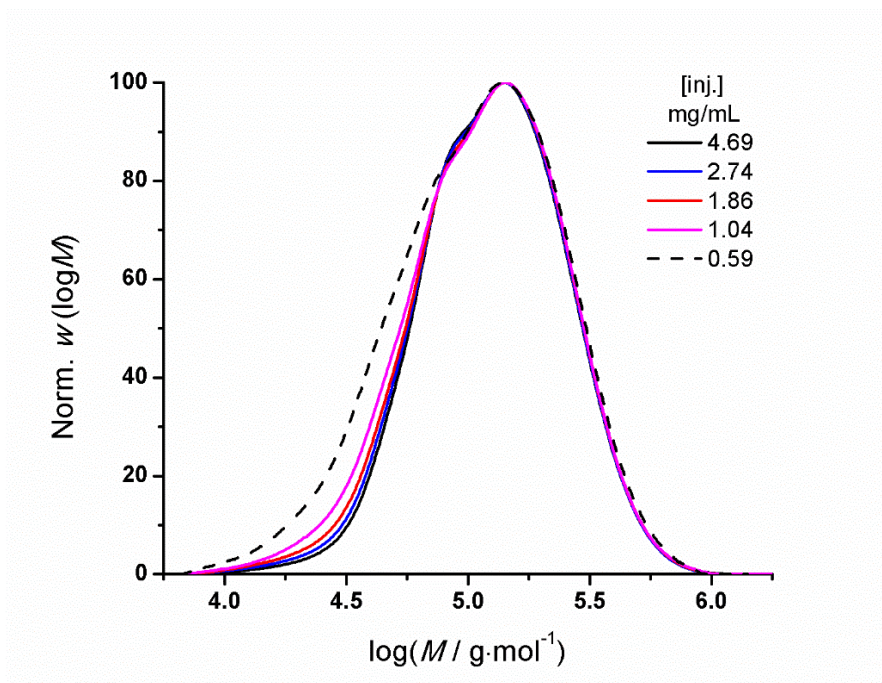
Figure D.5: RI detector response (normalized by amount with pullulan calibration) for a low-conversion poly(PCL₂ChMA) sample injected at concentrations ranging from 0.59–4.69 mg·mL⁻¹.

Figure D.6: MALLS output for MMD of a low-conversion poly(PCL$_2$ChMA) sample injected as 1.04, 1.86, 2.74, and 4.69 g·mL^{-1} in panels A, B, C, and D, respectively.

Table D.3: Reproducibility of MALLS output (corresponding to Figure D.6) for inflection point identification in PLP-SEC samples.

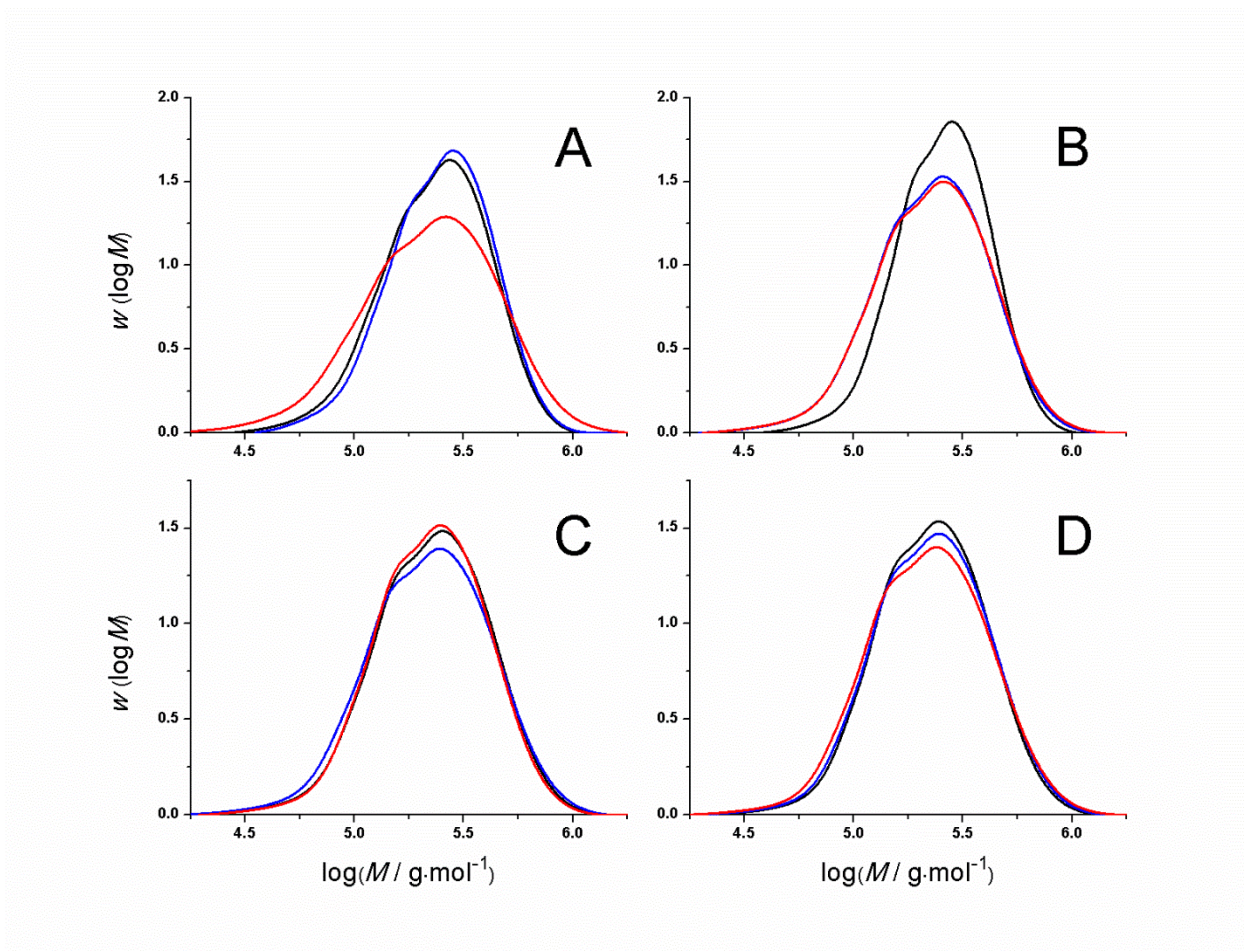| wt%	[LiTPO] (mmol/L)	# pulses	p.r.r. (Hz)	T (°C)	[inj] (mg·mL^{-1})	inj. #	$\log M_1$	$\log M_2$	M_2/M_1
10	10	1000	20	50	4.69	1	5.102	5.315	1.63
						2	5.088	5.312	1.67
						3	5.064	5.297	1.71
					2.74	1	5.105	5.322	1.65
						2	5.074	5.306	1.71
						3	5.102	5.316	1.64
					1.86	1	5.210	5.383	1.49
						2	5.119	5.327	1.61
						3	5.112	5.329	1.65
					1.04	1	5.162	5.355	1.56
						2	5.189	5.379	1.55
						3	5.076	5.315	1.73

Table D.4: Inflection point comparison between Pullulan direct calibration and MALLS.

[inj] (g·mL^{-1})	inj. #	MALLS		Elution Volume		Pullulan calib.		Pullulan calib. → MALLS		Avg.
		$\log M_1$	$\log M_2$	$\log M_1$	$\log M_2$	$\log M_1$	$\log M_2$	$\dfrac{M_{1,MALLS}}{M_{1,Pull.}}$	$\dfrac{M_{2,MALLS}}{M_{2,Pull.}}$	
4.69	1	5.102	5.315	24.0780	23.0462	4.816	5.063	1.93	1.79	1.83 ± 0.08
	2	5.088	5.312	24.0831	23.0538	4.815	5.061	1.87	1.78	
	3	5.064	5.297	24.0716	23.0551	4.818	5.061	1.76	1.72	
2.74	1	5.105	5.322	24.0908	23.0635	4.813	5.059	1.96	1.83	
	2	5.074	5.306	24.0824	23.0528	4.815	5.062	1.81	1.76	
	3	5.102	5.316	24.0865	23.0583	4.814	5.060	1.94	1.80	

Table D.5: PLP-SEC reaction conditions for PCL$_2$ChMA k_p determination at 25 °C.

Label	wt% macromer	[LiTPO] mmol·L^{-1}	# pulses	p.r.r. Hz	[NaCl] M	x %	Pullulan Calibration			MALLS			$\frac{M_{2,MALLS}}{M_{2,Pull}}$
							logM_2	M_2/M_1	$k_{p,2}\cdot$M	logM_2	$k_{p,2}\cdot$M	M_2/M_1	
201	10	10	300	5	0	4.9	5.298	1.95	941	5.551	1686	1.69	1.79
203	10	10	300	20	0	4.1	4.834	1.74	1294	5.072	2238	1.69	1.73
205	5	10	300	10	0	6.8	5.004	1.97	957	5.269	1761	2.17	1.84
206	5	10	300	20	0	6.4	4.796	1.64	1185	5.062	2187	1.58	1.85
207	20	10	300	5	0	3.3	5.334	1.74	1023	5.618	1967	1.46	1.92
208	20	10	300	10	0	3.2	5.124	1.89	1261	5.389	2322	1.52	1.84
209	20	10	300	20	0	3.8	4.89	1.68	1472	-	-	-	-
218	20	10DMPA	300	20	0	1.1	4.898	1.69	1499	-	-	-	-
213	10	10	600	20	0	11.6	4.831	1.74	1285	5.050	2127	1.59	1.66
214	10	10	900	20	0	16.8	4.837	1.80	1303	5.061	2182	1.58	1.67
215	10	10	1200	20	0	21.5	4.82	1.72	1253	-	-	-	-
216	10	10	1500	20	0	27.8	4.826	1.75	1270	5.079	2274	1.63	1.79
210	9.5	10	200	20	1.0	3.9	4.865	1.73	1390	5.105	2415	1.58	1.74
211	8.4	10	200	20	3.4	6.2	4.795	1.78	1183	5.085	2306	1.79	1.95
219	10	10	300	20	1.0	10.2	4.802	1.82	1202	-	-	-	-
220	10	10	300	20	3.4	14.9	4.816	1.75	1241	-	-	-	-

Table D.6: PLP-SEC reaction conditions for PCL₂ChMA k_p determination at 50 °C.

Label	wt% macromer	[LiTPO] mmol·L⁻¹	# pulses	p.r.r. Hz	x %	Pullulan Calibration			MALLS			$\dfrac{M_{2,MALLS}}{M_{2,Pull}}$
						$\log M_2$	M_2/M_1	$k_{p,2}\cdot M$	$\log M_2$	$k_{p,2}\cdot M$	M_2/M_1	
501	10	10	200	10	2.6	5.227	1.97	1599	5.492	2943	1.77	1.84
502	10	10	200	15	3.2	5.102	1.90	1799	5.400	3572	1.85	1.99
503	10	10	200	20	4.1	5.01	1.80	1940	5.275	3572	1.70	1.84
504	10	10	200	30	7.9	4.816	1.73	1862	-	-	-	-
505	5	10	200	10	5.7	5.04	1.87	1040	5.301	1896	1.94	1.82
506	5	10	200	15	12.5	4.944	2.05	1250	-	-	-	-
507	5	10	200	20	10.4	4.873	1.80	1415	-	-	-	-
509	20	10	200	10	2.1	5.292	1.82	1857	5.711	4873	1.73	2.62
510	20	10	200	15	2.4	5.042	1.91	1566	5.447	3980	1.77	2.54
511	20	10	200	20	2.4	4.953	1.85	1702	5.308	3854	1.82	2.26
515	20	10DMPA	200	20	0.8	5.038	1.81	2070	-	-	-	-

Table D.7: PLP-SEC reaction conditions for PCL₂ChMA k_p determination at 70 °C.

Label	wt% macromer	[LiTPO] mmol·L⁻¹	# pulses	p.r.r. Hz	[add.] mM	x %	Pullulan Calibration			MALLS			$\dfrac{M_{2,MALLS}}{M_{2,Pull}}$
							$\log M_2$	M_2/M_1	$k_{p,2}\cdot M$	$\log M_2$	$k_{p,2}\cdot M$	M_2/M_1	
703	10	10	200	30	0	3.5	4.983	1.75	2735	5.311	5820	1.55	2.13
710	10	10DMPA	200	20	0	1.8	5.102	2.02	2398	-	-	-	-
705	5	10	200	20	0	7.0	5.054	1.87	2147	5.390	4654	1.88	2.17
706	5	10	200	30	0	6.7	4.92	1.88	2366	-	-	-	-
711	5	10DMPA	200	20	0	1.4	5.157	2.33	2722	-	-	-	-
707	20	10	200	10	0	2.4	5.3	1.82	1892	5.650	4235	1.57	2.24
708	20	10	200	20	0	2.8	5.086	1.85	2311	5.504	6052	1.74	2.62
709	20	10	200	30	0	3.0	4.962	1.82	2606	5.330	6081	1.72	2.33
712	20	10DMPA	200	20	0	1.4	5.204	1.87	3033	5.546	6666	1.78	2.20

Table D.8: PLP-SEC reaction conditions for PCL₂ChMA k_p determination at 85 °C.

Label	T	wt%	[LiTPO]	#	p.r.r.	[NaCl]	x	Pullulan Calibration		
	°C	macromer	mmol·L^{-1}	pulses	Hz	M	%	logM_2	M_2/M_1	$k_{p,2}$·M
802	85	10	10	100	20	0	6.5	5.144	1.87	2642
803	85	10	10	100	30	0	5.9	5.018	1.81	2965
805	85	5	10	100	20	0	5.7	5.151	2.24	2685
806	85	5	10	100	30	0	9.4	4.957	2.15	2576
813	85	10	10	200	20	0	4.5	5.13	1.94	2558
814	85	10	10	300	20	0	9.9	5.146	1.94	2654
821	85	10	10	800	20	0	38.8	5.168	1.97	2792
810	85	9.5	10	100	20	1.0	7.6	4.829	2.52	3228
811	85	8.4	10	100	20	3.4	3.9	5.07	1.93	4294
819	85	10	10	100	20	1.0	2.2	4.913	1.91	2957
820	85	10	10	100	20	3.4	1.6	5.036	2.19	4517

Copolymerization Kinetics
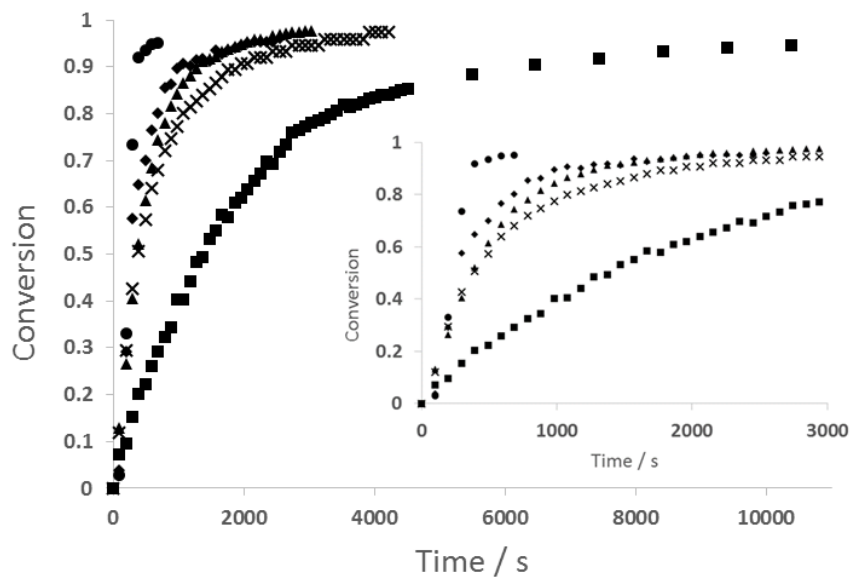
Figure D.7: Molar conversion profiles for 5 wt% PCL₃ChMA/AM copolymerizations in D₂O at 50 °C with 0.22 wt% V-50 initiator for initial AM compositions $f_{AM,0}$ = 0 (●), 0.1 (♦), 0.5 (■), 0.9 (▲), and 1.0 (×).
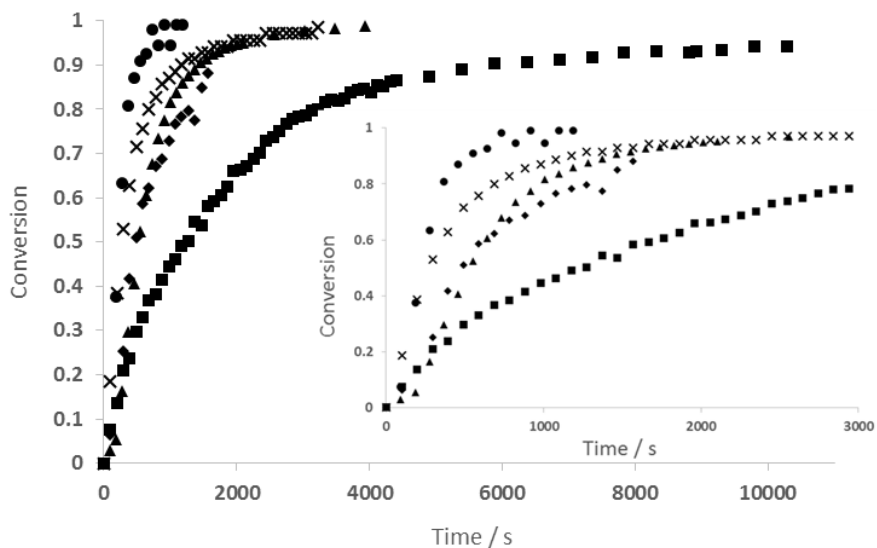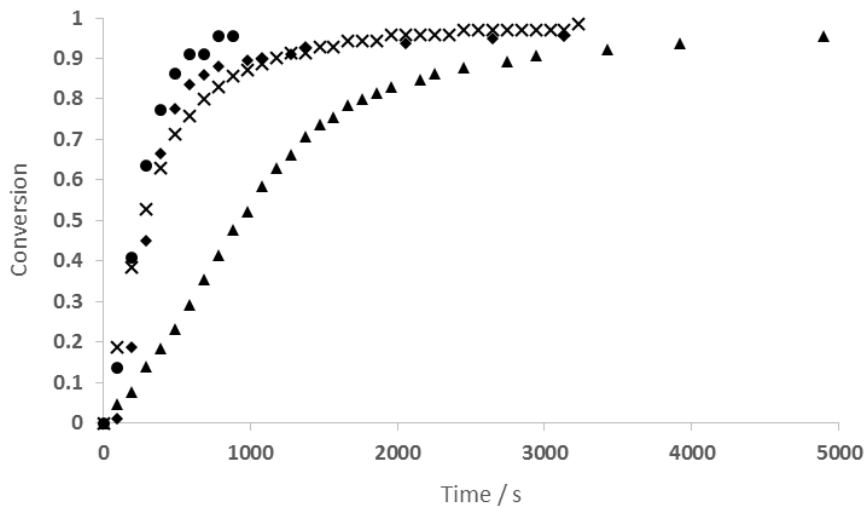
Figure D.8: Molar conversion profiles for 10 wt% PCL₃ChMA/AM copolymerizations in D₂O at 50 °C with 0.22 wt% V-50 initiator for initial AM compositions $f_{AM,0}$ = 0 (●), 0.1 (♦), 0.5 (■), 0.9 (▲), and 1.0 (×).

Figure D.9: Molar conversion profiles for 10 wt% PCL₂ChMA/AM copolymerizations in D₂O at 50 °C with 0.22 wt% V-50 initiator for initial AM compositions $f_{AM,0}$ = 0 (●), 0.1 (♦), 0.9 (▲), and 1.0 (×).

Table D.9: Inhibition times (hr) for PCL$_n$ChMA copolymerizations with AM at 50 °C with 0.22 wt% V-50 initiator in D$_2$O. Corresponding conversion plots are summarized by Figures D.7-9.

$f_{AM,0}$	5 wt%	10 wt%	
	$n=3$	$n=3$	$n=2$
0	0.30	0.20	0.60
0.1	0.57	0.79	0.52
0.5	1.77	1.33	-
0.9	0.14	0.92	1.25
1.0	0.35	0.16	-
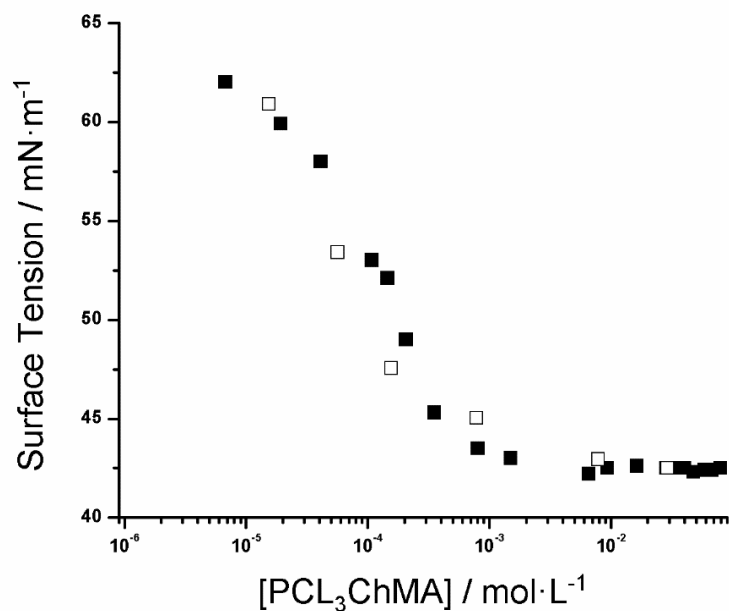
Figure D.10: Surface tension measurements for PCL$_3$ChMA at room temperature in pure H$_2$O (■) and in 1 wt% AM aqueous solution (□).
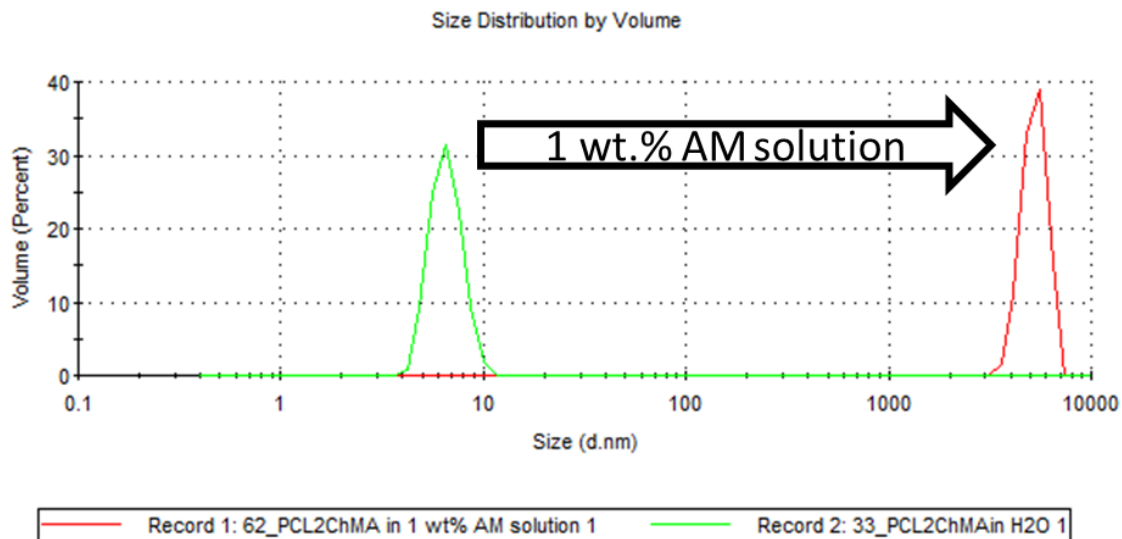
Figure D.11: Particle size distributions in volume percent measured at room temperature for PCL$_2$ChMA above its CMC in pure H$_2$O and in 1 wt% AM aqueous solution (at room temperature for over one hour).

Appendix E

Supporting Information for Chapter 8: Polyester Macromonomer Radical Copolymerization Kinetics with Styrene

In order to estimate monomer conversion, a reference peak invariant with time must be established from the proton NMR spectra, as shown in Figure E.1. The integral of the aromatic region does not change with time, but the broadness of the copolymer aromatic signals overlaps peak C of styrene (ST) monomer. Since the integrations of peaks C and A are equivalent throughout the reaction, a reference integral is established as the difference in integrations of peak A (which is distinct) and the aromatic region, as summarized by Eqn. E.1. Then, the absolute moles of methacrylate (xMA) and ST are calculated as a function of time by Eqn. E.2 and E.3 in order to determine monomer molar composition and molar conversion by Eqn. E.4 and E.5, respectively. The composition drift is normalized by initial composition according to Eqn. E.6.

$$Ref. = \int Aromatics - \int A \tag{E.1}$$

$$n_{xMA} = \frac{\int E}{Ref.} \tag{E.2}$$

$$n_{ST} = \frac{\int A}{Ref} \tag{E.3}$$

$$f_{xMA} = \frac{\int E}{\int A + \int E} \tag{E.4}$$

$$x = 1 - \frac{n_{xMA} + n_{ST}}{n_{xMA,0} + n_{ST,0}} \tag{E.5}$$

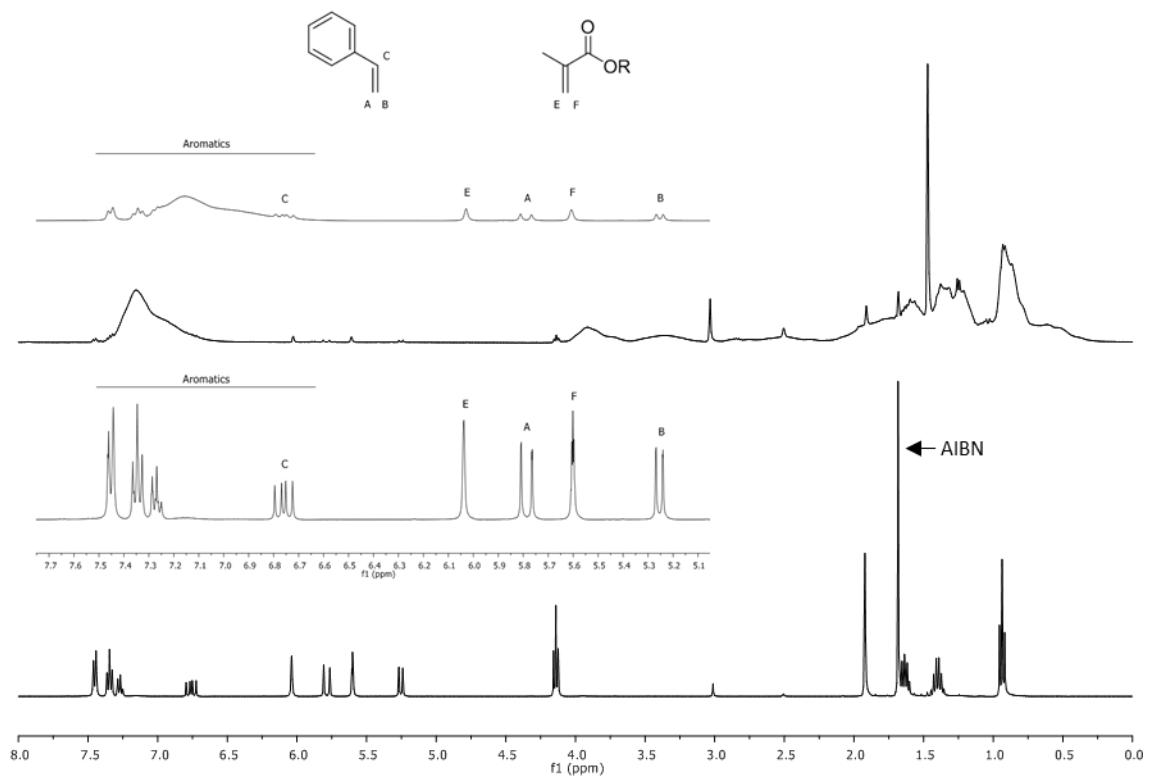$$Normalized\ f_{xMA} = \frac{f_{xMA}}{f_{xMA,0}} \tag{E.6}$$

Figure E.1: Relevant peak assignments for representative ^{1}H NMR spectra of BMA/ST copolymerization at 0% (bottom) and at 98% (top; inset at 80%) conversions performed in 80 wt% DMSO-d6 at 80 °C with $f_{xMA,0} = 0.5$ and 3.5 wt% AIBN.
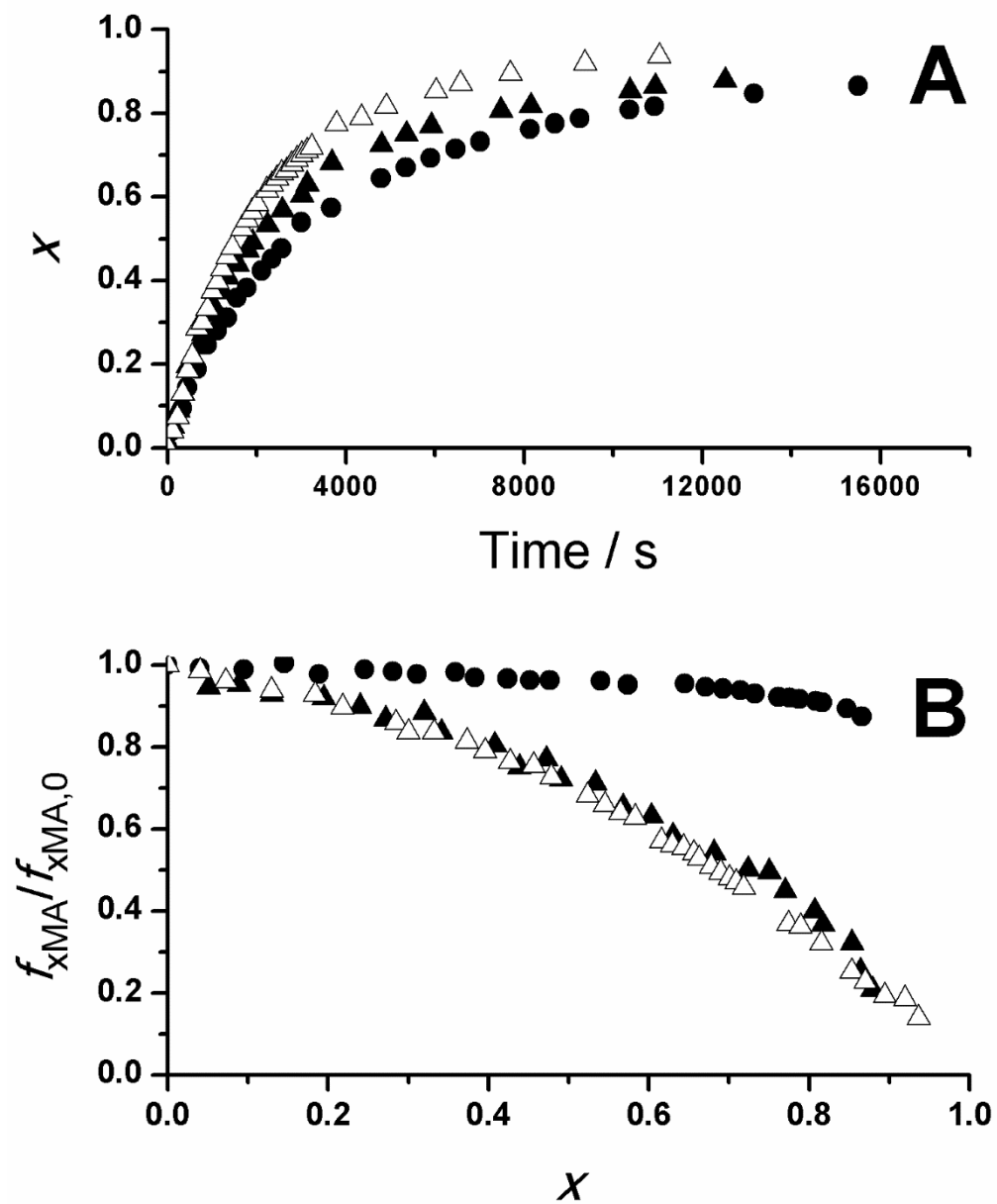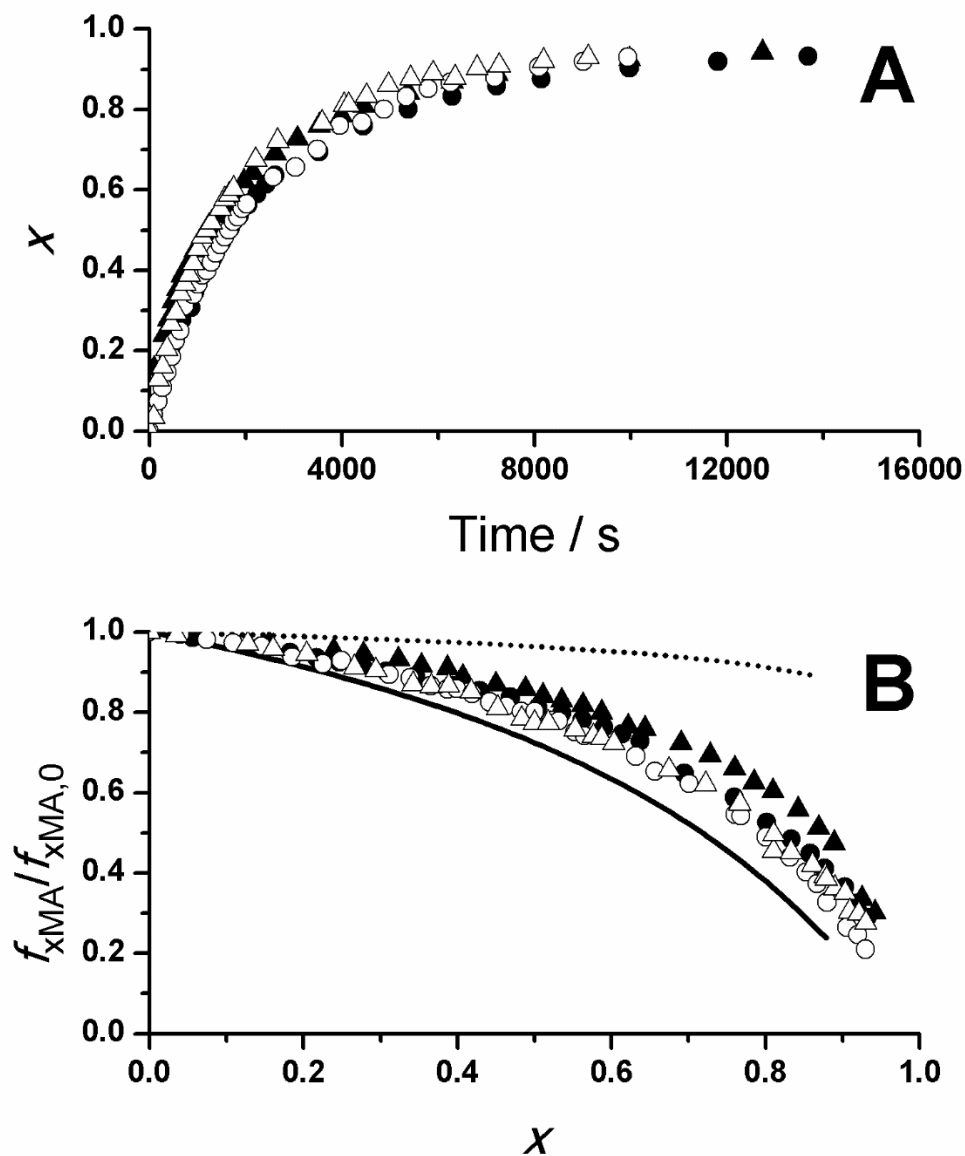
Figure E.2: Overall monomer conversion vs time profiles (panel A) and normalized monomer composition vs conversion (panel B) for ST copolymerizations with $f_{xMA,0} = 0.2$ for BMA (circles) and HEMA (triangles) in 80 wt% (closed symbols) as well as 60 wt% (open symbols) toluene-d8 performed at 80 °C with 3.5 wt% AIBN.

Figure E.3: Overall monomer conversion vs time profiles (panel A) and normalized monomer composition vs conversion (panel B) for ST copolymerizations with $f_{xMA,0} = 0.2$ for BMA (circles) and HEMA (triangles) in 80 wt% (closed symbols) as well as 60 wt% (open symbols) DMSO-d6 performed at 80 °C with 3.5 wt% AIBN. Best fit lines for HEMA/ST (solid line) and BMA/ST (dotted line) in 80 wt% toluene-d8 are provided as visual guides.
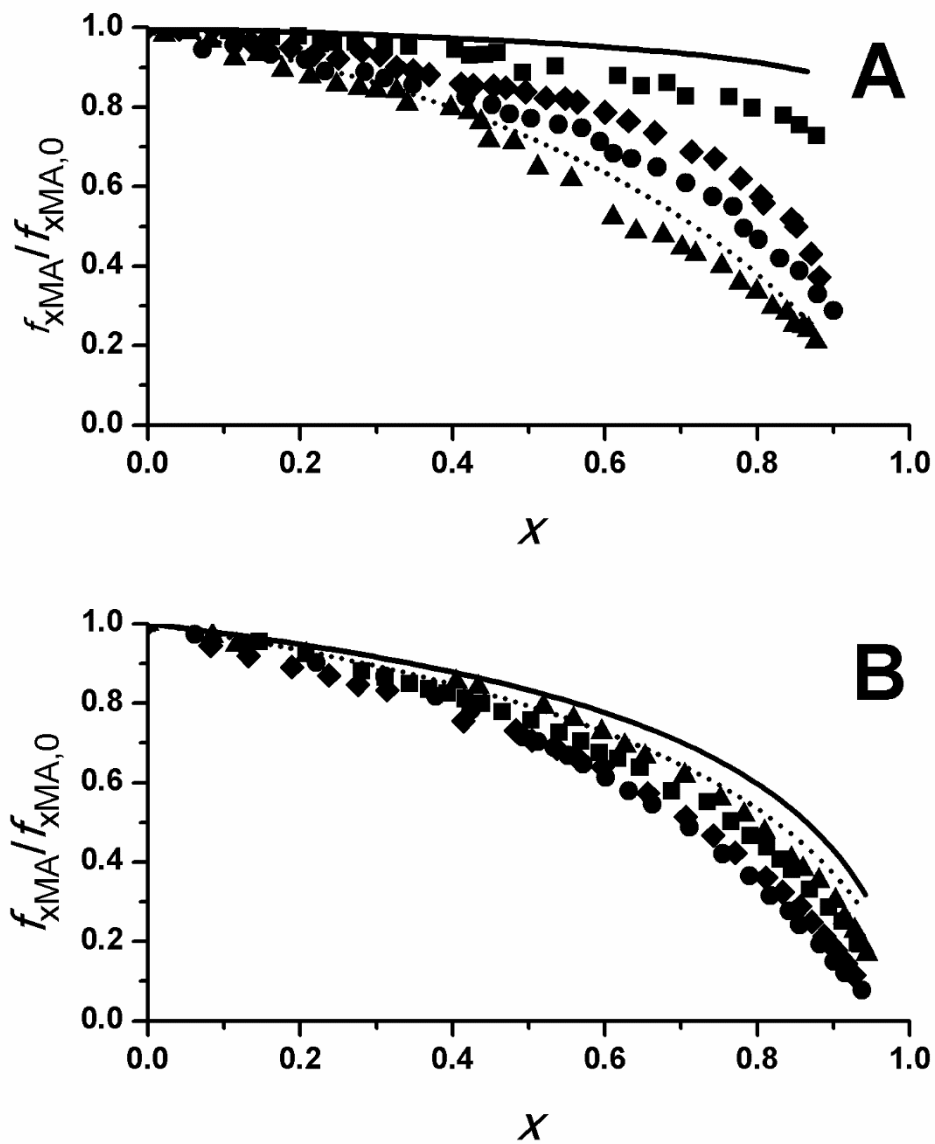
Figure E.4: Normalized monomer composition drifts of ST copolymerizations with $f_{xMA,0}$ = 0.2 for PLA₁EMA (●), HEMA-COOH (▲), DMAEMA (■), and GMA (◆) in 80 wt% toluene-d8 (panel A) and 80 wt% DMSO-d6 (panel B) performed at 80 °C with 3.5 wt% AIBN. Best fit lines for HEMA/ST (solid lines) and BMA/ST (dotted lines) in their respective solutions are provided as visual guides.
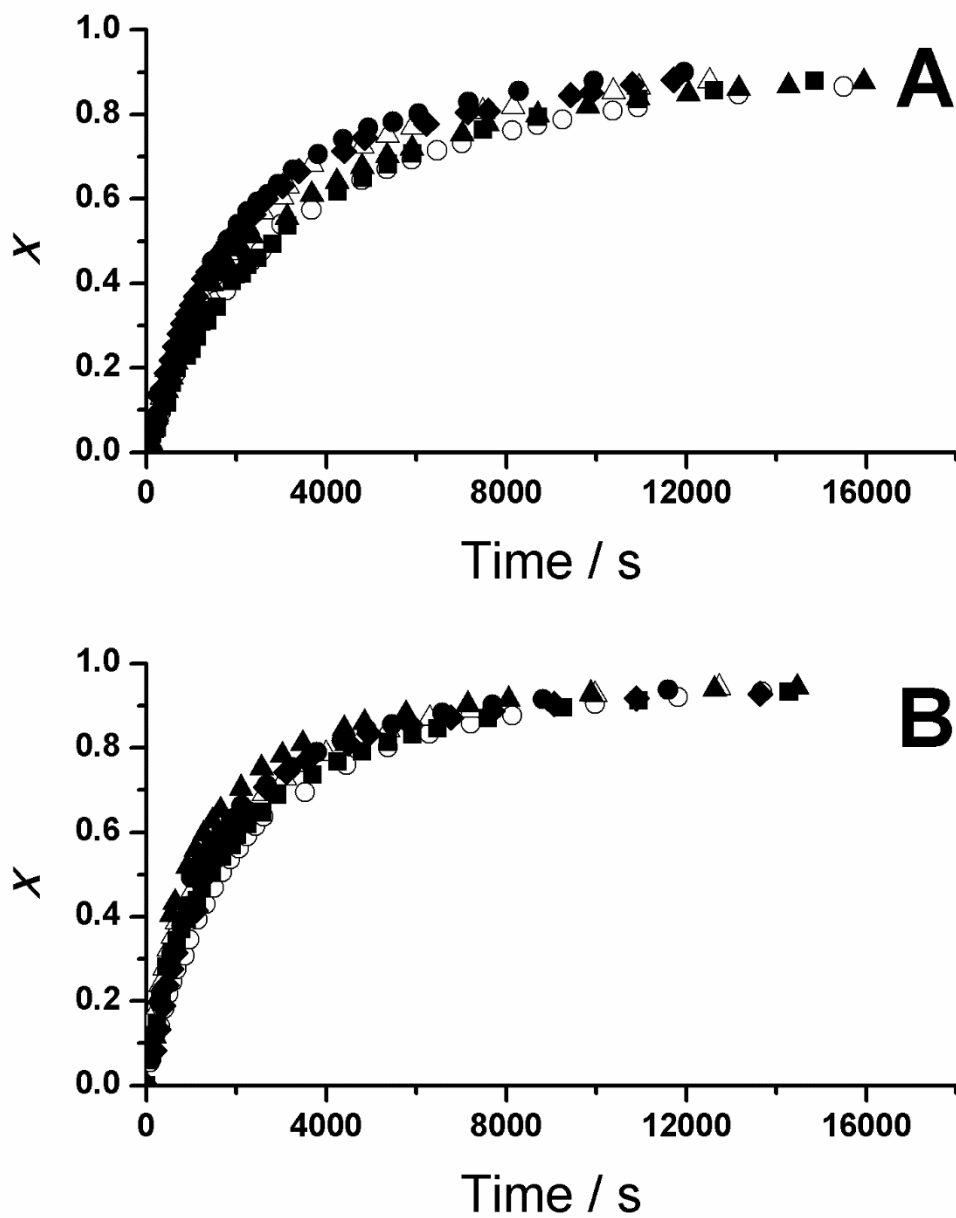
Figure E.5: Overall monomer conversion profiles for ST copolymerizations with $f_{xMA,0} = 0.2$ **for BMA (○), HEMA (△), PLA₁EMA (●), HEMA-COOH (▲), DMAEMA (■), and GMA (◆) in 80 wt% toluene-d8 (panel A) and 80 wt% DMSO-d6 (panel B) performed at 80 °C with 3.5 wt% AIBN.**
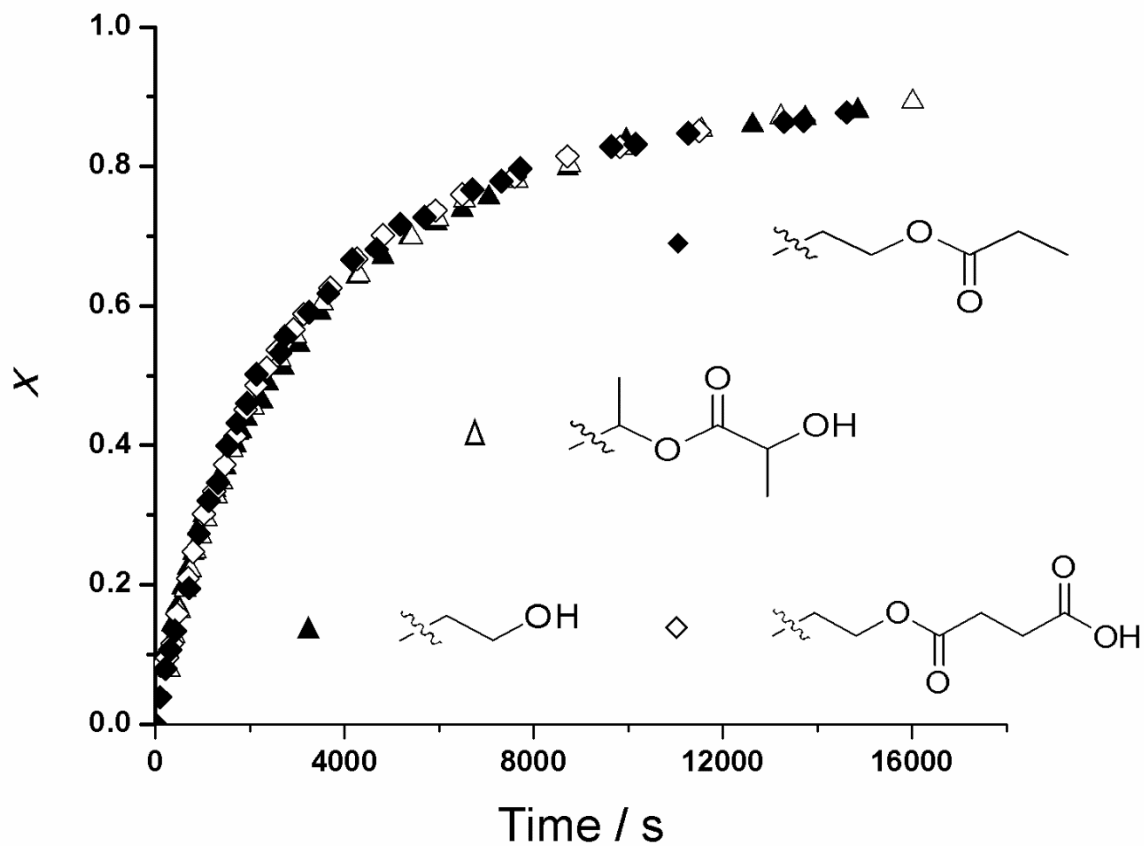
Figure E.6: Overall monomer conversion profiles for ST copolymerizations with $f_{xMA,0} = 0.2$ for HEMA-PCL$_3$ (▲), HEMA-PLA$_5$ (△), HEMA-PCL$_3$-COOH (◆), and HEMA-PCL$_3$-PR (◇) in 80 wt% toluene-d8 performed at 80 °C with 3.5 wt% AIBN.
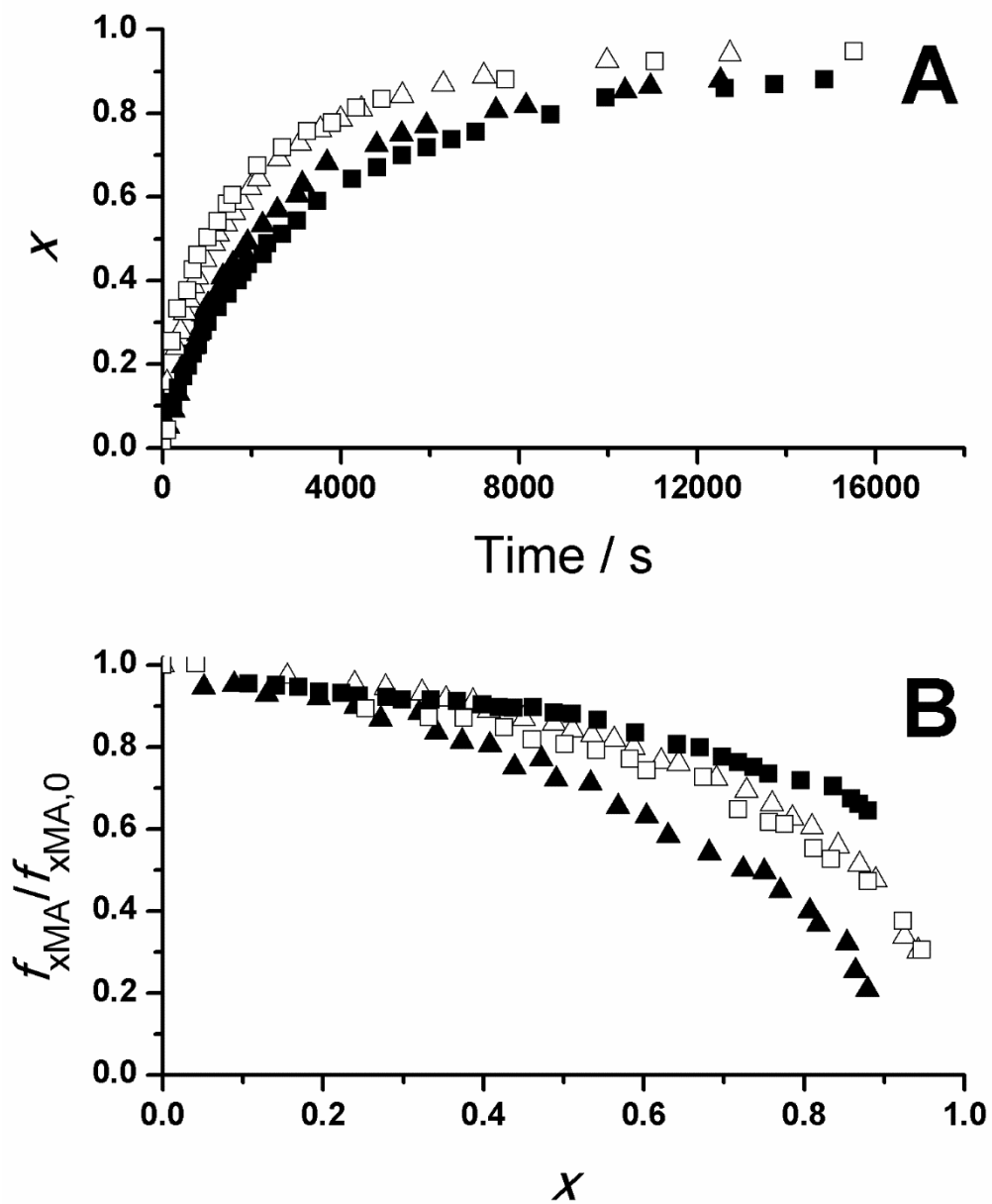
Figure E.7: Overall monomer conversion vs time profiles (panel A) and normalized monomer composition vs conversion (panel B) for ST copolymerizations with $f_{\text{xMA,0}} = 0.2$ for HEMA (triangles) and HEMA-PCL$_3$ (squares) in 80 wt% toluene-d8 (closed symbols) and 80 wt% DMSO-d6 (open symbols) performed at 80 °C with 3.5 wt% AIBN.

Table E.1: Weight-average molar masses (M_w) and dispersities ($Đ$) measured by light scattering for high conversion batch xMA/ST ($f_{xMA,0} = 0.2$) copolymers produced at 80 °C in 80 wt% toluene-d8 with 3.5 wt% AIBN.

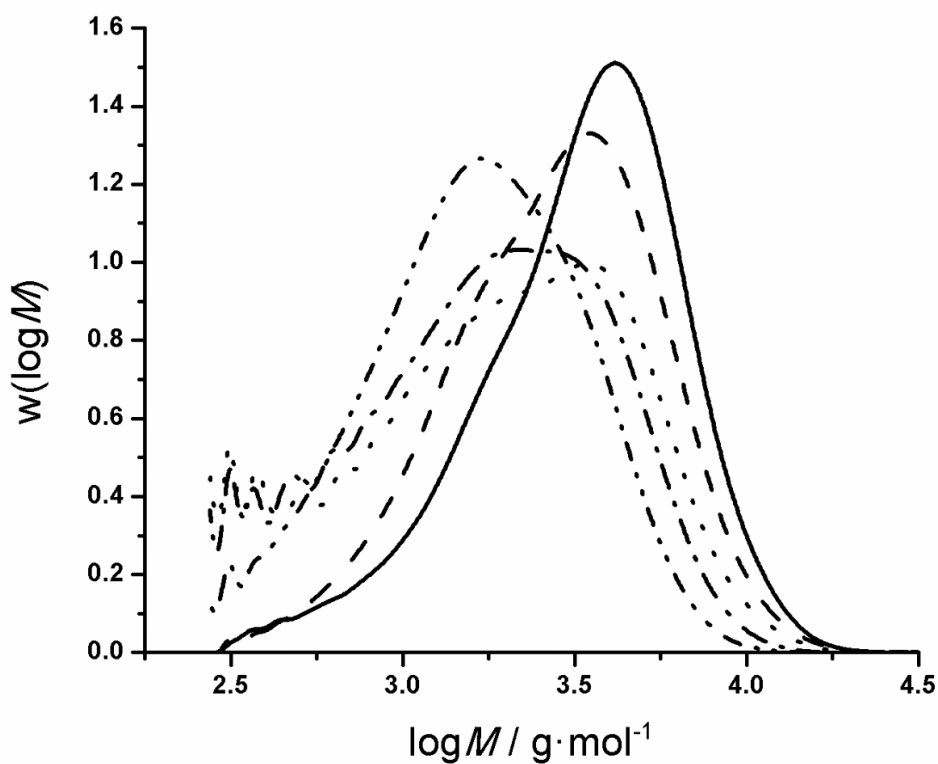| xMA	M_w kg·mol^{-1}	$Đ$
PLA$_5$EMA	5.3	-
HEMA	3.7	1.4
HEMA-PCL$_3$	3.0	1.7
PCL$_3$DeMA	3.0	1.3
BMA	2.2	1.5

Figure E.8: Polymer molar mass distributions in polystyrene equivalents for high conversion batch xMA/ST ($f_{xMA,0} = 0.2$) copolymers produced at 80 °C in 80 wt% toluene-d8 with 3.5 wt% AIBN for PLA$_5$EMA (solid), HEMA (dash), HEMA-PCL$_3$ (dot), PCL$_3$DeMA (dash dot), and BMA (dash dot dot) as xMA comonomer.